SIMPLIFIED BOW MODEL
FOR A STRIKING SHIP IN COLLISION

by

Suryanarayana Vakkalanka

Thesis submitted to the faculty of the
Virginia Polytechnic Institute and State University
In partial fulfillment of the requirements for the degree of

MASTER OF SCIENCE
in
Ocean Engineering

APPROVED:

A.J. Brown, Chairman

R.K Kapania **O. Hughes**

March 2000
Virginia Tech, Blacksburg, VA, USA
Keywords: ship, collision, bow, damage, accident

ABSTRACT

SIMPLIFIED BOW MODEL
FOR A STRIKING SHIP IN COLLISION

by

Suryanarayana Vakkalanka

The serious consequences of ship collisions necessitate the development of regulations and requirements for the subdivision and structural design of ships to reduce damage and environmental pollution, and improve safety.

Differences in striking ship bow stiffness, draft, bow height and shape have an important influence on the allocation of absorbed energy between striking and struck ships. The energy absorbed by the striking ship may be significant. The assumption of a "rigid" striking bow may no longer hold good and typical simplifying assumptions may not be sufficient.

The bow collision process is simulated by developing a striking ship bow model that uses Pedersen's super-element approach and the explicit non-linear FE code LS-DYNA. This model is applied to a series of collision scenarios. Results are compared with conventional FE model results, closed-form calculations, DAMAGE, DTU, ALPS/SCOL and SIMCOL. The results demonstrate that the universal assumption of a rigid striking ship bow is not valid. Bow deformation should be included in future versions of SIMCOL.

A simplified bow model is proposed which approximates the results predicted by the three collision models (closed-form, conventional and intersection elements) to a reasonable degree of accuracy. This simplified bow model can be used in further calculations and damage predictions. A single stiffness can be defined for all striking ships in collision, irrespective of size.

ACKNOWLEDGEMENTS

The completion of this thesis would have been impossible without the support of many people. First of all, I would like to express my sincere appreciation to my advisor, Professor Alan Brown, for his continuous support and guidance throughout the duration of this work. He has been a constant source of inspiration and it has been a pleasure working under his supervision.

This thesis is dedicated to my parents, Sri V.N Pratap & Smt. V. Ramavathi and my sister, Sita who have been a constant source of encouragement. Their love and support have helped me through difficult times and keep up challenges.

Also, I would like to acknowledge the support of several research students working on the ship collision project, particularly Donghui Chen, Bo Jin, Marie Lutzen and Jianjun Xia for helpful discussions.

I am grateful to the Department of Aerospace & Ocean Engineering at Virginia Tech. for providing me with research assistantship throughout the course of my study. I would like to thank ETA (Engineering Technology Associates), MI and LSTC (Livermore Software Technology Corporation), CA for providing technical support when needed and for providing introductory training in LS-DYNA. I am also thankful to the Society of Naval Architects and Marine Engineers (SNAME) and Ship Structure Committee (SSC) for funding this project.

I am thankful to Dr. Rakesh Kapania and Dr. Owen Hughes for serving on the committee and for their valuable suggestions. Finally, I would like to thank “our gang”, especially Susmitha Akula, who made my stay in Blacksburg and in the U.S.A a very pleasant and memorable one.

TABLE OF CONTENTS

LIST OF TABLES

LIST OF FIGURES

Chapter 1 Introduction

1.1 Motivation [1, 2, 3, 4]

The serious consequences of ship collisions necessitate the development of regulations and requirements for the subdivision and structural design of ships so that damage and environmental pollution is reduced, and safety is improved.

The International Maritime Organization (IMO) is responsible for regulating the design of oil tankers and other ships to provide for ship safety and environmental protection. Their ongoing transition to probabilistic performance-based standards requires the ability to predict the environmental performance and safety of specific ship designs. This is a difficult problem requiring the application of fundamental engineering principles and risk analysis [2,3,4].

This thesis addresses one aspect of this problem, the probabilistic definition of a collision scenario with emphasis on the striking ship bow, as required to predict ship damage in collision for a specific ship structural-design.

1.1.1 Revision of IMO Regulations

IMO's first attempt at probabilistic performance-based standards for oil tankers was in response to the U.S Oil Pollution Act of 1990 (OPA 90). In OPA 90, the U.S requires that all oil tankers entering the U.S waters must have double hulls. IMO responded to this unilateral action by requiring double hulls or their equivalent. Equivalency is determined based on probabilistic oil outflow calculations specified in the "Interim Guidelines for the Approval of Alternative Methods of Design and Construction of Oil Tankers Under Regulation 13F(5) of Annex I of MARPOL 73/78" [4], hereunder referred to as the Interim Guidelines.

The Interim Guidelines are an excellent beginning, but they have a number of significant shortcomings:

- They use a single set of damage extent pdfs from limited single hull data applied to all ships, independent of structural design.
- IMO damage pdfs consider only damage significant enough to breach the outer hull. This penalizes structures able to resist rupture.
- Damage extents are treated as independent random variables when they are actually dependent variables, and ideally should be described using a joint pdf.
- Damage pdf's are normalized with respect to ship length, breadth and depth when damage may depend to a large extent on local structural features and scantlings vice global ship dimensions.

1.1.2 SNAME/SSC Collision and Grounding Research Project

Research sponsored by the Society of Naval Architects and Marine Engineers (SNAME) and the Ship Structure Committee (SSC) addresses the shortcomings in the IMO Interim Guidelines. This research uses physics-based models to predict probabilistic damage in collision and grounding for a specific design, vice basing damage prediction on a single set of limited data.

SNAME Ad Hoc Panel #6 was established specifically to consider structural design and response in collision and grounding. Ad Hoc Panel #6 objectives include the consideration of structural design or crashworthiness in predicting probabilistic damage response. This panel was formed under the SNAME T&R Steering Committee on May 14, 1998 with support from SNAME and the SSC. It has four working groups studying: 1) tools for predicting damage in grounding and collision; 2) data; 3) collision and grounding scenarios; and 4) innovative design concepts. Funded research is centered at Virginia Tech and Webb Institute of Naval Architecture. Virginia Tech is specifically tasked with:

- Developing collision and grounding scenarios
- Assessing and developing a simplified collision model sufficient for probabilistic analysis

Figure 1.1 illustrates the process being used at Virginia Tech to predict probabilistic damage as a function of ship structural design.

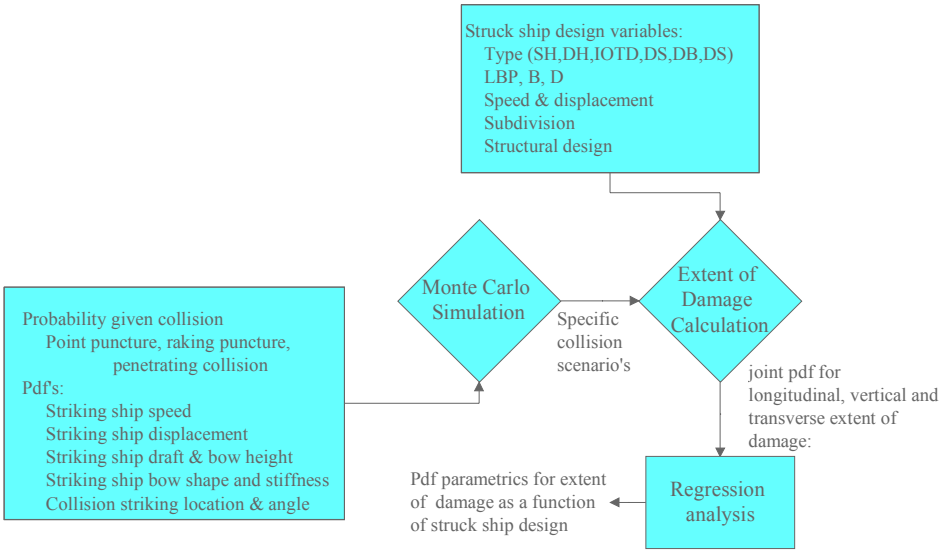

Figure 1.1 - Methodology to Predict Probabilistic Damage in Collision [1, 2]

The process begins with a set of probability density functions (pdfs) defining possible collision scenarios. Based on these pdfs, a specific scenario is selected using a Monte Carlo simulation, and combined with a specific ship structural design to predict collision damage. This process is repeated for thousands of scenarios and a range of structural designs until sufficient data is generated to build a set of parametric equations relating probabilistic damage extent to structural design. These parametric equations can then be used in oil outflow or damage stability calculations.

Critical to this process is a simple, but sufficient probabilistic definition of the collision scenario, including the striking ship bow.

1.1.3 Collision Model for Probabilistic Analysis

The collision problem consists of two sub-problems:

- **External problem** - includes the principal characteristics of the striking and struck ships and their motion before, during and after collision;
- **Internal problem** - includes the internal mechanics and structural response of the struck ship and the striking ship bow during collision.

The responses of the colliding structures are highly transient and non-linear, and involve a continuous change in geometry. An early approach to collision damage

evaluation was made by Minorsky [40, 57], who developed a simple linear relationship between damaged structural volume and absorbed energy in collision, as illustrated in Figure 1.2.

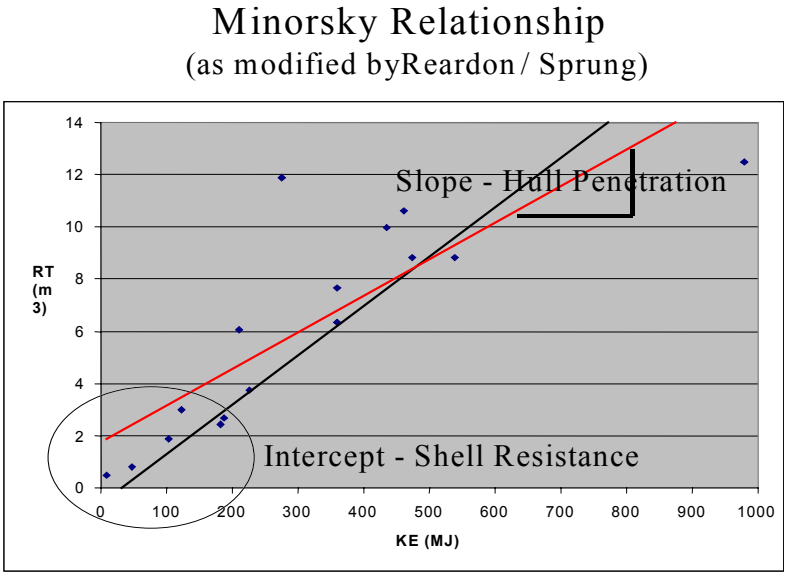

Figure 1.2 - Minorsky Model [40, 57]

SNAME Ad Hoc Panel #6 identified three types of side damage to consider, with emphasis on penetrating collision:

- Low energy puncture at point
- Low energy raking puncture
- Penetrating Collision – right angle and oblique sufficient to penetrate outer hull with significant damage extending in at least 2 directions (penetration, horizontal, vertical).

At Virginia Tech, initial work is focused on the penetrating collision using SIMCOL (Simplified Collision Model) [17], a modified Minorsky collision model for internal damage with three degree-of-freedom external ship dynamics. SIMCOL requires a compatible striking ship definition, and collision scenarios that are simple, but sufficient for accurate results.

Most of the existing theories for ship collisions assume that the bow of the striking ship is infinitely stiff and that all energy-absorbing deformation occurs in the side structure of the struck ship. The baseline collision model, SIMCOL Version 0.1, assumes:

- Absorbed energy during crushing and tearing of internal structured can be estimated using a "Modified Minorsky" method [40, 57].
- 3 degrees of freedom (sway, yaw, surge) are required for both ships.
- The striking ship bow is a rigid, vertically infinite wedge.
- A membrane model can be used to estimate shell resistance (Van Mater, Jones, et. al. - plastic membrane tension and rupture).
- A fully coupled time-step solution is required.

The strengths of SIMCOL are:

- Speed
- Simple input
- The ability to consider oblique collision angles and damage length.

Its limitations are:

- Some structural details are not considered.
- There is only limited data to define appropriate probabilistic scenarios.
- The sufficiency of the striking ship bow model is suspect.

General improvements in SIMCOL are addressed in Chen [17]. This thesis examines the sufficiency of the SIMCOL bow model. Questions examined in this thesis are:

- Is it sufficient to assume that the striking ship bow is rigid?
- Is the energy absorbed by the striking ship bow significant and does it vary in different collision scenarios?
- Is it sufficient to assume that the striking bow is an infinite wedge?

1.2 Hypothesis

The universal assumption of a rigid striking ship bow in ship collision analysis is not valid. Differences in striking ship bow stiffness, draft, bow height and shape have an

important influence on the allocation of absorbed energy between striking and struck ships and the extent of damage in the struck ship. The energy absorbed by the striking ship can be significant and varies in different collision scenarios.

1.3 Plan

The scope of work in this thesis includes the development and validation of a striking ship model that uses Pedersen's super-element approach [45,52] and the explicit non-linear FE code LS-DYNA 3D [22, 23, 24] to simulate the bow collision event. Important striking ship bow attributes, including a simplified striking ship sub-model for use in future collision models are defined. Application of this bow model demonstrates that the universal assumption of a rigid striking ship bow is not valid. Necessary tasks include:

- Identify necessary collision scenario variables [9, 63].
- Propose a framework for defining the relationship of collision scenario variables, and collect preliminary scenario data.
- Describe and compare various bow models in the current literature.
- Support the striking bow hypothesis using results from prior analysis.
- Reproduce and compare closed-form load vs. indentation results by Amdahl [5, 6, 52], Yang and Caldwell [70, 52] and Pedersen [52] for four bow designs: (500 DWT coaster, 23K DWT container ship, 40K DWT container ship and 150K DWT bulk carrier) striking a rigid wall at various speeds.
- Create four coarse mesh "intersection" bow models (500 DWT coaster, 23K DWT container ship, 40K DWT container ship and 150K DWT bulk carrier) in LS-DYNA 3D using intersection and rigid elements. Review potential element models and compare to available elements in LS-DYNA 3D. Run simulations of bows striking a rigid wall at various speeds.
- Create fine mesh, "conventional" bow models (23K DWT container ship and 150K DWT bulk carrier). Run simulations of bows striking a rigid wall at various speeds.

- Compare closed-form, "conventional" and "intersection" results for bows striking a rigid wall at various speeds.
- Create fine mesh "conventional" tanker side models (100K DWT SH tanker and 150K DWT DH tanker) in LS-DYNA. Run simulations of bow models striking these stationary tankers and tankers with sway at various speeds.
- Create coarse mesh "super-element" tanker side models (100K DWT SH tanker and 150K DWT DH tanker) in LS-DYNA using super-elements. Run simulations of bow models striking these stationary tankers and tankers with sway at various speeds.
- Compare "conventional" and "intersection" results for striking a tanker at various speeds, with and without sway and propose a simplified bow model that duplicates results to a reasonable accuracy level.
- Propose a simplified and sufficient bow model.

1.4 Thesis Organization

After a survey of the literature and data available on ship collisions, data available from various sources is compiled, organized and presented in Chapter 2. Chapter 2 also proposes a sufficient set of collision scenario variables and a relationship framework. Chapter 3 describes the theories behind various striking ship models developed by different researchers. Chapter 4 shows that the energy absorbed by the striking ship bow is significant and variable in a number of documented collision cases, and therefore needs more examination.

Some of the salient features of LS-DYNA 3D and modeling techniques using Finite Element Model Builder (FEMB) are discussed in Chapter 5. Chapter 6 describes the finite element models developed using FEMB in more detail. The results from the various simulations and calculations are analyzed and presented in Chapter 7. Chapter 8 discusses conclusions and suggested improvements for future work.

Chapter 2 Collision Scenarios and Data

2.1 Collision Scenario Variables

An important objective of this research is to specify a simplified, but sufficient collision scenario definition for application in probabilistic collision analysis using SIMCOL [17]. Although the primary emphasis of this thesis is to describe the striking ship bow, this chapter discusses other scenario variables, proposes a framework for defining their relationship, and provides preliminary scenario data. Variables considered to describe the collision event include:

- Struck ship random variables - all other characteristics of the struck ship are design parameters and are not random variables
  - Speed
  - Trim
  - Displacement
- Event random variables – these variables are shown in Figure 2.1
  - Collision angle (ϕ)
  - Strike location (l)
- Striking ship random variables
  - Speed
  - Displacement
  - Bow stiffness
  - Bow geometry – wedge or more detailed geometry
    - Half-angle
    - Bow extents: depth and draft at the bow
    - Other principal characteristics

Figure 2.2 illustrates the external collision geometry and Figure 2.3 illustrates various alternatives for vertical alignment between the struck ship and the striking ship

bow. Figure 2.4 shows probability density functions (pdfs) used in the earlier MIT study [3].

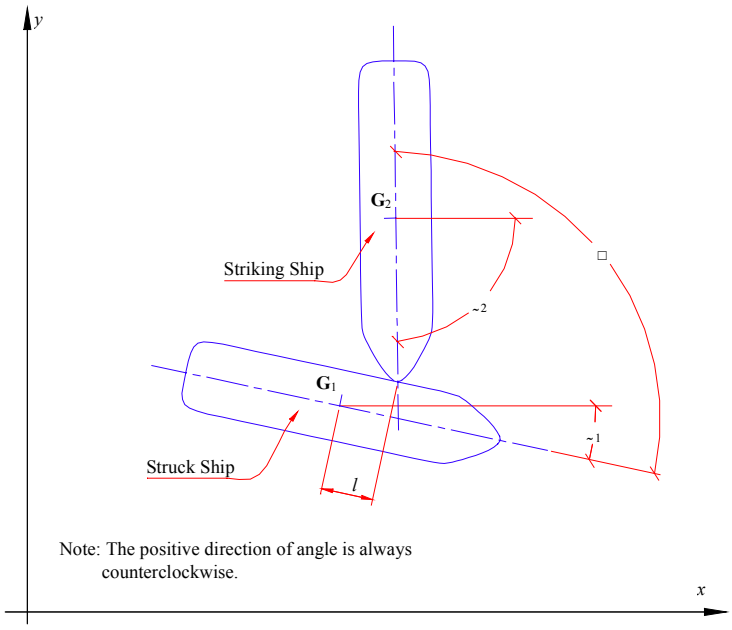

Figure 2.1 - General Collision Scenario [1, 2]

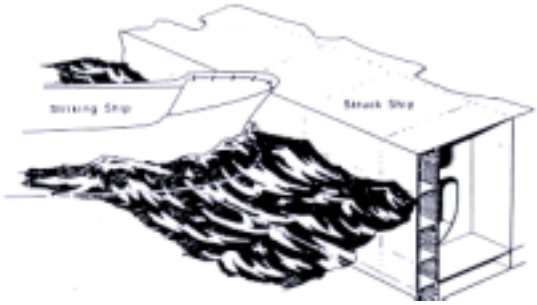

Figure 2.2 - External Collision Geometry [53]

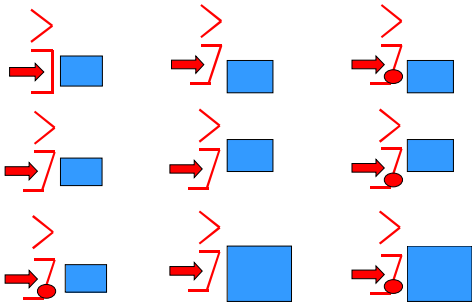

Figure 2.3 - Possible Variations of Striking Bow Geometry

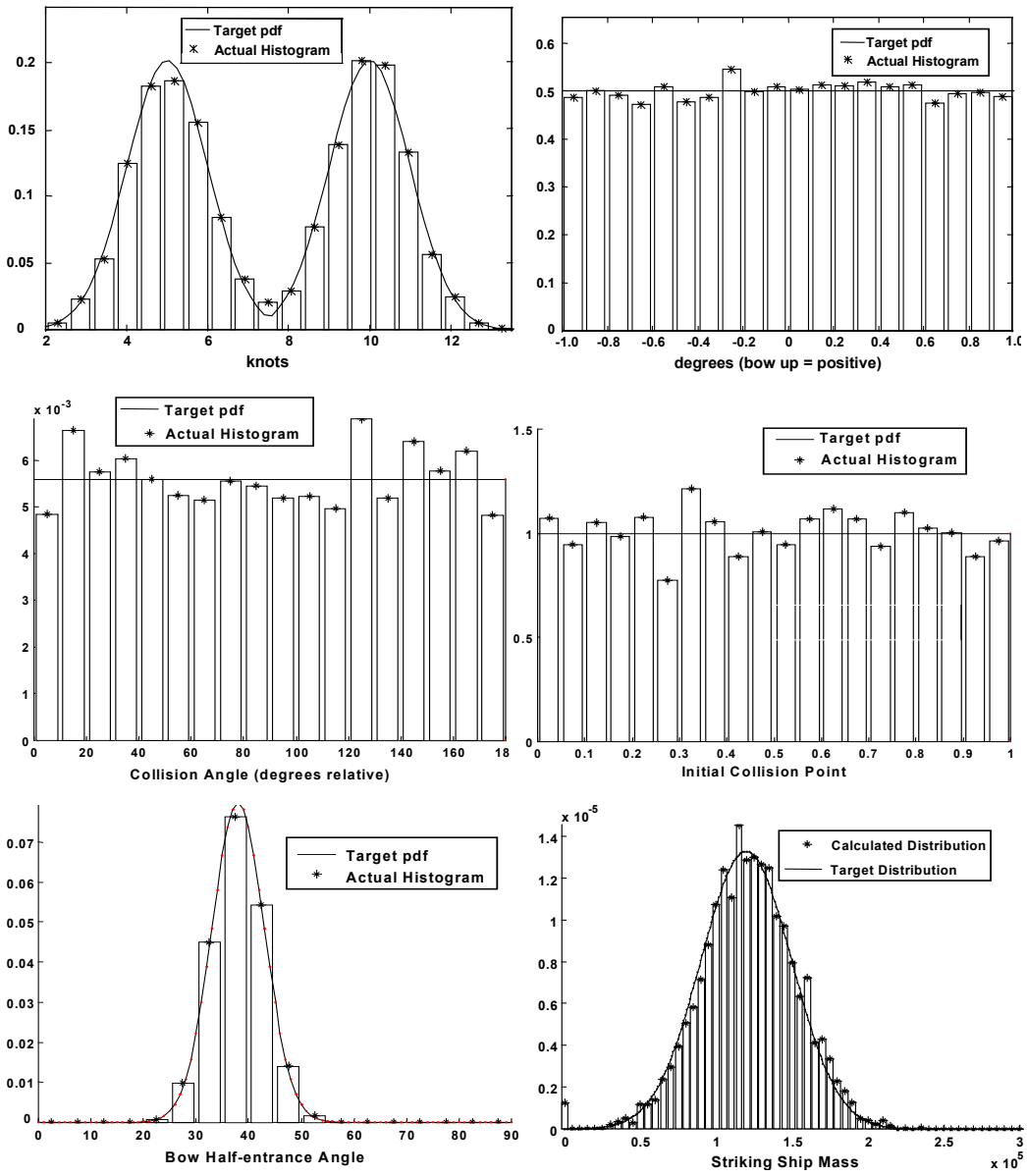

Figure 2.4 - MIT Input Scenario - pdfs for Ship velocity, trim, collision angle, impact point, bow 1/2-entrance angle and striking ship mass

Scenario variables are not expected to be independent, but their interdependence is difficult to quantify because of limited collision data. Figure 2.5 provides a framework for the relationship of scenario variables. Expected dependencies are labeled 1 through 4:

1. Striking ship design variable distributions may be inferred from their distributions in the worldwide population of ships, but it is expected that there is some degree of bias

for striking ships to be similar in size and type to struck ships. Similar ships operate on similar routes. Data required to access the extent of this bias is very limited.

2. A specific struck ship with known design characteristics in a specific trade will also have related distributions for draft, trim and speed. Note: this speed is the speed at the moment of the collision, and not necessarily operating speed.

3. Given a specific type and tonnage of striking ship, its other characteristics will also be related including displacement/mass, bow half entrance angle, bow height, draft, bow stiffness or structural design and speed. Again, this is speed at the moment of collision, not operating speed.

4. When two ships are maneuvering to avoid a collision (in-extremis), the resulting collision angle and strike location are expected to be related.

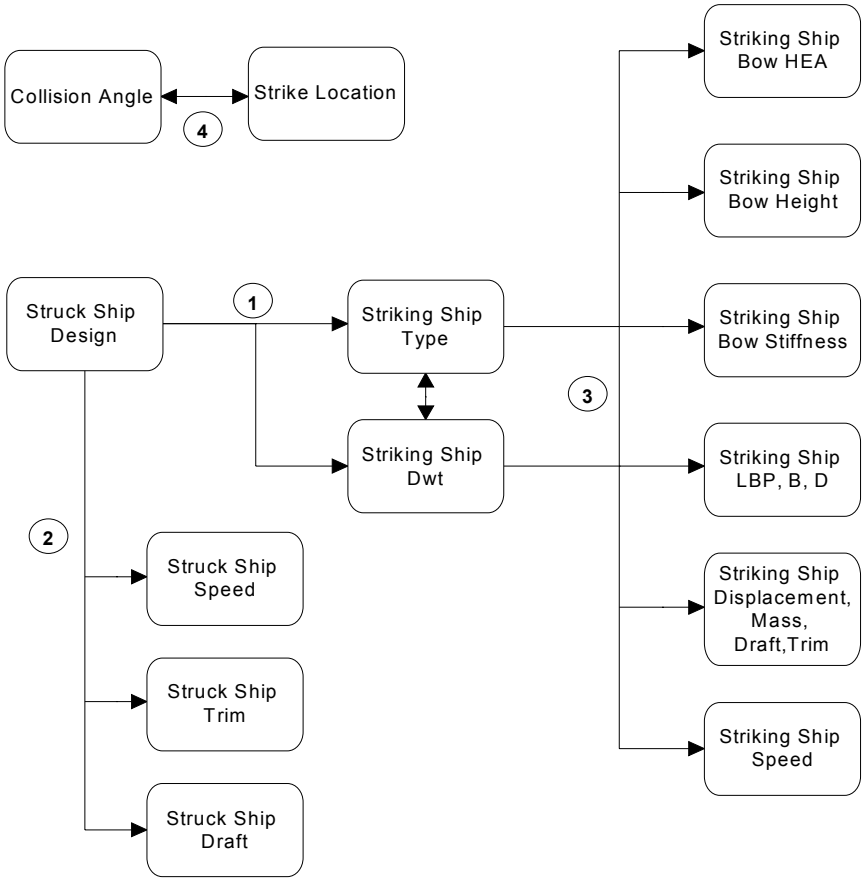

Figure 2.5 - Relationship between Scenario Variables

Event	Ship name and type	Deadweight tons	Displacement tons	L.O.A (ft)	Breadth (ft)	Depth (ft)	Mean Draft (ft)	Impact Angle (degrees)	Damage Length (ft)	Damage Height (ft)	Speed (knots)	Penetration (ft)
Atlantic Ocean, Off Nantucket Island, July 25, 1956	Passenger Liner Stockholm	4,700	16,500	525.2	69.1	38.50	24.6	90	30	29.0	18.0	
	Passenger Liner Andrea Doria	8,145	21,200	697.0	89.9	50.08	18.8		50	29.0	22.0	30
San Fransisco Bay Entrance, January 18, 1971	Tanker Arizona Standard	17,350	22,578	504.0	68.2	39.20	31.0	45	17	39.2	11.4	
	Tanker Oregon Standard	17,265	22,575	504.0	68.2	39.20	31.0		72	39.2	4.00	12
Punta Indio Channel, River Plate May 11, 1972	Passenger Royston Grange	10,385	14,660	489.0	65.7	35.3	22.5	40	110	30.0	13.0	
	Tanker Tien Chee	18,750	25,975	579.6	70.0	39.8	29.6		100	30.0	11.0	10
Off S. African Coast Between Alphard Banks and Yzervarkpunt August 21, 1972	Tanker Oswedo Guardian	95,608	109,870	899.6	128	62	43.7	50	25.0	43.0	16.0	
	Tanker Texanita	100,613	62,075	872.2	128	61.3	25.0		80.0	43.0	15.0	25
New York Harbour June 2, 1973	Containership C.V Sea Witch	16,343	26,670	610.0	78.2	54.5	27.3	60	21.0	36.0	15.5	
	Tanker Esso Brussels	43,121	52,500	699.5	97.3	49.3	38.0		40.0	36.0	0.0	25
Gulf of Mexico January 7, 1978	Tanker Stolt Viking	21,150	28,500	565.0	72.2	42.2	33.2	45	NIL	NIL	12.0	
	Crewboat Candy Bar	N/A	72	95.0	21.0	8.9	3.8		Cut in half	8.9	14.0	21
Chesapeake Bay, Mouth of the Potomac River, Maryland October 20, 1978	General Cargo Santa Cruz II	20,373	25,855	520.0	74.0	44.0	32.5	5	Indent	Indent	13.5	
	USCG Cutter Cuyahoga	N/A	460	125.0	24.0	18.0	10.0		15.0	10.0	11.3	10
Atlantic Ocean, Sea of Cape Cod, June 18, 1979	Tanker Exxon Chester	29,210	36,630	627.9	82.7	42.5	33.6	60	31.0	40.0	10.0	
	Bulk Carrier Regal Sword	27,464	34,714	576.9	75.0	48.6	36.0		150.0	25.0	12.0	20
Tampa Bay, January 28, 1980	Tanker Capricorn	24,796	29,950	604.9	75.2	41.8	31.5	18	Hawse pipe	Haws pipe	12.0	
	USCG Buoy tender Blackthorn	N/A	1,025	180.0	37.0	17.3	12.8		80.0	10.0	7.5	4
Lower Missisippi River, Near Venice, Louisiana November 24, 1980	Chemical Tanker Coastal Transport	14,428	20,160	490.0	64.0	38.0	30.0	90	Bow to frm 110	22.0	17.3	
	Offshore Supply Sallee P	N/A	395	115.0	26.0	8.0	7.0		34.0	8.0	14.0	20
Missisippi River December 27, 1980	Tanker Pisces	24,438	31,070	604.9	75.3	41.8	33.3	90	45.0	50.0	11.5	
	Bulk Carrier Trade Master	33,448	41,768	628.3	86.9	50.2	37.0		55.0	50.0	11.1	18
Atlantic Ocean May 6, 1981	Barge Carrier Lash Atlantico	29,820	44,606	819.8	100.2	60.0	32.1	120	70.0	30.0	18.0	
	General Cargo Hellenic Carrier	15,153	18,725	470.0	67.1	38.5	20.8		70.0	32.0	14.0	30
Gulf of Mexico, February 19, 1982	Barge Carrier Delta Norte	41,223	57,800	893.1	100.2	60.0	34.0	45	42.0	40.0	19.0	
	General Cargo African Pioneer	12,391	18,600	495.0	71.4	39.7	18.3		80.0	33.0	15.0	30

Rhode Island Sound July 2, 1983	Passenger / General Cargo Yankee	N/A	450	136.5	29.0	9.5	7.5	70	10.0	15.0	11.5	
	General Cargo Harbel Tapper	N/A	17,525	435.0	72.0	35.0	26.5		Indent only	Indent only	5.0	0
Galveston Bay Entrance November 10, 1988	Auto Carrier Figaro	27,764	35,894	649.6	105.9	102.4	29.8	30	72.0	70.0	10.0	
	Tanker Camargue	133,360	158,210	918.9	135.0	72.0	36.4		75.0	45.0	10.0	12
Lower Missisippi, March 24, 1993	Bulk Carrier Atticos	29,165	17,176	593.1	75.9	47.6	15.1	120	Bulb	16.0	10.5	
	Offshore Supply Galveston	N/A	630	180.0	40.0	14.3	8.2		15.0	14.3	13.5	12
Port Pusan May 2, 1994	Containership Hanjin Hongkong	20,000	27,780	796.6	105.6	62.3	17.1	90	55.0	62.3	10.0	
	Containership President Washington	49,310	56,534	860.2	105.8	66.0	38.1		105.6	40.0	6.0	55
Bay of Tokyo, Japan November 9, 1974	General Cargo Pacific Ares	N/A	21,620	505.5	72.8	39.7	28.8	90	40.0	35.0	5.5	
	Tanker Yuyo Maru No. 10	52,836	73,790	740.3	117.4	68.1	39.1		78.7	35.0	10.0	15
Mississippi River, Pilottown, Louisiana October 3, 1978	Tanker Texaco Iowa	41,282	53,850	699.5	97.0	49.0	38.6	15	30.0	1.0	8.0	
	Tanker Burmah Spar	74,350	81,135	785.0	121.0	54.0	40.0		Indent only	Indent only	6.0	0
Lower Mississippi River, Near New Orleans, Louisiana November 9, 1978	Bulk Carrier Maritime Justice	34,196	41,089	608.0	85.0	51.0	31.3	0	30.0	20.0	7.2	
	Bulk Carrier Irene S. Lemos	43,285	44,910	657.0	95.0	53.0	34.5		33.0	20.0	8.0	25
Neches River, Near Beaumont, Texas February 25, 1979	Tanker Mobil Vigilant	53,490	56,950	735.0	104.0	51.0	36.3	42	45.0	20.0	4.0	
	Tanker Marine Duval	24,734	34,224	612.0	80.0	42.0	33.4		160.0	20.0	6.6	18
Lower Mississippi River, Near Bonnet Carre Point, Louisiana January 27, 1980	Bulk Carrier Frotaleste	24,622	30,753	582.2	75.7	45.9	33.1	135	150.0	40.0	7.4	
	General Cargo Cunene	16,311	18,050	522.7	69.5	44.1	25.0		22.0	40.0	0.0	12
Under Greater New Orleans Bridge at New Orleans, Louisiana, March 29, 1980	Sternwheel passenger Natchez	N/A	1,550	237.5	40.0	7.8	6.0	55	20.0	8.0	6.0	
	Tanker Exxon Baltimore	50,311	62,852	743.0	102.0	50.0	38.5		34.0	2.5	15.8	2.0
Missisippi River, Gulf Outlet Near Shell Beach, Louisiana July 22, 1980	Bulk Carrier Sea Daniel	N/A	28,300	551.2	75.0	46.4	32.0	45	35.0	30.0	6.0	
	Containership Test Bank	N/A	18,060	467.5	68.9	35.5	28.0		45.0	30.0	4.0	10
Seattle Harbor, Washington D.C Jan 13, 1981	Ferry Klahowya	N/A	1,334	310.0	73.0	17.0	N/A	40	30.0	17.0	10.0	
	General Cargo / Vehicle freighter Sankograin	20,138	13,570	514.0	75.0	44.3	19.2		Indent only	Indent only	2.0	0
Upper New York Bay May 6, 1981	General Cargo Hoegh Orchid	18,207	26,450	599.8	67.7	41.3	30.8	90	6.5	6.0	4.0	
	Ferry American Legion	N/A	5,025	294.0	69.0	20.6	14.3		9.0	50.0	2.0	15
Upper New York Bay – Feb 18, 1988	Tanker Maersk Neptune	68,800	85,100	811.0	105.5	57.1	43.2	45	Bow indent	Bow indent	1.5	
	Bulk Carrier Mont Fort	26,748	34,868	600.6	73.7	46.6	34.5		16.0	34.0	0.0	10

Table 2.1 - Ship Collision Scenario data from Sandia Report [63]

The relationships shown in Figure 2.5 require data to quantify, and this data is very limited and/or difficult to obtain.

Table 2.1 presents data available on various collisions that took place between 1979 and 1993 [63]. The information presented is derived from various sources, including the Sandia report [63]. This data may be used together with worldwide ship data to quantify the relationships shown in Figure 2.5. This will be accomplished in future work.

2.2 Rigid Bow Geometry

This section compares the geometry of the striking ships used in DAMAGE, the DTU model, ALPS/SCOL and SIMCOL.

Both DAMAGE and the DTU model calculate the absorbed energy for direct contact deformation of struck ship super-elements by the striking ship bow. This is not a finite element method. Deformation away from the actual striking ship penetration is not considered. Both methods are based on the same deformation and energy evaluation procedure and folding mechanisms developed by Wierzbicki [68]. By summing the deformation energy absorbed by various sections and intersections, i.e. angles, T-sections and cruciforms (Figure 2.6) during the folding process, and the membrane tension energy absorbed in the shell plate, the total crushing force is obtained. These sections and intersections are called Super-Elements. Figure 2.7 shows the idealized bow geometry used in the DAMAGE and DTU models. The striking bow is assumed to be rigid.

ALPS/SCOL is based on the Idealized Structural Unit Method (ISUM). ISUM is a non-linear finite element method developed by Paik [44,45]. A coarse mesh is used to model a segment of the struck ship with elements the size of whole panels supported by web frames and stringers. These are super-elements, but solved in a finite element solution vice by direct contact. ISUM considers the coupling between local and global deformation and failure modes inside model. It uses a course mesh rigid model of the actual bow geometry.

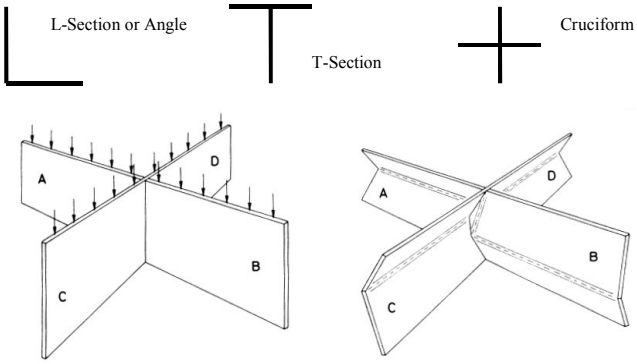

Figure 2.6 - Crushing mechanism of basic structural elements

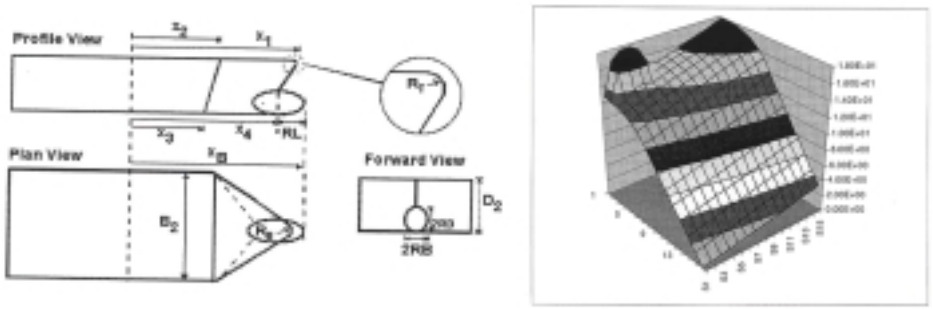

Figure 2.7 - Idealization of a bulbous bow in DAMAGE [62]

SIMCOL uses a very simple wedge-shaped bow geometry. SIMCOL Versions 0.0 to 2.0 assume that the striking bow is rigid and has a wedge shape defined by a half entrance angle with infinite vertical extents. SIMCOL Version 2.1 considers the upper and lower extents of the bow relative to the struck ship.

The SIMCOL wedge with infinite vertical extents was initially preferred because of its simplicity, however subsequent testing and comparison to the other models demonstrated that this simple geometry is not sufficient. Table 2.2 shows the collision scenarios for Test Matrices 1 and 2 used to evaluate this geometry. DAMAGE, DTU, SIMCOL and ALPS/SCOL models were tested using these matrices.

Figure 2.6 shows the results from Matrix 1 for penetration, as a function of speed. SIMCOL 2.0 with the infinite wedge assumption predicts low penetrations for all speeds because it overestimates the damage volume. SIMCOL 2.1 with limited vertical extents predicts penetrations that correlate well with DAMAGE, DTU and ALPS/SCOL. This

trend is consistent in Matrix 2 and in other SIMCOL results. SIMCOL 2.1 is the preferred model. The use of a wedge greatly simplifies the damage geometry and provides good results when compared to more complex models.

	MATRIX 1		MATRIX 2	
	STRUCK SHIP	**STRIKING SHIP**	**STRUCK SHIP**	**STRIKING SHIP**
DWT	150,000	150,000	150,000	150,000
Type	DH Tanker	Bulk Carrier	DH Tanker	Bulk Carrier
Speed (knt)	$V_A = 0$	$V_B = 3, 4, 5, 6, 7$	$V_A = 0$	$V_B = 3,4,5,6,7$
Draft (m)	T = 16.8	T=15.96	T = 16.8	T=15.96
Displacement (MT)	Δ = 178,867	Δ = 174,850	Δ = 178,867	Δ = 174,850
Impact Location fwd of midship (m)	62.5, 29.5 aft and 3.5, 36.5, 69.5 102.5 fwd		1.85, 2.68, 3.5, 4.32, 5.15	

Table 2.2 – Collision Model Scenario Test Matrices

Models:

SIMCOL 2.0 - Infinite wedge; 1/2 angle = 49 deg; (Virginia Tech)

SIMCOL 2.1 - Wedge with limited bow height and draft; 1/2 angle = 49 deg

DAMAGE - MIT model

DTU - Technical University of Denmark model

ALPS/SCOL - Paik model

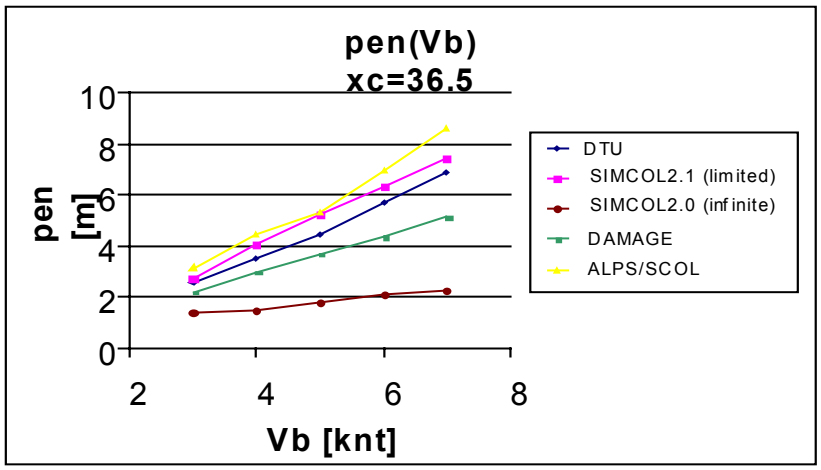

Figure 2.8 - Penetration vs speed for Matrix 1 [17]

The choice of the half-entrance angle to be used in a simplified wedge-shaped bow is critical to the estimation of damage results. The MIT study [3] proposed the pdf shown in Figure 2.9 for tanker bows. Sandia data, Table 2.3, provides mean bow half-angles for ships of different size and type [63]. These results are based on very limited data, and no distributions were provided with the mean values.

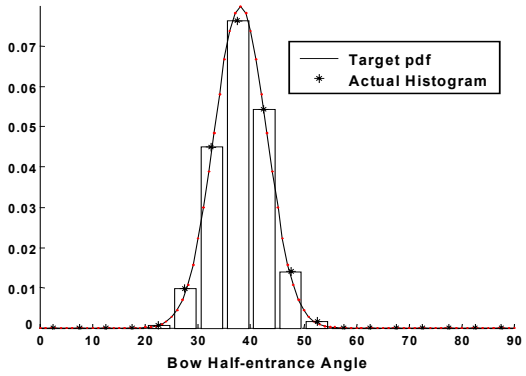

Figure 2.9 - Scenario–Bow Half-Entrance Angle

Displacement	Tanker/ Bulker	General Cargo	Container Ship	Passenger Liner
0 - 10,160	28	29	17	17
10,160 – 20,320	30	20	17	17
10,320 – 30,480	30	20	17	17
30,480 – 40,640	38	20	17	17
40,640 – 50,800	38	20	17	17
50,800 – 60,960	38	20	17	17
60,960 – 71,120	38	20	17	17
71,120 – 81,280	38	20	17	-
81,280 – above	38	20	17	-

Table 2.3 – Representative bow half angles for ships of different type and size

2.3 SIMCOL Bow Model

Based on this preliminary assessment of scenario and striking bow definitions, the following process is recommended.

- Assume that a wedge with limited vertical extent is sufficient for the simplified collision model.

- Continue to collect and analyze statistical collision data for collision angle and strike location. Propose pdf(s) for these variables. Use the MIT pdfs in Figure 2.4 as the baseline definition.
- Define striking ship characteristics using the relationships proposed in Figure 2.5. Use worldwide ship data to define the baseline distributions, and modify these when actual collision data or ship encounter data is available and sufficient.
- Analyze the structural design and stiffness of the striking ship bow and propose a simplified relationship between bow penetration and force for application in SIMCOL.

The remainder of this thesis will focus on bow models, with emphasis on bow stiffness.

Chapter 3 Bow Damage Models

3.1 INTRODUCTION

This chapter describes bow models developed by various researchers. A brief overview of each model is presented. There are two main types of bow models: rigid and deformable. Although Minorsky [40] considers bow deformation, extensions of his theory typically use a rigid bow. Because of this, Minorsky's model is presented separately in Section 3.2. Rigid bow models are described in Section 3.3 and Section 3.4 describes deformable bow models. A summary table is provided in Section 3.5.

3.2 Minorsky [40]

Minorsky's work is among the earliest in the field of ship collisions. Minorsky examined fifty major collision cases that occurred before 1959. He developed an empirical "Resistance Factor" for predicting energy absorption based on the volume of damaged steel components in the striking and struck ships, and correlated it with the absorbed kinetic energy causing major damage.

Since an attempt to produce an analytical solution would of necessity rest on many doubtful assumptions, Minorsky preferred to follow a semi-empirical approach based on the data from 50 actual collisions, which were supplied by the U.S Coast Guard. The data included speeds, angles of encounter, displacements, drafts and extents and location of damage. Of these collisions, those with very oblique collision angles were eliminated.

The twenty-six cases remaining were analyzed for absorbed kinetic energy and extent of damage. As only right-angle penetration is calculated, only velocity components normal to the struck ship's centerline are considered. The effect of the added mass of water *dm* and the ratio ($R = M_B/M_A$) of the mass of the striking ship (M_B) to that

of the struck ship (M_A) is considered. A coefficient of energy absorption, K is defined as a function of M_A, M_B and *dm*.

$$K = \frac{M_A + dm}{M_B + M_A + dm} \tag{3.1}$$

Where:

K is the percentage of the initial kinetic energy in the direction normal to the struck ship's centerline that is absorbed in the collision.

When R $\rightarrow$ 0, i.e, when the striking ship is very small compared to the struck ship, K $\rightarrow$ 1and most of the initial kinetic energy normal to the struck ship's centerline is absorbed in the collision. When R $\rightarrow \infty$, the case where a very large vessel strikes a small shallow draft vessel, K $\rightarrow$ 0, and the small vessel is pushed away without absorbing significant kinetic energy.

Based on the assumption of a wholly inelastic impact, the absorbed kinetic energy is expressed as a function of the displacements of the colliding vessels, velocity of the striking ship (V_B) and angle of impact (θ) [40]:

$$\frac{\Delta_A \Delta_B}{1.43\Delta_B + 2\Delta_B} (V_B Sin\theta)^2 \tag{3.2}$$

Where:

Δ_A is the displacement of the struck ship;

Δ_B is the displacement of the striking ship

Those members having little depth in the direction of penetration, such as the shell of the struck ship, do not contribute to the resistance factor. Members having depth in the direction of penetration, such as decks, transverses, flats and inner and outer bottoms of both vessels and the shell of the striking ship, are considered. A resistance factor, R_T is calculated based on damage to the following structural members:

- Decks, flats and double bottoms in both struck and striking vessels
- Transverse bulkheads in struck vessel
- Longitudinal bulkheads in striking vessel

- The component in the direction of collision of the shell of the striking vessel (assumed at 0.7 of shell area)

The resistance factor is given by the equation:

$$R_T = \quad P_N L_N t_N + \quad P_n L_n t_n \tag{3.3}$$

Where:

P_N is the depth of damage in the Nth member of the striking vessel;

L_N is the length of damage in the Nth member of the striking vessel;

t_N is the thickness of the Nth member of the striking vessel;

P_n is the depth of damage in the nth member of the struck vessel;

L_n is the length of damage in the nth member of the struck vessel;

t_n is the thickness of the nth member of the struck vessel

Figure 3.1 shows a typical calculation for resistance factor and absorbed energy. For each collision that Minorsky studied, a similar figure is made, showing the transverse section of the struck ship at the point of collision and a profile of the striking ship, both at the correct drafts and showing the reported maximum penetration.

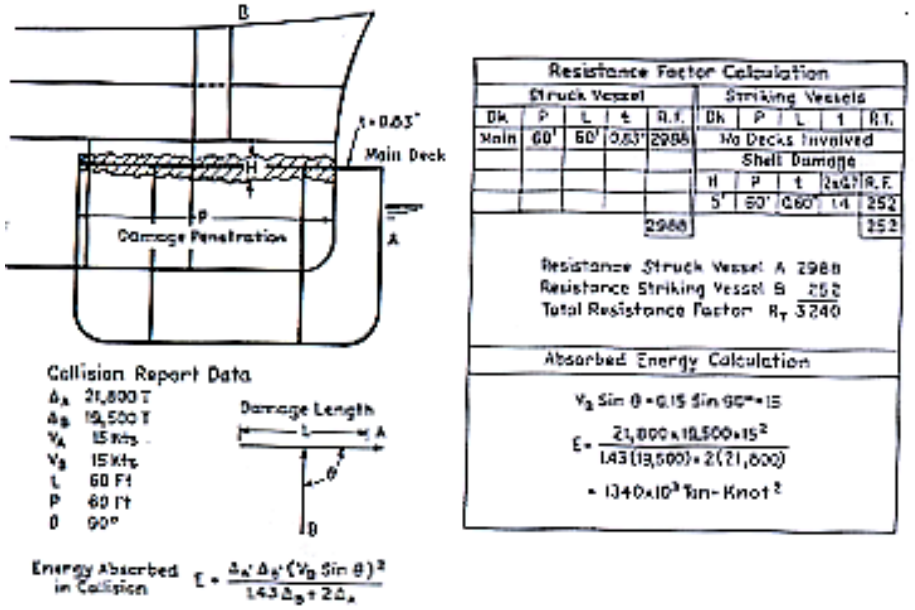

Figure 3.1 - Resistance factor calculations [40]

Figure 3.2 shows a correlation between resistance factor and the lost kinetic energy. At low speeds there is considerable scattering of points. The area of low-energy points is indicated in Figure 3.2, by cross-hatching.

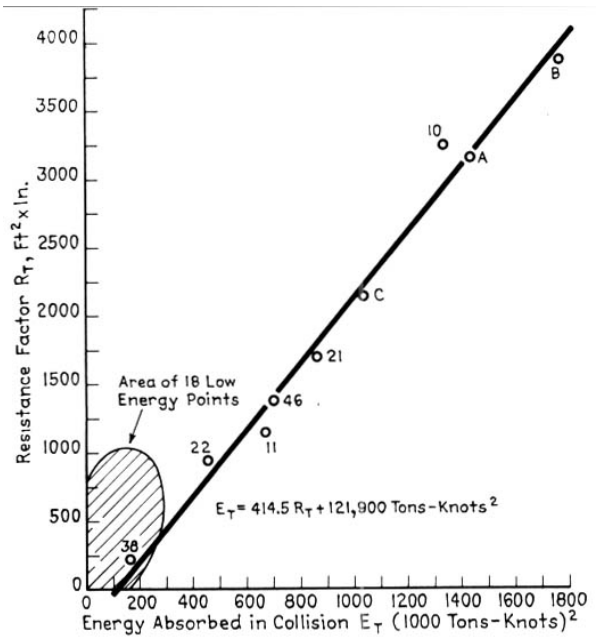

Figure 3. 2 – Empirical correlation between resistance to penetration and energy absorbed in collision [40]

Consideration of the striking ship in the resistance calculations indicates that the striking ship may also absorb a significant portion of the collision energy. This is discussed in Section 4.6.

3.3 Rigid Bow Models

3.3.1 Hutchison [25]

Hutchison uses a generalized Minorsky [40] method applied to barge collisions. Minorsky's original model, as described in section 3.1, is further developed to include hull membrane structural resistance, up to the point of hull rupture. A time-domain simulation computer program is used to run a total of 12,500 barge collision scenarios randomly chosen based on statistics from the U.S Coast Guard commercial accident

database. Distributions are estimated for: 1) collision energy absorbed; 2) penetration; 3) peak acceleration, and whether or not the hull membrane is ruptured.

The bow model used in this time-domain simulation is a sharp, rigid wedge-shaped bow with a half-entrance angle of α and infinite vertical extent. The wedge shaped bow penetration process is of considerable interest since it is characteristic of high-speed ships. According to Hutchison, these assumptions are conservative, and not unreasonable, particularly when the collision is between a large ship and a barge. However, when the striking bow encounters an object as substantial as a RAM (Radio-Active Material) cask, significant bow damage is expected. The assumption of a rigid bow is justified by its relative ease of calculation and its prediction of conservative damage extents in the struck ship. Since it is difficult to characterize the diverse population of striking bows in terms of shape, vertical extent and stiffness and relative vertical position, the infinite rigid bow assumption is retained. A similar model is used in the early versions of SIMCOL [17]. Figure 3.3 shows the bow model used by Hutchison.

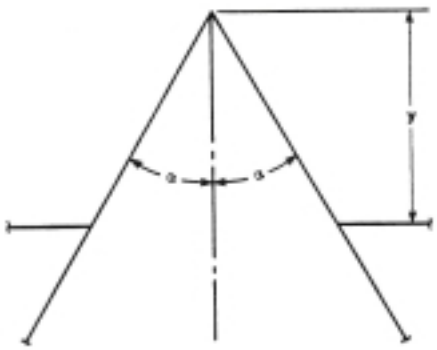

Figure 3.3 - Rigid wedge-like bow model used by Hutchison [25]

The geometry of the damage area created by the triangular shape is readily defined. The assumption of a rigid bow leads to conservative results for struck ship damage because in an actual collision a significant portion of the total collision energy may be absorbed by the striking ship bow.

With a change of units, the energy absorbed, E_A is expressed as a function of the damaged volume of the structure, V (ft^3):

$$E_A = 150{,}000\ V \text{ (lbf-ft)} \quad \textbf{(3.4)}$$

The penetrated structure is assumed to have a composite thickness of t. The energy absorbed in deforming the structure is dE = dW = Fdu = 150,000 V = 150,000 t dw du. So the damaged material volume up to any penetration distance, y, is:

$$E(y) = 150{,}000ty^2 \tan(\alpha) \tag{3.5}$$

and the force acting in the negative y-direction to oppose the penetration is:

$$F(y) = 2[150{,}000ty \tan(\alpha)] \tag{3.6}$$

If the force on the wedge is regarded as a normal force (i.e, no force acting tangent to the wedge surfaces), as shown in Figure 3.4, then the forces acting normal to each wedge face, f_1 and f_2 are:

$$f_1 = f_2 = F(y) / 2 \text{ Sin } \alpha \tag{3.7}$$

Figure 3.4 shows the forces that act on the advancing rigid wedge-like bow. The time domain simulation is an Euler integration of the dynamic equations of motion in the horizontal plane for the two vessels subject to Minorsky structural interaction mechanism. The simulation incorporates added mass, and friction.

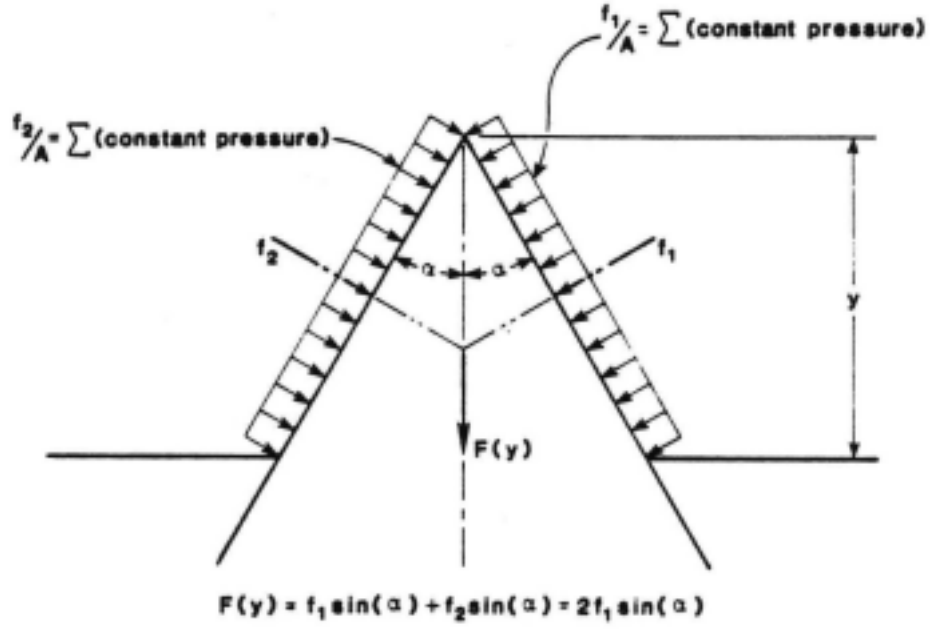

Figure 3.4 - Constant pressure forces acting on advancing bow [25]

3.3.2 Ito [27]

Ito investigates the effects of various design parameters on the strength of double-hulled structures in collision. The collisions are classified into five types, two of which are examined, one where a stem collides against the ship's side and the other where a bulbous bow collides against it. Static destruction tests are carried out using a series of double hull models, which cover a wide strength-distribution range. Two different bow models, one using the stem of the bow and the other using the bulb are created and tested. Model tests are performed and used to validate calculated results. The stem and the bulb used in the calculations are assumed rigid.

Figure 3.5 shows a classification of various collision scenarios based on the relative vertical position of the strike. Types a, b and c are generally the most critical of all cases from what is observed from actual collisions. Only types b and c are analyzed in this study so that a comparison of the results for a stem test (type c) against those of a bulb test (type b) can be made independently.

Figure 3.6 shows the two types of indenters tested in this study. Figure 3.6 (a) shows the stem used in the stem test and Figure 3.6 (b) shows the bulb in the bulb test.

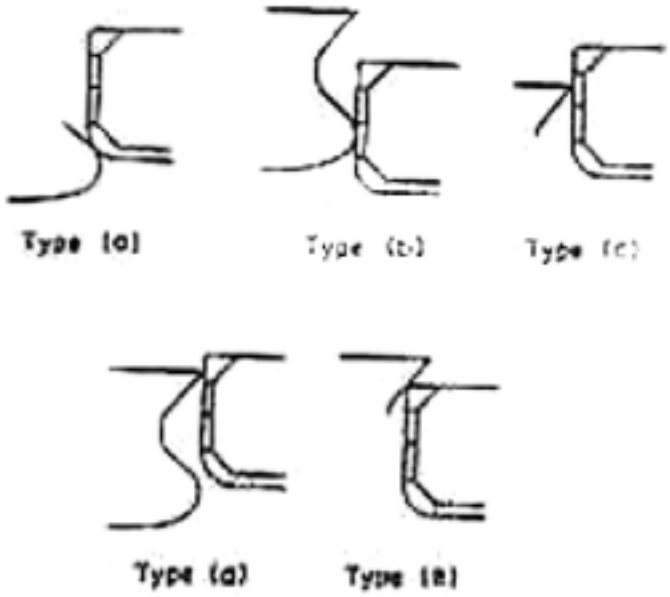

Figure 3.5 - Different contacts analyzed, based on type [27]

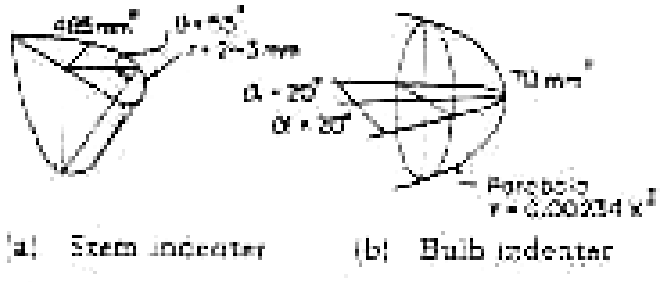

Figure 3.6 - Rigid bow model used by Ito [27]

Figure 3.7 shows the double hull ship used in the experiments. As can be seen from the figure, the ship model is very coarse, without much detail. The collision point is midway between two transverse bulkheads along the centerline of the two side stringers. The bow models are gradually pushed into the double-hulled structure using a hydraulic jack. Measurements of load, penetration, deformation and strain are made.

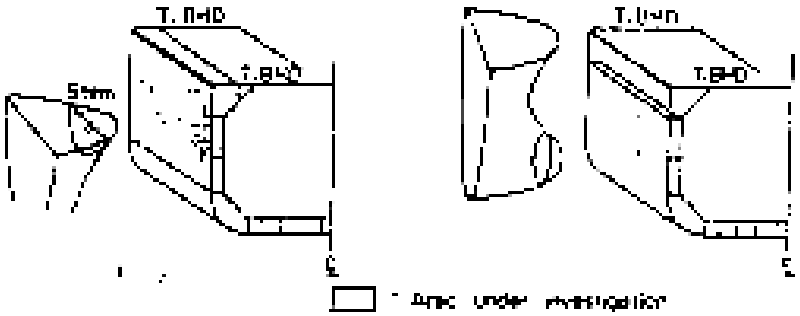

Figure 3.7 - The two types of experiments performed by Ito [27]

The assumptions made in the analysis are as follows:

- The striking bow is rigid
- Collisions are right-angled
- The double-hulled structure is damaged only in the vicinity of the point of contact. It does not collapse in its entirety.
- When the bow strikes the side shell of the double-hulled structure, the side shell behaves as a plastic membrane. Transverse webs and stringers are buckling members.
- The damage penetration does not extend beyond the inner hull

3.3.3 Wierzbicki [68]

Wierzbicki provides a benchmark study on several closed-form solutions for the mean crushing strengths and the cutting resistance of plated structures during collision, by comparing theoretical solutions with experimental data. Based on expressions derived for unstiffened structures, an extension of the methods is proposed for longitudinally and/or transversely stiffened structures.

The process of ship collision is dynamic in nature and the applicability of the formulations derived under quasi-static loading conditions to analyze the crushing and cutting damage of the structure in the dynamic situations is also discussed.

Several empirical relations are derived for the mean crushing strengths of various intersection elements. The general expressions, which can be employed for both stiffened and unstiffened intersections in both bow and side structure may be written as:

For T-sections,

$$\frac{\sigma_m}{\sigma_y} = \frac{1.1608}{\eta}\left(\frac{t_{eq}}{b}\right)^{2/3} \tag{3.8}$$

For X-sections,

$$\frac{\sigma_m}{\sigma_y} = \frac{0.7606}{\eta}\left[0.87\left(\frac{t_{eq}}{b}\right) + 0.63\left(\frac{t_{eq}}{b}\right)^{3/4}\right]^{2/3} \tag{3.9}$$

For L-sections,

$$\frac{\sigma_m}{\sigma_y} = \frac{2.3910}{\eta}\left(\frac{t_{eq}}{b}\right)^{2/3} \tag{3.10}$$

Where:

σ_m is the static mean crushing strength (stress)

σ_y is the static yield strength (stress) of the material

η is the normalized effective crushing length of unit without transverse stiffeners

t_{eq} is the equivalent plate thickness

b is the plate width

Paik and Pedersen derived the following formula based on the Wierzbicki models:

$$\frac{\sigma_m}{\sigma_y} = \frac{1}{\eta}[1.4245\left(\frac{t_{eq}}{b}\right)^{0.5} + 0.2673\left(\frac{t_{eq}}{b}\right)] \quad \textbf{(3.11)}$$

Several closed-form solutions for the mean crushing strengths of plated structures during collision are derived [68], by comparing theoretical solutions with experimental data. Figure 3.8 shows the wedge-like rigid bow model used by Wierzbicki [68] in his experiments. Although Wierzbicki uses a rigid wedge for the bow to develop equations for the stiffened plate, his intersection elements are used to establish relations for predicting crushing forces on deformable bows. Wierzbicki's work provides the basis for deformable bows used by other researchers. His experiments and DAMAGE [62] use a rigid bow.

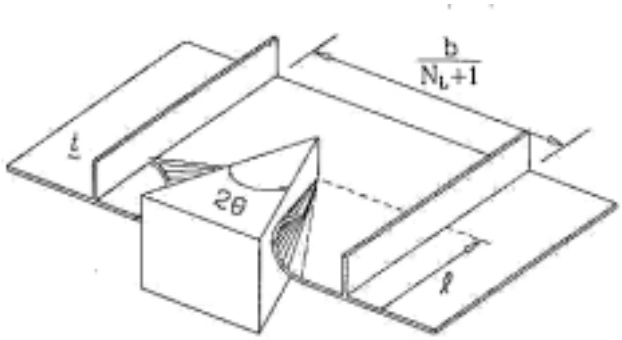

Figure 3.8 – Wedge-like Bow model used by Wierzbicki [68]

3.3.4 MIT "DAMAGE" – Simonsen [62]

Various researchers have developed closed-form solutions for crushing strength. Wierzbicki, as described in Section 3.3.3, developed several fundamental solutions that are used to estimate the energy absorption in axial crushing of plate intersections like X-forms, T-forms etc. These special solutions – often termed "super-element" solutions, are known to predict the energy absorption quite accurately but at the same time, they only apply to specific load cases.

This means, for example, that the solution for axial crushing of a T-section is accurate if the section is crushed axially, but if the loading is slightly different, the solution may not work. Therefore, it is essential to be able to re-mesh or re-discretize the structure as the solution proceeds. The methodology used by Simonsen is based on such

a successive adaptive-discretization of the side structure into super-elements, as the solution proceeds. This methodology applies to deformable side structure, but still uses a rigid bow. Figure 3.9 shows how a bulbous bow is idealized in this model.

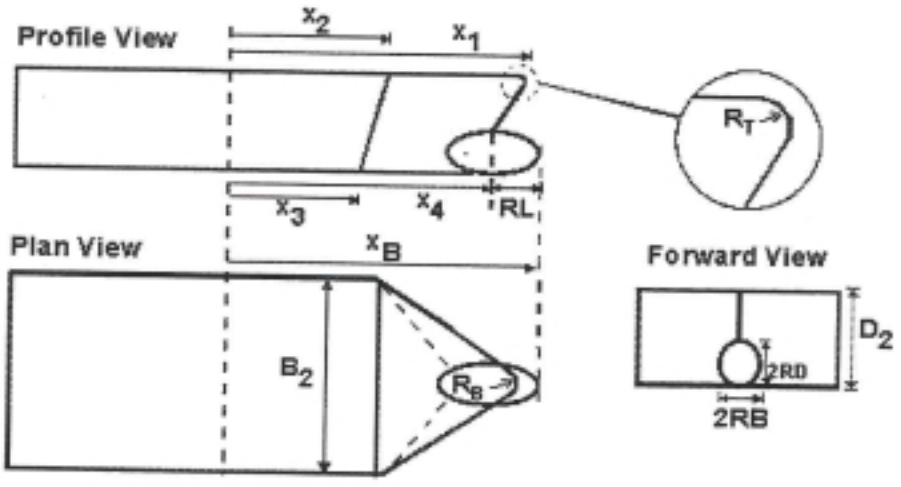

Figure 3.9 - Idealization of a bulbous bow in DAMAGE [62]

Figure 3.10 shows an Excel surface plot of the bow model used by DAMAGE. The salient features and assumptions of this model are:

- The striking ship has a user-defined forward speed
- Struck ship has no forward speed
- Right-angled collision
- Point of impact is not at the extremities of the ship.
- Depending on the height of the struck ship, on the geometry of the striking ship bow, and on the relative ship drafts, various configurations are captured.
- Bow modeled using idealized geometric shapes – rigid.

The configuration at the time of impact is illustrated in Figure 3.11.

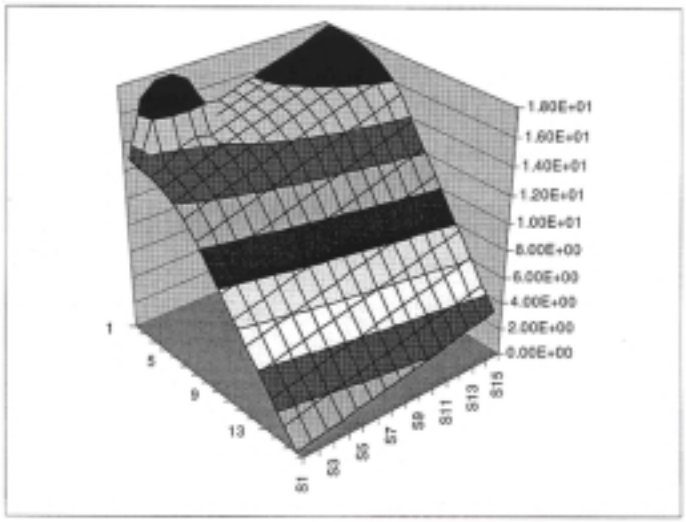

Figure 3.10 - Excel surface plot of bow model [62]

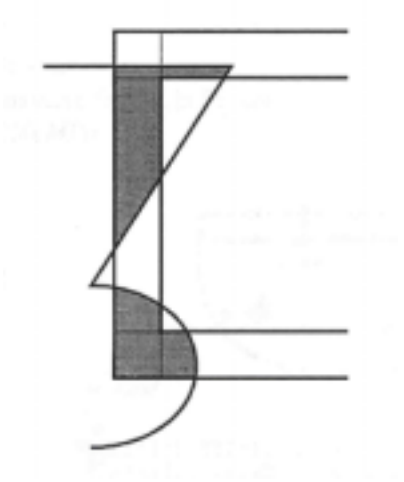

Figure 3.11 - DAMAGE Impact scenario [62]

Six validation examples are presented in this study, four of which are with small-scale specimens with a plate thickness of 1-2 mm. The tests are performed by forcing cylinders of various radii into longitudinally and transversely stiffened ships. The validation cases show good agreement with theoretical predictions with an error of 15% in the estimated energy absorption. Two other examples are presented where a rigid bulb penetrates the side. Although a rigid bow used in this study gives good results, the author recommends the use of deformable bows in future studies as there is significant amount of energy absorption in striking bows.

3.3.5 SIMCOL [17]

Chen [17] proposes a Simplified Collision model (SIMCOL). In order to keep the model as simple as possible, SIMCOL Versions 0.0 to 2.0 assume that the striking bow is rigid and has a wedge shape defined by a half entrance angle. SIMCOL Version 2.1 considers the upper and lower extents of the bow relative to the struck ship.

The geometry calculation used in Version 0.1 was not descriptive of the actual damage volume when:

- the striking bow moves along the longitudinal axis of the struck ship; or
- there is relative rotation between the striking and struck ships.

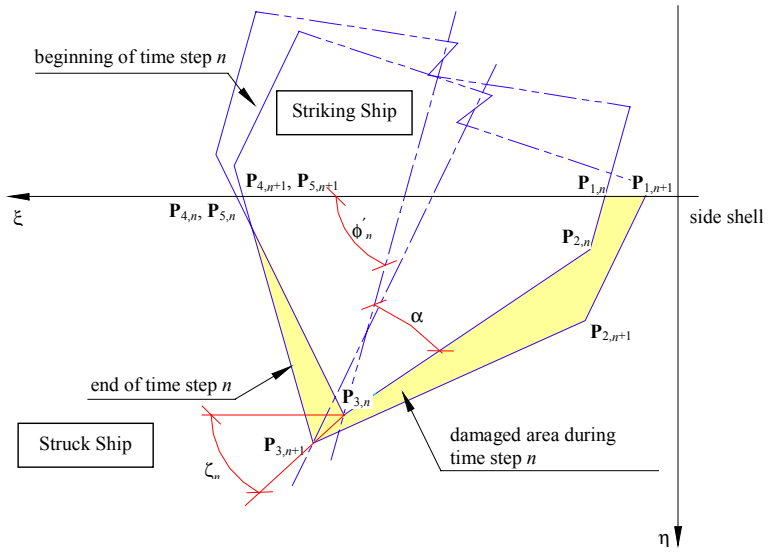

Figure 3. 12 – SIMCOL [17]

The damaged geometry is changed in later versions to solve these problems. With the assumption of a wedge-shaped rigid striking bow, the intrusion portion of the bow is described with five nodes, as shown in Figure 3.12. The shaded area in Figure 3.12 is exactly the damaged area of decks and/or bottoms during the time step.

Prior to SIMCOL Version 2.1, the striking bow is assumed to have infinite depth. As discussed in Section 2.2, this is not a good assumption even though it simplifies the problem dramatically. A vertical striking bow with limited depth is introduced in Version

2.1. It is assumed that the deflection of the side shell or longitudinal bulkhead is linear from the top and/or bottom of the striking bow to the next horizontal support that has not been struck. This is shown in Figure 3.13. It is also assumed that the lateral deformation of web frames is similar to the incursion of the striking bow as shown in Figure 3.13.

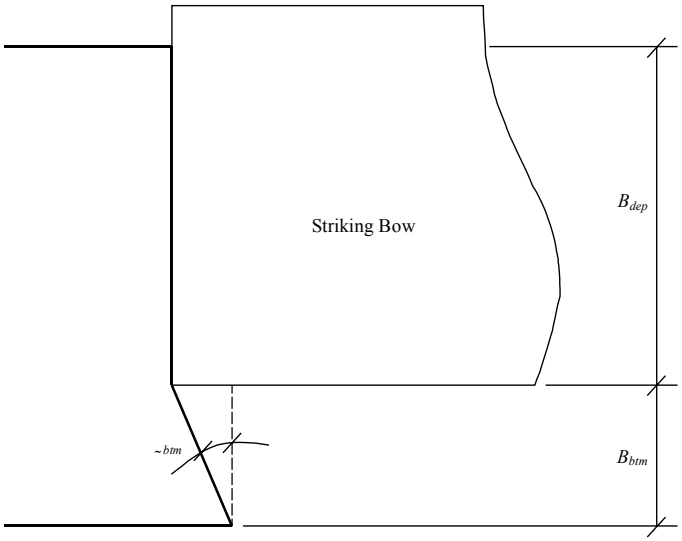

Figure 3.13 – SIMCOL Version 2.1 [17]

3.4 Deformable Bow Models

3.4.1 Woisin [69]

Woisin analyses the structural design of nuclear ships to reduce damage from collision. The differences in design of chemical and gas tankers are also discussed. A survey of model testing techniques is presented, including scale laws, scale effects and differences with real collisions. Some calculation methods for the mechanics of collision are provided, but a comprehensive theory is lacking. Calculations of critical collision speeds of different ships ramming gas and chemical tankers are reported. Some structural reinforcements of the ships' sides are proposed. He proposes the theory of "soft bows" to minimize penetration into other ships.

A modified Minorsky [40] method is used for calculation. A total of 12 pairs of collision structure models were tested in Hamburg from 1967 to 1976. Figure 3.14 shows a schematic diagram of the collision model tests performed in Hamburg.

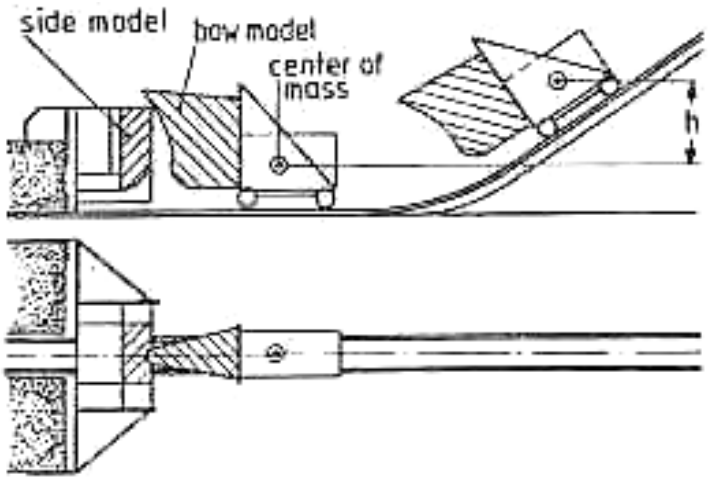

Figure 3.14 - Schematic diagram of test techniques in Hamburg [69]

The test stand (Figure 3.14) consists of a carriage of up to 25 tonnes with a fore-ship model attached to its forward end, which rams a ship's side model attached to a rigid counter bearing. The necessary velocity and energy of impact are achieved by an incline on which the carriage, after release of an arresting device, accelerates until it coasts without acceleration on a horizontal plane. Significant damage is caused to the bow model. The development of soft or non-penetrating bows was also addressed by Woisin. Potential methods for soft bows are:

- transverse, instead of longitudinal stiffeners
- water filling
- fewer breast hooks and reduced stem plate thickness
- no hard points
- design of bulbous bows and raking parts above water as crushable zones

Woisin proposes the following formula for predicting the maximum collision force P_{max} of bow structures, as a function of the DWT of the striking ship:

$$P_{\max} = 0.88\sqrt{DWT} \pm 50\% \quad \textbf{(3.12)}$$

Significant bow damage is recorded from the model tests performed in Hamburg. The author suggests the use of soft bows in future to minimize damage to the struck ship.

3.4.2 Kim [30]

Kim considers the finite strength of the striking bow in the overall collision simulation. The bow structural members considered are the side shell and the decks. Transverse and longitudinal stiffeners are considered using a smearing technique. Based on actual collision pictures, two alternative bow models are developed, that account for the deformation modes evident in the photographs (see Figure 3.15). The model with inward folds (Model B) gives superior results compared to the model with outward folds (Model A) and these results compare well with model test results. Five scale model tests are run and the force-deflection characteristics are recorded and compared, showing good correlation.

In Kim's analysis, a ship with an orthogonal stiffened bow moving with a forward velocity of V is considered to strike an embankment at an angle of 90^0 vertically and ϕ (bow angle) horizontally. Bow elevation and trim effects are neglected. No friction between the bow and the embankment is considered. The embankment is treated as a rigid, right-angle-edged wall. The collision is assumed to be perfectly inelastic, thus the dissipation of external kinetic energy is fully converted to the structural damage of the striking ship.

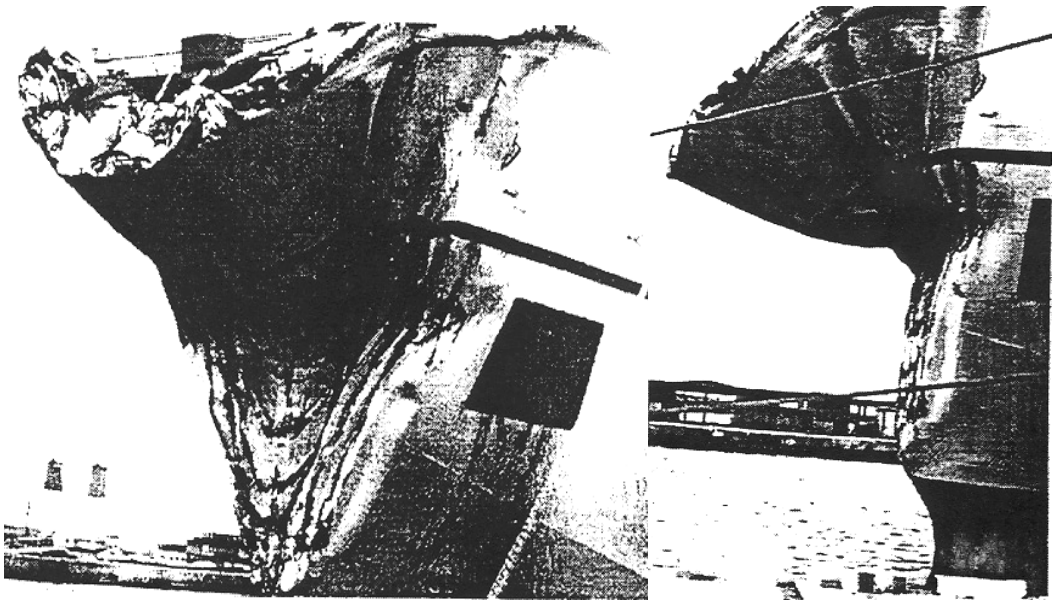

Figure 3.15 – Photographs of actual collision [30]

Since the bow has complex three-dimensional geometry, it is necessary to simplify the bow geometry. First, the contact point between the ship and the rigid obstacle is specified. It is observed from actual accidents and tests that the contact point divides the bow length in two parts with same length and the vertical extension of the line from the end of the bow length to the deck plate gives the boundary of the deforming part of the bow. The bow model in this study is defined using three independent variables, bow length (l), bow angle (ϕ) and deck angle (θ). All edge lines in the bow are then defined in terms of these 3 parameters.

Photographs of the actual collision shown in Figure3.15 show quite a complex deformation mode. However, by careful inspection, it is observed that there are four major internal energy dissipation areas, which are side shell folding, deck tilting, frontal bow stretching and side shell stretching. It is also noticed that one fold of the side shell of the bow matches one bend on the deck and the large stretching area from the contact point and small stretching area on the sides.

The mean crushing forces for models A and B respectively are [30]:

Model A:

$$P_m = 18N_0 \frac{H^2}{l\sin\phi} + 8(N_0 H Sin^2\varphi Cos\varphi + N_0 \varphi l Sin\varphi Cos^2\varphi) + 4\pi M_0 Sin\varphi \frac{l}{H} + 4M_0 Cos\varphi Tan\varphi \qquad \textbf{(3.13)}$$

Model B:

$$P_m = \sigma_0 (0.134lt + 6.28t^2) \qquad \textbf{(3.14)}$$

Where:

P_m is the mean crushing force;

N_0 is the fully plastic membrane force per unit length;

φ is the bow angle (assumed to be 60 degree);

θ is the approximate side angle between forefront and collision bulkhead (assumed to be 30 degree);

l is the distance from the bow tip to the point of application of the load;

t is the bow shell plate thickness (0.21mm and 1.2mm are the two values used in this study);

H is the folding length;

M_0 is the bending energy per unit length

Table 3.1 compares the mean crushing loads calculated for 4 different bows using Models A and B to the test results.

	BOW1	BOW2	BOW3	BOW4
Model A	5305.8	3557	4278	3587
Model B	4846	2917	3558	9343
Model Test	4038	2652	4137	10991

Table 3.1 - Comparison of P_m calculated for Model A and Model B [30]

Both of these models consider only the upper bow and not the bulb. Although Pedersen [52] shows calculations for the bow uncoupled from the bulb, the solutions from these models cannot be compared to his solutions because the basis ships considered are different. Of the two models developed, Model B gives better results than Model A and hence the simplified equation for mean crushing load for Model B can be used in future studies.

3.4.3 Gerard [52]

Gerard developed a semi-empirical method for the estimation of crushing loads of structures based on the correlation of the results of a series of panel tests with various stiffener types.

This method is very conservative. It predicts loads, which are approximately 50% higher than the experimental results. The maximum crushing strength σ_c, according to Gerard is given by the following equation:

$$\sigma_c = \sigma_0 \beta_g \left[\left(nt^2 / A \right) \sqrt{E / \sigma_y} \right]^m \tag{3.15}$$

The total crushing load is then given by:

$$P_c = \sigma_c A \tag{3.16}$$

Where:

σ_y	is the yield stress;
σ_0	is the compressive flow stress (inclusive strain rate effects);
E	is the Young's Modulus for steel;
β_g=0.56, m=0.85	coefficients depending on edge restraint. The values applied are for undistorted edges
n	sum of cuts and flanges for the cross-section under consideration (See Figure 3.16)
t	average thickness for the cross-section under consideration;
A	cross-sectional area

The strain rate is taken as:

$$\dot{\varepsilon} = v_x / s \tag{3.17}$$

Where:

v_x	is the velocity in longitudinal direction during impact;
s	frame spacing

The magnitude of the dynamic flow stress is calculated from the following relationship:

$$\sigma_0(\dot{\varepsilon}) = 1.29\sigma_{0_s}\dot{\varepsilon}^{0.037} \tag{3.18}$$

where σ_{0s} is the static ultimate strength of the steel material.

The load formula given above predicts the maximum crushing load of plated structures within ± 10% of the experimental results. One of the major drawbacks of the model is that it has been derived from the crushing of fairly simple and regular plate constructions where the range of plating to stiffener thickness ratios and stiffener spacing are limited. Normal bow structures consist of a number of plate panels of different dimensions and stiffener sizes.

3.4.4 Amdahl [5, 6]

Amdahl developed a model using intersection elements, correlated against model test results. Amdahl's method is a modified Wierzbicki [68] method, based on the energy dissipated during plastic deformation of basic structural elements such as angles, T-sections and cruciforms (see Figure 3.16). The total crushing load of a specific structure is obtained by adding up all the basic elements' crushing loads. Amdahl's method predicts values that are non-conservative, unlike Gerard's method.

Amdahl's procedure leads to the following equation for the average crushing strength:

$$\sigma_c = 2.42\sigma_0[n_{AT}t^2/A]^{0.67}[0.87+1.27\frac{n_c+0.31n_T}{n_{AT}}(\frac{A}{(n_c+0.31n_T)t^2})^{0.25}]^{0.67} \quad \textbf{(3.19)}$$

The total crushing load is found by multiplying σ_c by the associated cross-sectional area of the deformed steel material:

$$P_c = \sigma_c A \quad \textbf{(3.20)}$$

Where:

σ_c is the average crushing strength of the bow;

σ_0 is the ultimate strength of steel (incl. strain rate effects);

t is the average thickness of the cross-section under consideration;

A is the cross-sectional area of the deformed steel material;

n_c is the number of cruciforms in the cross-section (See Figure 3.16);

n_T is the number of T-sections in the cross-section (See Figure 3.16);

n_{AT} is the number of angle- and T-sections in the cross-section (See Figure 3.16)

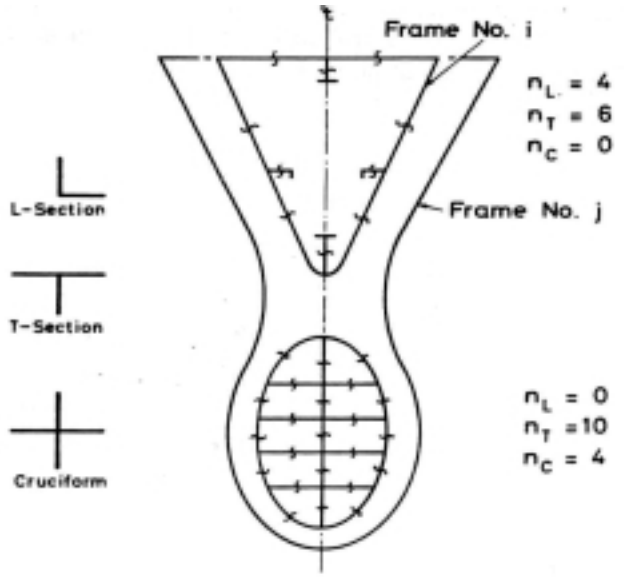

Figure 3.16 – Method of cross-sections to determine the number of intersections [52]

3.4.5 Yang and Caldwell [70]

In Yang and Caldwell, the bow section is modeled as an assembly of basic elements as shown in Figure 3.16. The mean crushing strength is obtained by summing the energy dissipated in all individual structural elements.

Figure 3.17 and Figure 3.18 show the different folding mechanisms of the basic elements and their plane descriptions. The following equations specify the energy absorbed in the various mechanisms:

- **Mechanism a)** $E_1 = \pi M_0 c \quad E_2 = {4 I_2 M_0 H^2}/{r} \qquad E_3 = {16 I_3 M_0 r H}/{t}$

$$I_2 = 1.1478 \qquad I_3 = 0.5779 \tag{3.21}$$

Where:

E_1 is the energy absorbed due to bending about horizontal hinge lines;

M_0 is the corresponding bending moment;

c is the side length of the cross-section of the angle element;

E_2 is the energy absorbed by rolling about the moving hinge lines;

E_3 is the energy absorbed due to inverting of curvature at the junction;

H is the half-folding length;

r is the radius of the toroidal shell element;

I_2 and I_3 depend on the joint angle of the basic element;

t is the plate thickness

- **Mechanism b)** $E_4 = \sigma H^2 t \qquad E_5 = 4 M_0 H$ **(3.22)**

Where:

E_4 is the energy absorbed during extensional distortion of one plate flange;

E_5 is the plastic work in the stationary line at the joint

- **Mechanism c)** $E_6 = \sqrt{2}\sigma_0 {H^2}/{t} \qquad E_7 = \pi M_0 H$ **(3.23)**

Where:

E_6 is the energy absorbed during extensional distortion in the flange after neglecting shear;

E_7 is the plastic work in the stationary line at the joint after neglecting shear

- **Mechanism d)** $E_8 = 1.29\sigma_0 H^2 t \qquad E_9 = \pi M_0 \, H/2$ **(3.24)**

Where:

E_8 is the energy absorbed during distortion of one plate flange;

E_9 is the energy absorbed by folding of plate along the inclined hinge lines

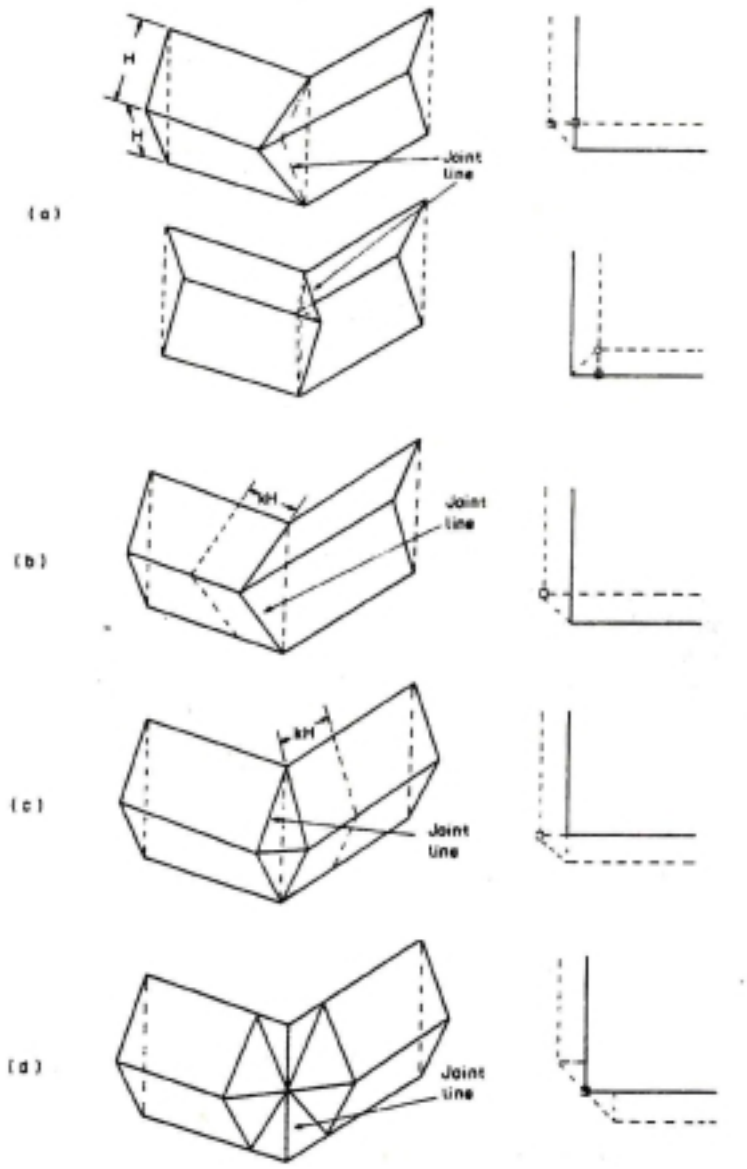

Figure 3.17 - Folding mechanisms of basic intersection type elements [70]

Crushing strengths for T-sections and cruciform sections are obtained from the mean crushing strengths for basic elements, with slight modifications. The cruciform,

which collapses in the asymmetric mode, i.e mechanism (i), has lower capacity than the other modes, while collapse in mechanism (iii) leads to the greatest mean crushing strength. Most of the plate intersections in a complex structure will be of a T-section or cruciform shape. The basic crushing modes of T-sections and cruciforms are shown in Figure 3.19.

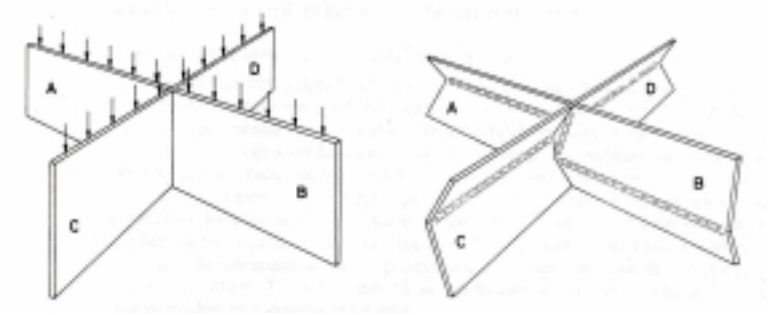

Figure 3.18 - Crushing mechanism for a cruciformed structural element [52]

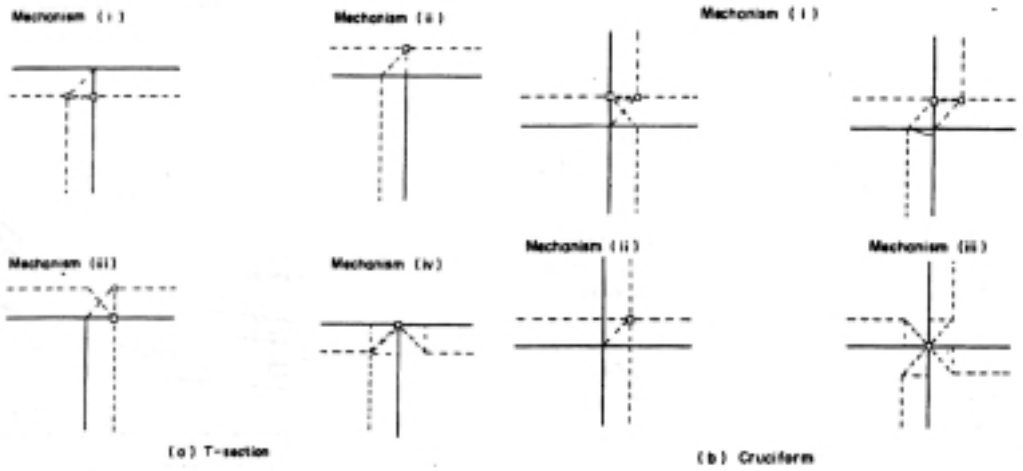

Figure 3.19 - Crushing mechanisms of T-Sections and cruciforms [70]

The empirical relation for the mean crushing force P_m thus developed [70] based on the crushing strengths of these basic elements is given below. See Appendix B for an explanation of symbols.

$$P_m = 1.178\sigma_0 / H^{n_T} b_i t_i^2 + 0.215\sigma_0 H^{n_A+n_T} t_i + 6.935\sigma_0^{n_A+n_T} t_i^2 + 0.265\sigma_0 H^{n_T} t_i + 0.589\sigma_0^{n_T} t_i^2 + 0.75\sigma_0 H^{n_C\ 4} t_i + 0.375\sigma_0^{n_C\ 4} t_i^2 \quad \textbf{(3.25)}$$

Where:

P_m is the mean crushing load of the structure;

σ_0 is the flow stress based on the mean value of the yield and the ultimate strength of the steel;

b_i is the width of the ith plate flange;

t_I is the thickness of the ith plate flange;

H is the folding length of the distorted plate flanges;

n_c is the number of cruciforms in the cross-section (See Figure 3.16);

n_T is the number of T-sections in the cross-section (See Figure 3.16);

n_{AT} is the number of angle- and T-sections in the cross-section (See Figure 3.16);

n_f is the number of flanges of angles, T-sections and cruciforms

The theory is applied to a tanker collision with a concrete bridge pier. In the results of the analysis, the mean crushing strength of the bow structure increases by about 10% due to the strain-rate effects. Figure 3.20 shows a comparison of the force-penetration curves developed using Gerard's, Amdahl's and Yang and Caldwell's methods.

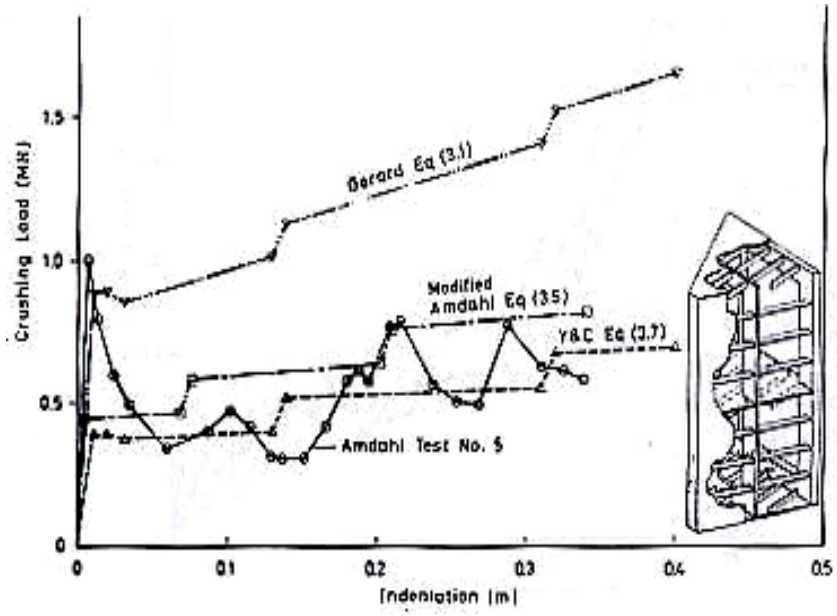

Figure 3.20 – Comparison of Gerard's, Amdahl's and Yang and Caldwell's results [52]

As can be seen in Figure 3.20, Gerard's results are conservative and predict almost 50% higher loads as compared to Amdahl's and Yang and Caldwell's results for larger penetration. For small penetrations, Gerard's results agree well with Amdahl's results.

3.4.6 Kierkegaard [29]

Kierkegaard also develops a mathematical model for force-indentation relations for high-energy collisions involving bow structures. The theory is based on axial crushing mechanisms for basic elements such as L-, T- and X-elements. The internal energy is determined for these elements under the assumption of a rigid plastic material. The energy is related to an external mean crushing force. Stiffened plates are included in the crushing mechanism. The crushing force is calculated in a simple time simulation, where the strain rate effect on flow stress is also included. The structure is crushed from the front and the simulation procedure is able to handle rigid body motions of crushed and non-crushed structure.

In a numeric calculation, the bow is modeled as an assembly of basic axial elements (L-, T- and X-elements). The flanges in these elements are formed from the main structural items such as: shell plates, stringers, stem plate, bulkheads and decks. Four basic folding mechanisms are considered, which are all related to an L-element:

a) *Sliding toroidal surface mechanism* - mechanism forms a part of a toroidal surface in the center of the junction. Under the folding process, the toroidal surface moves to the left and material from the flange on the left will pass continuously to the other flange. No in-plane deformations. The total energy absorption for an L-element over one folding length, 2H, is given as:

$$E_a = 2E_1 + 4E_2 + 2E_3 \tag{3.26}$$

Where:

E_1 is the energy absorbed during extension/compression in vertical direction on the toroidal surface;

E_2 is the energy absorbed due to bending about horizontal hinge lines at the center and at the top and bottom clamped ends;

E_2 is the energy absorbed due to bending about vertical moving hinge lines

b) *One flange extension mechanism* - The intersection line breaks to the side without any material transfer across the intersection. The energy in this case is:

$$E_b = 4E_2 + E_4 + E_5 \quad \textbf{(3.27)}$$

Where E_4 is the energy from extension and E_5 is the energy from bending.

c) *Straight edge mechanism* - Under the folding process, the intersection line between the flanges will remain straight and vertical. Then the triangular sections with a side coinciding with the intersection line will be compressed in-plane in the x-direction and the other triangular plate sections will be transformed by shear and extension in the horizontal direction. The energy absorbed in this case is:

$$E_c = 4E_2 + 2E_6 + 2E_7 \quad \textbf{(3.28)}$$

Where E_6 and E_7 are the energies dissipated in bending along the vertical hinge lines.

d) *In-plane deformation mechanism* - Energy is absorbed through shape distortion of each of the four rectangular sections. These plane deformations are dominated by extension/compression in the y-direction. Also, a minor part is absorbed in bending about the joint-line. The energy absorbed here is:

$$E_d = 4E_2 + 2E_8 + 2E_9 \quad \textbf{(3.29)}$$

Where E_8 and E_9 are the energies dissipated in one flange during extension and bending in the joint line.

The mean crushing force can then be found as:

$$P_m = \frac{E_i}{\partial_e} \quad \textbf{(3.30)}$$

Where E_I is the energy absorption over one folding length 2H and

$$\partial_e = \frac{2}{3} 2H \quad \textbf{(3.31)}$$

The mean crushing force for the four mechanisms is shown in the Figure 3.21. Crushing mechanisms for T- and X-elements can be generated from the four basic

mechanisms by adding extra flanges or by combining the methods. The energy absorption for a T-element with clamped ends is:

$$E_T = 2E_1 + 6E_2 + 2E_3 + E_4 + E_5 \tag{3.32}$$

An X-element is assumed to crush in the straight edge mechanism, and hence,

$$E_c = 8E_2 + 4E_6 + E_7 \tag{3.33}$$

In complex ship bow structures, the crushing mechanisms are not fully compatible as the common folding length in each transverse section could result in an unrealistically high collision force when stiffeners are involved. These mechanisms for the basic elements are extended to apply for the complex bow structure, taking into consideration the strain rate effects on the flow stress.

This method is applied and compared to crushing tests of bow models given in the literature by Arita [10], Amdahl [6] and Hagiwara [21]. Scale models are built of unstiffened plates and they are crushed quasi-statically. One of the models developed is shown in Figure 3.21.

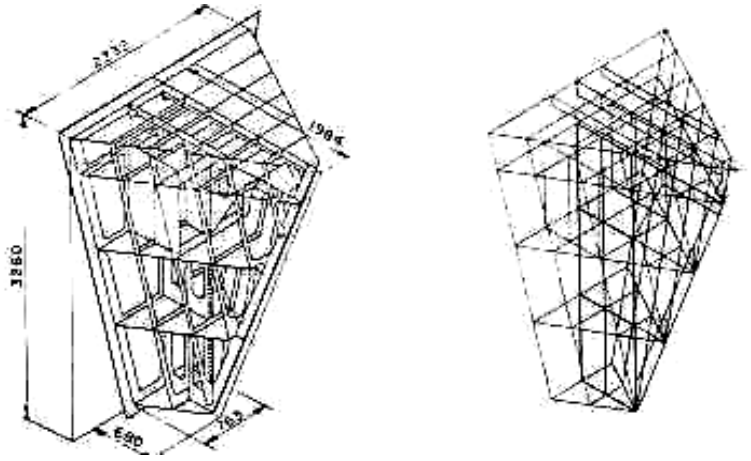

Figure 3.21 - Intersection element model by Kierkegaard [29]

Hagiwara's test model is a 1/5-scale bow of a 17,000 DWT cargo ship, which is typical of a small ship having a transverse framing. For simplicity of fabrication, the model omits some of the inner structural members, as seen in Figure 3.21. The flow stress is taken to be 250 MN/m^2 and the quasi-static crushing is simulated using a constant

speed $V_0 = 10^{-4}$ m/s as in the test. The simulation is done in 1400 steps. The calculated results agree very well with the test results.

In another study, a large ship with a longitudinal stiffened bow, a 150,000 DWT Bulk Carrier is considered. A bulbous bow is proposed due to higher collision loads. The steel used in the ship has a static yield stress of 315 MN/m^2. The structure is divided into axial elements consisting of 185 L-elements, 67 T-elements and 2 X-elements, as seen in Figure 3.22.

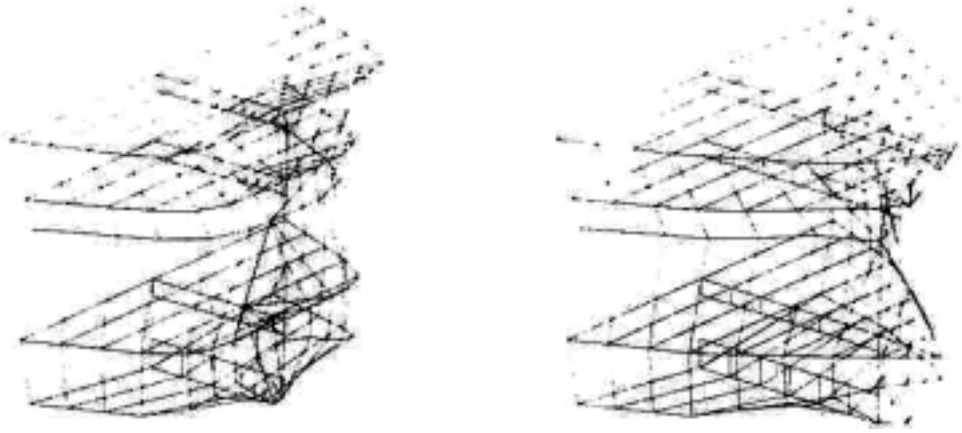

Figure 3.22 – 150,000 DWT Bulk Carrier Intersection Model [29]

The collision scenario is assumed to be a right-angled head-on collision against a rigid object. An initial velocity of 7.72 m/s and an added mass of 5% of the ship's mass are used in the calculation. The simulation ended at time 3.78 sec where a penetration of 16.5 m is reached. The absorbed energy in the striking ship is calculated to be 5453 MJ as compared to only 2617 MJ using Minorsky's method. As documented above, this method predicts high values for absorbed energy in the longitudinally stiffened case, as compared to reasonably good values for the transversely stiffened case.

3.4.7 Valsgard and Pettersen [66]

Valsgard and Pettersen provide a procedure capable of estimating the damage to the striking bow and the struck ship side, to predict the collision force, and to determine the associated energies and energy absorption ratio between side and bow. A bulbous

bow is used in their example, for which the stiffness is represented as a set of non-linear springs (Figure 3.23) evaluated using a semi-empirical approach.

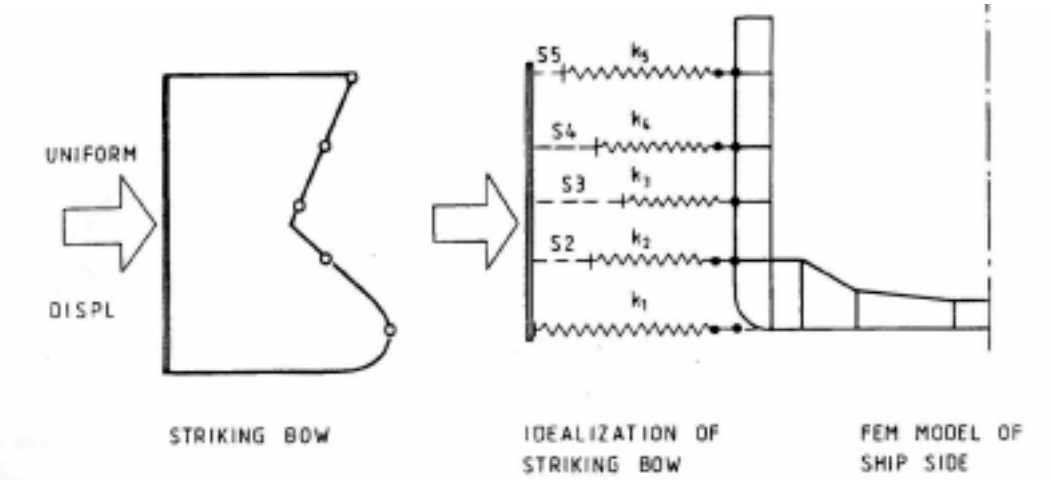

Figure 3.23 - Idealization of striking bow by a set of non-linear springs [66]

The collision situation is characterized by the following conditions:

- The struck ship has zero speed before the collision and after the collision, both ships have a common speed, as determined by the momentum of impact before and after the collision.
- Collisions are considered to be perpendicular to a midship tank. Thus no energy is supposed to go into the struck ship rotation.
- The impact energy is absorbed by both the side and the bow structures. The calculated stiffness characteristics (load vs. indentation) are used in determining the damage and energy absorption in each part.
- A realistic bulbous bow is used. This is the bow of a sister ship at an increased draft for simulating the bow of a 126,000 tonne displacement tanker as shown in Figure 3.23.
- Various longitudinal striking positions and striking speeds are investigated.

The relative position of the striking bow and the struck ship is shown in Figure 3.24:

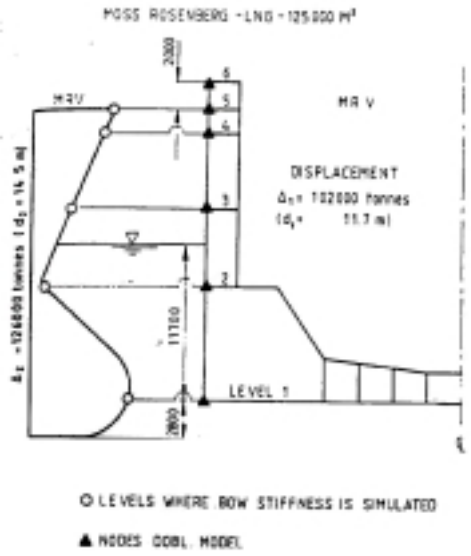

Figure 3.24 - Relative position of striking bow and struck ship [66]

The striking bow is simulated by a set of non-linear springs (k1-k5) with associated slacks (S2-S5) which represent the geometrical bow form. These springs are attached to the nodes in the ship's side in which the stiffness characteristics are determined by a nonlinear simplified FE procedure. Figure 3.25 shows the bow model approximated using a set of non-linear springs. In this way the relative damage and energy absorption of the side and the bow are determined. The results depend on the relative stiffness of the bow and for this reason, results for two different bow stiffnesses are produced in this study.

The spring constants of the bow are represented as discrete linear functions of force-deformation values supplied as input to the computer program. Non-linear bow springs for the striking bow of the MRV sister ship are evaluated by Bach-Gansmo and Valsgard [12] for 10 vertical levels in the ship bow. These springs are established by using a combination of crippling loads determined from Gerard's test [52] and elastic buckling loads. The load-deformation behavior of the structural elements in the bow is then constructed as proposed by Chang et.al. [16], as shown in Figure 3.25. The relative stiffness of the ship's side and the bow determines which structure suffers the most damage in a collision.

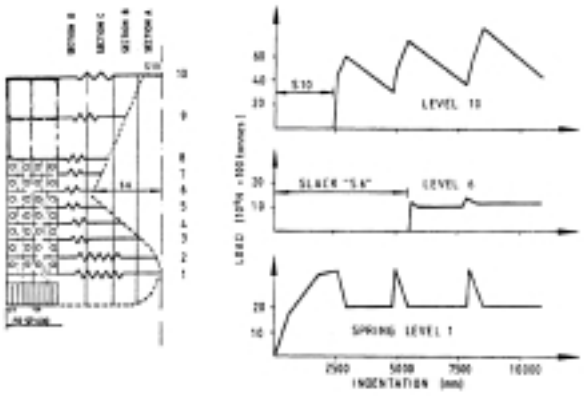

Figure 3.25 - Approximation of bow stiffness with non-linear springs [66]

The results, as discussed in Section 4.4, show that the bow of the striking ship in this case absorbs about 55% of the total energy, as compared to 15% when the stiffness of the striking ship's bow is assumed to be ten times the actual stiffness. These results indicate that the stiffness of the bow of the striking ship plays a very important role in the energy absorption in ship collisions.

3.4.8 Pedersen [52]

Pedersen presents a method for estimating the collision forces between conventional merchant vessels and large volume offshore structures. The main emphasis is on impact loads on fixed offshore structures due to bow collisions. The crushing loads are determined as a function of vessel size, vessel speed, bow profile, collision angles and eccentric impacts.

Pedersen discusses the various methods and theories for calculating the crush loads during collisions, including Amdahl's method, Gerard's method and Yang and Caldwell's approach and applies these various methods to six different ships in order to compare and validate the theories. After a series of numerical calculations, Pedersen concludes that Gerard's results are approximately 50% higher than the experimental results.

These are based on the assumption of collision against an infinite rigid wall. For cases where the vessel strikes a pier of limited width, or with a step or recess, the

collision force needs to be adjusted by multiplying the ratio of the deformed steel area in actual contact with the pier to the total steel area of the bow section under consideration. In addition, shear forces are to be included as shown in the equation below:

$$P_{cl} = P_c A_c / A + \sum^{n_d} \tau_{cr} t_d S_{FR} \quad \textbf{(3.34)}$$

Where:

P_{cl} is the collision load on the pier based on contact area assessment;

P_c is the collision load on plane infinite wall;

A_c is the cross-sectional area of the steel material in direct contact with the pier during deformation of bow;

A is the total cross-sectional area of the steel material at the section of the bow under consideration;

n_d is the number of decks and sides extending outside the pier width;

τ_{cr} is the shear buckling stress of decks and sides extending outside the pier

Six different ships are considered: 1) 150,000 DWT Bulk Carrier, 2) 40,000 DWT containership, 3) 3000 DWT general cargo vessel, 4) 2000 DWT tanker, 5) 1000 DWT pallet carrier 6) 500 DWT coaster. All these ships have bulbs. The main particulars and the bow scantlings of these ships are given in Appendix C.

Figure 3.26 shows the calculated crushing load-indentation curves using Amdahl's modified method and Yang and Caldwell's method for the 150,000 DWT bulk vessel in a fully loaded condition, striking head-on with a rigid wall at an initial impact speed of 18 knots. Similar results for the 40,000 DWT container vessel for a head-on collision with a rigid wall at an initial speed of 12.9 m/s are obtained.

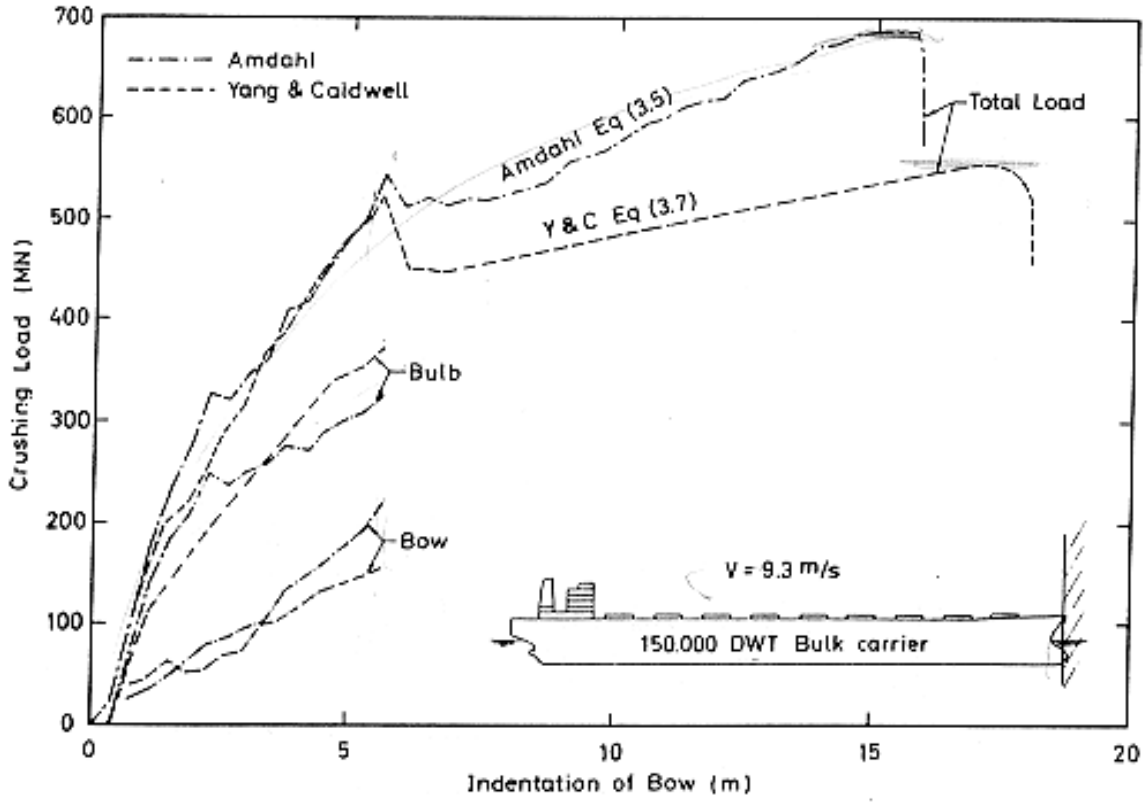

Figure 3.26 – Force-indentation curves for 150,000 DWT Bulk ship [52]

As can be seen in Figure 3.26, the force-penetration curve is uncoupled into two curves – one for the bow and the other for the bulb. The overall force curve represents a sum of the bow and bulb forces at that instant of time. Also, the force-penetration curve is approximated by using a sine curve, the peak of which represents the maximum bow crushing force.

Similar results are obtained for the remaining 4 ships. An empirical expression is derived to estimate maximum bow collision loads, as a function of strain rate, impact velocity, vessel displacement and vessel length. For a vessel between 500 DWT and 300,000 DWT the crushing load is given by:

$$\begin{aligned} P_{bow} &= P_0 \overline{L}[\overline{E}_{imp} + (5.0 - \overline{L})\overline{L}^{1.6}]^{0.5} \quad \text{for} \quad \overline{E}_{imp} \geq \overline{L}^{2.6} \\ P_{bow} &= 2.24 P_0 [\overline{E}_{imp} \overline{L}]^{0.5} \qquad\qquad\quad \overline{E}_{imp} < \overline{L}^{2.6} \end{aligned} \tag{3.35}$$

Where:

$\bar{L}$ = L_{pp}/275 m;

$\bar{E}_{imp}$ = E_{imp}/1425 MN;

E_{imp} = ½ $m_x V^2_0$;

P_{bow} is the maximum collision load in MN;

P_o is the reference collision load equal to 210 MN;

E_{imp} is the enrgy to be absorbed by plastic deformations;

L_{pp} is the length of the vessel (m);

m_x is the mass plus added mass (5%) w.r.t longitudinal position [10^6 kg];

V_o is the initial speed of the vessel in ms^{-1}

The maximum indentation s_{max} is found as:

$$S_{\max} = \frac{\pi}{2} \frac{E_{imp}}{P_{bow}} \tag{3.36}$$

and the associated impact duration is derived as:

$$T_0 \approx 1.67 \frac{S_{\max}}{V_0} \tag{3.37}$$

Tables 3.2, 3.3 and 3.4 show the bow collision loads for seven different vessels based on the empirical equations developed above. The collision loads in the tables vary between 20 and 900 MN, which is a variation caused by the variation of vessel size and impact energy. In view of the uncertainties naturally involved in the actual collision scenario, it is reasonable to use the expression as an integral part of the probabilistic risk analysis [36, 37].

Vessel size	500 DWT	1000 DWT	2000 DWT	3000 DWT	270,000† DWT
L_{pp} (m)	41.00	53.80	69.00	78.00	330.7
B_m (m)	9.00	11.00	12.30	16.00	51.80
D (m)	6.40	6.70	8.60	10.50	27.60
Mass (10^3 kg)	886	1650	3020	4600	312.384
V_0 (m s^{-1})	5.0	5.5	7.0	7.5	7.5
P_{bow} Eqn (3.10) (MN)	15.3 (21)‡	25.0 (24)‡	39.9 (32)‡	50.7 (72)‡	859.2 (900)‡
s_{max} Eqn (3.12) (m)	1.19 (1.1)‡	1.64 (2.0)‡	3.06 (3.3)‡	4.21 (3.6)‡	16.82 (17.00)‡
T_0 Eqn (3.13) (s)	0.40 (0.35)‡	0.50 (0.67)‡	0.73 (0.85)‡	0.94 (0.93)‡	3.76 (4.0)‡
P_{bow} W–G Eqn (3.14) (MN)	19.7	27.8	39.4	48.2	457.3
P_{bow} US-Guide Eqn (3.15) (MN)	13.4	20.9	37.6	49.3	467.7

Table 3.2 – F, d and t for five fully loaded ships [52]

Vessel size	150,000 DWT			
L_{pp} (m)	274.0			
B_m (m)	47.0			
D (m)	21.6			
Mass (10^3 kg)	174,900			
V_0 (m s^{-1})	9.3	7.7	5.2	2.6
P_{bow} Eqn (3.10) (MN)	646.7 (570–680)†	584.4 {514}‡	500.5 {462}‡	309.9 {270}‡
s_{max} Eqn (3.12) (m)	19.3 (16–18)†	14.6 {14.6}‡	7.8 {8.4}‡	3.2 {3.8}‡
T_0 Eqn (3.13) (s)	3.46 (3.0–3.5)†	3.17 {3.35}‡	2.50 {2.79}‡	2.2 {2.41}‡
P_{bow} S–S Eqn (3.14) (MN)	340.8	—	—	—
P_{bow} US-Guide Eqn (3.15) (MN)	432.2	357.9	241.7	120.8

Table 3.3 –F, d and t for a bulk carrier at various speeds [52]

Vessel size	40,000 DWT		
L_{pp} (m)		211.5	
B_m (m)		32.2	
D (m)		21.0	
Mass (10^3 kg)		54,000	
V_0 (m s^{-1})	12.9	9.3	5.2
P_{bow} Eqn (3.10)	398.6	342.6	294.2
(MN)	(350–450)†	{345}‡	{224}‡
s_{max} Eqn (3.12)	18.6	11.2	4.1
(m)	(15–19)†	{10.5}‡	{5.2}‡
T_0 Eqn (3.13)	2.41	2.02	1.31
(s)	(2.0–2.6)†	{1.95}‡	{1.72}‡
P_{bow} S–S Eqn (3.14) (MN)	176.0	—	—
P_{bow} US-Guide Eqn (3.15) (MN)	309.6	223.2	124.8

Table 3.4 – Maximum bow crushing forces, indentation and collision duration for a container ship at various speeds [52]

The empirical equations are used to obtain plots of bow crushing force, crushing distance and collision duration as functions of ship size and velocity, as seen in Figure 3.27, Figure 3.28 and Figure3.29.

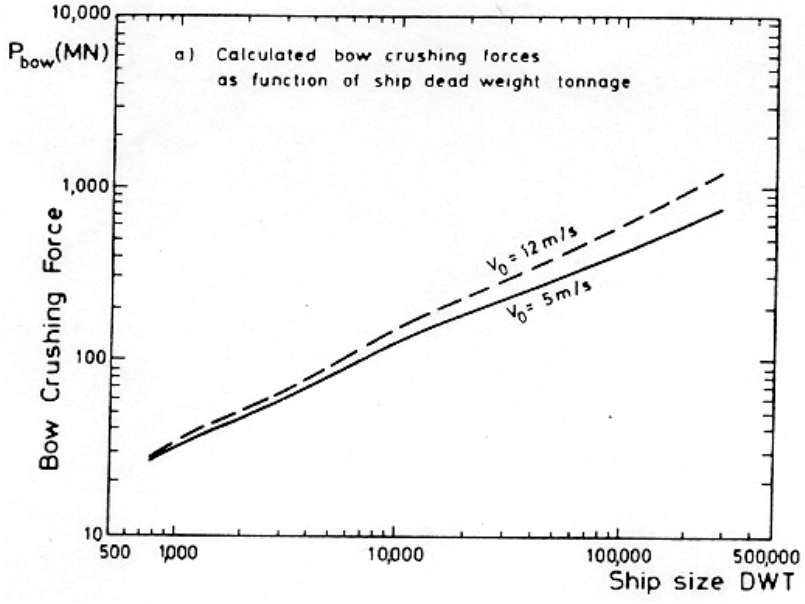

Figure 3.27 – F vs DWT for different speeds [52]

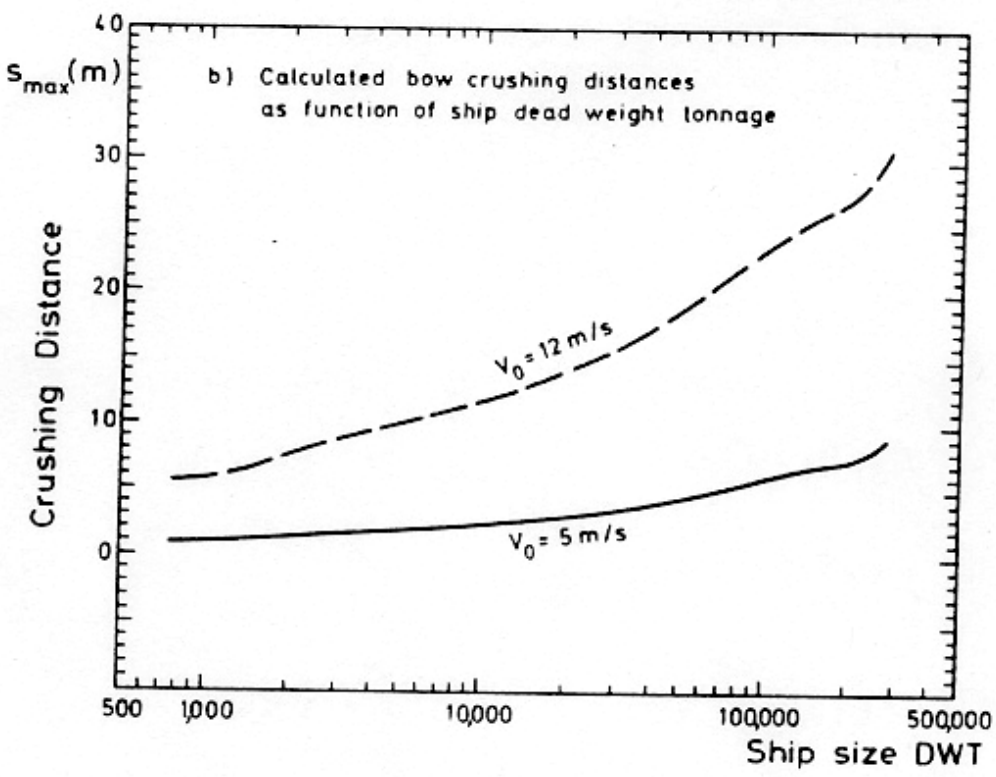

Figure 3.28 – Crushing distance vs DWT for different speeds [52]

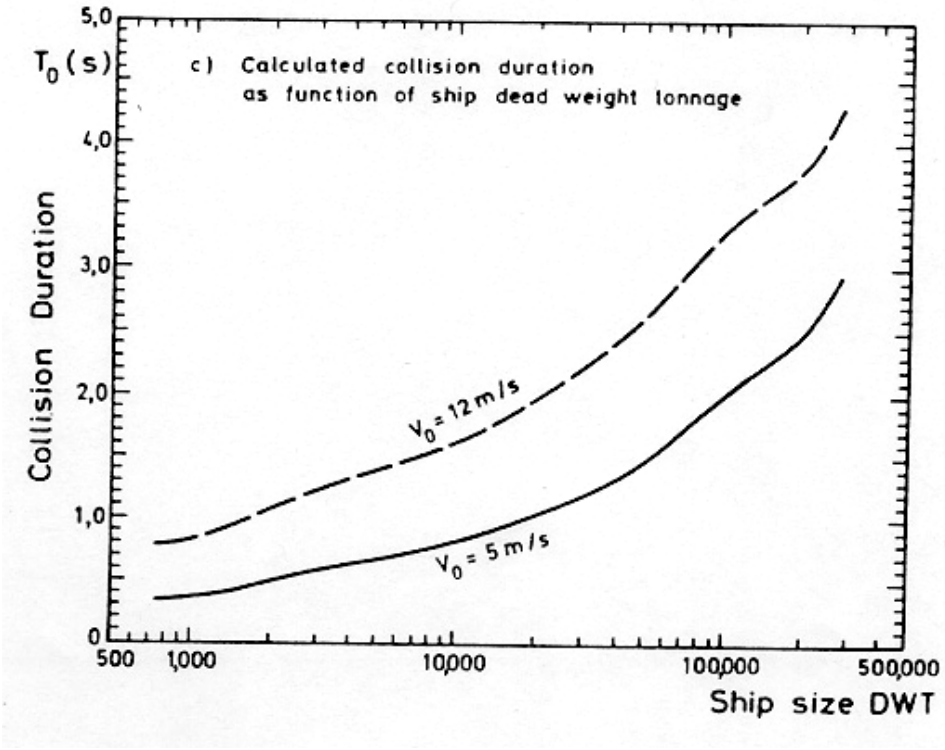

Figure 3.29 – Collision duration vs DWT for different speeds [52]

3.5 Comparison of the models

Table 3.1 below summarizes the various bow models described in the sections above and reviews the salient points to be remembered from each of these models.

Model	Rigid	Deformable	Closed-Form Equation	FE-Based	Empirical	Intersection Elements	Bow Infinite Wedge	Numerical Examples	Relative Draft	Uuncoupled Bulb, Bow
Minorsky [40]										
Hutchison [25]										
Ito [27]										
Wierzbicki [68]										
Simonsen [62]										
SIMCOL 0.1 – 2.0 [17]										
SIMCOL 2.1 [17]										
Woisin [69]										
Kim [20]										
Gerard [52]										
Amdahl [52]										
Kierkegaard [29]										
Yang and Caldwell [70]										
Pedersen [52]										
Valsgard, Pettersen [66]										

Table 3.5 – Comparison of important features of various bow models

Chapter 4 Evidence Supporting the Hypothesis

4.1 INTRODUCTION

If the energy absorbed by the striking ship bow is small or a constant percentage of the total absorbed energy then calculation of striking ship damage and absorbed energy is unnecessary. However, various types of evidence including pictures of actual collisions, numerical analyses of actual collisions and FE simulations indicate that this is not the case.

4.2 PICTORIAL EVIDENCE

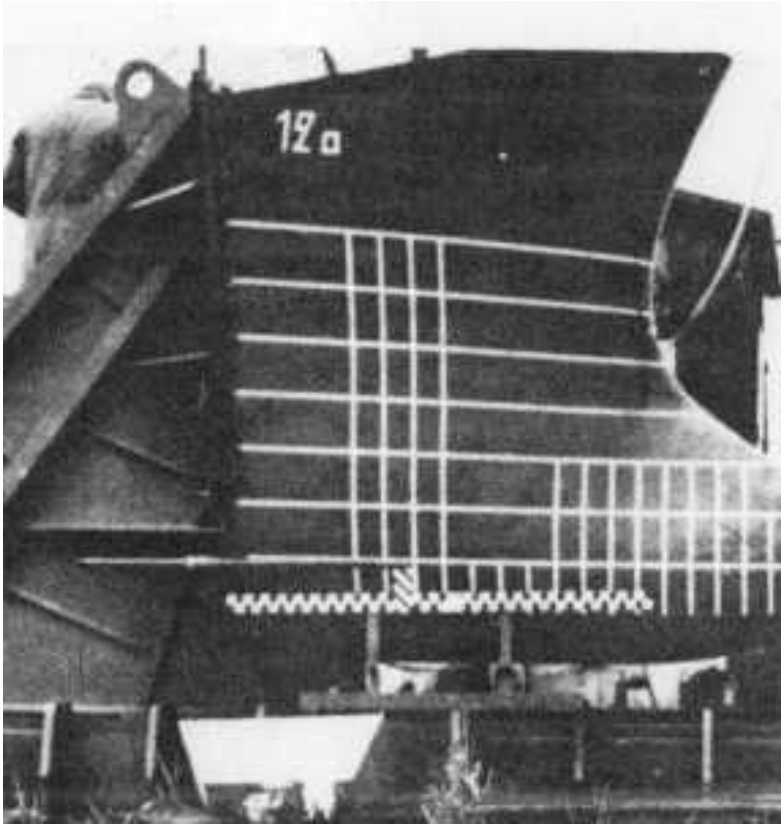

Figure 4.1 – Scale Model of a Bulbous Bow Before Collision [43]

Figure 4.2 – Scale Model of a Bulbous Bow After Collision [43]

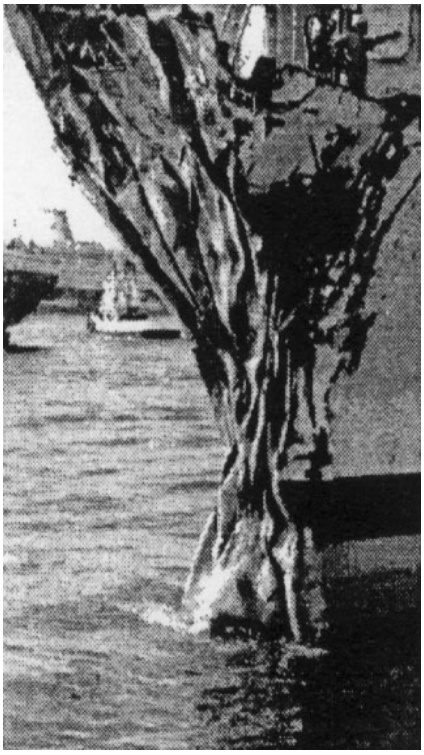

Figure 4.3 – Bulbous Bow of a Real Ship After Collision [43]

Figures 4.1 through 4.3 show that the striking ship bow is deformable and may play an important role in the energy absorption process during a collision.

4.3 RECKLING ANALYSIS OF ABSORBED ENERGY [58]

Reckling [58] presents a method to compute energies absorbed in striking and struck ships during collision.

For evaluation of the force functions $F_i(x_i)$, Reckling recommends using the distance d of the contact area between the collision opponents. The distance d is the total relative translation between the struck and striking ships measured after the moment of first contact. This distance uniquely determines the engaged contact area of the striking ship bow with the struck ship. It is the sum of the penetration into the struck ship's side and the collapse of the striking ship bow. When the resultant forces $F_i(x_i)$ (with i=1,2 for the striking and struck ships respectively) are computed as functions of their individual deformations x_i, the total absorbed energy E_p is obtained by integration up to the maximum deformations l_i. For every integration interval $0,\ldots,l_i$, the conditions of equal forces $F_1(x_1) = F_2(x_2)$ and equal contact area must be satisfied.

The resultant maximum force $F_1(d)$ transmitted by the bow through a certain material cross-sectional area in the distance d behind the fore-end of the bow is a function of d or of the contact area A. This force is calculated by summing up the collapse forces of the individual components for a suitable number of frame sections using the methods described in the paper [58]. It is valid irrespective of the bow having collapsed partially, totally or not at all up to the distance d. The distance d is not to be confused with the deformations, l_i. It is the sum of l_1 and l_2. The function $F_1(d)$ or $F_1(A)$ is plotted schematically in Figure 4.4. The function $F_2(d)$ or $F_2(A)$ is also evaluated and plotted in Figure 4.4.

In Figure 4.4, in the first collision phase (up to the point b), the bow is stronger than the side structure and presses into it as a rigid body with $F_2(d)$ as the actual force. Up to the point a of the force curve $F_2(d)$ of the side structure, the collapse load is governed only by plastic bending moments in the hull panel loaded by a force distributed over the

contact area. Subsequently, the membrane action of the hull and the web frame forces are activated so that the $F_2(d)$ curve grows more steeply than the $F_1(d)$ curve, which, after point b, is the actual force. At point c, the gradient of the $F_2(d)$ curve diminishes considerably so that, at the critical point d, both curves intersect a second time and the side structure collapses. The energy absorbed by the bow is the shaded area under the $F_1(d)$ curve. The total energy absorbed overall is the area under the lowest F_i curve integrated from zero to d.

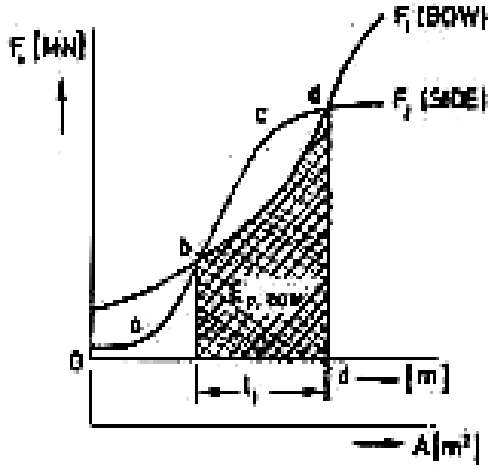

Figure 4.4 – Schematic plot of the maximum collision forces [58]

Reckling models the collision of two equal 141,000 TSDW tankers in the same loading condition [58]. The masses of the vessels are $m_{10}= m_{20}= 170$ MNs^2m^{-1}. The transverse bulkheads are 25m apart with 4 web frames between them. The frame distance is 0.6m. In Figure 4.5 (scale 1:250), the frames 141, 139 and 137 with distances 0.3, 1.5 and 2.7m behind the fore-end of the bow are shown in a cross-section (a), in a side view (b) and in a plan view at the height of bow stringer I (c).

The upper and lower regions of the contact area are treated independently in this calculation due to their different collapse behavior. The bulb and turn of the bilge are much more rigid than the upper bow and side shell. All calculations are performed with a yield stress of 270 MNm^{-2}. The independent force functions $F_{iu}(d)$ for the upper region and $F_{il}(d)$ for the lower region of the collision opponents are plotted in Figure 4.6.

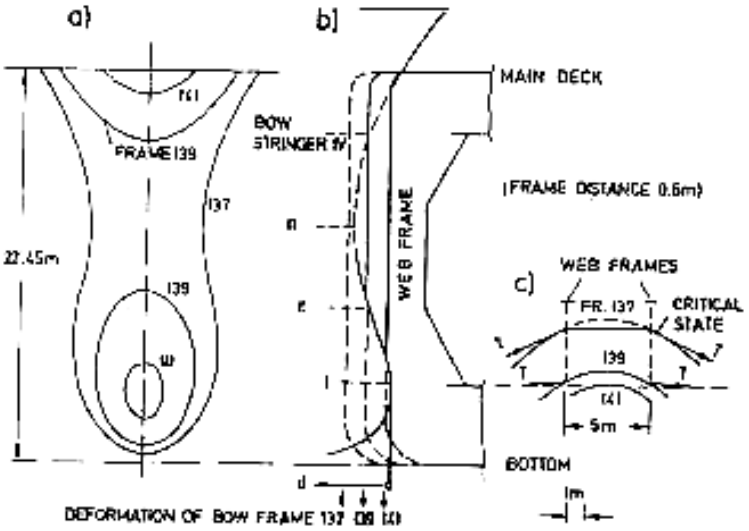

Figure 4.5 – Progress of collision of two equal tankers [58]

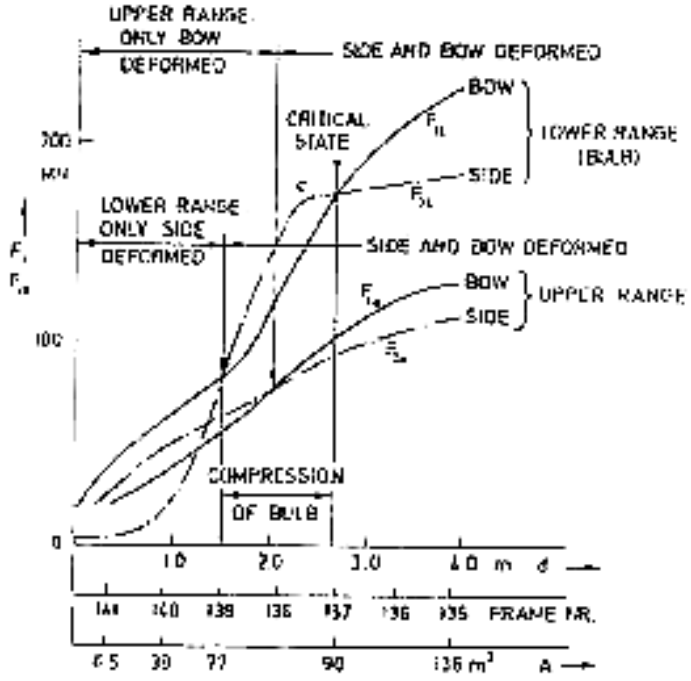

Figure 4.6 - Energy absorption ratios between side and bow [57]

The lower force functions, $F_{il}(d)$, show the same behavior as in Figure 4.4 (side collapses first). The upper force functions, $F_{iu}(d)$, show the opposite tendency (bow collapses first) in the first collision phase.

The collision process advances essentially in two phases, as shown by comparing the force functions of Figure 4.6. In the first phase, the bulb squeezes into the side hull and begins to activate membrane stresses until cross-section 139 is loaded (end of first phase). In the same phase, the undeformed upper side of the struck ship compresses the upper structure of the bow.

In the second phase, the bulb is deformed and intrudes simultaneously into the side hull in which the membrane stresses are activated more and more until, in point (c) of the $F_{21}(d)$ curve, they are nearly exhausted.

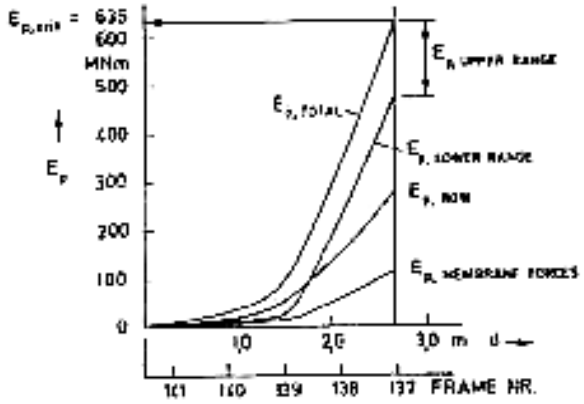

Figure 4.7 - Plots of energy absorbed [57]

Figure 4.7 shows absorbed energy, plotted against d. The E_p curve for the lower range rises sharply after cross-section 139 comes into contact, so that the predominant percentage (86% of the total energy in the critical state) is absorbed in the second phase. The percentages of the total energy absorbed in the individual component groups can be sub-divided as follows:

Energy absorbed in hull of side structure by membrane action	18 %
Energy absorbed in web frames, deck, bottom, etc of side structure	40 %
Energy absorbed in bow structure	42 %
Or for both the collision opponents together;	
Energy absorbed in structures of the lower range	75 %
Energy absorbed in structures of the upper range	25 %

Table 4.1 - Energy absorption in striking bows

This study shows that 42% of the total absorbed energy is absorbed in the bow structure, and a relatively low percentage of the energy (18%) is absorbed by membrane tension in the side structure. In this case, the bow absorbs a significant fraction of the total energy. It is not rigid.

4.4 EXPERIMENTAL RESULTS [31, 66]

Valsgard and Pettersen [66] use a two-step finite element analysis to study the collision resistance of an LNG tanker. This analysis includes a deformable bow modeled using non-linear springs. The stiffness of these springs is adjusted to match experimental results. The first part of the analysis considers side shell penetration using a Side Shell Membrane Model (SSMM). After rupture of the side shell, continued penetration of the deck and bottom structure is modeled using DOBL. Results are presented in Table 4.2.

EVENT	RELATIVE BOW STIFFNESS	STRIKING SHIP MASS (TONNES)	E_{BOW}	E_{TOTAL}	% OF E_{TOTAL} ABSORBED BY THE BOW
First Side Rupture	actual	126,000	62.200	69.860	89.03 %
Max. Coll. Force			68.140	78.580	86.71 %
Final Side Rupture			84.450	108.730	77.67 %
Tank Contact			84.450	123.330	68.47 %
Tank Rupture			84.450	135.230	62.45 %
First Side Rupture	10 x actual	126,000	1.740	3.760	46.27 %
Max. Coll. Force			9.530	26.030	36.61 %
Final Side Rupture			10.830	33.950	31.89 %
Tank Contact			10.830	41.450	26.12 %
Tank Rupture			10.830	53.350	20.29 %

Table 4.2 Energy Absorption in the Striking Ship [66]

Table 4.2 shows that the percentage of the total energy absorbed by the bow of the striking ship is dependent on the stiffness of the bow to a large extent. As the stiffness of the bow is increased, there is a decrease in the percentage of the total energy absorbed by

the bow. The assumption of an infinitely stiff bow, where the energy absorbed by the bow is neglected, is not valid in this case.

4.5 MINORSKY CALCULATIONS

Table 4.3 presents data for collision cases from Reardon and Sprung [63] that were originally from Minorsky. In Minorsky's original calculations he included damage and absorbed energy in the striking ship bow. Minorsky calculated the total absorbed kinetic energy to be:

$$\frac{\Delta_A \Delta_B}{1.43\Delta_B + 2\Delta_B}(V_B Sin\theta)^2 \quad \textbf{(4.1)}$$

Where:

Δ_A is the displacement of the struck ship;

Δ_B is the displacement of the striking ship;

V_B is the striking speed;

θ is the collision angle

Minorsky's values for energy absorbed by the striking ship bow which are not provided in the open literature can be calculated by subtracting the energy absorbed in the struck ship from the total kinetic energy. The damage volume in the struck ship is estimated using the formula:

$$D_{vol} = Nwdt \quad \textbf{(4.2)}$$

Where:

D_{vol} damage volume in the struck ship, in m^3;

w damage width in m; (from [63])

d Damage depth in m; (from [63])

t thickness of decks, assumed at 0.021m;

N number of decks damaged in the struck ship; (from [63])

MINORSKY COLLISION CASE		Mass (tonne)	N	T (m)	V (m/s)	θ(deg)	W (m)	D (m)	H (m)	D vol (Struck) m^3	R_T (m^3)	KE From V (MJ)	KE Given (MJ)	KE from R_T (MJ)	KE Struck (MJ)	KE Striking (MJ)	% Striking
10	**Esso Greensboro**	22150	1	0.021	7.72	90	18.3	18.3	11.9	7.03	7.65	360.24	360	388.72	331.17	29.07	8.07
	Esso Suez	19813			7.72					0							
11	**Tullahoma**	22252	2	0.021	514	90	6.1	7.62	11.9	1.95	2.45	181.66	182	143.80	144.75	36.91	20.32
	P&T Adventurer	9043			7.2					0							
21	**Gulf Glow**	22252	2	0.021	0	65	6.1	11.6	12.2	2.97	3.73	227.43	227	204.08	181.21	46.22	20.32
	Imperial Toronto	16257			7.2					0							
22	**Mojave**	5690	2	0.021	5.14	70	8.53	7.01	11.3	2.51	2.98	122.36	122	168.76	103.12	19.24	15.72
	Prometed	16257			7.2					0							
38	**Catawba Ford**	22150	1	0.021	5.14	90	8.23	3.05	8.53	0.53	0.8	46.56	46.7	66.08	30.68	15.88	34.11
	Hoegh Clair	6706			4.11					0							
46	**David E Day**	8840	2	0.021	8.38	55	10.7	5.18	14.6	2.33	2.67	187.40	187	154.16	163.38	24.01	12.81
	Marine Flyer	20728			8.49					0							
B	**Texanita**	63100	3	0.021	7.72	50	24.4	7.62	13.1	11.71	12.5	981.48	979	617.15	919.73	61.76	6.29
	Osweto Guardian	112000			8.23					0							
G	**African Pioneer**	18900	1	0.021	7.72	45	24.4	9.14	10.1	4.68	9.99	435.23	435	498.93	204.03	231.19	53.12
	Delta Norte	58700			9.77					0							
H	**Galvenston**	640	1	0.021	6.94	60	4.57	3.66	4.36	0.35	0.47	9.32	9.31	50.537	6.96	2.35	25.27
	Atticos	17500			5.4					0							
I	**President Washington**	57400	1	0.021	3.09	90	32.2	16.8	12.2	11.36	11.9	275.75	276	588.89	263.24	12.51	4.54
	Hanjin Hongkong	28200			5.14					0							

Table 4.3 – Percentage of energy absorbed by striking ship

Energy absorbed by the struck ship is given by:

$$KE_{struck} = \frac{D_{vol}}{R_T} KE_{given} \tag{4.3}$$

The percentage of energy absorbed by the striking ship is calculated to be:

$$\% \text{ Striking } = \frac{\text{KE}_{\text{given}} - KE_{struck}}{KE_{given}} * 100 \tag{4.4}$$

It is observed that in all the cases, the percentage of energy absorbed by the striking ship is significant and is not constant. This supports the hypothesis that the striking bow absorbs significant energy in a collision and hence the universal assumption of a rigid bow is not valid.

Chapter 5 An overview of FEMB,LS-DYNA3D and PostGL

5.1 Introduction

The three basic software packages used in the present study for pre-processing, simulating and post-processing the finite element collision models are eta (Engineering Technology Associates) FEMB (Finite Element Model Builder), LS-DYNA3D and eta-PostGL. This chapter provides a brief introduction and description of the basic concepts that are necessary to understand and use this software.

5.2 Features of the Pre-Processor, FEMB 26 NT

FEMB (Finite Element Model Builder) version 26NT is a finite element pre-processor for use with LS-DYNA. FEMB's CAD interface allows the input of CAD line data from CAD packages like AutoCAD. Once the CAD line data is received, FEMB is used to manipulate both line and surface data. If CAD data is not available, the Geometry Builder in FEMB can be used to create points, lines, splines and surfaces and build a finite element model. It is very difficult to mesh surfaces manually with fine mesh models. Auto Meshing is one of the key features of FEMB that is critical to the development of large conventional-element bow models. This feature does not require common end-points or intersections between lines.

A variety of finite element pre-processor packages are available, but FEMB 26 NT is designed specifically for LS-DYNA, and is most suitable for pre-processing the bow models required for analysis in this study. All material models supported by LS-DYNA are available in FEMB. FEMB is used to develop the various bow models for the study, starting from a line drawing to the development of a detailed finite element model that includes the definition of element properties, material properties, contact interfaces, initial conditions and boundary conditions.

5.2.1 Mesh Generation

The development of a reliable finite element model depends on the FE mesh size, density and continuity. A mesh that is not sufficiently dense, or has discontinuities, may lead to unpredictable problems and incorrect results. Mesh generation is the most important stage in the development of a good finite element model. The various commands within FEMB's element menu can be used to generate a finite element mesh that is free from these problems.

Auto-Meshing is one of the key features of FEMB that is critical to the development of the conventional element bow models. Auto-meshing doesn't require creating elements manually from node data. This reduces the time required to mesh trimmed and standard IGES surfaces.

The various mesh-editing tools in FEMB are used to manipulate displayed elements. This includes such as splitting, coarsening, copying, mirroring, reversing element-normal, changing connectivity and renumbering elements. Other tools can be used to project F.E. meshes onto surfaces, an existing mesh or a plane. Tools can be used to scale, move, rotate, reflect and copy partial or entire models.

5.2.2 Material Properties

Material properties are directly assigned to the currently displayed part of the model, without the user having to enter data in LS-DYNA CARD or KEYWORD format. Pop-up menus appear at specific junctions in the session, prompting for material/element properties. This allows for the assignment of specific materials and properties to the F.E. model as a whole or in parts.

Currently FEMB supports the nineteen LS-DYNA material types listed:

Material Number	Material Title	Bricks	Beams	Thin shells	Thick shells	Strain-Rate Effects	Failure	Equation of state	Thermal effects	NOTES Gn General Fl Fluid Cm Composites Mt Metal Pl Plastic Rb Rubber
1	Elastic	Y	Y	Y	Y					Gn, Fl
2	Orthotropic Elastic	Y		Y	Y					Cm, Mt
3	**Plastic Kinematic/Isotropic**	**Y**	**Y**	**Y**	**Y**	**Y**	**Y**			**Cm, Mt, Pl**
6	Linear Viscoelastic	Y	Y	Y		Y				Rb
7	Blatz-Ko Rubber	Y		Y						Rb, Polyurethane
12	Isotropic Elastic Plastic	Y		Y	Y					Mt
20	**Rigid**	**Y**	**Y**	**Y**	**Y**					
24	Piecewise Linear Plasticity	Y	Y	Y	Y	Y	Y			Mt, Pl
26	Honeycomb	Y				Y	Y			Cm, Fm, Fl
27	Mooney-Rivlin Rubber	Y		Y						Rb
37	Transversely Anisotropic Elastic Plastic			Y	Y					Mt
57	Low Density Urethane Foam	Y					Y	Y		Fm
66	Linear Elastic Discrete Beam		Y				Y			
67	Nonlinear Elastic Discrete Beam		Y				Y	Y		
68	Nonlinear Plastic Discrete Beam		Y				Y			
69	SID Damper Discrete Beam		Y				Y			
70	Hydraulic Gas Damper Discrete Beam		Y				Y			
71	Cable Discrete Beam (Elastic)		Y							
75	Bilkhu/Dubois Foam (Isotropic)	Y					Y			Fm

Table 5.1 – LS-DYNA Material types available in FEMB [23]

Of these materials, the ones shown in bold are the ones that are used in the various bow models developed in this study.

5.2.3 Contact Interface

The Interface Menu option within FEMB's Main menu allows the user to create and assign sliding or rigid wall interfaces for LS-DYNA applications. Once the interface type is defined, the contact type is easily edited and modified to simulate the actual collision. The *CONTACT section in the input allows the user to define many different

contact types. These contact options are for treating the contact of deformable bodies, single surface contact in deformable bodies, and deformable body to rigid body contact. The type of interface can be defined directly within FEMB, without the user having to enter the input in KEYWORD format.

5.2.4 Specifications/database limitations

Currently FEMB has the following specifications/limitations per database:

200,000	POINTS
100,000	LINES
2,500	SURFACES
100,000	EDGE POINTS (SURFACE)
150,000	CONTROL POINTS (SURFACE)
100,000	GRIDS
225,000	ELEMENTS (Full Version)
10,000	ELEMENTS (Student Version)
1,000	PROPERTIES
1,000	PIDS
225,000	NODES

5.2.5 Line data

FEMB converts and filters the following (optional) line data to FEMB neutral line format directly:

IGES (line and surface)

DXF (line data file format)

PDGS (standard format)

5.2.6 Recommended Practice (.fmb, .his, .lin, .bin, etc.)

To open/read files while in the FEMB program, the user should select File/Open from the Main Menu bar. Specific file types would be listed within the Pop-Up menu. The following extensions for specific file types is recommended:

- FEMB database file name: *filename*.**fmb**
- FEMB line data file name: *filename*.**lin**
- IGES line/surface data name: *filename*.**igs**
- DXF line data name: *filename*.**dxf**
- PDGS line data: *filename*.**pdgs**

When reading a line data file into FEMB, the user should select File/Open from the Main Menu bar. By default, all existing FEMB database files (*.fmb) will be listed. Beneath the list of FEMB database files, there is a prompt for FILES OF TYPE. If the user selects FEMB line data, all file names in that directory with the extension .lin will be listed. The user may then select the appropriate file name. The user may choose ALL FILES to display files with different extensions than those listed above.

5.2.7 Local coordinate system

FEMB refers to the local or global coordinate system to translate, rotate, mirror, copy and generate points, lines, nodes and elements. When such a function is selected, the program automatically prompts the user to generate a local coordinate system designated as the U, V, W, coordinate frame.

One, two, or three reference points are required to establish a local coordinate system. The first reference point defines the local origin. For a three point system the second reference point defines the direction of the local U axis which is extended from the first reference point. The third reference point, along with the first two reference points, defines the local U-V plane. The local V axis is defined in the U-V plane and perpendicular to the U axis. The local W axis is then defined according to the right hand rule perpendicular to the U-V plane. For the two-reference point option, End Select should be selected after the second reference point is defined. The local W axis lies along the vector from the origin to the second reference point and the V axis lies in the V-W plane. The U axis is defined by the right hand rule.

All rotational commands (i.e., generating arcs, copy with rotating, etc.) execute around the local W or global Z-axes.

For a one-reference-point system, the user selects a point or node on the screen as the local origin, and then selects one of the X, Y, or Z options available to define the local W axis along one of the global axes.

5.2.8 Getting started with FEMB

There are three basic scenarios that the user will encounter when starting FEMB:

- Supplied CAD line/surface data is read into FEMB.
- Supplied model data (e.g., LS-DYNA, etc.) is read directly into FEMB.
- CAD or model data is not supplied so the user starts with an empty database and generates or 'digitizes' line data from a drawing.

5.2.9 Getting started with CAD data

In the LS-DYNA program manager, FEMB is started by clicking the Pre-/Post-Processing button, or by pulling down the Builder/Viewer menu and selecting the Pre-/Post-Processing menu item.

When reading a line data file into FEMB, by default all existing FEMB database files (*.fmb) will be listed. Beneath the list of FEMB database files there is a prompt for FILES OF TYPE. The user may select FEMB line data. All file names in that directory with the extension .lin will be listed. The user may then select the appropriate file name. Once the appropriate file has been selected, FEMB will create a database called UNKNOWN.fmb containing the selected line data. The user may then save the database under a new name. File types are read in directly without external translation.

When reading model data (LSDYNA type .dyn) into FEMB, by default, all existing FEMB database files will be listed. Beneath the list of FEMB database files there is a prompt for LIST OF FILE TYPE. The user may select the desired file type. All file names in that directory with the extension .dyn will be listed. The user may then select the appropriate file name. Once the appropriate file has been selected FEMB will create a database called UNKNOWN.fmb containing the selected file type data. The user may then save the database under a new name. File types are read in directly without external translation.

In case CAD line data or model data from LSDYNA is not available, the user will need to digitize a drawing thus generating one's own line data. The line data can then be modeled using FEMB. Once FEMB is started as described above, a window pops up listing FEMB database files with the extension .fmb. Enter a new file name.

- The first thing that needs to be done is to create a new part in the Part Menu. FEMB will not allow entities to be created in an empty database unless there is an existing part for the information.
- Upon creating a new part, the user will be prompted, via Pop-Up window, to define/assign material and element property. The user may either assign properties or disregard this prompt by selecting the Cancel/End button. Once a part has been created, the next step is to generate the desired line data.
- Enter the Geom Menu (Geometry Builder).
- Select the Generate Lines command and click the right most mouse button for the available options.
- Select KEY IN X, Y, Z if the coordinates of the line are known.
- Once this is done the prompt will ask for the X, Y, Z coordinate. The prompt will keep asking for the coordinates until you select End Select.

The user may continue generating line data or executing the other CAD functions available in the menu.Generating a finite element model from line data is described in Element Options (ELEM).

5.2.10 Main menu

This is the first menu the user sees when FEMB starts. The 15 initial options will open an additional series of menus. The functions in the Main Menu are organized as follows:

File - FILE MANAGER
Geom - GEOMETRY BUILDER
Surf - SURFACE MENU
Elem - ELEMENT OPTIONS
Node - NODE OPTIONS

Check - MODEL CHECKER

Part - PART CONTROL

Matl - MATERIAL PROPERTY

Prop - ELEMENT PROPERTY

I.F. - INTERFACE MENU

B.C. - BOUNDARY CONDITIONS

Set - LOAD SET

Help - “ABOUT” WINDOW

Figure 5.1 shows how the FEMB’s main menu looks and also, how the important icons in the main menu look, and where they are located.

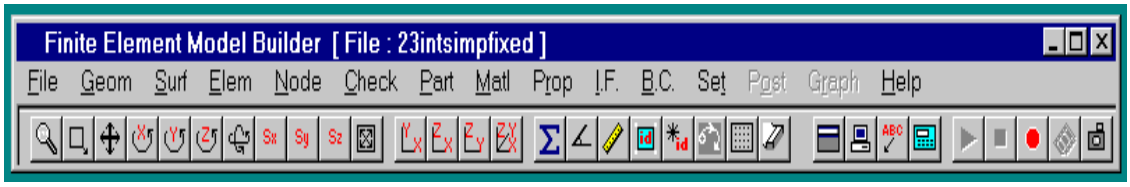

Figure 5.1 - Main Menu of FEMB

5.2.10.1 File menu

The options available in the File menu allow the user to input (open) data to or output (save) data from FEMB. The user has the ability to input LS-DYNA, IGES, DXF, LS-DYNA animation/graph data, and FEMB line data formats.

FILES OF TYPE allows the user to specify the type of file to open/save. The available file types are:

FEMB Database	*.fmb
FEMB Line	*.lin
LS-DYNA	*.dyn, *.dat
NASTRAN	*.nas
IGES	*.igs, *.iges
IDEA-S Universal	*.unv
DXF	*.dxf

5.2.10.2 Geometry builder menu

The functions of the Geometry Builder Menu are used to create a new set of line data or modify existing line data. FEMB has 100,000 lines or 200,000 points per database limitation. Figure 5.2 shows the important features of the Geometry-builder.

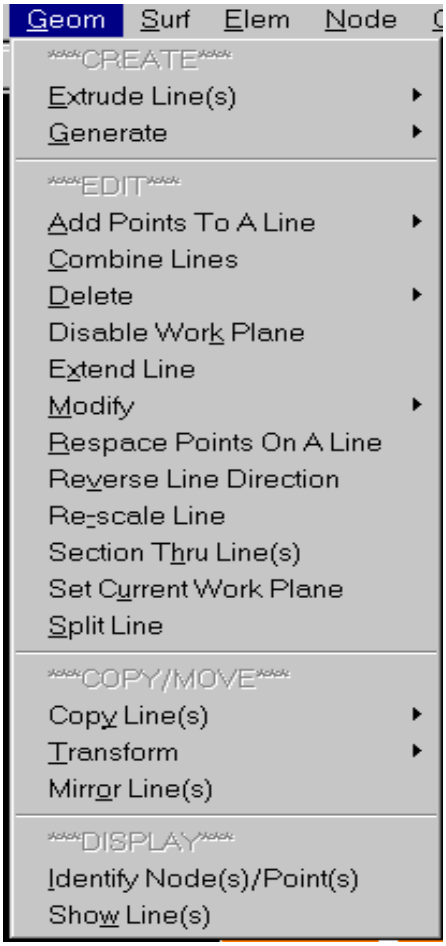

Figure 5.2 – Geometry Builder Menu of FEMB

5.2.10.3 Surface menu

The functions in the Surface menu allow the user to create and modify surfaces in a FEMB database. The IGES translator is updated to convert IGES surface data into FEMB format. FEMB line data file format is expanded to include surface data. Figure 5.3 shows the surface menu of FEMB and all the important functions available in this sub-menu.

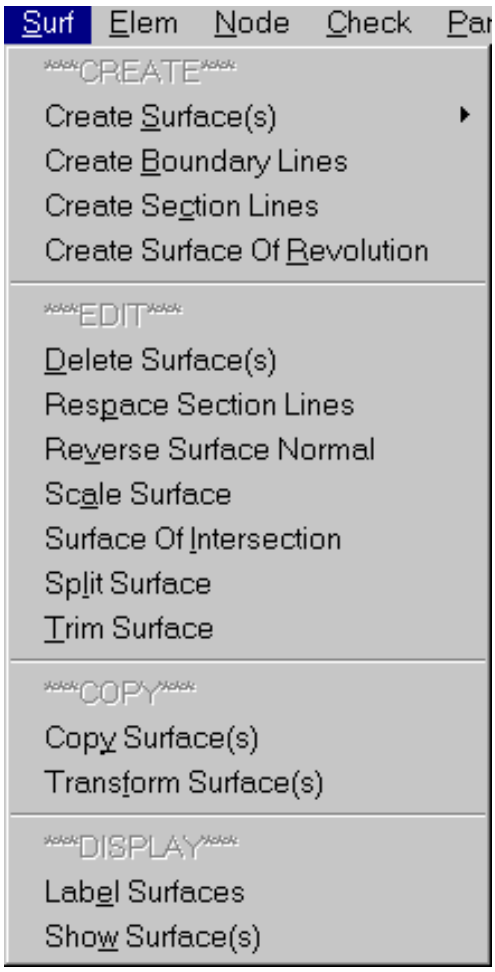

Figure 5.3 – Surface Menu of FEMB

5.2.10.4 Element menu

The Element Menu contains commands used to create and modify elements. Elements, the basis for finite element modeling, are created from within this menu. The user can create elements through Surface Mesh, which automatically meshes IGES surfaces substantially faster than creating a mesh by hand. The Line Mesh and Line Solid Mesh options create plate and solid elements via line data selection, respectively. Elements can be modified to suit a particular model by using commands such as Modify, Split and Coarse elements. Figure 5.4 shows the key features available in the element menu

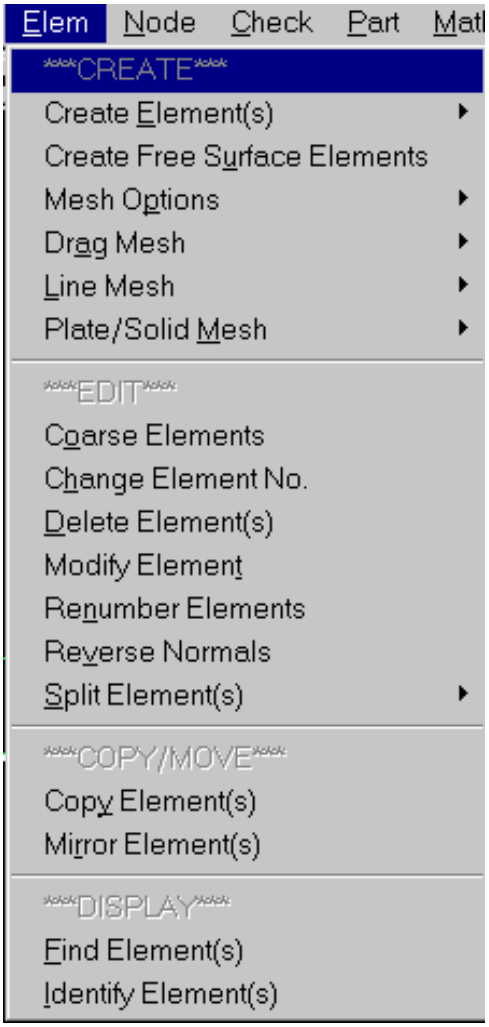

Figure 5.4 – Element Menu of FEMB

5.2.10.5 Node

The functions in this menu are used for node related operations. Two types of nodes are defined in FEMB. The referenced nodes (connected by elements) are represented by dots (•) and the un-referenced nodes are represented with asterisks (*). Useful applications include moving nodes (node to node or node to point), checking for and merging common or coincident nodes, transforming and rotating nodes, etc. Figure 5.5 shows the salient features and functions available in the node menu of FEMB.

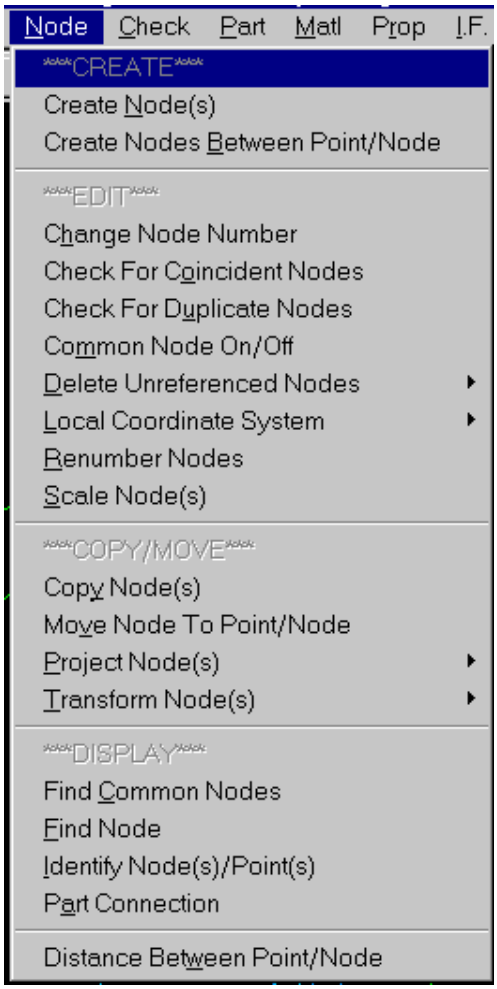

Figure 5.5 – Node Menu of FEMB

5.2.10.6 Check

The Check Menu is used to validate FEMB models. The criteria values for model validation are set to defaults in FEMB but may be adjusted to suit the user's needs. Element orientation, size, skewness, connectivity and interior angles are compared to the specified criteria. Figure 5.6 shows the salient features and functions available in the Check menu of FEMB.

Figure 5.6 – Check Menu of FEMB

5.2.10.7 Part

The functions of the Part Control Menu are intended to organize line, surface, and element data in a structure. A part is a set of lines, surfaces and/or elements grouped under a part name. The part name is defined as a label consisting of alpha and/or numeric data no more than eight characters long. Presently, up to 1000 parts may be defined in a database. Each part has a unique part identification number, PID. Figure 5.7 shows the salient features and functions available in the part menu of FEMB.

Figure 5.7 – Part Menu of FEMB

5.2.10.8 Material property

The functions in this menu are designed to define and modify material properties in the database. Once a Material Property menu function is selected, the displayed parts are shown in the property color. The parts that do not have material properties defined are shown in white upon entering the Material Property menu. All subsequent materials assigned and created will be LS-DYNA specific. The user may assign and create materials at the beginning or end of a FEMB session. Figure 5.8 shows the salient features and functions available in the material menu of FEMB.

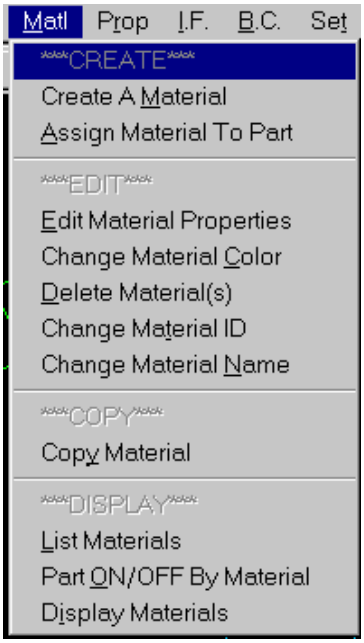

Figure 5.8 – Material Menu of FEMB

5.2.10.9 Element property

The functions in this menu are designed to define and modify the element (physical) properties in the database. Once the Element Property Menu is selected, the displayed parts will be shown in the property color. Parts without property definitions will be shown in white. The element properties created will be LS-DYNA specific. The user may assign and create materials at the beginning or end of the FEMB session. Figure 5.9 shows the salient features and functions available in the element property menu of FEMB.

Figure 5.9 – Element Property Menu of FEMB

5.2.10.10 Interface menu

The functions in the Interface Menu define and modify contact interface data (sliding and rigidwall) for LS-DYNA analysis. The functions are organized as below. Once the Interface Menu is selected, the actives (on) interfaces are displayed with the active parts. Figure 5.10 shows the salient features and functions available in the interface menu of FEMB.

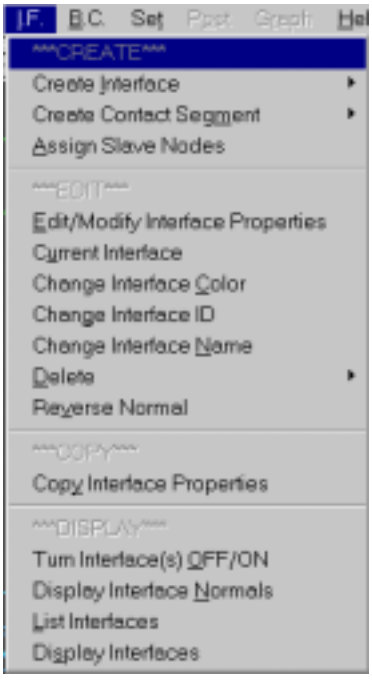

Figure 5.10 – Interface Menu of FEMB

The master segments are drawn as interior outlines of the elements where the segments are defined and labeled as “M”. The letter “M” is labeled in color filled squares. The slave segments are drawn similarly to the master segments except that they are labeled with a “S”.

5.2.10.11 Boundary conditions

The functions of the BOUNDARY CONDITIONS MENU create and verify constraints and loads and define initial velocities on finite element models. Figure 5.11 shows the salient features and functions available in the BC menu of FEMB.

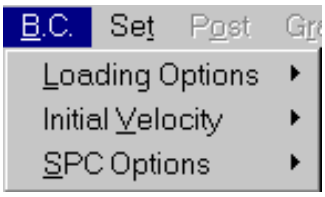

Figure 5.11 – Boundary Conditions Menu of FEMB

5.2.10.12 Display properties

The Display Properties Menu is accessible through its icon on the tool bar. It is a menu of toggle switches, which allow the user to select from various ways to display information contained in the FEMB database.

5.3 LS-DYNA VERSION 950

LS-DYNA is a general-purpose, explicit finite element program used to analyze the nonlinear dynamic response of three-dimensional inelastic structures. Its fully automated contact analysis capability and error-checking features have enabled users worldwide to solve successfully many complex crash and forming problems [23,24,25].

The basic procedure for working with the LS-DYNA package is to:

- Use the pre-processor to create a desired model.
- Run LS-DYNA to solve a simulation using the model.

- Use the post- and/or graph-processor to obtain/review the simulation results.

The components for working with the LS-DYNA package are located within a "Program Manager", a basic "starting point" screen for the program. The menu bar and toolbar of the LS-DYNA Program Manager screen are shown below. The buttons on the toolbar are shortcuts for the most frequently used operations in LS-DYNA. Figure 5.12 shows the main menu of LSDYNA 3D.

Figure 5.12 – Main Menu of LS-DYNA 3D

5.3.1 Sense switch controls

Sense switches are control points that are used to interrupt the LS-DYNA program to retrieve useful information in the midst of a simulation run. This is done by first typing a "^C" (Control-C), which sends an interrupt message to LS-DYNA which is trapped, and the user is prompted to input (type in) the sense switch code. LS-DYNA has four terminal sense switch controls:

SW1 A restart file is written and LS-DYNA terminates.
SW2 LS-DYNA responds with time and cycle numbers.
SW3 A restart file is written and LS-DYNA continues.
SW4 A plot state is written and LS-DYNA continues.

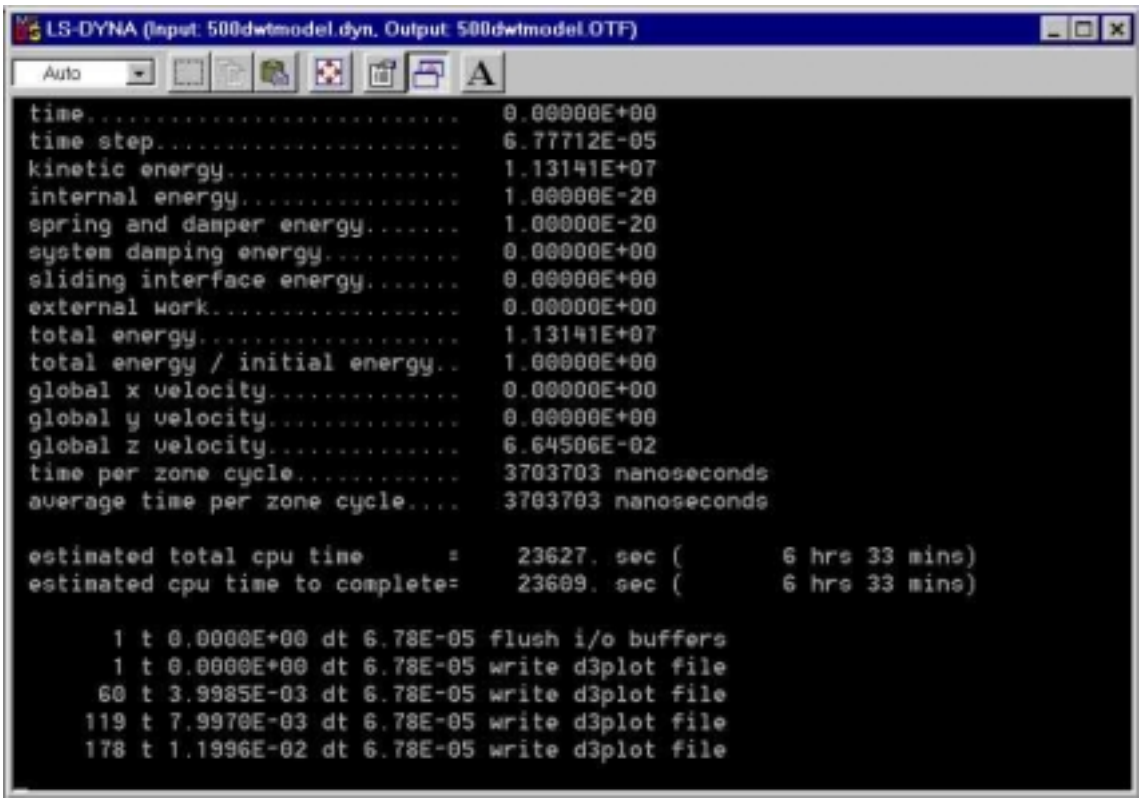

Figure 5.13 - Screenshot of an LS-DYNA run

5.3.2 LS-DYNA contact algorithm

Figure 5.14 shows how contact is defined in LSDYNA 3D. The dots indicate slave nodes and the surfaces are the master segments.

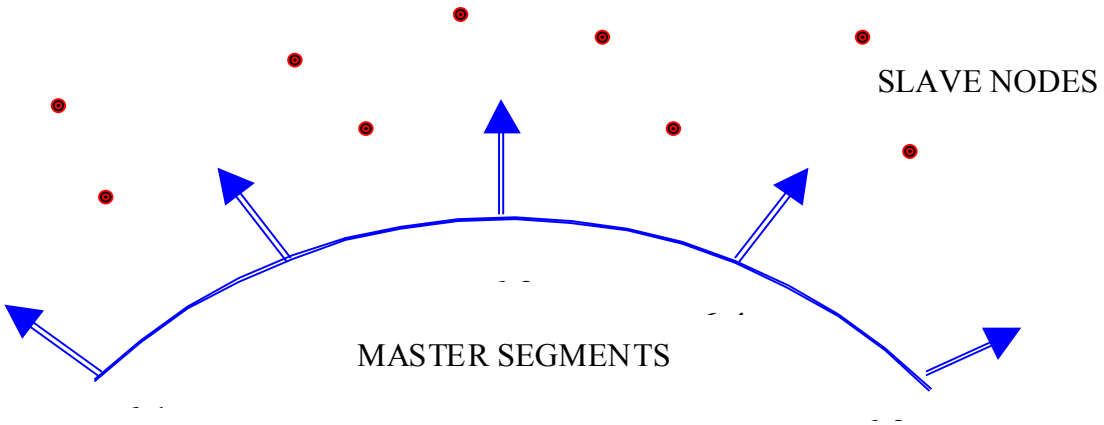

Figure 5.14 – LS-DYNA Contact Algorithm

Slave nodes must always be on the positive side of the master segment normals. Contact type 5 and contact type 10 are one-sided searches whereas contact type 3 is a two-sided search, as described in the example below.

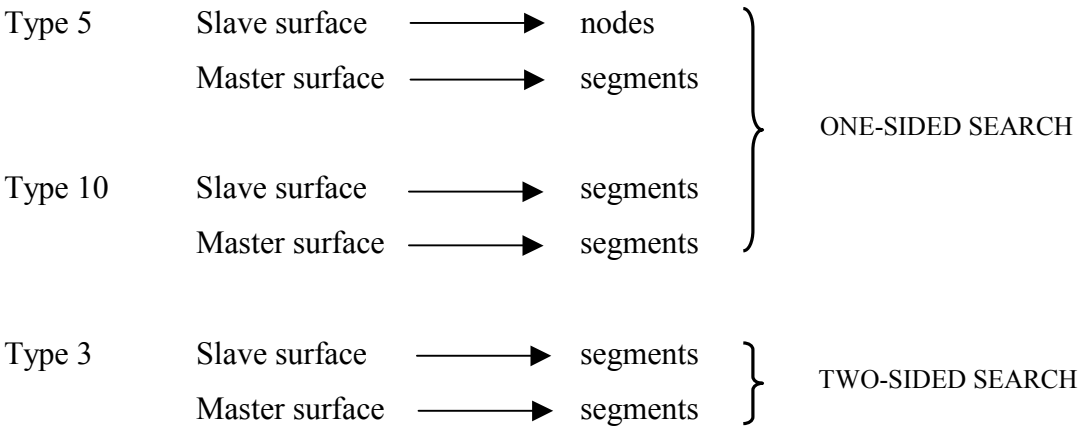

One-sided search:

Slave nodes are prevented from going through the master surface

Ex.: Types 5 and 10

Symmetric search:

Slaved nodes are prevented from going through master segments and vice versa

Ex.: Type 3

For instance, the example below shows the difference between a type 3 and a type 5 contact, in the way these contacts deal with penetration.

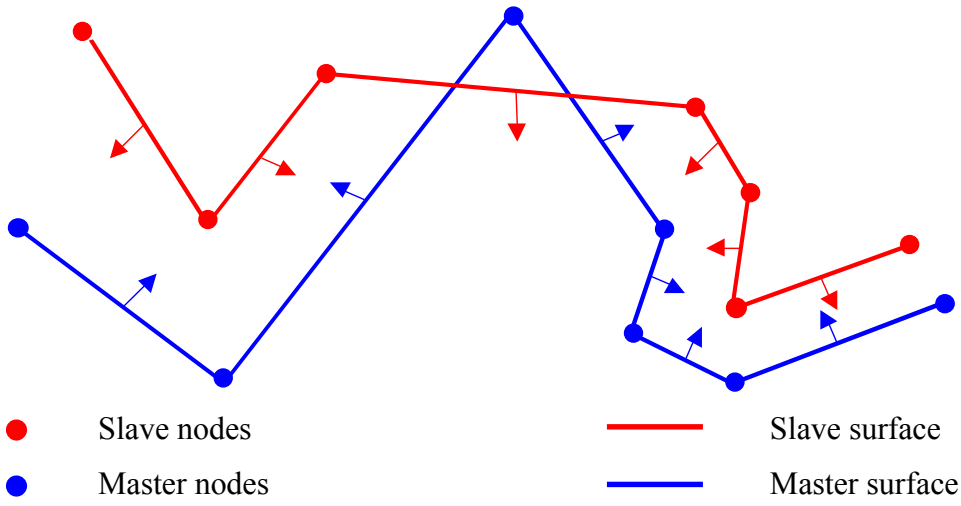

Figure 5.15 – Contact Definition in LS-DYNA 3D

In Figure 5.15, although there is an obvious penetration, type 5 contact ignores this because all it checks for is that the slave nodes are on the positive side of the master segment normal, which they are. On the other hand, type 3 contact would detect this penetration because the master node has penetrated the slave surface.

5.4 Post processor, eta PostGl

eta/PostGL is a general purpose post-processor for use with LS-DYNA. Developed by Engineering Technology Associates Inc., eta/PostGL quickly post-processes result data including the real time animation of stresses, strain energy, displacements and time history curves. Its dynamic allocation of memory optimizes system resources allowing for models up to 250,000 elements and nodes. eta/PostGL™s OPENGL, workstation-quality, 3D graphics add clarity and realism to model animations for easy interpretation of analysis results. Animated frames can number up to 500 for highly detailed analysis. Model animations can be edited using a variety of different functions and saved as an AVI file for use on or over the internet.

eta/PostGL™s interface allows the user to cut and paste plots and graph data directly from eta/PostGL to other windows-based programs. eta/PostGL also allows the

user to drag and drop files and double click on recognized file extensions for easy access of result data. Figure 5.16 shows a screenshot of the post-processor PostGL.

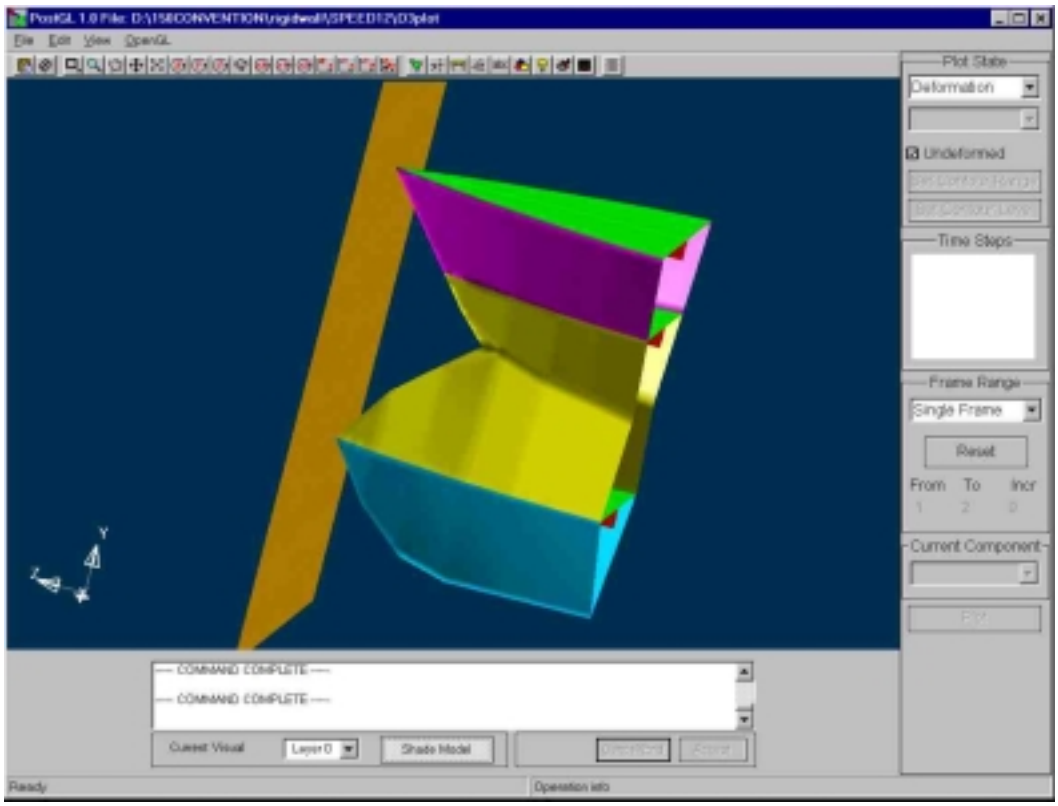

Figure 5.16 - Screenshot of PostGL

The user interface is divided into several parts: the MENU BAR, the TOOL BAR, the GRAPHICS DISPLAY WINDOW, the USER INPUT/OUTPUT WINDOW, and the CONTROL WINDOW. The current geometry/model/graph appears in the graphics display area. Figure 5.3 shows a screenshot of the POSTPROCESSOR.

5.4.1 PostGL/Graph

eta (Engineering Technology Associates) Post-GL/Graph is the Graph processor that comes with FEMB. PostGL/Graph is a general purpose program that is used to analyze the post-processing data in the form of graphs and curves that are plotted using the post-processing information available from the glstat (global statistics) and rcforc (force) files that are outputted by LS-DYNA. Figure 5.3 shows a typical screenshot of the Post-GL program.

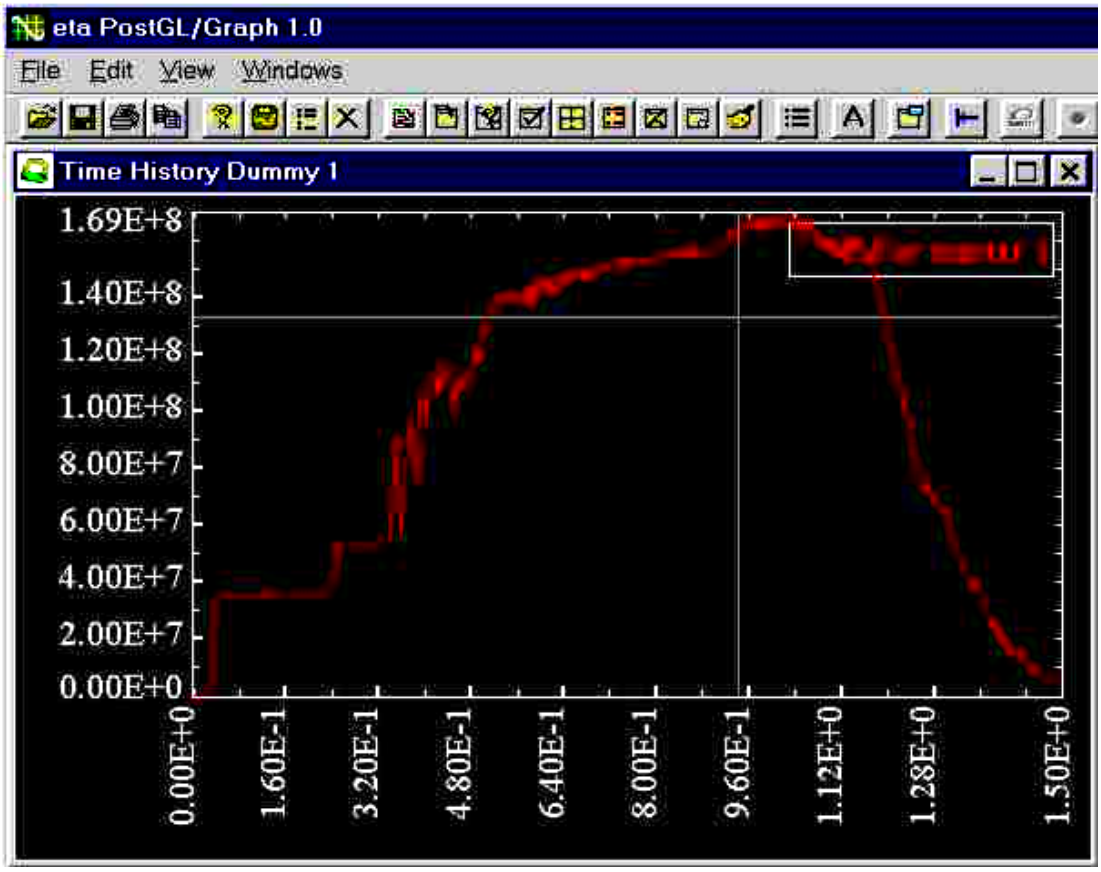

Figure 5.17 - Screenshot of eta PostGL/Graph

Figure 5.17 shows a screenshot of the Graph Processor. Useful curves such as force-penetration curves, energy plots and velocity plots are obtained using PostGL/Graph. Chapter 6 describes in detail, the various bow models developed and used in the simulations.

Chapter 6 Bow and Hull Models Developed in LSDYNA

6.1 Introduction

This chapter describes the methodology used to develop bow and hull models in LS-DYNA. Table 6.1 lists the various models that were developed. The principal characteristics, bow profile, structural design and scantlings for the striking bows and struck tankers used in this study are provided in Section 6.3.2, Section 6.3.3 and Appendix B. The striking ships include a 500 dwt coaster, 23000 dwt containership, 40000 dwt containership and a 150000 dwt bulk carrier. The struck ships include a 150000 dwt double hull tanker (DH150) and a 100000 dwt single hull tanker (SH100).

6.2 Test case matrix

Cases I-1 to I-4 in Table 6.1 use the closed-form Yang and Caldwell equation [70] to calculate force versus deflection for the bows striking a rigid wall at different speeds. This equation sums the force-deflection behavior of individual intersection elements. These calculations are provided in Appendix A. Cases I-5 to I-8 use "intersection"-elements in an LS-DYNA course-mesh finite element analysis to model the bows striking a rigid wall at different speeds. The cross-sectional area of these elements is chosen to duplicate the intersection element stiffness as calculated using the Yang and Caldwell equation [70]. Actual plastic material properties are used, and element areas are calculated to match element terms in Yang and Caldwell. These calculations are also provided in Appendix A.

In Cases I-9 and I-10, the LSDYNA intersection element model of the 23000 dwt containership strikes a conventional SH100 model at 5m/s. The conventional models use a fine mesh and Belytscko-Tsay shell elements. SH100 is fixed in Case I-9 and free-in-sway only in Case I-10. In Cases I-11 and I-12 the LSDYNA intersection element model of the 150000 dwt bulk carrier strikes the conventional DH150 at 5m/s. DH150 is fixed

in Case I-11 and free in sway-only in Case I-12. In Cases I-13 to I-16 the intersection element models for the 23000 dwt containership and the 150000 dwt bulk carrier strike simplified models of SH100 and DH150, fixed and free-in-sway. The simplified struck ship models use a course mesh and Belytscko-Tsay shell elements. Analyses using the simplified struck ship models did not run successfully.

STRUCK OBJECT CONVENTIONAL = FINE MESH FEA SIMPLIFIED = COURSE MESH SUPERELEMENT FEA		BOW MODEL							
		CONVENTIONAL FINE MESH FEA		INTERSECTION ELEMENT COURSE MESH FEA				RIGID	
		23K DWT	150K DWT	500 DWT	23K DWT	40K DWT	150K DWT	23K DWT	150K DWT
RIGID WALL	Closed Form			I-1	I-2	I-3	I-4		
	LS-DYNA	C-1	C-2	I-5	I-6	I-7	I-8		
100K SH TANKER SIMPLIFIED	LS-DYNA Fixed	C-7			I-13				
	LS-DYNA Sway	C-8			I-14				
100K SH TANKER CONVENTIONAL	LS-DYNA Fixed	C-3			I-9			R-1	
	LS-DYNA Sway	C-4			I-10			R-2	
150K DH TANKER SIMPLIFIED	LS-DYNA Fixed		C-9				I-15		
	LS-DYNA Sway		C-10				I-16		
150K DH TANKER CONVENTIONAL	LS-DYNA Fixed		C-5				I-11		R-3
	LS-DYNA Sway		C-6				I-12		R-4

Table 6.1 - Case Scenario Test Matrix

In Cases C-1 and C-2 the LSDYNA conventional model of the 23000 dwt containership and the 150000 dwt bulk carrier strike the rigid wall at two speeds (5m/s and 12m/s). In Cases C-3 and C-4 the conventional 23000 dwt containership strikes the

conventional SH100 at two speeds (5m/s and 12m/s), in fixed and sway-only conditions. In Cases C-5 and C-6 conventional models of the 150000 dwt bulk carrier strike the conventional DH150 at 5m/s, in fixed and sway-only conditions. In Cases C-7 to C-10 the conventional 23000 dwt containership and the conventional 150000 dwt bulk carrier strike the simplified SH100 and DH150, in fixed and sway-only conditions. These cases using the simplified struck ship models also did not run successfully.

In Cases R-1 through R-4 a rigid 23000 dwt containership and a rigid 150000 dwt bulk carrier strike the conventional SH100 and DH100. These tests were run to compare rigid bow collision results in LSDYNA to those calculated using SIMCOL, which also assumes a rigid bow.

6.3 GENERAL MODEL DESCRIPTION

This section describes the general modeling features common to all the cases. A flowchart showing the important steps in developing the various models is shown in Figure 6.1. Section 6.4 discusses the important modeling parameters specific to each of the eighteen cases.

6.3.1 Bow and the Side Structure Drawings

The bow model of the 500 dwt striking bow was created using AutoCAD-R14 and saved as a .DXF file that was later imported to the pre-processor FEMB. This file was then saved as an FEMB line data file (.LIN). After developing expertise in FEMB, the remaining bow models and side-ship models are created using the geometry builder features of FEMB in order to avoid exporting and importing of CAD line data. Principal particulars and dimensions for the striking ships were taken from Pedersen [52], as detailed in Section 6.3.2 and Appendix B. Section 6.3.3 and Appendix B provide characteristics of the struck ships.

6.3.2 Bow Geometry

Various bow models are analyzed as part of this thesis. Four different ships are considered: a 500 dwt coaster, 23000 dwt containership, 40000 dwt containership and a

150000 dwt bulk carrier. The choice of the striking ships is based on the availability of validation results and bow geometry data. 3-D drawings for these bows are created based on the 2-D information available from Pedersen [52], which is detailed in Appendix-B. The basic geometry of the various bows is derived from the scaled drawings of the bows as shown in Figure 6.2, Figure 6.3, Figure 6.4 and Figure 6.5.

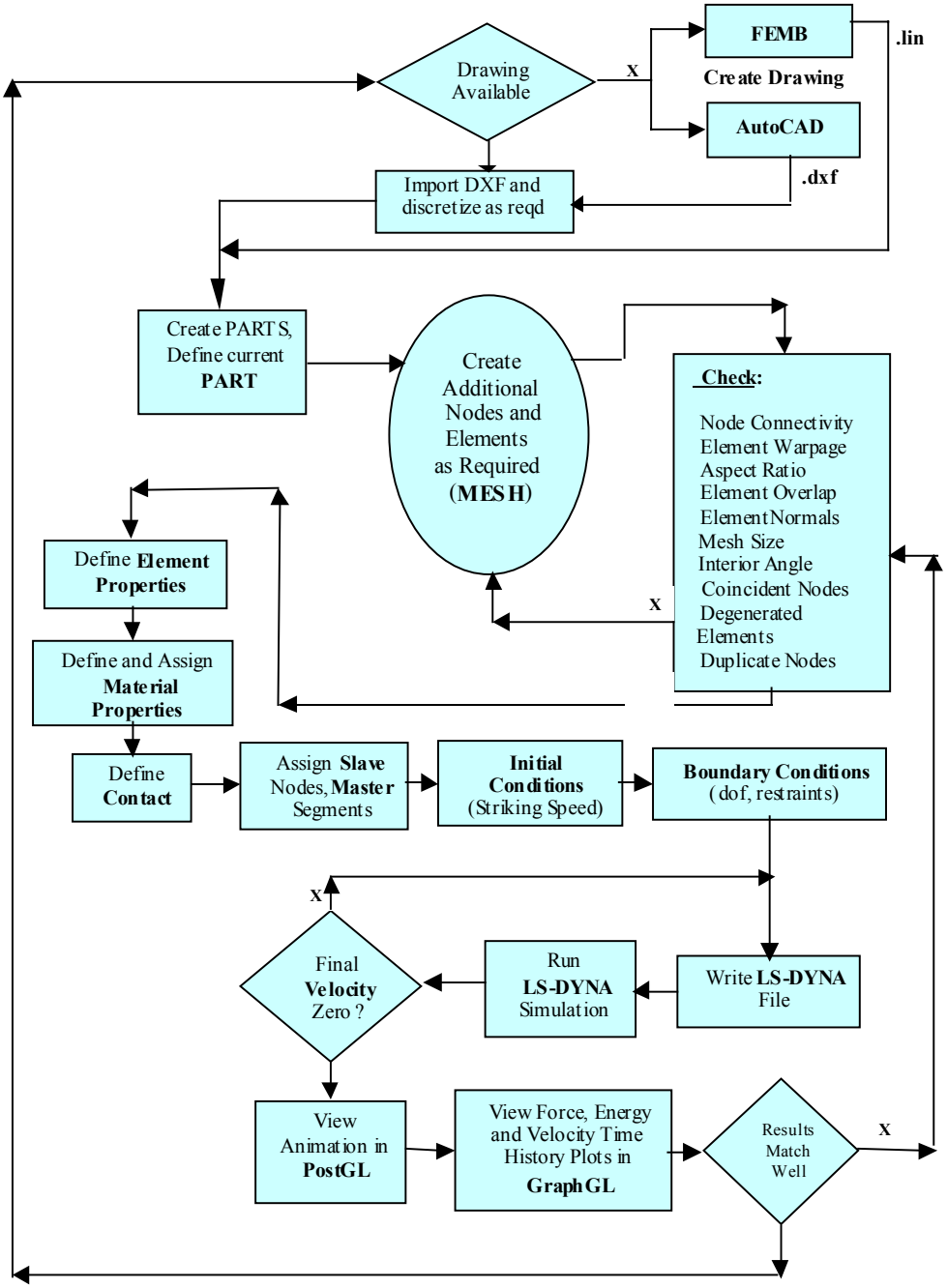

Figure 6.1 – Flowchart for FE Modeling and Simulation in LS-DYNA

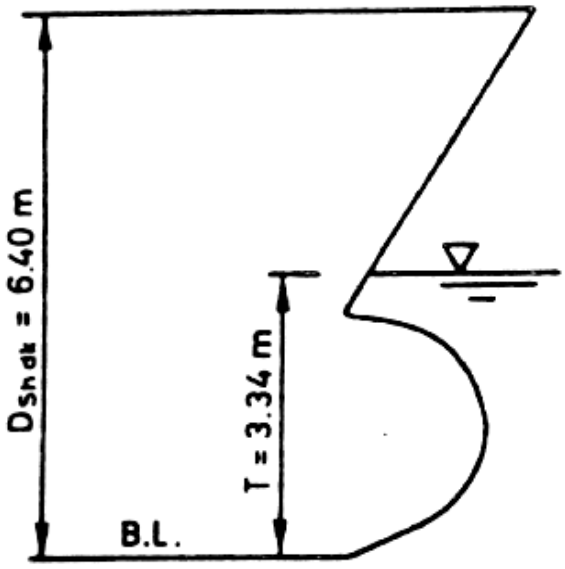

Figure 6.2 – Scaled Drawing of 500 dwt Coaster [52]

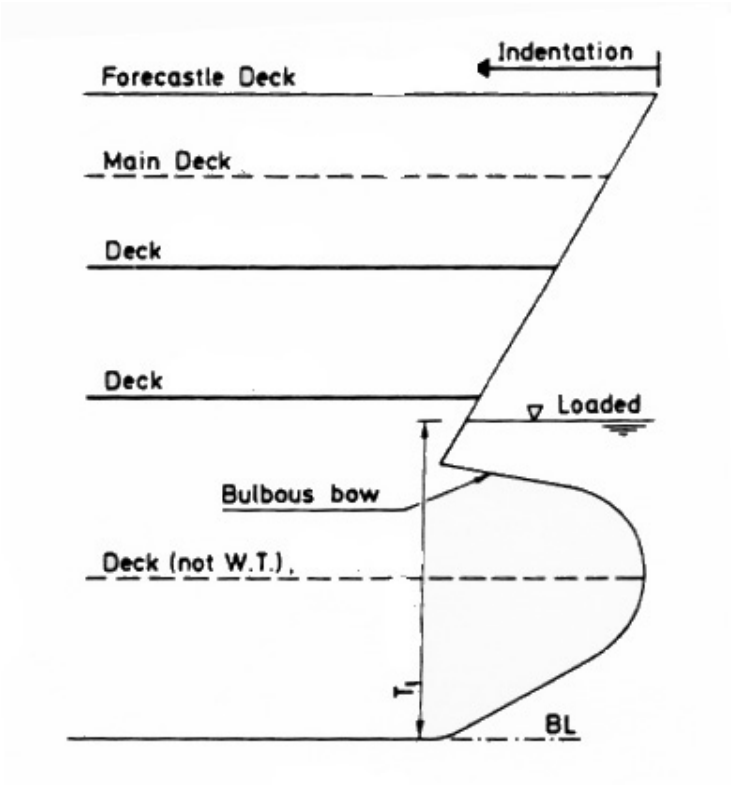

Figure 6.3 – Scaled Drawing of 23,000 dwt Containership [52]

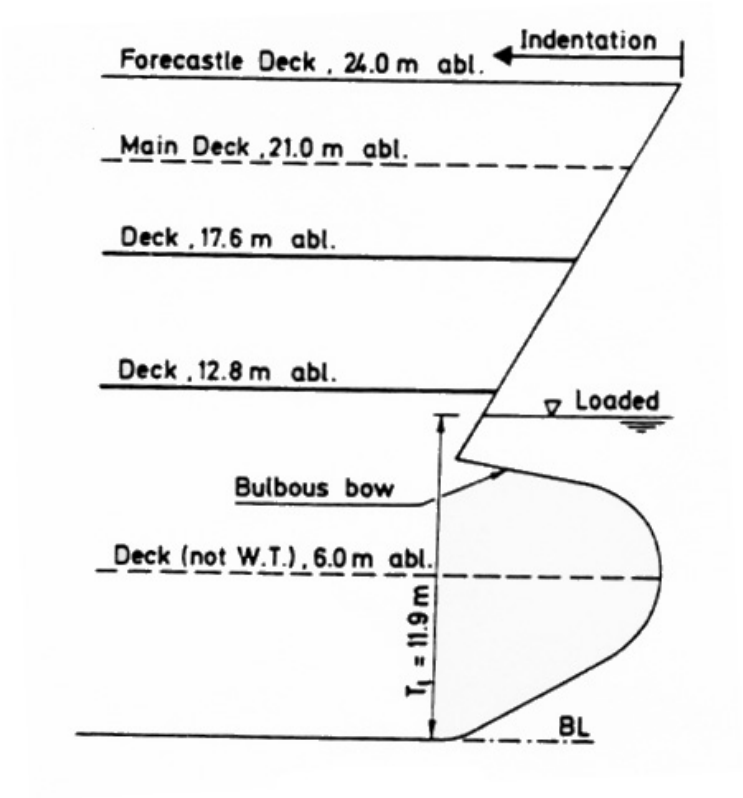

Figure 6.4 – Scaled Drawing of 43,000 dwt Containership [52]

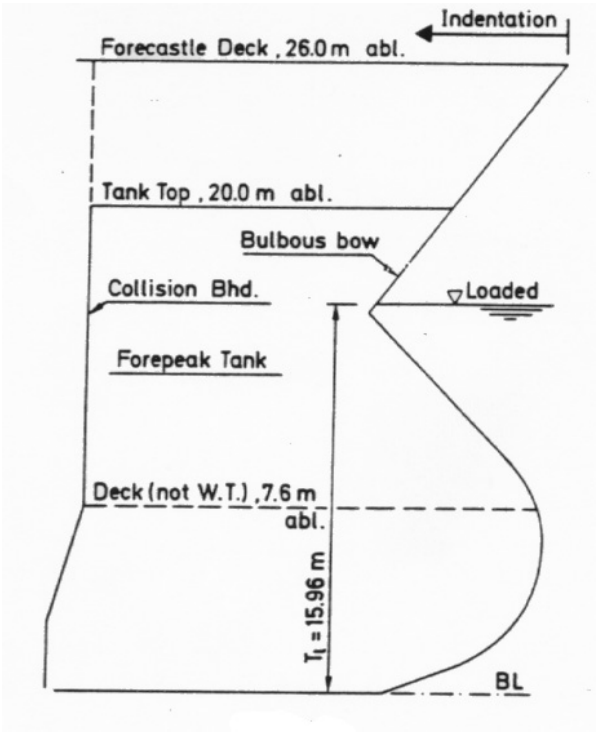

Figure 6.5 – Scaled Drawing of 150,000 dwt Bulk Carrier [52]

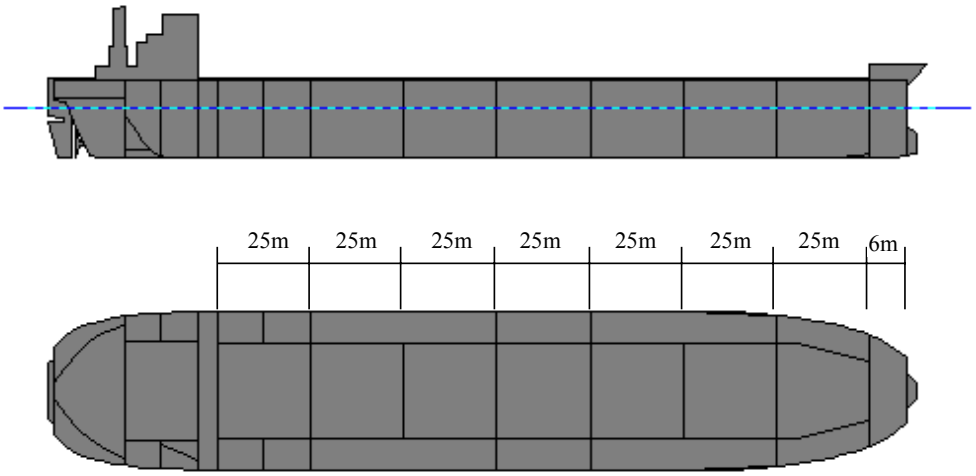

Figure 6.6 (a)– 100K dwt Single Hull Tanker from Kuroiwa (1996) [14]

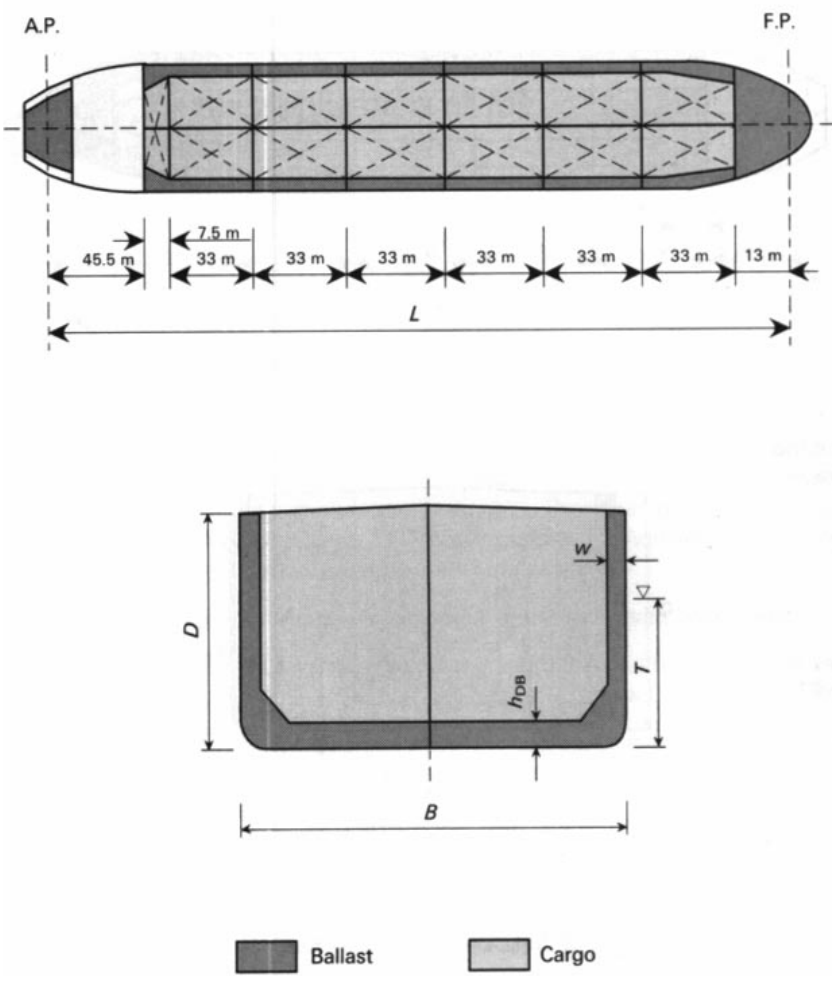

Figure 6.6 (b) – IMO 150K dwt Double Hull reference Tanker [15]

Ship		150,000 dwt double hull tanker	100,000 dwt single hull tanker
Web Frame Spacing L_s, m		3.30	5.00
Smeared Thickness t_h, mm	Deck	47.32	36.27
	Inner Bottom	26.92	--
	Bottom	28.29	44.20
	Stringers	3 ∇ 15.34	--
Smeared Thickness t_v, mm	Side Shell	21.92	26.78
	Inner Skin	22.94	--
	Bulkhead	22.28	27.82
Web Thickness t_w, mm	Upper	12.00	15.00
	Lower	18.00	15.00

TABLE 6.2 – MAJOR STRUCTURAL DATA OF THE STRUCK TANKERS

6.3.3 Side Structure Geometry

The geometry of the side structure of the two tankers is obtained from the information books available on these tankers [14,15] that were developed using SAFEHULL and HECSALV software. These designs satisfy ABS Class requirements. The principal particulars of the two basis side ships are given in Appendix B. Figures 6.6 (a) and (b) show drawings of the 100K dwt Single Hull Tanker and the 150K dwt Double Hull Tanker. Their major structural data are presented in Table 6.2.

6.3.4 Material Properties

Material type 20 (Rigid) is chosen for the rigid wall. All other parts in both the striking and the struck ships are assigned Material type 3 (Kinematic/Isotropic Elastic Plastic) with variable parameters.

The masses of the striking and the struck ship bow and side deformable elements are summed for each ship and subtracted from the total ship virtual mass for each ship. Total ship virtual mass is the product of their displacements and their added mass coefficients in surge (1.05) and sway (1.51), respectively. The mass differences are

assumed to be concentrated in one part for each ship called SHIPMASS. The necessary masses for the SHIPMASS parts are divided by the total volume of these parts to obtain their material densities. Material density is the required LSDYNA input. The part SHIPMASS is located in the midship section in the striking ships and along the length of the struck ships. This is acceptable for this limited one-degree-of-freedom problem. In the future, when this work is expanded to a three-degree-of-freedom problem (sway, surge, yaw), the ship masses must be distributed so that the yaw moments of inertia are modeled correctly.

Young's Modulus, Poisson's Ratio and Yield Stress are assigned values for the specified steel. For simplicity and to save computing time strain rate effects are neglected. In the analyses, a linear isotropic hardening law is used for the inelastic portion of the effective stress versus strain curve, as shown in Figure 6.7. No failure strain is specified so the intersection elements are assumed to be ductile through their entire range of deformation.

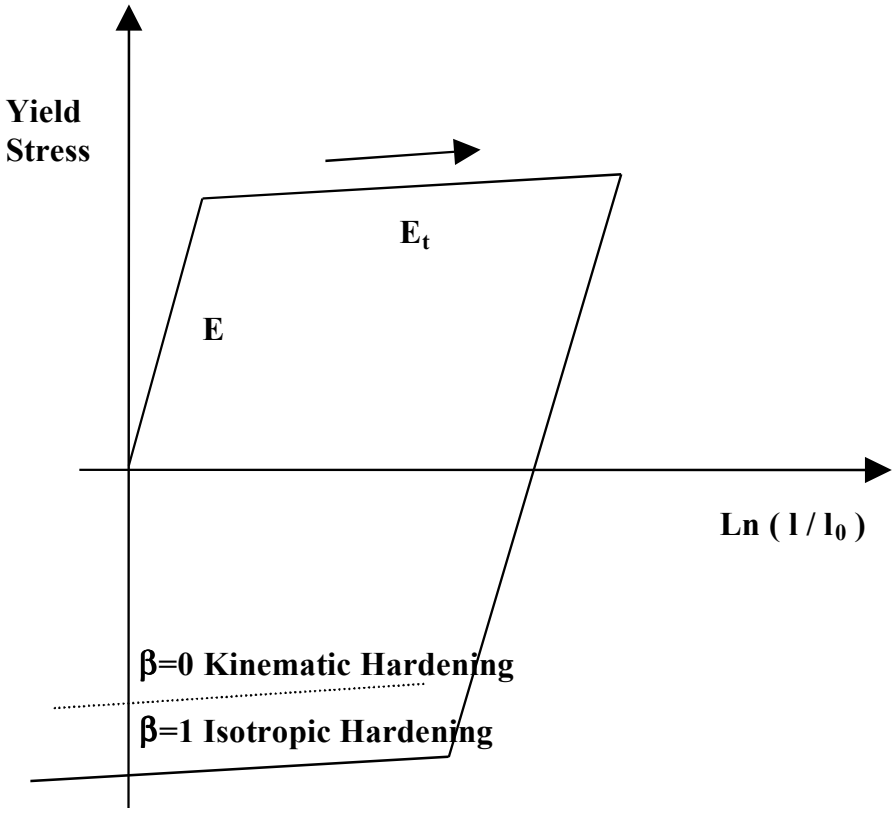

Fig. 6.7 – Material Properties for Type 3 LS-DYNA Material

Material type 3 uses the following input parameters:

MATERIAL TITLE	TRANS
MASS DENSITY	7.850000E+003
YOUNGS MODULUS	2.090000E+011
POISSONS RATIO	2.800000E-001
YIELD STRESS	4.567000E+008
HARDENING MODULUS	4.567000E+008
HARDENING PARAMETER	0.000000E+000
STRAIN RATE PARAM C	4.000000E+001
STRAIN RATE PARAM P	5.000000E+000
FAILURE STRAIN	0.000000E+000

Table 6.3 – Material input parameters (LS-DYNA type 3)

6.3.5 Element Properties

Three general types of models are used in this study:

- Intersection or truss element bow models – The cross-sectional area of these elements is chosen to duplicate the intersection element stiffness as calculated using the Yang and Caldwell equation [70]. Actual plastic material properties are used, and element areas are calculated to match element terms in Yang and Caldwell. These calculations are provided in Appendix A.
- Conventional or shell element models – The conventional models use a fine mesh and Belytscko-Tsay shell elements. Stiffeners are considered by smearing their area into the plate thickness. This type of model is used for bows and sides as indicated.
- Simplified side models - The simplified struck ship models use a course mesh and Belytscko-Tsay shell elements. Analyses using the simplified struck ship models did not run successfully.

6.3.6 Interface

Type 5 contact (NODES TO SURFACE) is used for all the contact cases. In this type of contact, all nodes in the striking ship are assigned as the slave nodes and all elements in the struck ship surface or rigid-wall are assigned as "Master Segments". The contact interface does not allow the slave nodes to penetrate the master segments. If a

rigid wall is defined as the master, then the striking ship must deform because of the contact definition. If the struck ship is assigned as the master, both the ships must deform because the slave nodes are not allowed to penetrate the master surfaces.

6.3.7 Boundary Conditions

The motion of the bow is restricted to the direction perpendicular to the un-deformed outer shell of the struck ship or rigid wall. Only collisions at right angles are considered. If this restraint is not imposed on the bow model, it was observed that the simulation results in modes of geometric unfeasibility. Various other dof combinations were tried. Until this limitation is removed, oblique collision angles cannot be considered. This will be addressed in future work.

The boundary conditions on the struck ship in the fixed case have all degrees of freedom fixed for the nodes lying on the centerline of the struck ship. Other nodes have only one dof, in the transverse direction of collision. In the case where sway is considered, the fixed nodes are released and are given one dof, in the sway direction. The ship mass is adjusted to include added mass in sway.

6.3.8 Initial Conditions

The initial velocity assigned to the nodes of the bow is equal to the speed of the striking vessel before collision. In some cases, this parameter has been varied to see the sensitivity of results to this variation. A velocity equaling the ship velocity is assigned to all nodes in the striking ship. Striking velocities of 5m/s and 12m/s are chosen for the analysis so that results can be compared with those from Pedersen [52].

6.3.9 Element Size

The accuracy of the results in finite element calculations generally increases if smaller elements are used. The size of the elements in the bow intersection models and the simplified side models are determined by their ship geometry's. They are both very course-mesh super-element models. The intersection bow models work very well because the intersection elements are true and valid super-elements. The simplified side models are not satisfactory because valid side panel super-elements are not currently

available to apply in LSDYNA. The element size in the conventional models are determined by trial and error in such a manner that the number of elements is sufficient and converges to the correct solution without having too many elements which greatly increases CPU time.

To further reduce CPU-time, calculations presented in this report are performed using the minimum number of three integration points for recovering internal forces in shell elements.

6.3.10 Hourglassing

Hourglassing is the indication for the occurrence of deformation modes, other than rigid body modes, which do not contribute to strains at the integration points. In order to suppress or overcome hourglassing, restoring forces are introduced on the hourglass modes. Since hourglass modes do not contribute to strains at the integration points, the energy causing hourglassing does not contribute to the internal energy of the system. Hourglassing of shell elements is a serious problem, if not dealt with properly. Care has been taken that there are no modes of hourglass energy in the energy time-history by insuring that mesh size is not too large.

6.3.11 Time-steps

Characteristic for explicit schemes is the use of a large number of small time steps. The maximum time step is restricted by stability criteria. For analyses on steel structures, the time step is typically of the order of 1×10^{-6} sec. As the duration of the collisions in the experiments is 1-3 sec, the configuration is evaluated at about 5×10^{5} points in time.

6.4 Intersection-Element bow models striking a rigid wall (Cases I-5, I-6, I-7, I-8)

6.4.1 Case I-5 (500 DWT Coaster Intersection Bow Striking Rigid Wall)

The geometry for the 500 dwt coaster bow model is created using AutoCAD R14 and exported to FEMB as a .DXF file. The AutoCAD generated .DXF file is shown in

Figure 6.8. After the geometry is discretized into points and lines, parts are created for each distinguishable set of nodes and elements sharing the same material and element properties. Seven distinct parts are created: WALL, TRANSVERSE, LONG1, LONG2, LONG3, LONG4 and SHIPMASS. Nodes are created at every intersection point in the bow model.

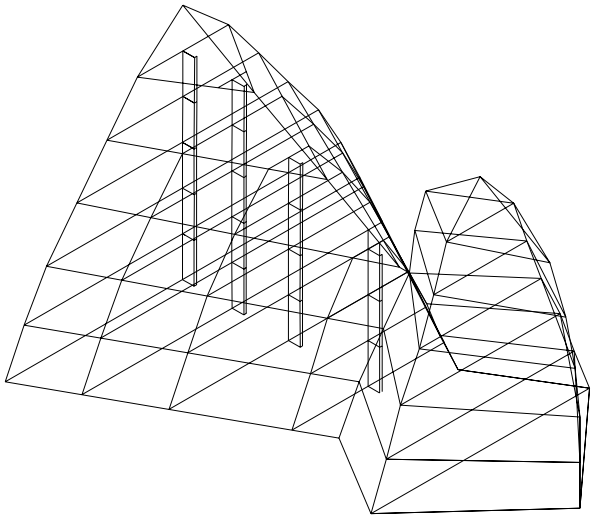

Figure 6.8 - AutoCAD drawing of 500 dwt Coaster Bow

The nodes in the striking ship are connected using beam (truss) elements. The wall is meshed by a 10 X 10 shell element mesh. The model is shown in Figs. 6.9 and 6.10. After generating nodes and elements for the various parts, appropriate material properties and element properties are assigned to the elements. Different colors are used representing various parts, material properties and element properties. Color-coding is helpful. The parts MASS, TRANSVERSE, LONG1, LONG2, LONG3 and LONG4 are assigned LS-DYNA Material Type 3 (Kinematic/Isotropic Elastic Plastic) and the rigid wall is assigned LS-DYNA Material Type 20 (Rigid).

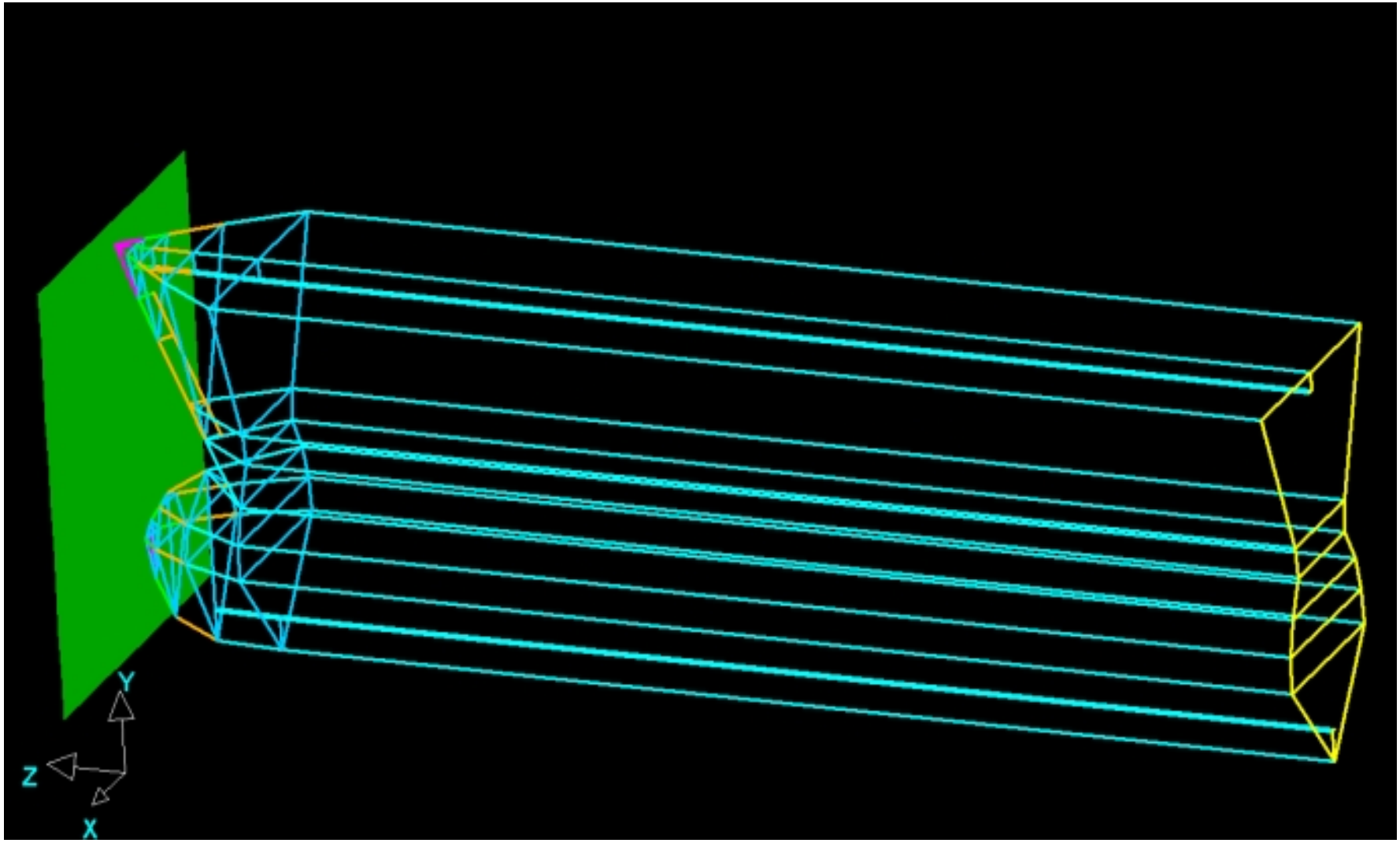

Figure 6.9 - FEMB discretized bow intersection model (500 dwt coaster, I-5)

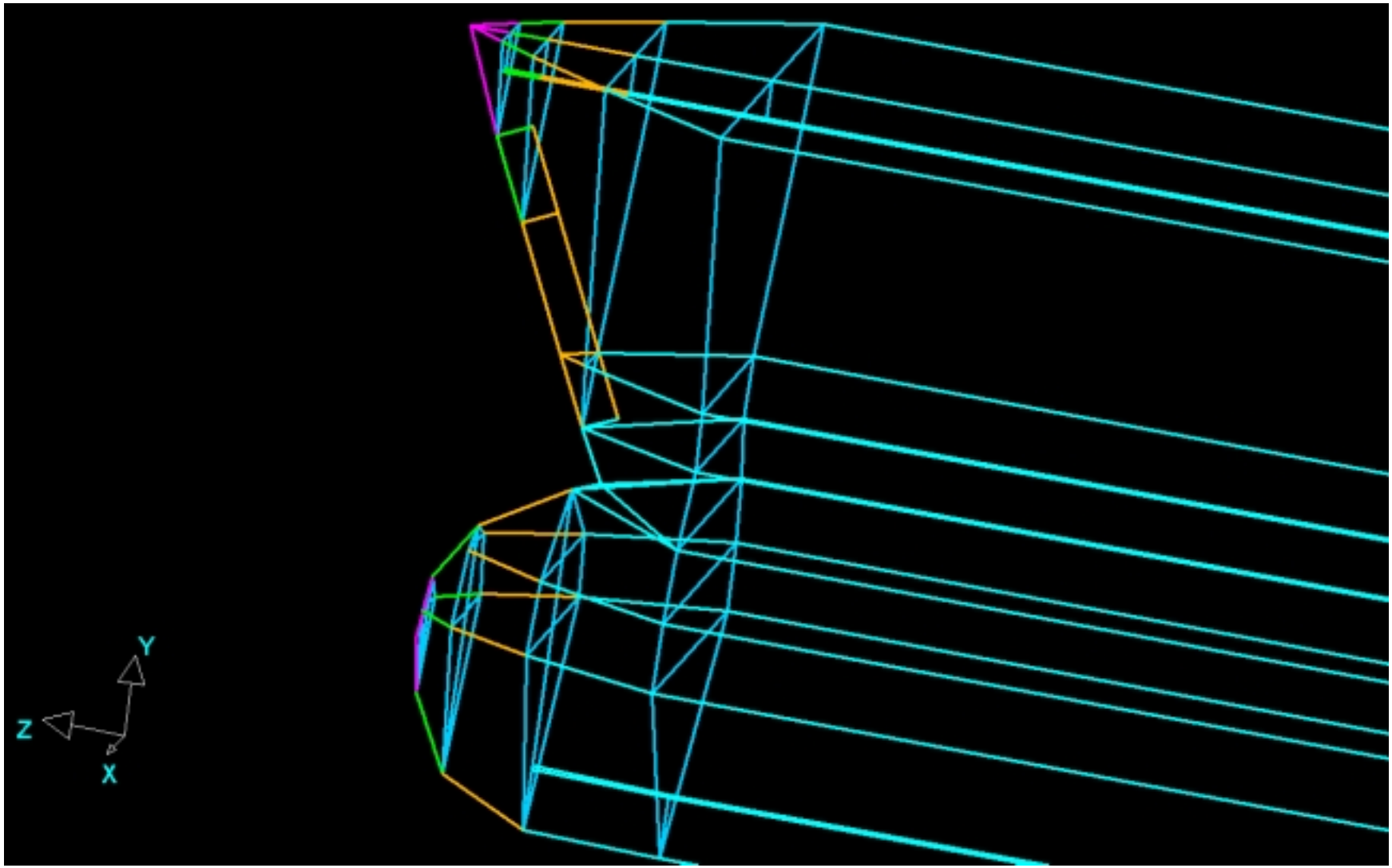

Figure 6.10 – Truss elements as intersection elements in the bow (500 dwt coaster, I-5)

500 DWT coaster (I-5) Model Summary:

No. of Parts	7
No. of Nodes	208
No. of Elements	280
No. of Beams	180
No. of Quads	100
No. of Trias	0
No. of Element Properties	7
No. of Materials	4
No. of Interfaces	1
No. of Master Segments	100
No. of Slave Nodes	87

Materials used

1. *WALL*

Material Type:	20 (Rigid)
Parts Assigned to:	WALL (Rigid Wall)
Mass Density:	7.85×10^{3}
Young's Modulus:	2.09×10^{11}
Poisson's Ratio:	0.28
Mass Constraint:	1
Local Coordinate No. (CON1):	7
SPC (CON2):	7

2. *LONG*

Material Type:	3 (Kinematic/Isotropic Elastic Plastic)
Parts Assigned to:	LONG1, LONG2, LONG3, LONG4
Mass Density:	7.85×10^{3}
Young's Modulus:	2.09×10^{11}
Poisson's Ratio:	0.28
Yield Stress:	470×10^{6}

3. *TRANS*

Material Type:	3 (Kinematic/Isotropic Elastic Plastic)
Parts Assigned to:	TRANSVERSE
Mass Density:	7.85×10^{3}
Young's Modulus:	2.09×10^{11}
Poisson's Ratio:	0.28
Yield Stress:	470×10^{6}

4. *MASS*

Material Type:	3 (Kinematic/Isotropic Elastic Plastic)
Parts Assigned to:	SHIPMASS
Mass Density:	3.0×10^{6}
Young's Modulus:	2.09×10^{11}
Poisson's Ratio:	0.28
Yield Stress:	470×10^{6}

Elements used:

Truss (beam) elements are used for the intersection elements in the bow and the rigid wall is meshed using Belytscko-Tsay shell elements with the following properties:

1. *Belytschko-Tsay shell* elements for rigid wall

Meshing:	10 X 10
Shear factor:	1
No. of integration points:	3
Uniform thickness:	1.00

2. *Beam (Truss) elements for ship*

LONG1:	3.80×10^{-3}
LONG2:	3.27×10^{-3}
LONG3:	3.11×10^{-3}
LONG4:	2.06×10^{-3}
TRANSVERSE:	1.00×10^{-2}
SHIPMASS:	1.00×10^{-2}

All nodes in the striking ship are assigned an initial velocity (see Figure 6.13) equaling $5ms^{-1}$ in the first simulation and 12m/s in the second. Simulation is performed on the model database file generated by FEMB after translating it into a .DYN file that is executable by LS-DYNA.

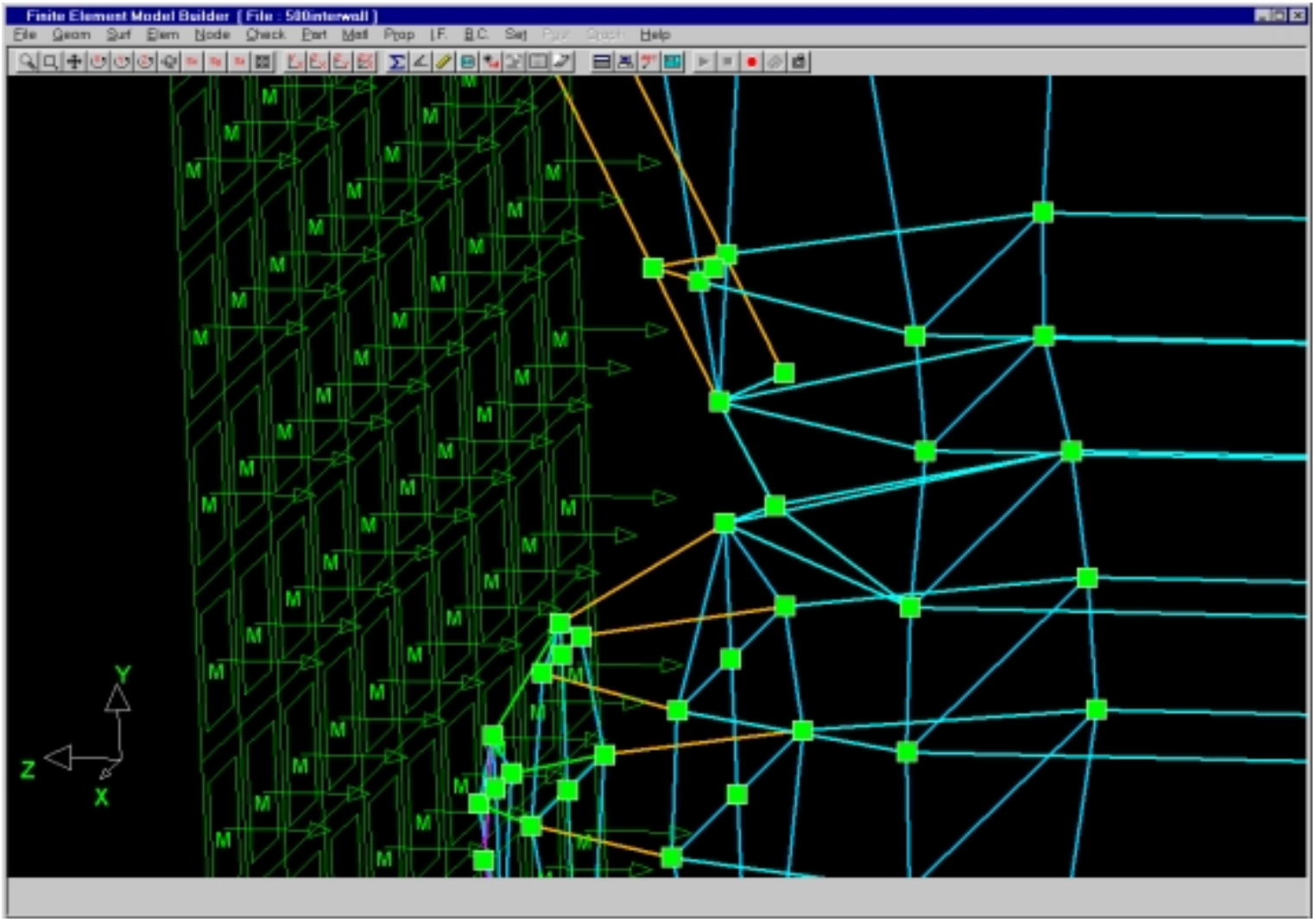

Figure 6.11 – Contact Definition Showing Master Segments in Rigid Wall and Slave Nodes in the Bow (500 dwt coaster, I-5)

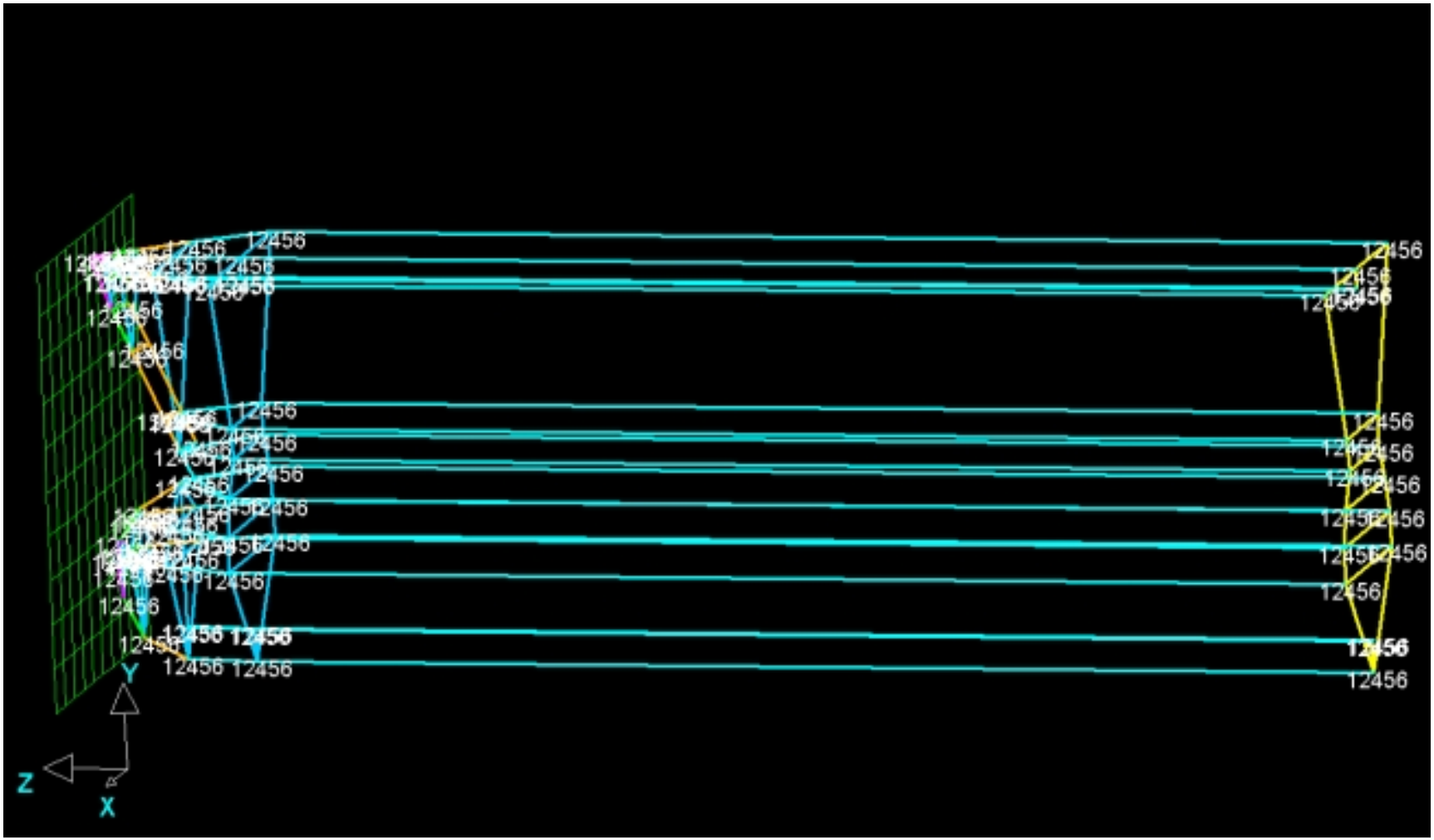

Figure 6.12 – Boundary Conditions on the Bow Model allow motion only in the direction of collision (500 dwt coaster, I-5)

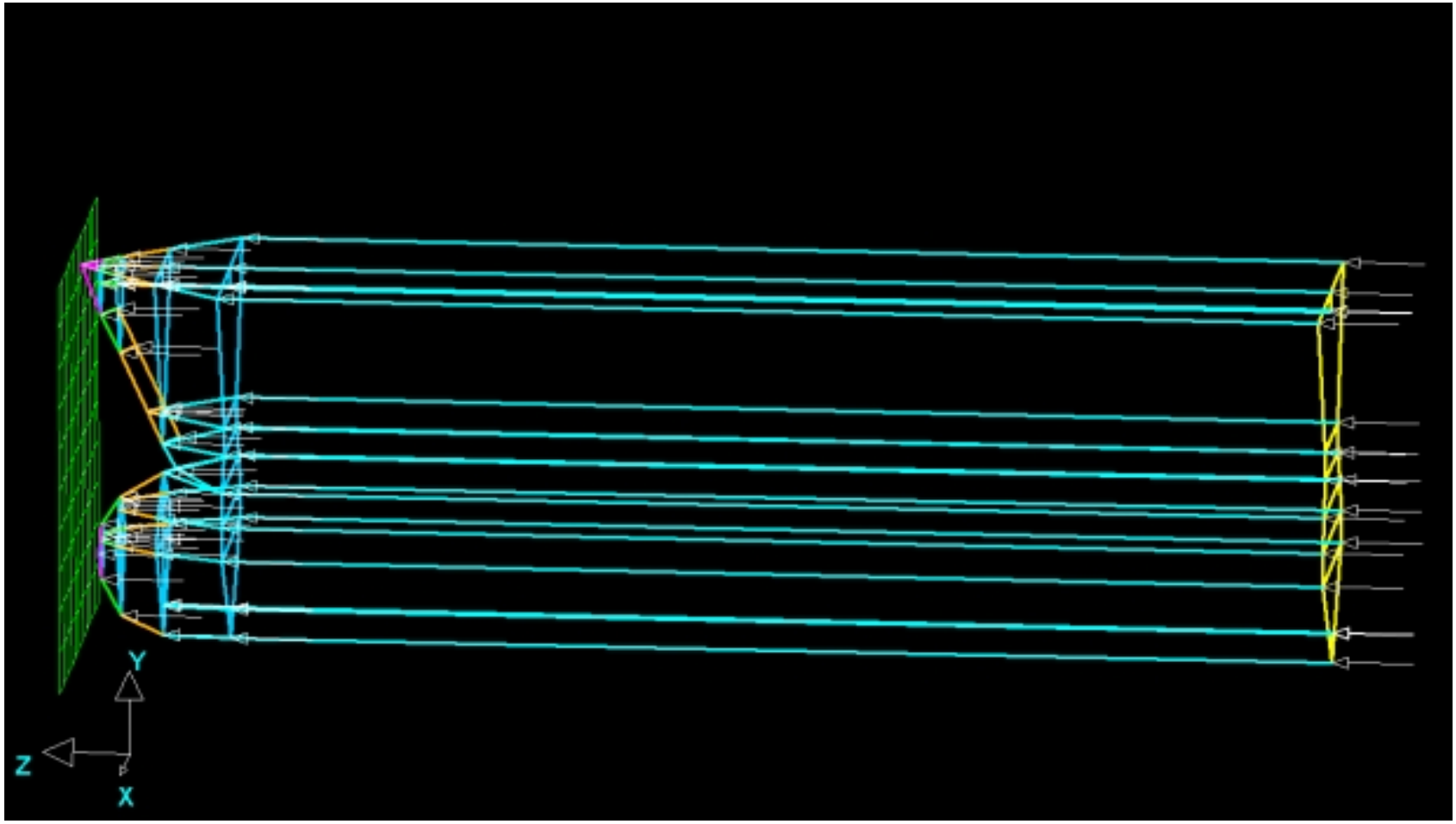

Figure 6.13 – All nodes in the bow model are assigned an initial velocity in a direction perpendicular to the rigid wall (500 dwt coaster, I-5)

6.4.2 Case I-6 (23000 DWT Containership Intersection Bow Striking Rigid Wall)

Due to the unavailability of scale drawings for the 23,000 dwt containership, this model is developed by linearly scaling the 40,000 dwt FEMB model [Section 6.4.3] so that its dimensions (L,B,D) match those of the 23K dwt Containership. A line drawing is created using FEMB. Therefore, the 23,000 dwt Containership model is the same as the 40,000 dwt Containership model, except for its size, mass and material.

Nine distinct parts are created: WALL, TRANSVERSE, LONG1, LONG2, LONG3, LONG4, LONG5, LONG6 and SHIPMASS. Nodes are created at every intersection point in the bow model. The nodes in the striking ship are connected by using beam (truss) elements. The wall is meshed by a 10 X 10 shell element mesh. The parts MASS, TRANSVERSE, LONG1, LONG2, LONG3, LONG4, LONG5 and LONG6 are assigned LS-DYNA Material Type 3 (Kinematic/Isotropic Elastic Plastic) and the rigid wall is assigned LS-DYNA Material Type 20 (Rigid). The mass of the striking ship is assumed concentrated in the part called SHIPMASS.

Model Summary (23000 dwt containership, I-6):

No. of Parts	9
No. of Nodes	306
No. of Elements	480
No. of Beams	380
No. of Quads	100
No. of Trias	0
No. of Element Properties	9
No. of Materials	4
No. of Interfaces	1
No. of Master Segments	100
No. of Slave Nodes	185

Materials used

1. *WALL*

Material Type:	20 (Rigid)
Parts Assigned to:	WALL (Rigid Wall)
Mass Density:	7.85×10^{3}
Young's Modulus:	2.09×10^{11}
Poisson's Ratio:	0.28
Mass Constraint:	1
Local Coordinate No. (CON1):	7
SPC (CON2):	7

2. *LONG*

Material Type:	3 (Kinematic/Isotropic Elastic Plastic)
Parts Assigned to:	LONG1, LONG2, LONG3, LONG4, LONG5, LONG6
Mass Density:	7.85×10^{3}
Young's Modulus:	2.09×10^{11}
Poisson's Ratio:	0.28
Yield Stress:	245×10^{6}

3. *TRANS*

Material Type:	3 (Kinematic/Isotropic Elastic Plastic)
Parts Assigned to:	TRANSVERSE
Mass Density:	7.85×10^{3}
Young's Modulus:	2.09×10^{11}
Poisson's Ratio:	0.28
Yield Stress:	490×10^{6}

4. *MASS*

Material Type:	3 (Kinematic/Isotropic Elastic Plastic)
Parts Assigned to:	SHIPMASS
Mass Density:	1.355×10^{5}
Young's Modulus:	2.09×10^{11}
Poisson's Ratio:	0.28

Yield Stress:	490×10^6

Elements used:

Truss (beam) elements are used for the intersection elements in the bow and the rigid wall is meshed using Belytschko-Tsay shell elements with the following properties:

1. *Belytschko-Tsay shell* elements for rigid wall

Meshing:	10 X 10
Shear factor:	1
No. of integration points:	3
Uniform thickness:	1.00

2. *Beam (Truss) elements for ship*

LONG1:	2.23×10^{-2}
LONG2:	2.53×10^{-2}
LONG3:	2.94×10^{-2}
LONG4:	3.18×10^{-2}
LONG5:	3.29×10^{-2}
LONG6:	3.69×10^{-2}
TRANSVERSE:	9.00×10^{-1}
SHIPMASS:	9.00×10^{-1}

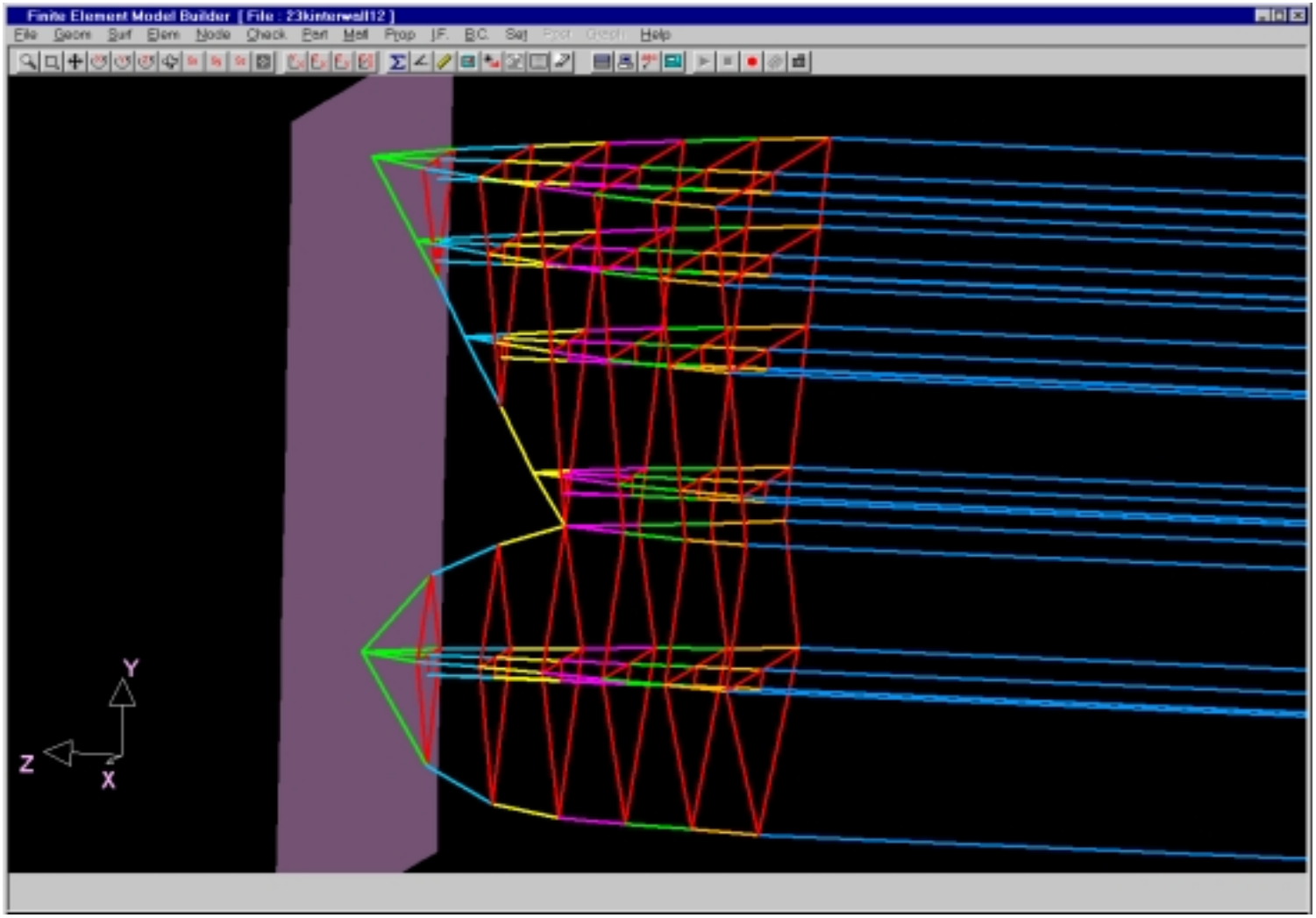

Figure 6.14 –23K dwt Containership Intersection Bow Model (I-6) Striking a Rigid Wall

6.4.3 Case I-7 (40000 DWT Containership Intersection Bow Striking Rigid Wall)

The initial line drawing is created using the Geometry Builder features of FEMB. Nine distinct parts are created: WALL, TRANSVERSE, LONG1, LONG2, LONG3, LONG4, LONG5, LONG6 and SHIPMASS. The parts MASS, TRANSVERSE, LONG1, LONG2, LONG3, LONG4, LONG5 and LONG6 are assigned LS-DYNA Material Type 3 (Kinematic/Isotropic Elastic Plastic) and the rigid wall is assigned LS-DYNA Material Type 20 (Rigid). The mass of the striking ship is assumed concentrated in the part called SHIPMASS.

Model Summary:

No. of Parts	9
No. of Nodes	306
No. of Elements	480
No. of Beams	380
No. of Quads	100
No. of Trias	0
No. of Element Properties	9
No. of Materials	4
No. of Interfaces	1
No. of Master Segments	100
No. of Slave Nodes	185

Materials used

1. WALL

Material Type:	20 (Rigid)
Parts Assigned to:	WALL (Rigid Wall)
Mass Density:	7.85×10^{3}
Young's Modulus:	2.09×10^{11}
Poisson's Ratio:	0.28
Mass Constraint:	1

Local Coordinate No. (CON1): 7

SPC (CON2): 7

2. *LONG*

Material Type: 3 (Kinematic/Isotropic Elastic Plastic)

Parts Assigned to: LONG1, LONG2, LONG3, LONG4, LONG5, LONG6.

Mass Density: 7.85×10^{3}

Young's Modulus: 2.09×10^{11}

Poisson's Ratio: 0.28

Yield Stress: 340.7×10^{6}

3. *TRANS*

Material Type: 3 (Kinematic/Isotropic Elastic Plastic)

Parts Assigned to: TRANSVERSE

Mass Density: 7.85×10^{3}

Young's Modulus: 2.09×10^{11}

Poisson's Ratio: 0.28

Yield Stress: 340.1×10^{6}

4. *MASS*

Material Type: 3 (Kinematic/Isotropic Elastic Plastic)

Parts Assigned to: SHIPMASS

Mass Density: 3.9×10^{5}

Young's Modulus: 2.09×10^{11}

Poisson's Ratio: 0.28

Yield Stress: 340.7×10^{6}

Elements used:

Truss (beam) elements are used for the intersection elements in the bow and the rigid wall is meshed using Belytschko-Tsay shell elements with the following properties:

1. *Belytschko-Tsay shell* elements for rigid wall

Meshing: 10 X 10

Shear factor:	1
No. of integration points:	3
Uniform thickness:	1.00

2. *Beam (Truss) elements for ship*

LONG1:	2.57×10^{-2}
LONG2:	2.80×10^{-2}
LONG3:	3.19×10^{-2}
LONG4:	3.22×10^{-2}
LONG5:	3.34×10^{-2}
LONG6:	3.43×10^{-2}
TRANSVERSE:	9.00×10^{-1}
SHIPMASS:	9.00×10^{-1}

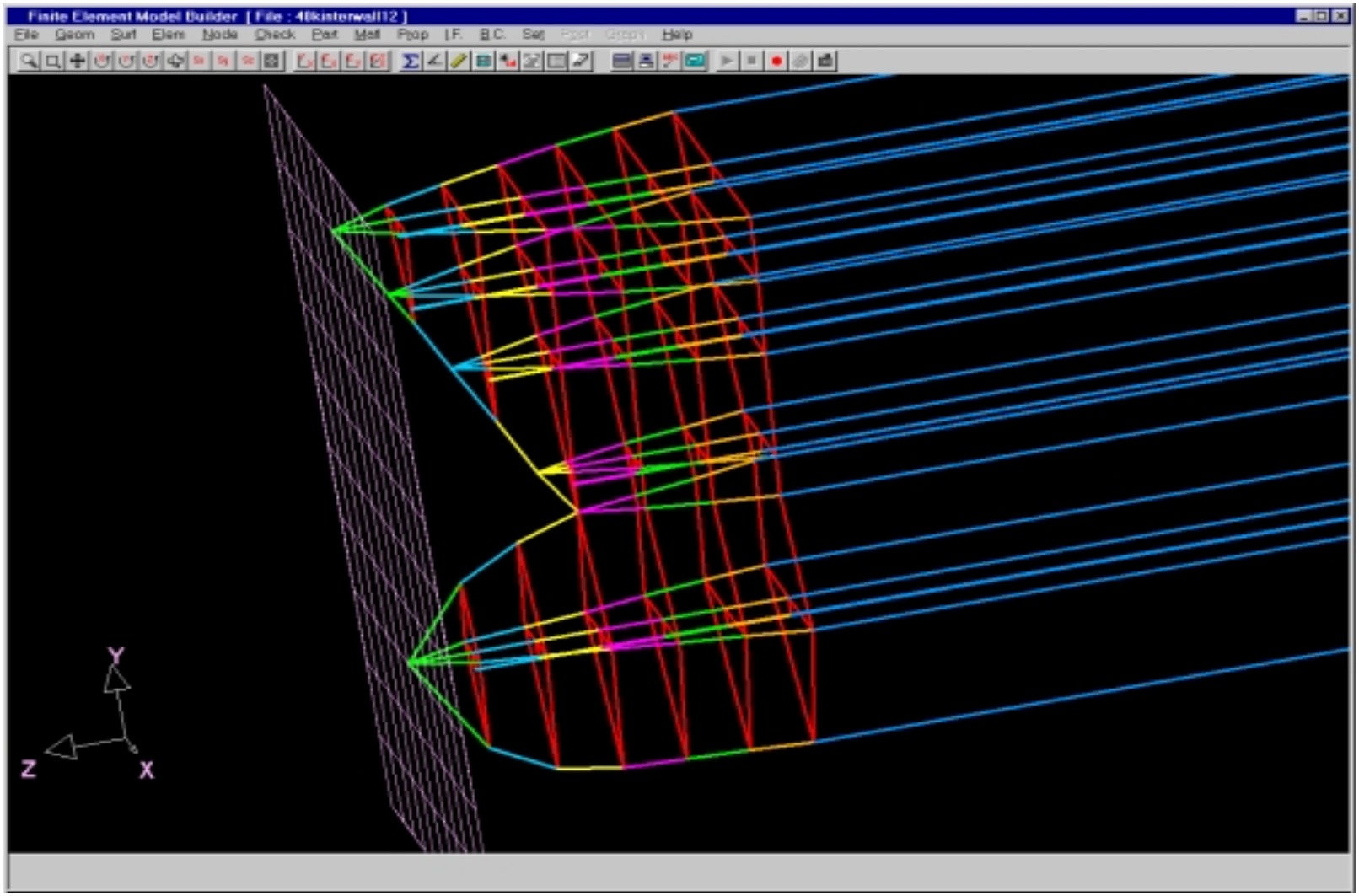

Figure 6.15 – 40 kdwt Containership (I-7) Intersection Bow Model Striking a Rigid Wall

6.4.4 Case I-8 (150000 DWT Bulk Carrier Intersection Bow Striking Rigid Wall)

The initial line drawing is created in FEMB. Nine distinct parts are created, namely: WALL, TRANSVERSE, LONG1, LONG2, LONG3, LONG4, LONG5, LONG6 and SHIPMASS. The parts MASS, TRANSVERSE, LONG1, LONG2, LONG3, LONG4, LONG5 and LONG6 are assigned LS-DYNA Material Type 3 (Kinematic/Isotropic Elastic Plastic) and the rigid wall is assigned LS-DYNA Material Type 20 (Rigid). The mass of the striking ship is assumed concentrated in the part called SHIPMASS.

Model Summary:

No. of Parts	9
No. of Nodes	228
No. of Elements	318
No. of Beams	218
No. of Quads	100
No. of Trias	0
No. of Element Properties	9
No. of Materials	4
No. of Interfaces	1
No. of Master Segments	100
No. of Slave Nodes	107

Materials used

1. WALL

Material Type:	20 (Rigid)
Parts Assigned to:	WALL (Rigid Wall)
Mass Density:	7.85×10^{3}
Young's Modulus:	2.09×10^{11}
Poisson's Ratio:	0.28
Mass Constraint:	1

Local Coordinate No. (CON1): 7

SPC (CON2): 7

2. *LONG*

Material Type: 3 (Kinematic/Isotropic Elastic Plastic)

Parts Assigned to: LONG1, LONG2, LONG3, LONG4, LONG5, LONG6

Mass Density: 7.85×10^{3}

Young's Modulus: 2.09×10^{11}

Poisson's Ratio: 0.28

Yield Stress: 457×10^{6}

3. *TRANS*

Material Type: 3 (Kinematic/Isotropic Elastic Plastic)

Parts Assigned to: TRANSVERSE

Mass Density: 7.85×10^{3}

Young's Modulus: 2.09×10^{11}

Poisson's Ratio: 0.28

Yield Stress: 457×10^{6}

4. *MASS*

Material Type: 3 (Kinematic/Isotropic Elastic Plastic)

Parts Assigned to: SHIPMASS

Mass Density: 1.53×10^{6}

Young's Modulus: 2.09×10^{11}

Poisson's Ratio: 0.28

Yield Stress: 340.7×10^{6}

Elements used:

Truss (beam) elements are used for the intersection elements in the bow and the rigid wall is meshed using Belytschko-Tsay shell elements with the following properties:

1. *Belytschko-Tsay shell* elements for rigid wall

Meshing: 10 X 10

Shear factor:	1
No. of integration points:	3
Uniform thickness:	1.00

2. *Beam (Truss) elements for ship*

LONG1:	7.73×10^{-2}
LONG2:	5.85×10^{-2}
LONG3:	4.25×10^{-2}
LONG4:	6.02×10^{-2}
LONG5:	6.24×10^{-2}
LONG6:	6.51×10^{-2}
TRANSVERSE:	9.00×10^{-1}
SHIPMASS:	9.00×10^{-1}

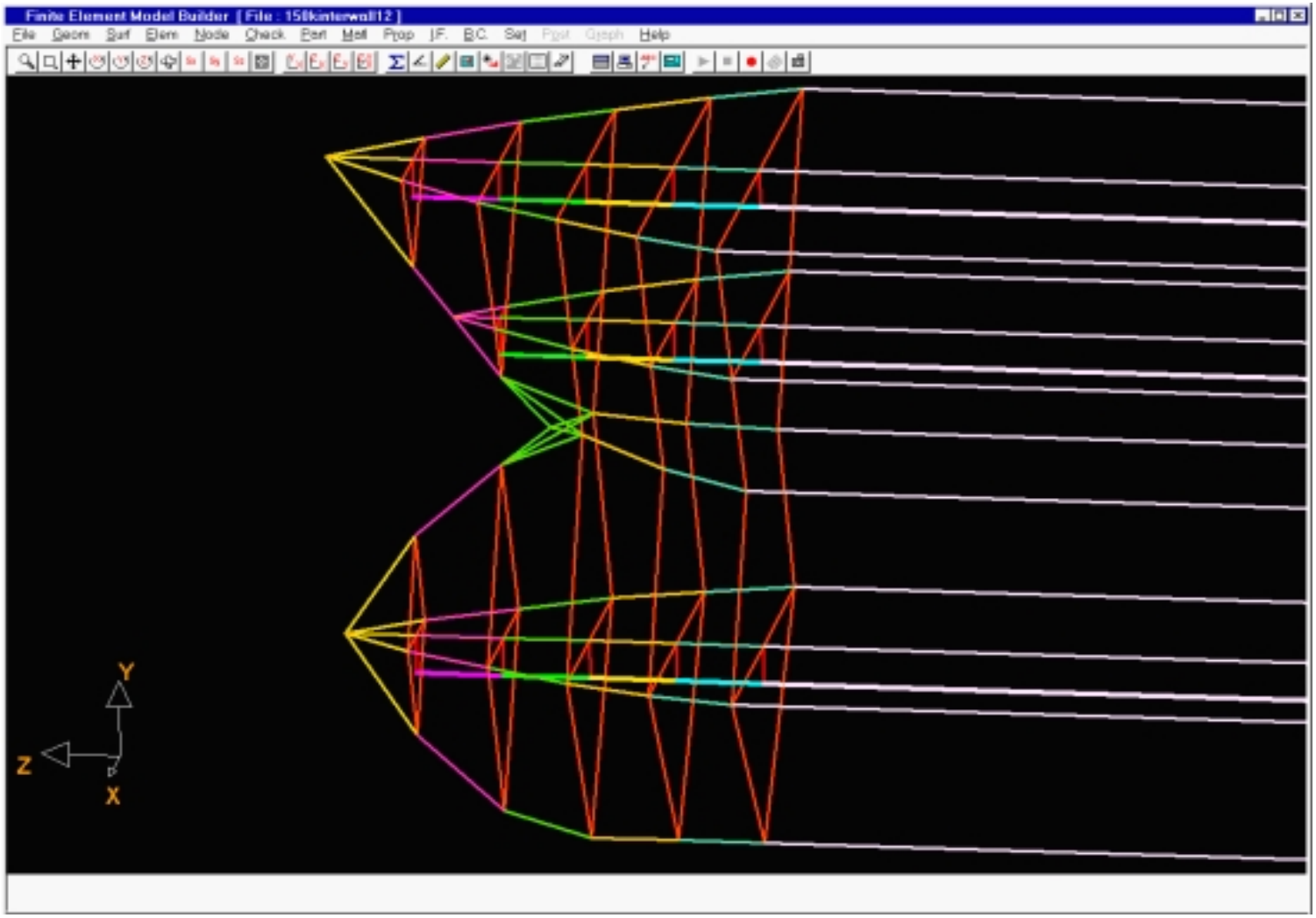

Figure 6.16 – Intersection Model for the 150000 dwt Bulk Carrier (I-8) showing Truss elements in the bow

6.5 Conventional Ship Side Models (Cases I-9, I-10, I-11 and I-12)

6.5.1 Cases I-9 and I-10 (23K DWT Intersection Containership Bow Striking SH100 Conventional Side)

In these cases, the striking ship model is the 23K dwt intersection model discussed in Section 6.4.2. A conventional model for the 100K dwt Single Hull struck ship is created using FEMB. For simplicity and due to symmetry, only half (breadth-wise) of the struck ship is modeled. Nine parts are created in the struck ship model:

STRKWEBS	Webs
TRBULKHD	Transverse Bulkheads
STRKSIDE	Side Shell
STRKDK	Decks
STRKBTM	Bottom Plating
TANKWALL	Tank Wall
STRKBILG	Bilge Plating
STRKGUNW	Gunwale Plating
STRKCL	Plating along the CL of the ship
STRKSHIP	Rest of the struck ship (mass distribution)

Model Summary:

No. of Parts	18 (9 in striking ship and 9 in struck ship)
No. of Nodes	1852
No. of Elements	2095
No. of Beams	444
No. of Quads	1509
No. of Trias	142
No. of Element Properties	15
No. of Materials	5
No. of Interfaces	1
No. of Master Segments	1609
No. of Slave Nodes	185

Materials used for the Struck Ship

1. *STRKMASS*

Material Type:	3 (Kinematic/Isotropic Elastic Plastic)
Parts Assigned to:	STRKSHIP
Mass Density:	5.2×10^5
Young's Modulus:	2.09×10^{11}
Poisson's Ratio:	0.28
Yield Stress:	315×10^6

2. *STRK*

Material Type:	3 (Kinematic/Isotropic Elastic Plastic)
Parts Assigned to:	all other parts in the struck ship.
Mass Density:	7.85×10^3
Young's Modulus:	2.09×10^{11}
Poisson's Ratio:	0.28
Yield Stress:	315×10^6

Truss (beam) elements are used for the intersection elements in the bow and the struck ship is meshed using Belytschko-Tsay shell elements with different shell thickness for each part, as defined in Table 6.2. Type 5 contact (NODES TO SURFACE) is defined. All nodes in the striking ship are assigned as the slave nodes and all elements in the struck ship are assigned as "Master Segments". Figure 6.17 shows the FE model of the conventional 100K SH Tanker. The motion of the bow has been restricted to the direction perpendicular to the undeformed outer shell of the struck ship. In case I-9, all nodes on the centerline of the struck ship are fixed, and the rest of the nodes have only one dof, in the direction of collision. In case I-10 (sway), all nodes have only the degree of freedom in the direction of collision. Figure 6.18 shows a closer view of the conventional struck ship model for the SH tanker.

Figures 6.19 and 6.20 show the collision between the 23 kdwt containership intersection-bow and conventional SH100 tanker.

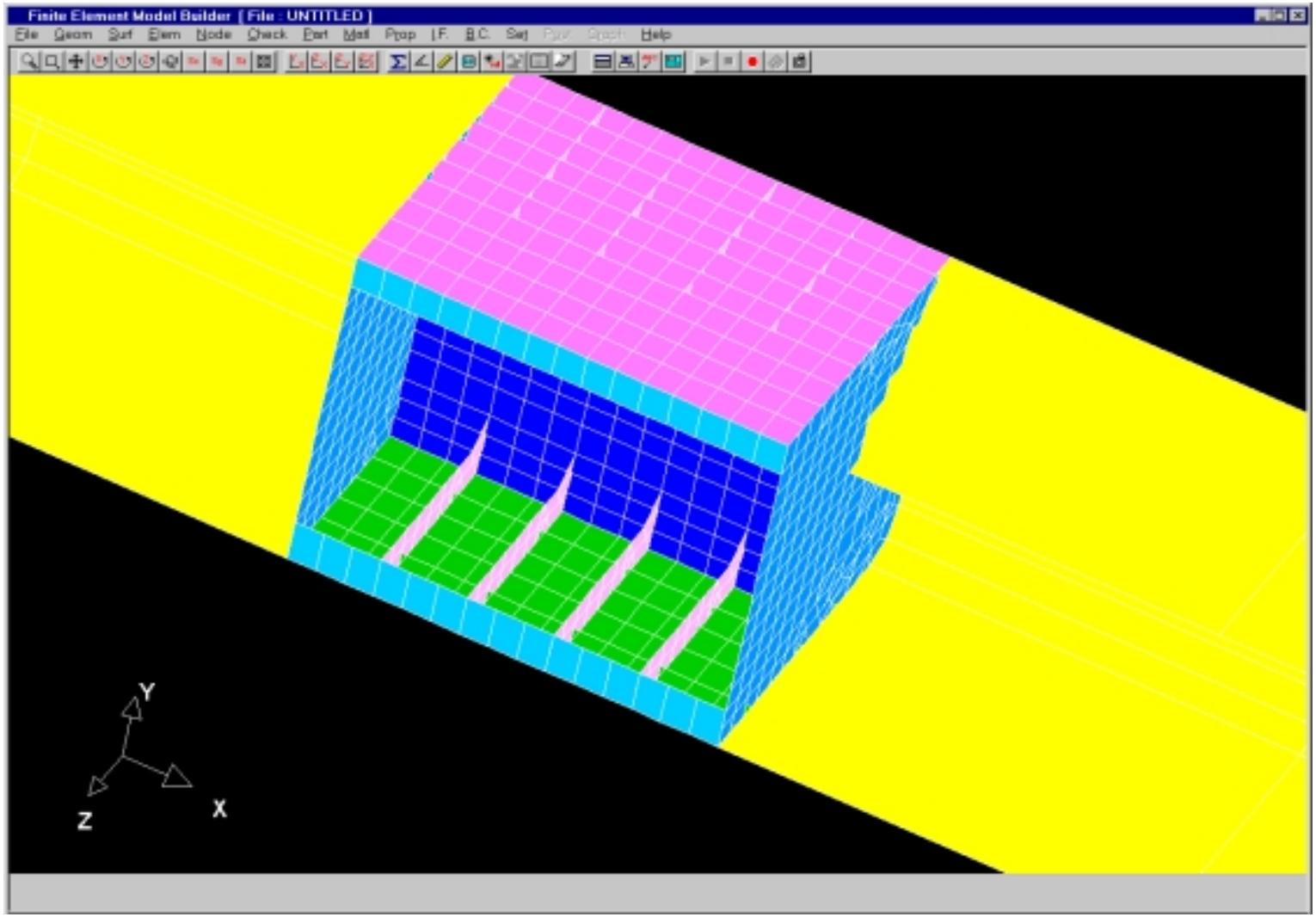

Figure 6.17 – Conventional SH100 Single Hull Tanker showing the region of strike, webs and bulkheads

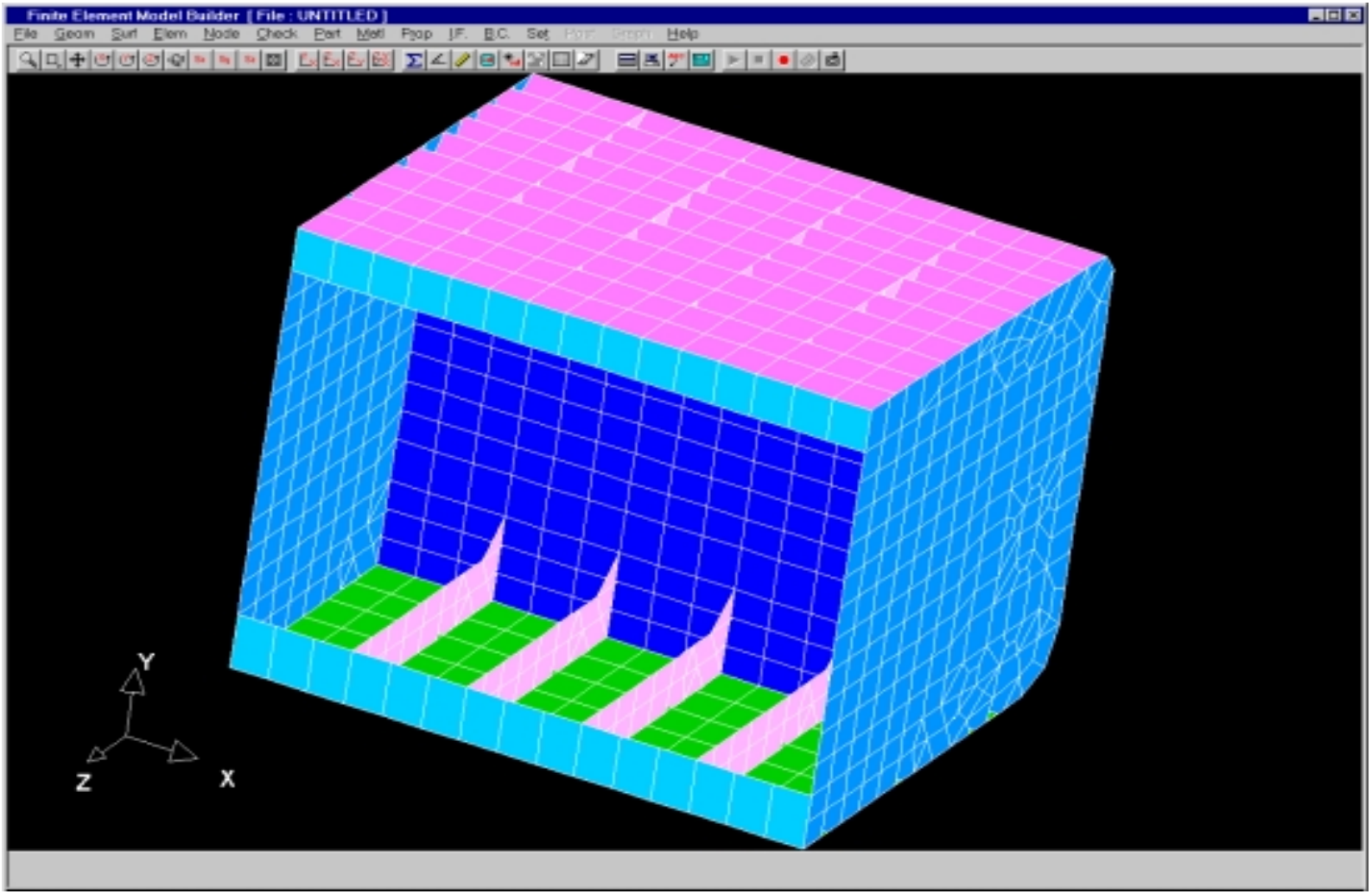

Figure 6.18 – Detailed view of the Conventional 100K SH Tanker showing the region of strike, webs and bulkheads

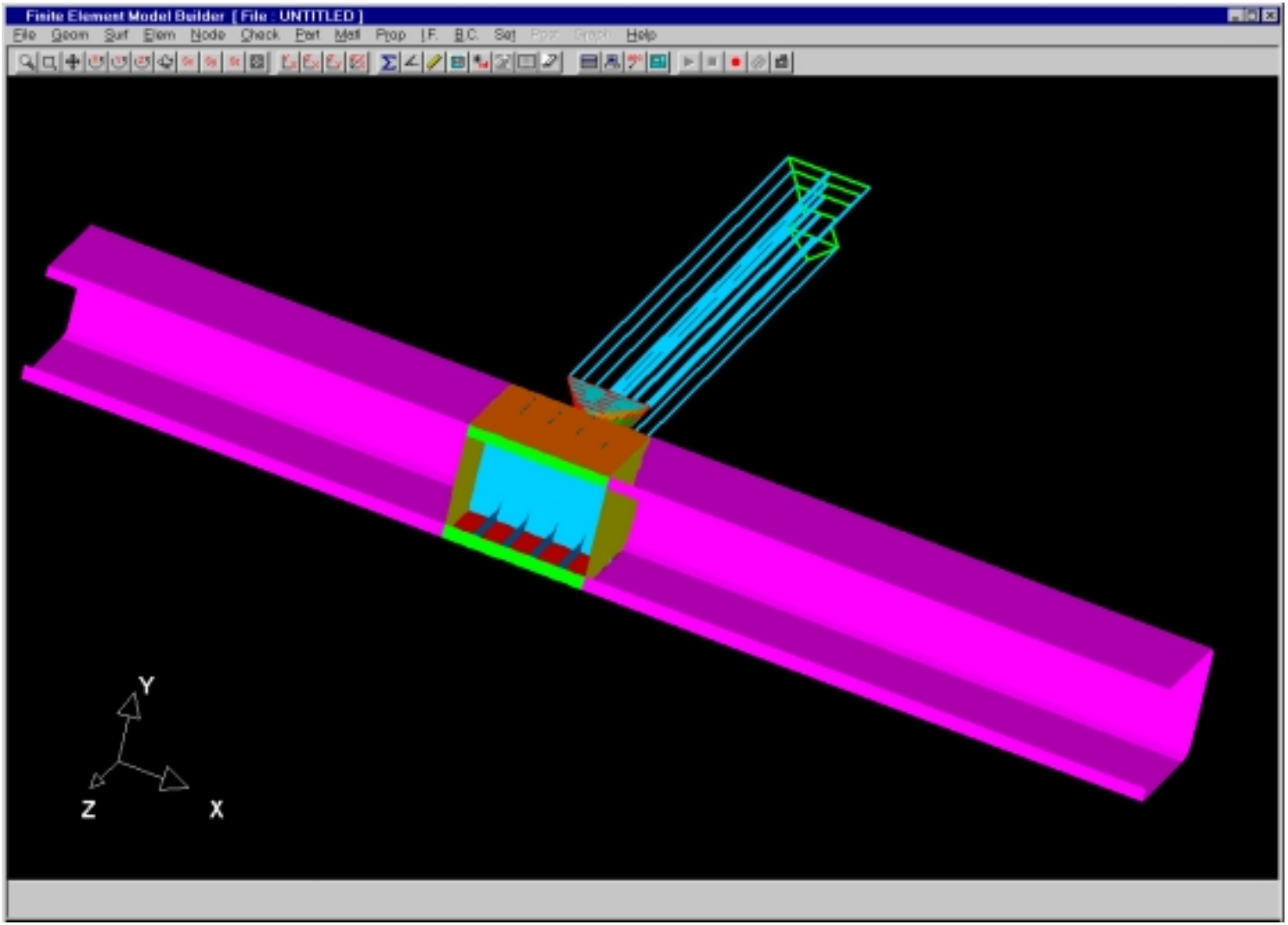

Figure 6.19 – Perspective of 23K dwt Intersection Model striking the Conventional SH100 Tanker (I-9 and I-10)

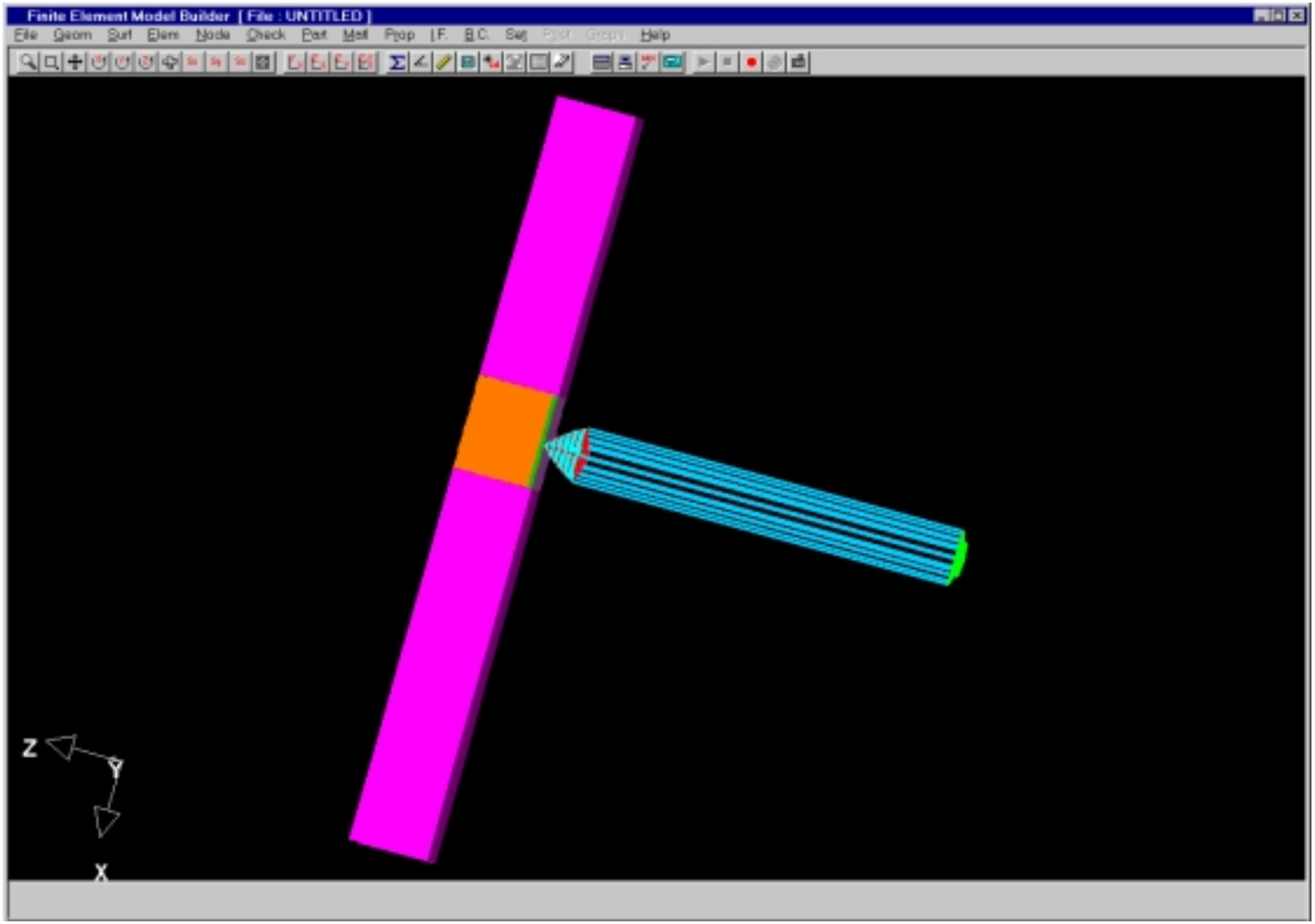

Figure 6.20 – Collision Scenario between 23K dwt Intersection Containership and the SH100 Tanker (I-9 and I-10)

6.5.2 Cases I-11 and I-12 (150K DWT Intersection Bulk Carrier Bow Striking DH150 Conventional Side)

The striking ship model is the same as that of the 150 kdwt intersection model, as discussed in Section 6.4.4. A conventional model for the 150 kdwt Double Hull tanker is created using FEMB. For simplicity and due to symmetry, only half (breadth-wise) of the struck ship is modeled. Nine parts are created in the struck ship model:

STRKWEBS	Webs
TRBULKHD	Transverse Bulkheads
STRKSIDE	Side Shell
STRKDK	Decks
STRKBTM	Bottom Plating
TANKWALL	Tank Wall
STRKGRDR	Girders in the struck ship
DBLBTM	Double Bottom Plating
DBLHULL	Plating in the Double Hull
STRKSHIP	Rest of the struck ship (mass distribution)

Model Summary:

No. of Parts	18 (9 in striking ship and 9 in struck ship)
No. of Nodes	1684
No. of Elements	2060
No. of Beams	132
No. of Quads	1868
No. of Trias	60
No. of Element Properties	15
No. of Materials	6
No. of Interfaces	1
No. of Master Segments	1932
No. of Slave Nodes	107

Materials used for the Struck Ship

1. *STRKMASS*

Material Type:	3 (Kinematic/Isotropic Elastic Plastic)
Parts Assigned to:	STRKSHIP
Mass Density:	5.2×10^5
Young's Modulus:	2.09×10^{11}
Poisson's Ratio:	0.28
Yield Stress:	315×10^6

2. *STRK*

Material Type:	3 (Kinematic/Isotropic Elastic Plastic)
Parts Assigned to:	all other parts in the struck ship.
Mass Density:	7.85×10^3
Young's Modulus:	2.09×10^{11}
Poisson's Ratio:	0.28
Yield Stress:	315×10^6

Truss (beam) elements are used for the intersection elements in the bow and the struck ship is meshed using Belytschko-Tsay shell elements with different shell thickness for each part, as defined in Table 6.2.

Type 5 contact (NODES TO SURFACE) is defined. All nodes in the striking ship are assigned as the slave nodes and all elements in the struck ship are assigned as "Master Segments". Figure 6.21 shows the FE model of the conventional 150K DH Tanker. The motion of the bow is restricted to the direction perpendicular to the un-deformed outer shell of the struck ship. In case I-11, all nodes on the centerline of the struck ship are fixed, and the rest of the nodes have only one dof, in the direction of collision. In case I-12 (sway), all nodes have only the degree of freedom in the direction of collision.

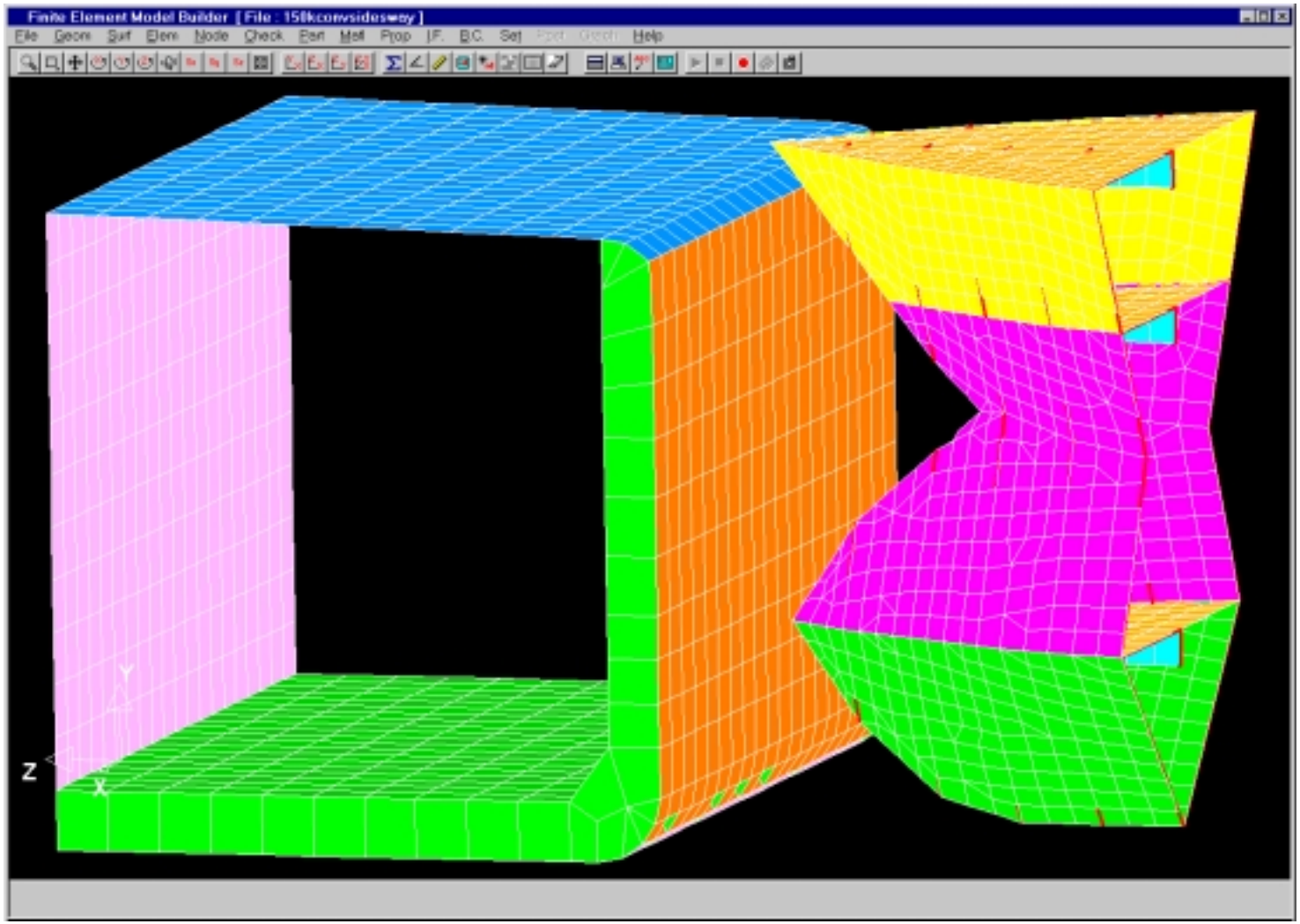

Figure 6.21 – 150K DWT DH Tanker

6.6 Simplified Ship Side Models (Cases I-13 through I-16)

A simplified model for the struck tankers was developed in an attempt to reduce the CPU time required for processing the FE model, in comparison with the conventional model. These models are used in the test cases I-13, I-14, I-15 and I-16. They do not provide satisfactory results because of the limitations in LSDYNA to define correct super-element properties. The striking ships are the 23 kdwt containership intersection model and the 150 kdwt bulk carrier intersection model. A summary of the simplified model developed for the two tankers is presented below:

100K SH Tanker (Cases I-13, I-14)		150K DH Tanker (Cases I-15, I-16)	
No. of Parts	18	No. of Parts	18
No. of Nodes	640	No. of Nodes	568
No. of Elements	871	No. of Elements	756
No. of Beams	380	No. of Beams	225
No. of Quads	452	No. of Quads	486
No. of Trias	39	No. of Trias	45
No. of Element Properties	14	No. of Element Properties	14
No. of Materials	6	No. of Materials	6
No. of Interfaces	1	No. of Interfaces	1
No. of Master Segments	491	No. of Master Segments	522
No. of Slave Nodes	185	No. of Slave Nodes	107

The difference between the conventional and the simplified models is that the simplified model has a coarser mesh. Elements whose normals are in the direction of the collision are chosen to be beam elements in order to simplify the CPU time. All other elements with normals in the direction of the collision are large plate elements. All plate elements in the struck ship are assigned the same materials as are defined in Section 6.5.1 for the conventional model.

Element thicknesses for the simplified struck ship are the same as for conventional model for the struck ship. Boundary conditions, interfaces and initial conditions are the same as defined for the conventional model. Figure 6.22 shows the simplified model of the 100K dwt SH tanker.

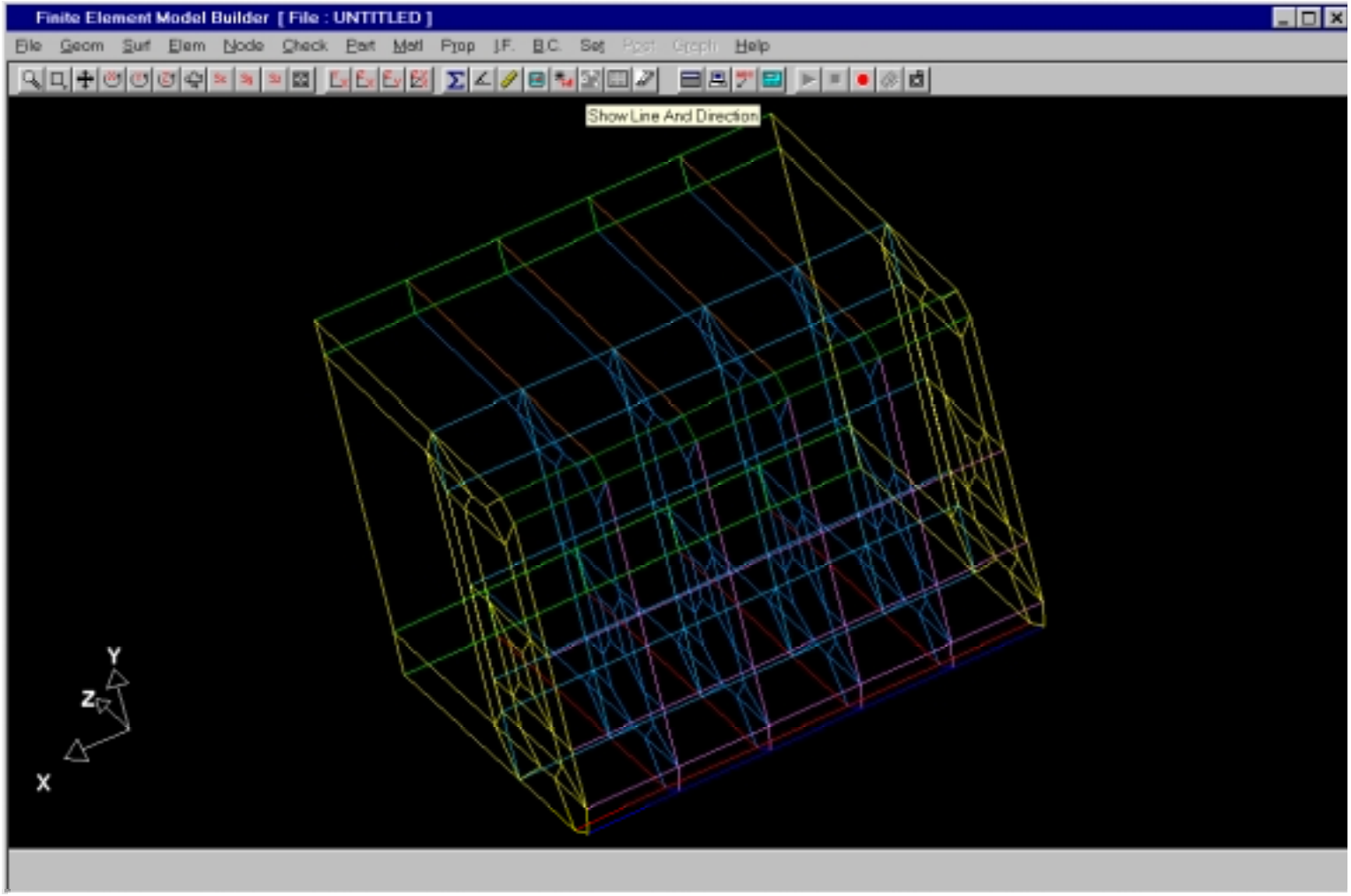

Figure 6.22– Simplified 100K SH Tanker Model (I-13 and I-14)

6.7 Conventional Bow Models

6.7.1 Cases C-1, C-3 and C-4 (23K DWT Conventional Bow Striking Rigid Wall and SH100 Conventional Side with and w/o Sway)

Parts created in the striking ship ship bow are:

SIDETOP	Side shell above Main Deck
SIDEMID1	Side shell between m WL and m WL
SIDEMID2	Side shell between m WL and m WL
SIDEBTM	Side Shell below m WL
TRANSVERSE	Transverse members
GIRDER	Longitudinal Girders
LONG6	Longitudinal Truss Elements
DECKS	Decks in the striking ship
SHIPMASS	Mass of ship concentrated

Model Summary:

No. of Parts	10
No. of Nodes	2196
No. of Elements	2491
No. of Beams	234
No. of Quads	1985
No. of Trias	272
No. of Element Properties	5
No. of Materials	5
No. of Interfaces	1
No. of Master Segments	100
No. of Slave Nodes	2077

Materials used

1. *LONG*

Material Type:	3 (Kinematic/Isotropic Elastic Plastic)
Parts Assigned to:	LONG6
Mass Density:	7.85×10^{3}
Young's Modulus:	2.09×10^{11}
Poisson's Ratio:	0.28
Yield Stress:	235×10^{6}

2. *TRANS*

Material Type:	3 (Kinematic/Isotropic Elastic Plastic)
Parts Assigned to:	TRANSVERSE
Mass Density:	7.85×10^{3}
Young's Modulus:	2.09×10^{11}
Poisson's Ratio:	0.28
Yield Stress:	235×10^{6}

3. *MASS*

Material Type:	3 (Kinematic/Isotropic Elastic Plastic)
Parts Assigned to:	SHIPMASS
Mass Density:	1.52×10^{5}
Young's Modulus:	2.09×10^{11}
Poisson's Ratio:	0.28
Yield Stress:	235×10^{6}

4. *SHELL*

Material Type:	3 (Kinematic/Isotropic Elastic Plastic)
Parts Assigned to:	Striking Ship Side Shell
Mass Density:	7.85×10^{3}
Young's Modulus:	2.09×10^{11}
Poisson's Ratio:	0.28
Yield Stress:	235×10^{6}

Type 5 contact (NODES TO SURFACE) is defined. All nodes in the striking ship are assigned as the slave nodes and all elements in the rigid-wall are assigned as "Master

Segments". Figure 6.23 shows the 23 kdwt conventional element bow model (C-1). Two speeds, 5m/s and 12m/s are analyzed. All nodes in the striking bow are allowed only one degree of freedom (in the direction of the collision).

6.7.2 Cases C-2, C-5 and C-6 (150K DWT Conventional Bow Striking Rigid Wall and Conventional DH150 Side with and w/o Sway)

Parts created in the striking ship ship bow are:

SIDETOP	Side shell above Main Deck
SIDEMID	Side shell between m WL and m WL
SIDEBTM	Side Shell below m WL
TRANSVERSE	Transverse members
GIRDER	Longitudinal Girders
LONG6	Longitudinal Truss Elements
SHIPMASS	Mass of ship concentrated

Model Summary:

No. of Parts	8
No. of Nodes	1587
No. of Elements	1740
No. of Beams	138
No. of Quads	1398
No. of Trias	210
No. of Element Properties	5
No. of Materials	5
No. of Interfaces	1
No. of Master Segments	100
No. of Slave Nodes	1466

Materials used

1. *LONG*

Material Type:	3 (Kinematic/Isotropic Elastic Plastic)
Parts Assigned to:	LONG6
Mass Density:	7.85×10^{3}
Young's Modulus:	2.09×10^{11}
Poisson's Ratio:	0.28
Yield Stress:	456.75×10^{6}

2. *TRANS*

Material Type:	3 (Kinematic/Isotropic Elastic Plastic)
Parts Assigned to:	TRANSVERSE
Mass Density:	7.85×10^{3}
Young's Modulus:	2.09×10^{11}
Poisson's Ratio:	0.28
Yield Stress:	456.75×10^{6}

3. *MASS*

Material Type:	3 (Kinematic/Isotropic Elastic Plastic)
Parts Assigned to:	SHIPMASS
Mass Density:	1.52×10^{5}
Young's Modulus:	2.09×10^{11}
Poisson's Ratio:	0.28
Yield Stress:	456.75×10^{6}

4. *SHELL*

Material Type:	3 (Kinematic/Isotropic Elastic Plastic)
Parts Assigned to:	Striking Ship Side Shell
Mass Density:	7.85×10^{3}
Young's Modulus:	2.09×10^{11}
Poisson's Ratio:	0.28
Yield Stress:	456.75×10^{6}

Type 5 contact (NODES TO SURFACE) is defined. All nodes in the striking ship are assigned as the slave nodes and all elements in the rigid-wall are assigned as "Master

Segments". Figure 6.24 shows the 150 kdwt conventional element bow model (C-2). Two speeds, 5m/s and 12m/s are analyzed. All nodes in the striking bow are allowed only one degree of freedom (in the direction of the collision). Figures 6.25 and 6.26 show the 150 kdwt conventional bow model striking the DH150 and SH100 conventional side models (C-3 and C-5). These models were described in Section 6.5.

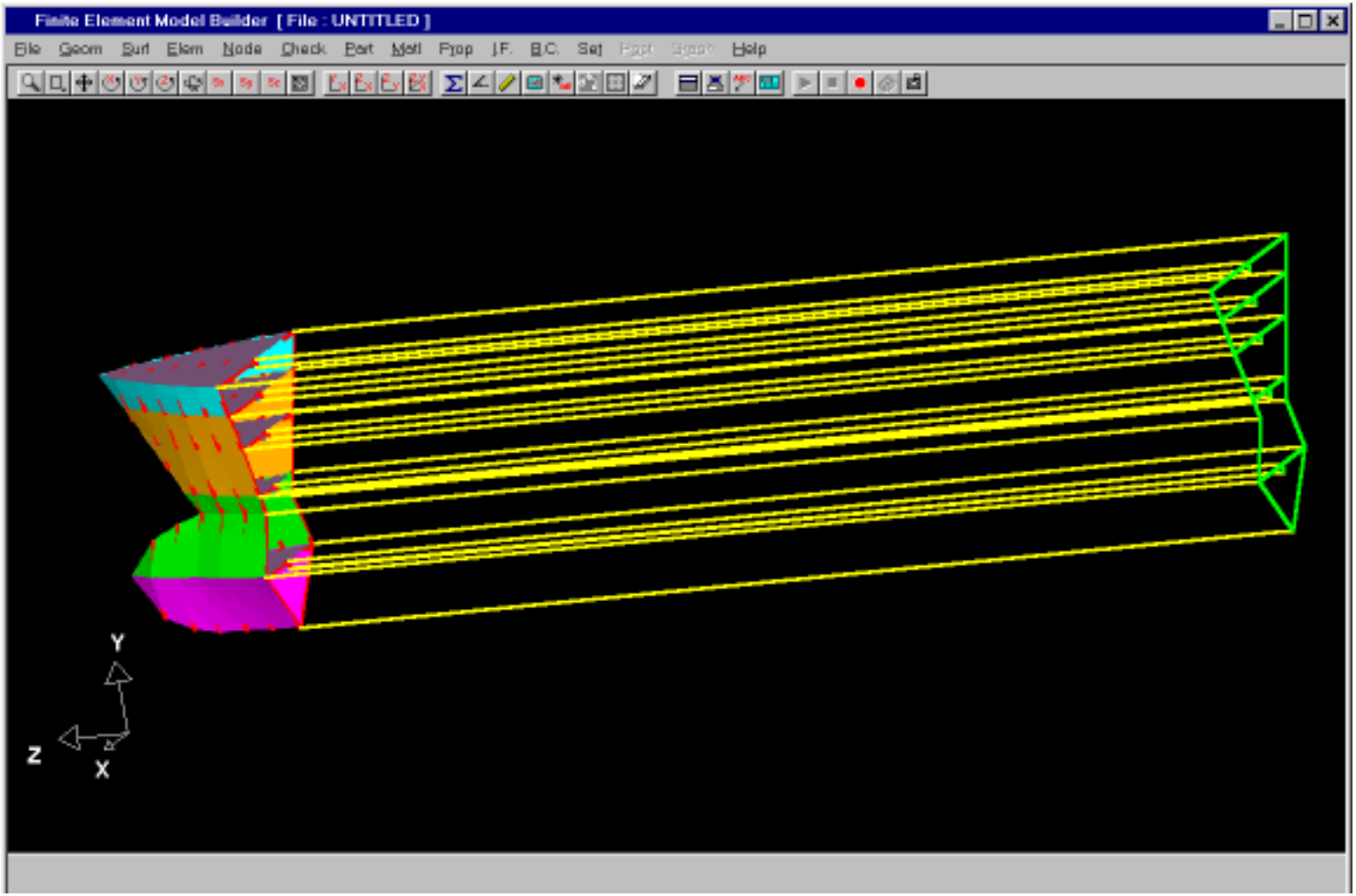

Figure 6.23– 23K dwt Containership Conventional Bow Model (C-1)

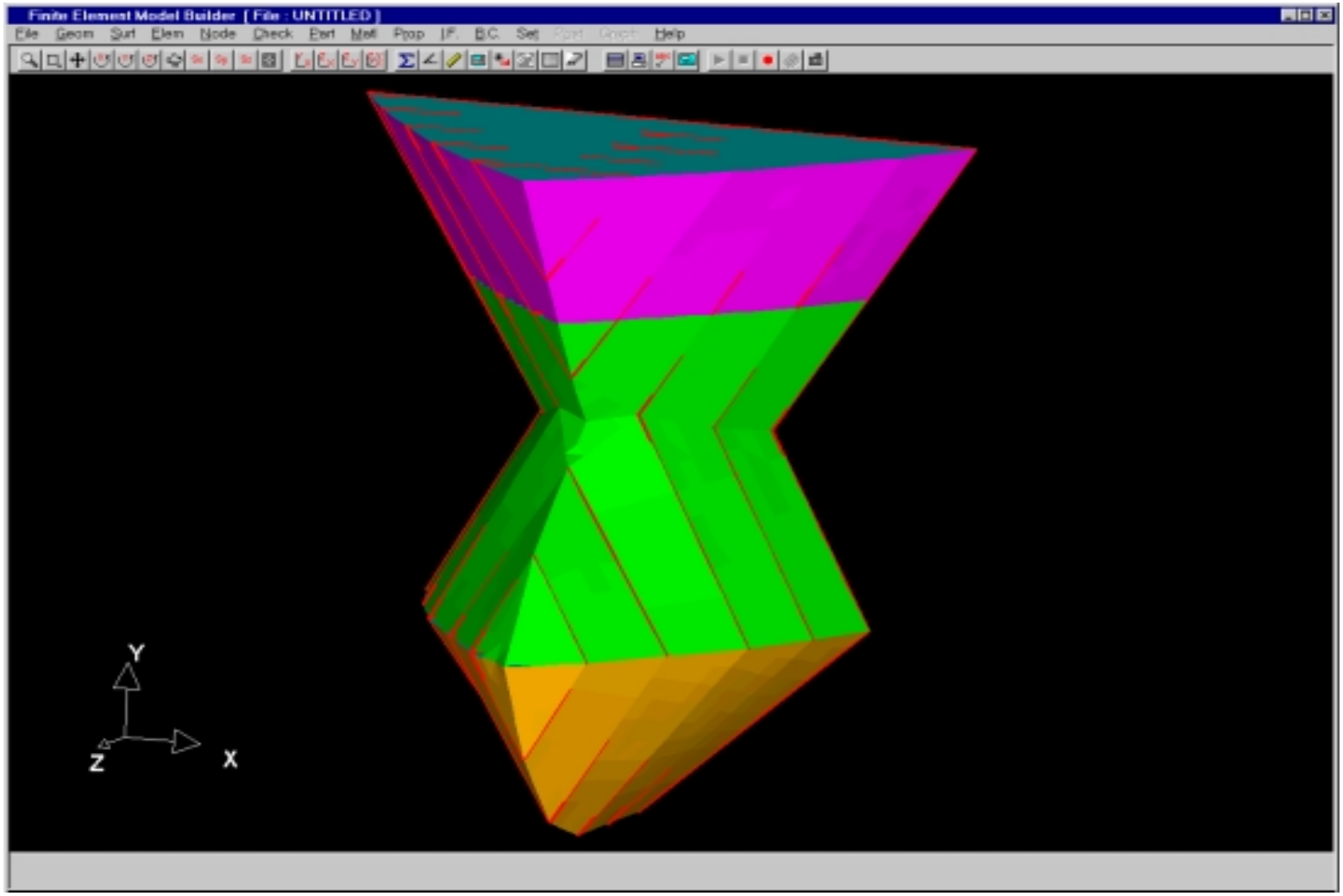

Figure 6.24– 150K dwt Bulk Carrier Bow Conventional Model (C-2)

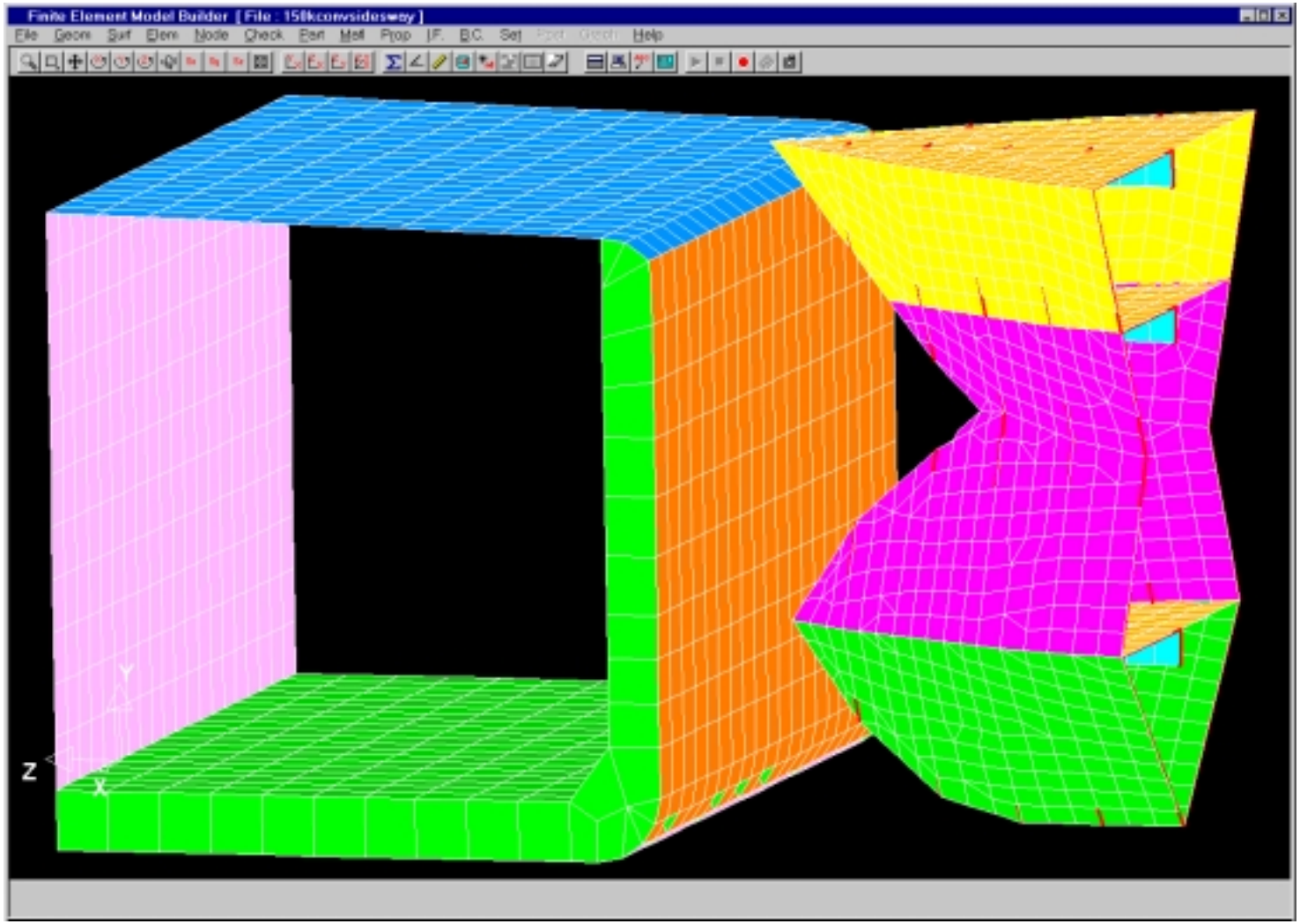

Figure 6.25– Conventional 150K dwt Containership Striking Conventional DH150 Tanker (C-5)

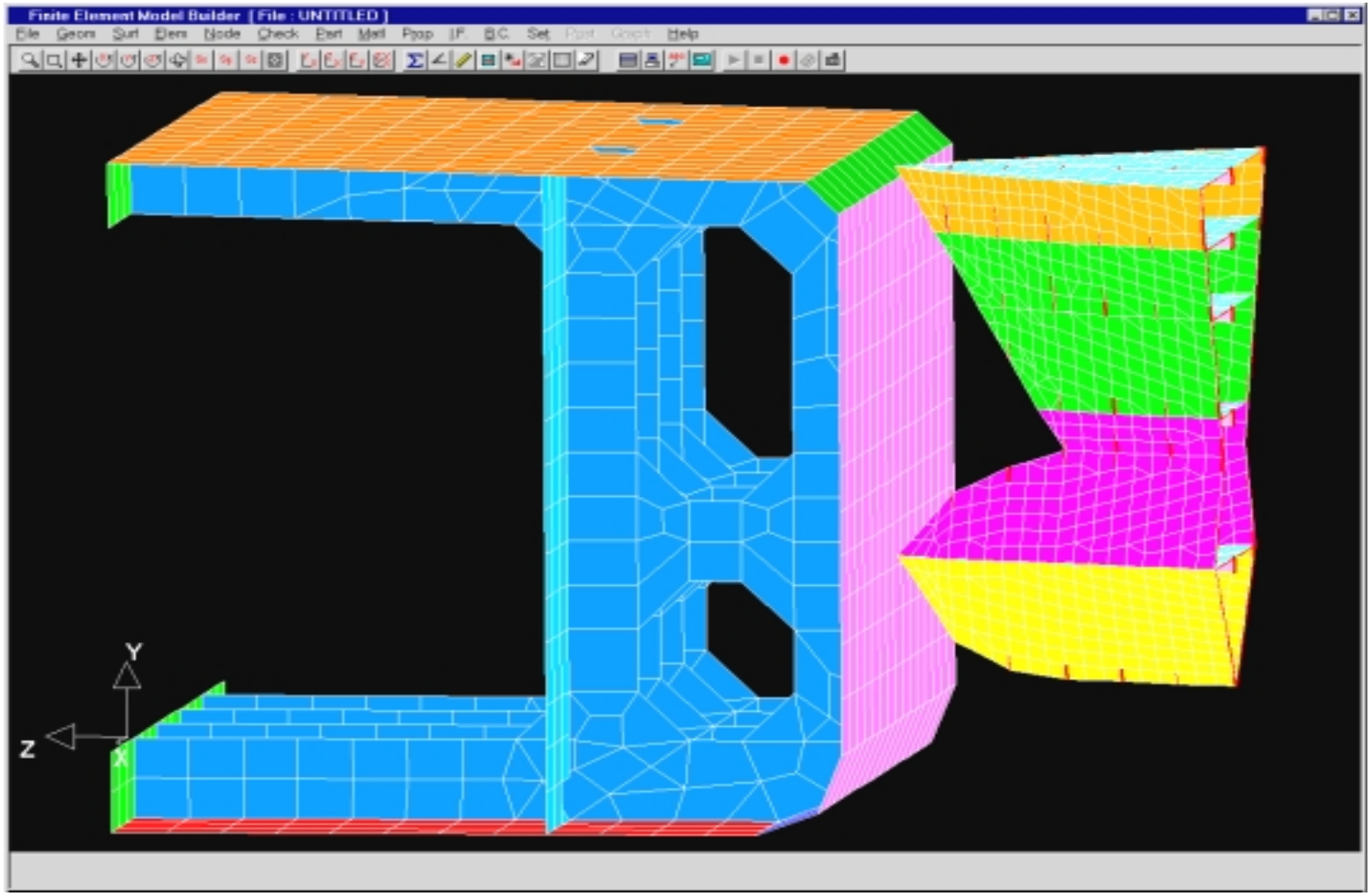

Figure 6.26– Conventional 23K dwt Containership Bow Striking a Conventional SH100 Tanker (C-3)

Chapter 7 Comparison of Results and Validation

7.1 Collision with a Rigid Wall (Cases I-5 to I-8, C-1 and C-2)

This section presents the results obtained from the simulations of the "intersection" element bow models striking a rigid wall at various speeds.

Plots of force, velocity and energy as functions of time are obtained from the simulations. The velocity-time curve is integrated to obtain the penetration-time curve, which is used to plot the force as a function of penetration. Information like collision duration is extracted from the velocity vs time plots so that the maximum collision duration is that corresponding to a striking ship velocity of zero. Conservation of energy can be seen in the energy-time plots. In the figures presented in this chapter, Case (a) denotes the case where the striking speed is 5m/s and Case (b) represents a speed of 12m/s. Figure 7.1 shows the collision force plotted against time, for Case I-5 (a).

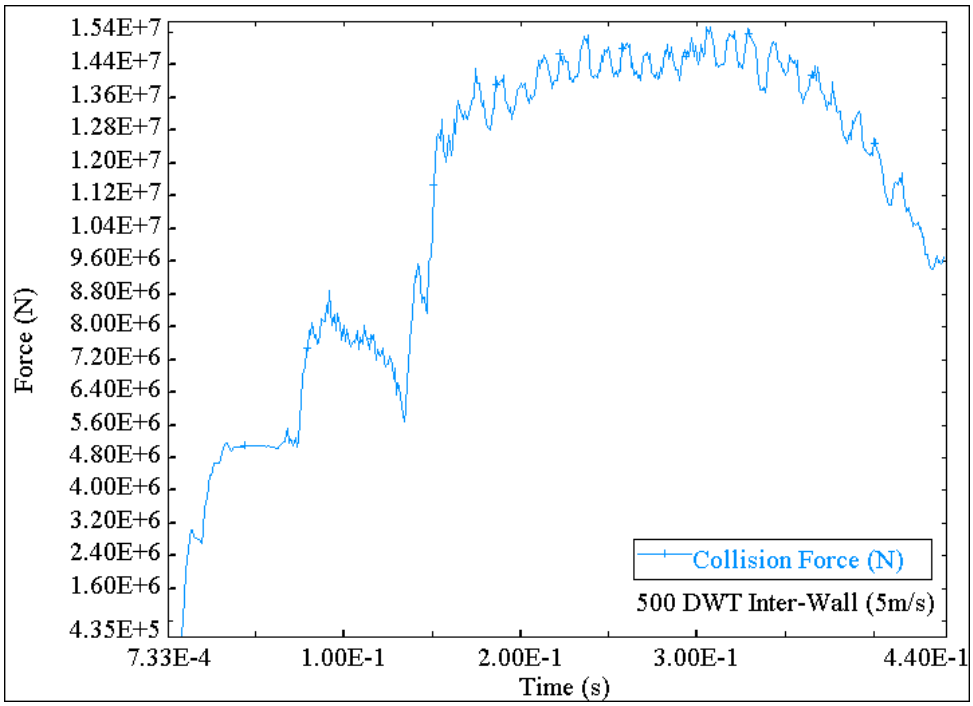

Figure 7.1 - Collision force vs time for Case I-5 (a)

Figure 7.2 shows the velocity time history for case I-5 (a). Figure 7.3 shows a plot of the energy during the collision process. As can be seen in Figure 7.2, the velocity decreases with time in a nearly linear fashion. A plot of penetration as a function of time is made, by integrating the velocity-time curve.

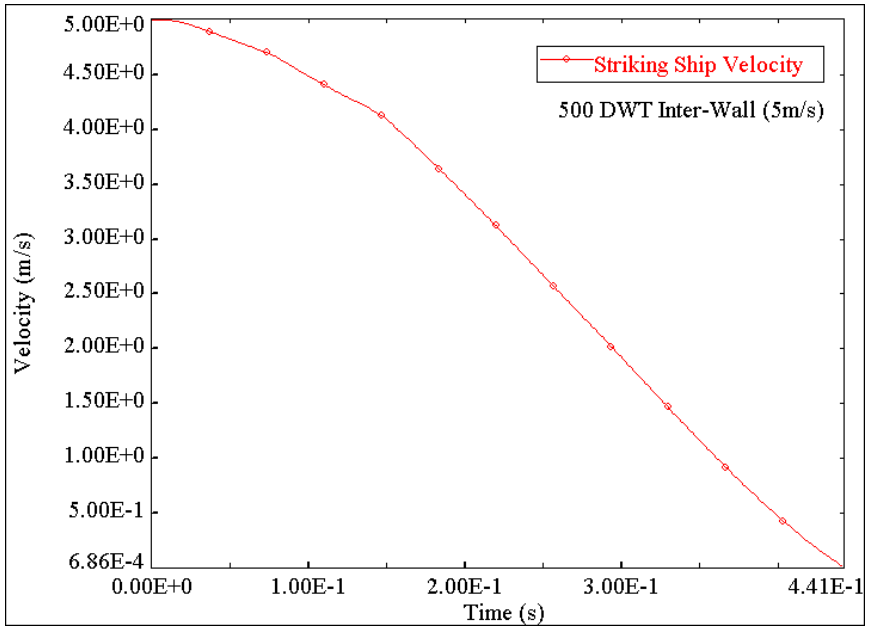

Figure 7.2 – Velocity time history for Case I-5 (a)

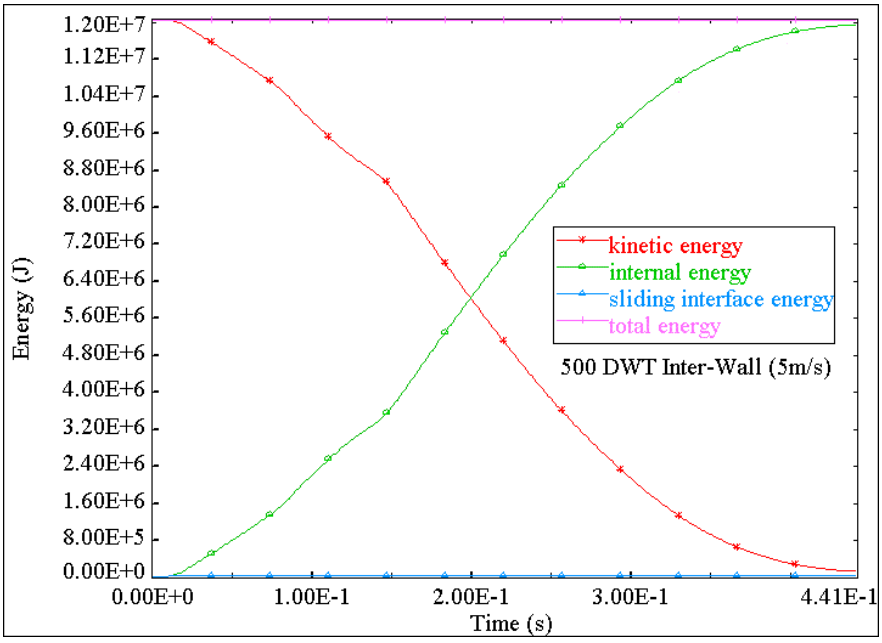

Figure 7.3 – Energy Time history for Case I-5 (a)

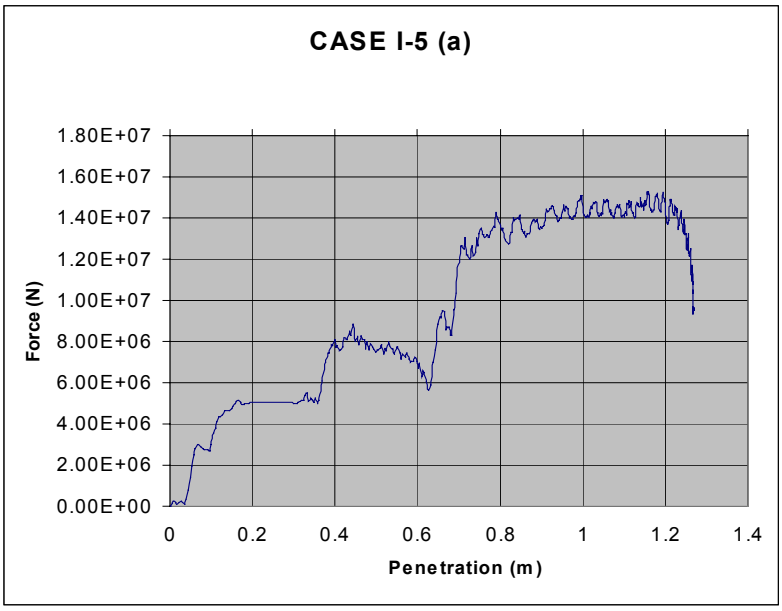

Figure 7.4 – Force vs Penetration plot for Case I-5 (a)

Values for maximum collision force, collision duration and maximum penetration have been recorded to be 15.3MN, 0.44s and 1.27m respectively.

Figure 7.5 shows the force-time plot for case I-5 (b). Figure 7.6 shows the velocity time history and Figure 7.7 shows the energy history. Force-penetration plots are obtained in the same way as in Case I-5 (a).

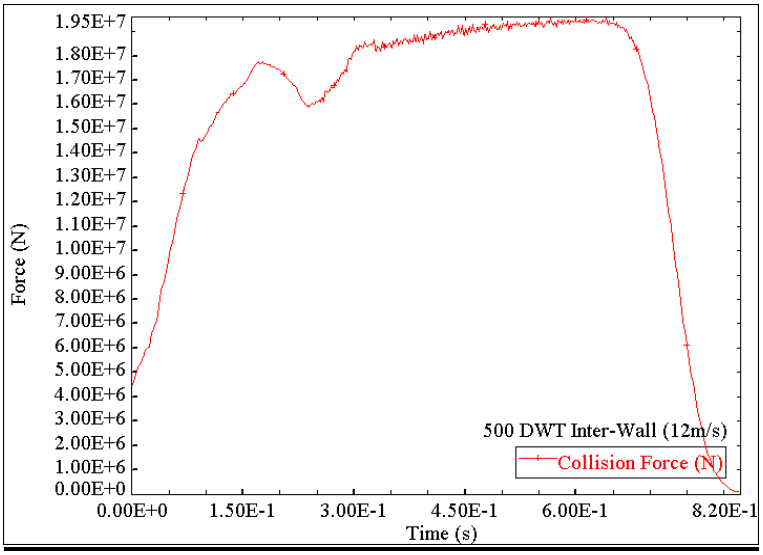

Figure 7.5 – Force vs time for Case I-5 (b)

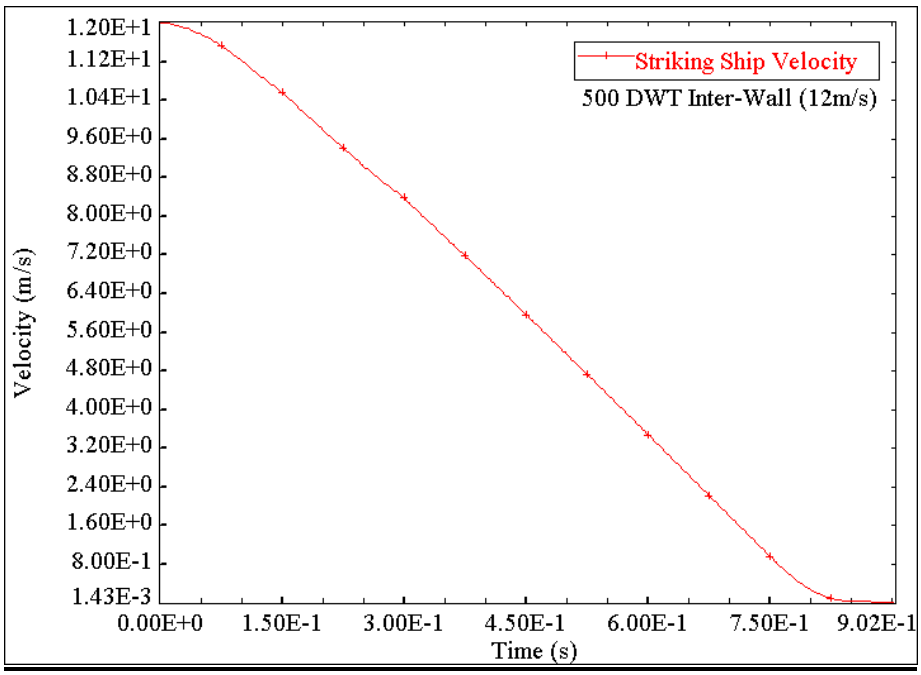

Figure 7.6 – Velocity vs time for Case I-5 (b)

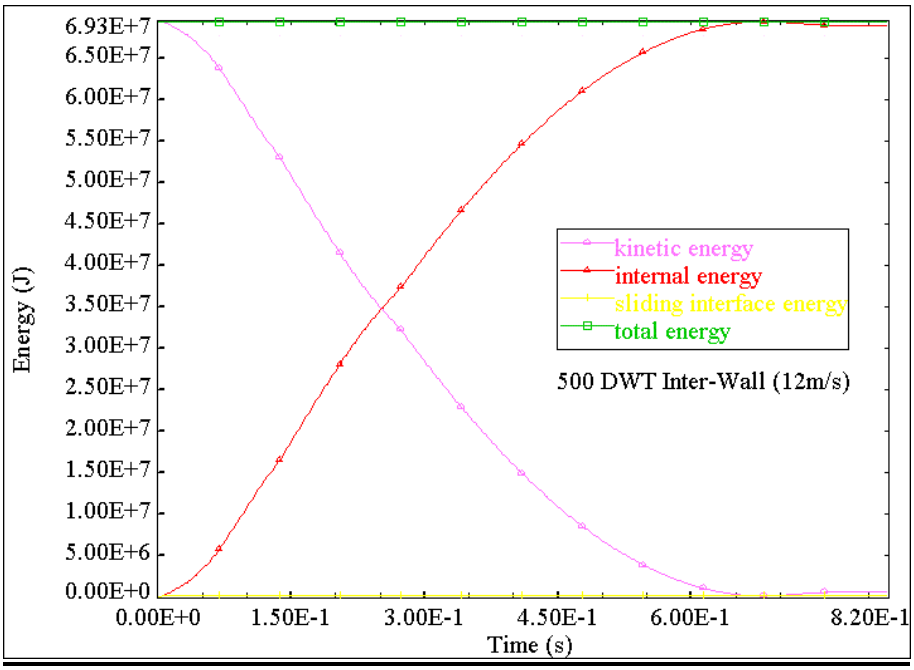

Figure 7.7 – Energy vs time for Case I-5 (b)

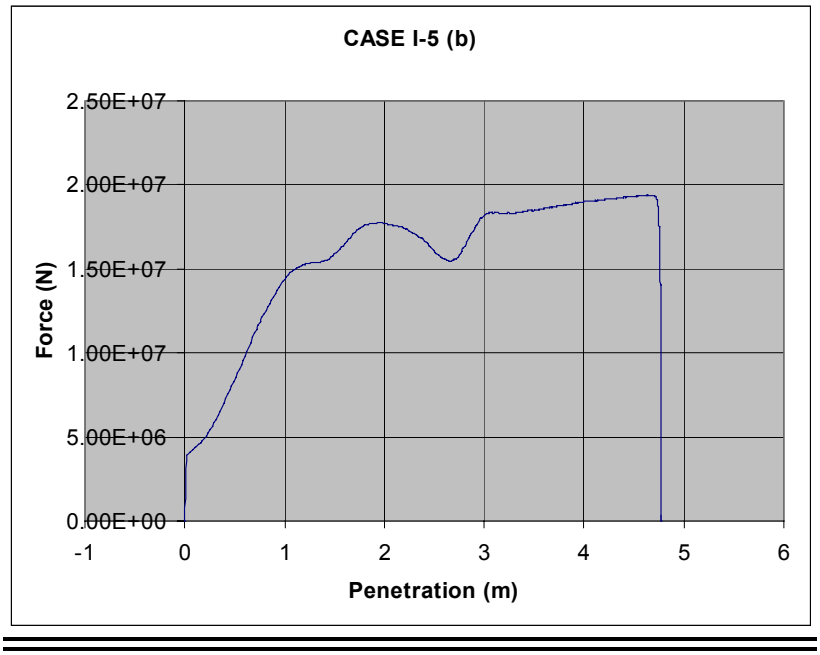

Figure 7.8 – Force vs penetration for Case I-5 (b)

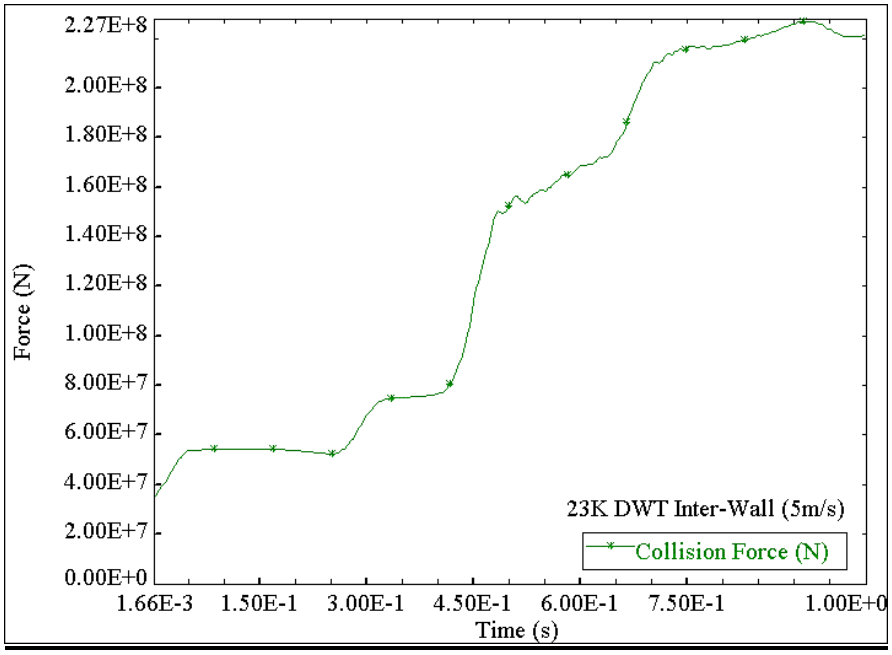

Figure 7.9 - Collision force vs time for case I-6 (a)

Figure 7.9 shows the collision force plotted against time, for Case I-6 (a). Figure 7.10 shows the force-penetration curve for the same case. Values for maximum collision force, collision duration and maximum penetration have been recorded to be 227MN, 1.0s and 3.42m respectively.

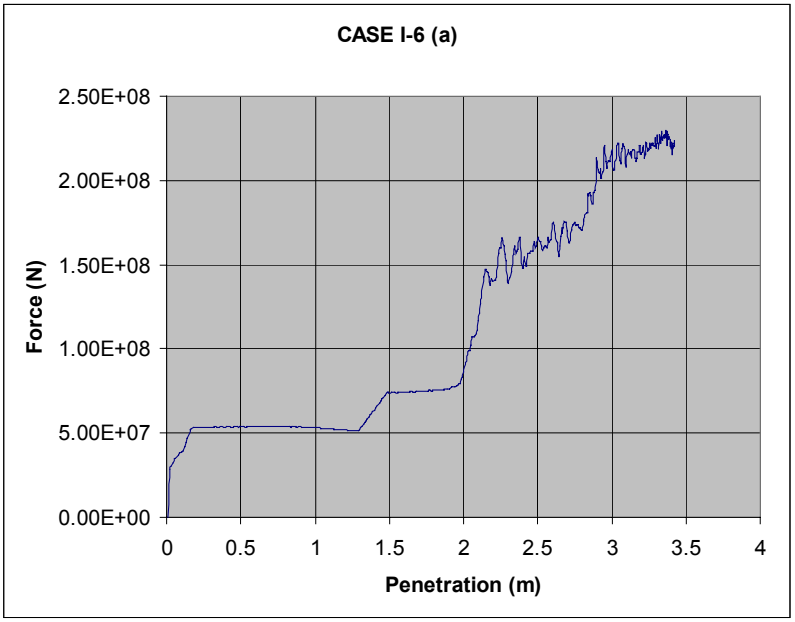

Figure 7.10 – Force vs penetration for CASE I-6 (a)

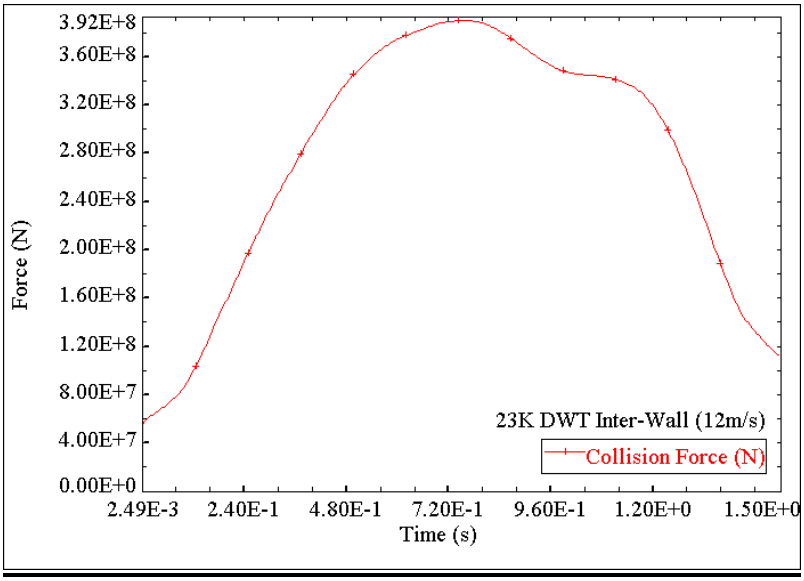

Figure 7.11 - Collision force vs time for case I-6 (b)

Figure 7.11 shows the collision force plotted against time, for Case I-6 (b). Figure 7.12 shows the force-penetration curve for the same case. Values for maximum collision force, collision duration and maximum penetration have been recorded to be 392MN, 1.5s and 9.49m respectively.

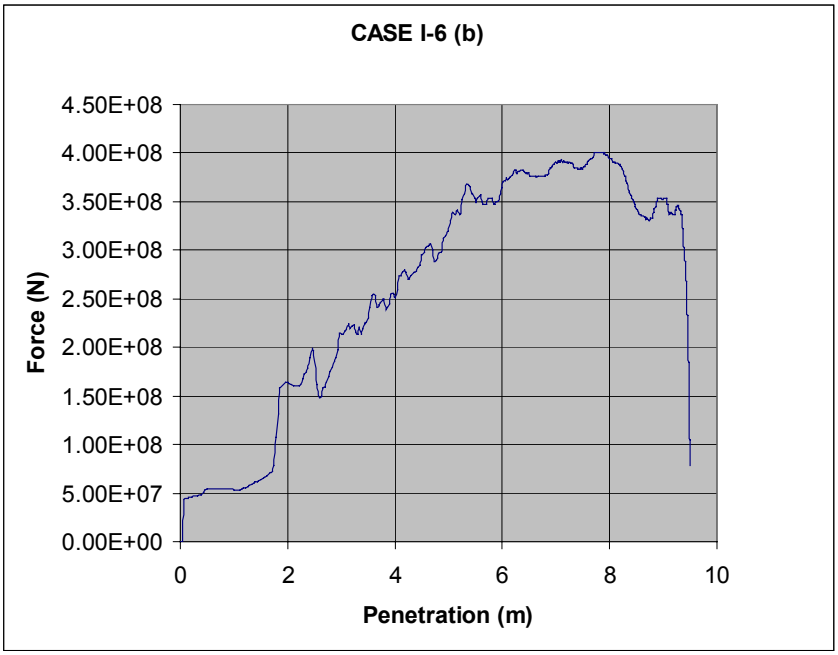

Figure 7.12 – Force vs penetration for Case I-6 (b)

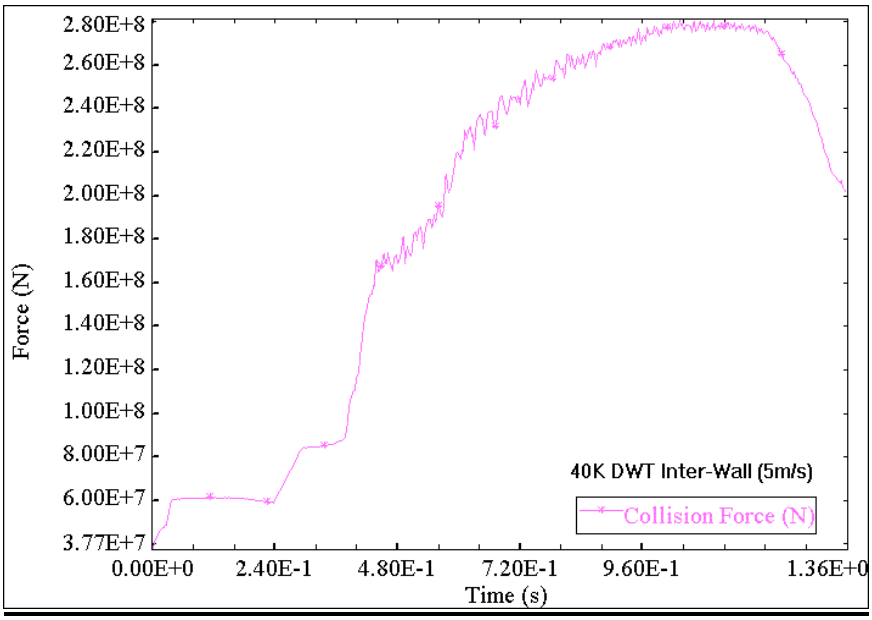

Figure 7.13 - Collision force vs time for Case I-7(a)

Figure 7.13 shows the collision force plotted against time, for Case I-7 (a). Figure 7.14 shows the force-penetration curve for the same case. Values for maximum collision force, collision duration and maximum penetration have been recorded to be 279MN, 1.36s and 4.18m respectively.

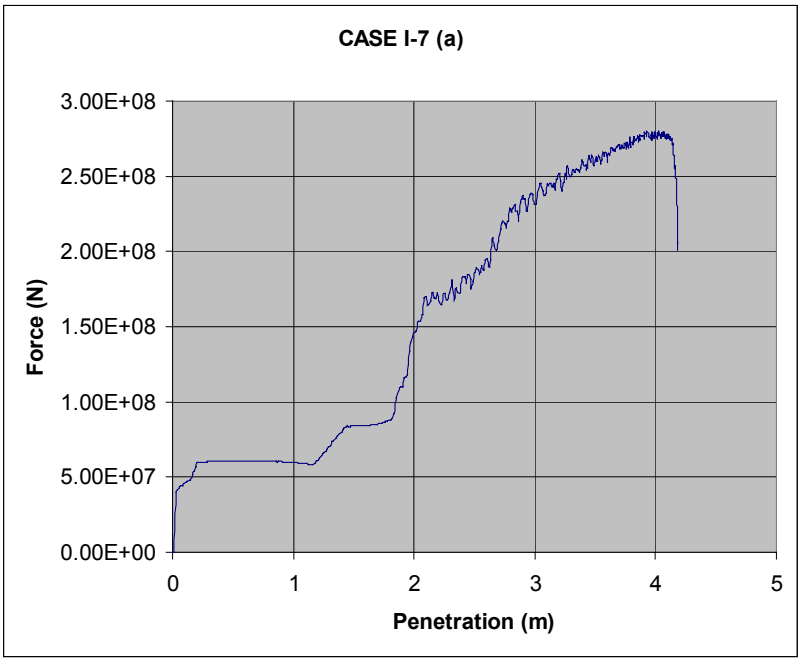

Figure 7.14 – Force vs penetration for Case I-7 (a)

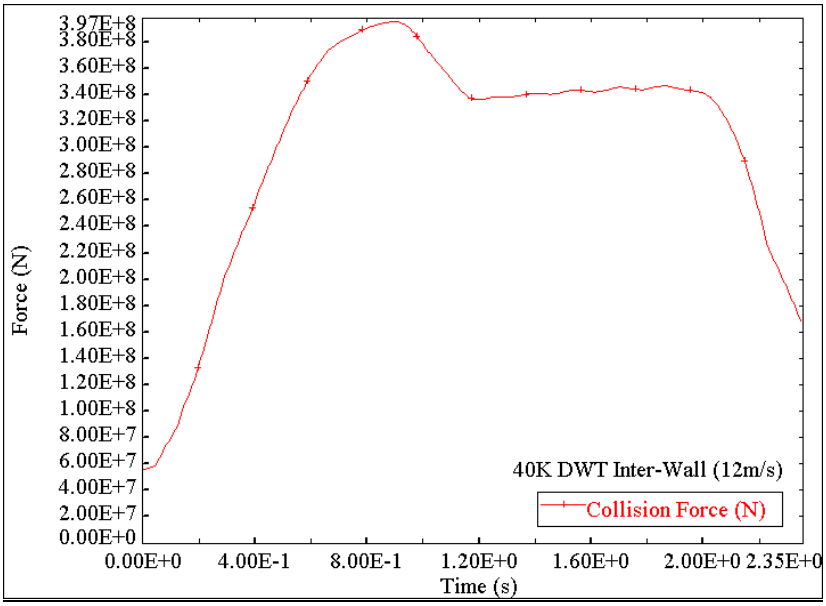

Figure 7.15 - Collision force vs time for case I-7 (b)

Figure 7.15 shows the collision force plotted against time, for Case I-7 (b). Figure 7.16 shows the force-penetration curve for the same case. Values for maximum collision force, collision duration and maximum penetration have been recorded to be 395MN, 2.35s and 14.91m respectively.

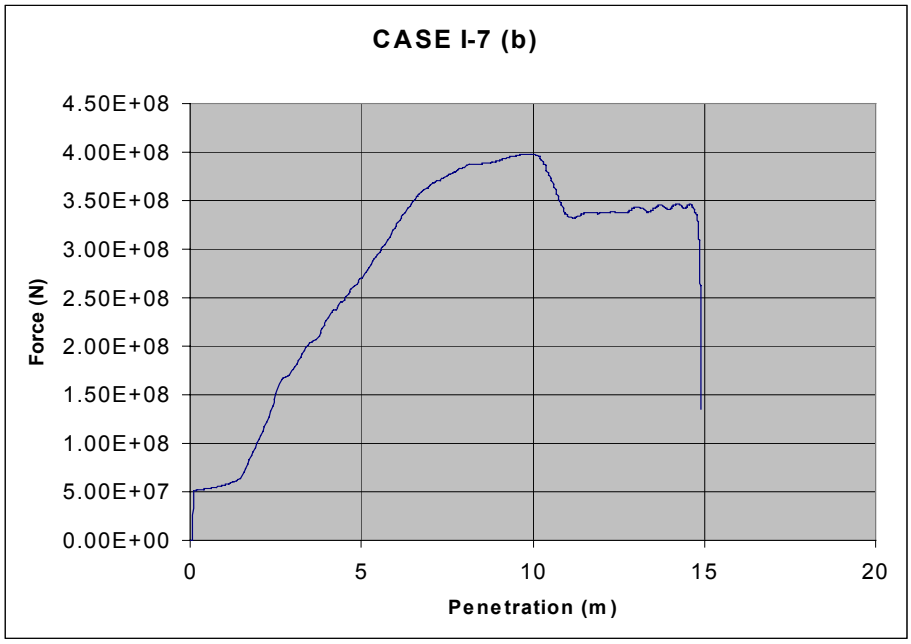

Figure 7.16 – Force vs penetration for Case I-7 (b)

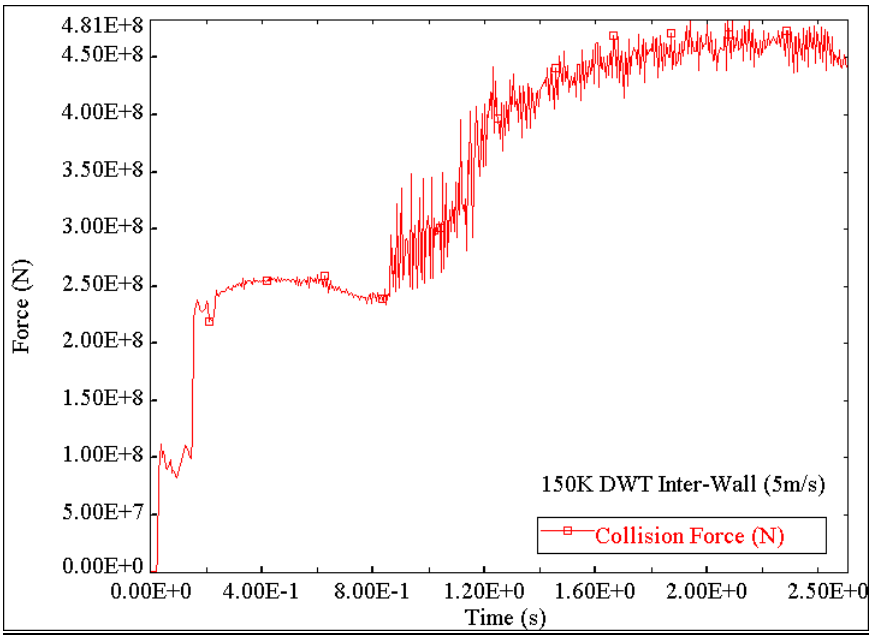

Figure 7.17 - Collision force vs time for Case I-8(a)

Figure 7.17 shows the collision force plotted against time, for Case I-8 (a). Figure 7.18 shows the force-penetration curve for the same case. Values for maximum collision force, collision duration and maximum penetration have been recorded to be 481MN, 2.5s and 7.33m respectively.

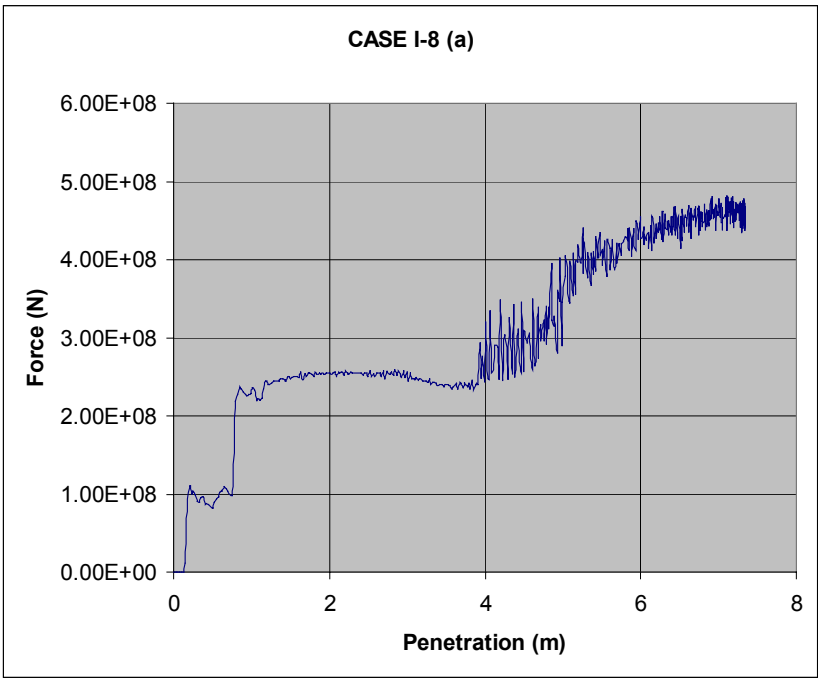

Figure 7.18 – Force vs penetration for Case I-8 (a)

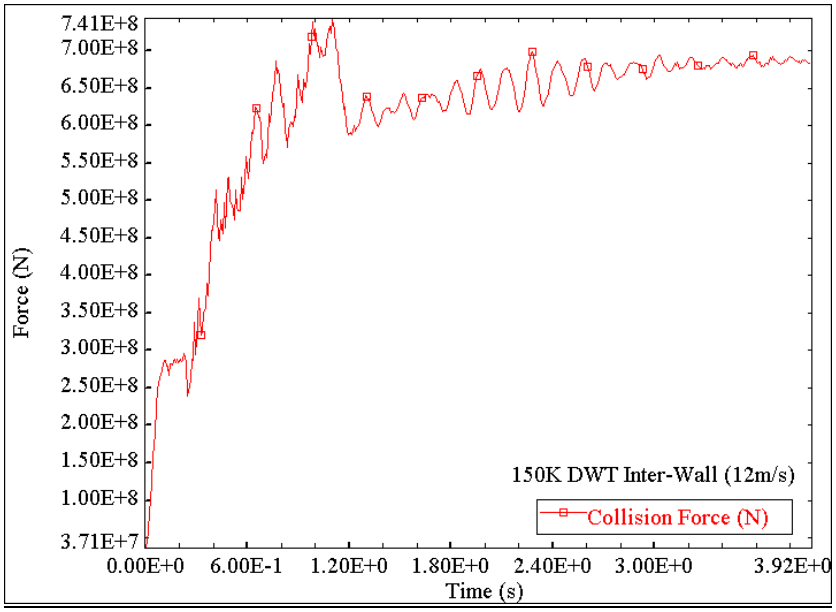

Figure 7.19 - Collision force vs time for Case I-8 (b)

Figure 7.19 shows the collision force plotted against time, for Case I-8 (b). Figure 7.20 shows the force-penetration curve for the same case. Values for maximum collision force, collision duration and maximum penetration have been recorded to be 741MN, 3.92s and 25.39m respectively.

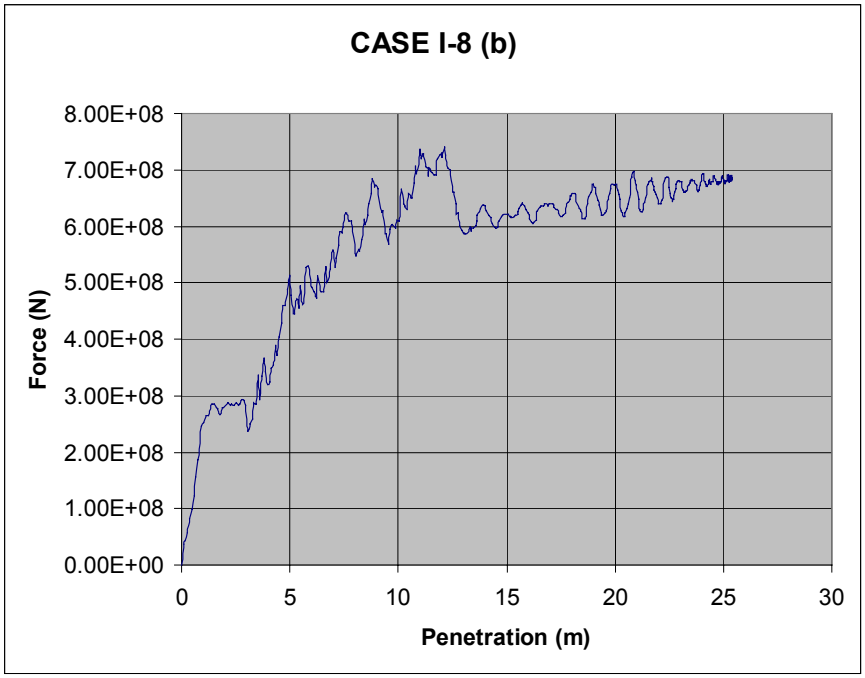

Figure 7.20 – Force vs penetration for Case I-8 (b)

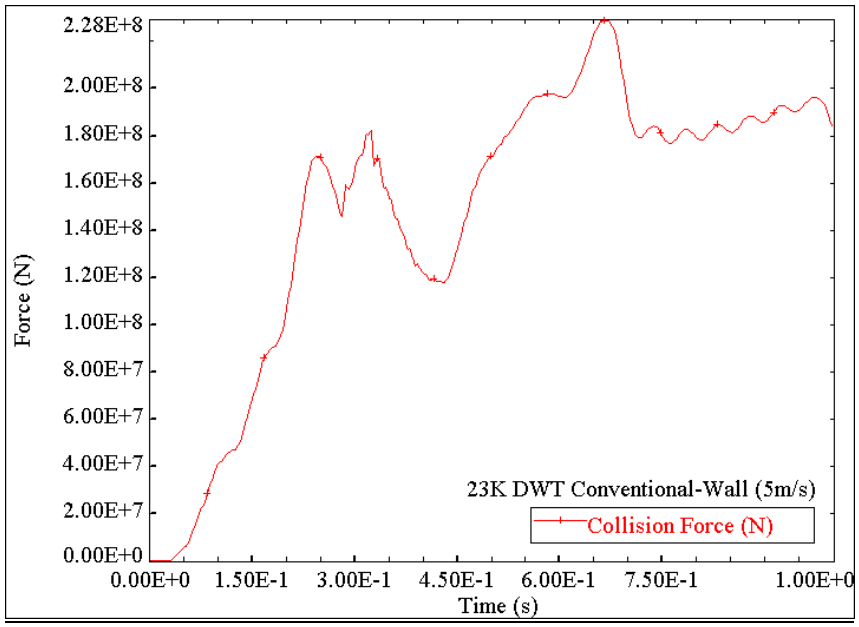

Figure 7.21 - Collision force vs time for Case C-1 (a)

Figure 7.21 shows the collision force plotted against time, for Case C-1 (a). Figure 7.22 shows the force-penetration curve for the same case. Values for maximum collision force, collision duration and maximum penetration have been recorded to be 228MN, 1s and 2.92m respectively.

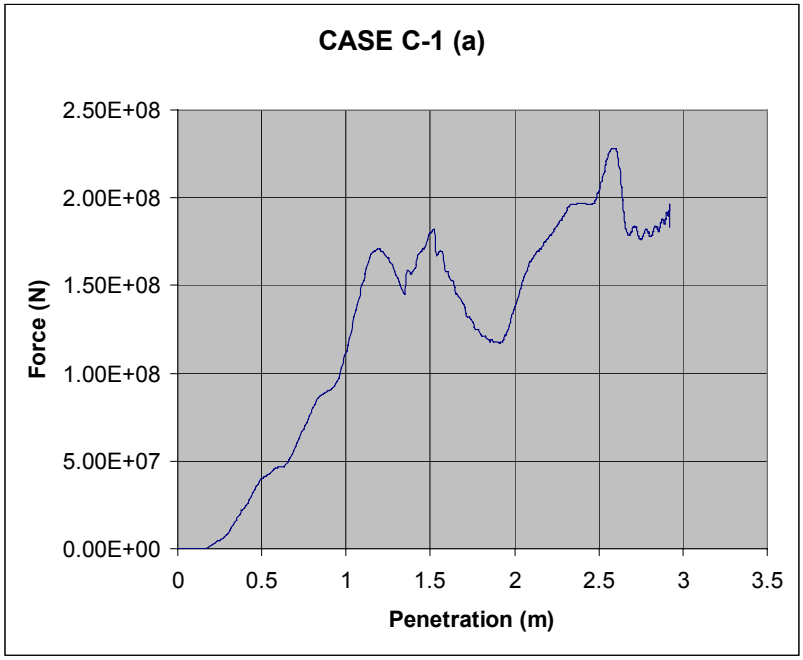

Figure 7.22 – Force vs penetration for Case C-1 (a)

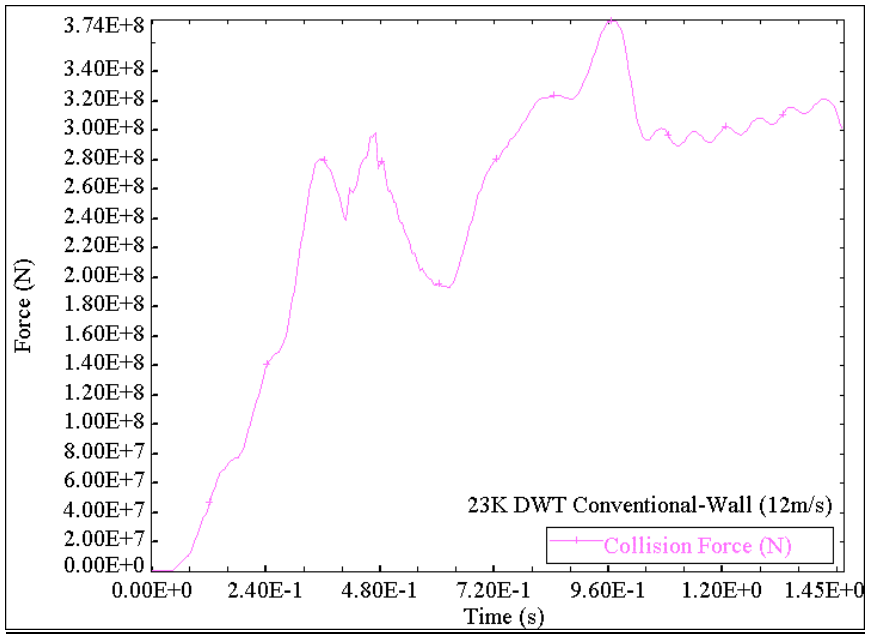

Figure 7.23 – Collision Force vs time for Case C-1 (b)

Figure 7.23 shows the collision force plotted against time, for Case C-1 (b). Figure 7.24 shows the force-penetration curve for the same case. Values for maximum collision force, collision duration and maximum penetration have been recorded to be 374MN, 1.45s and 9.2m respectively.

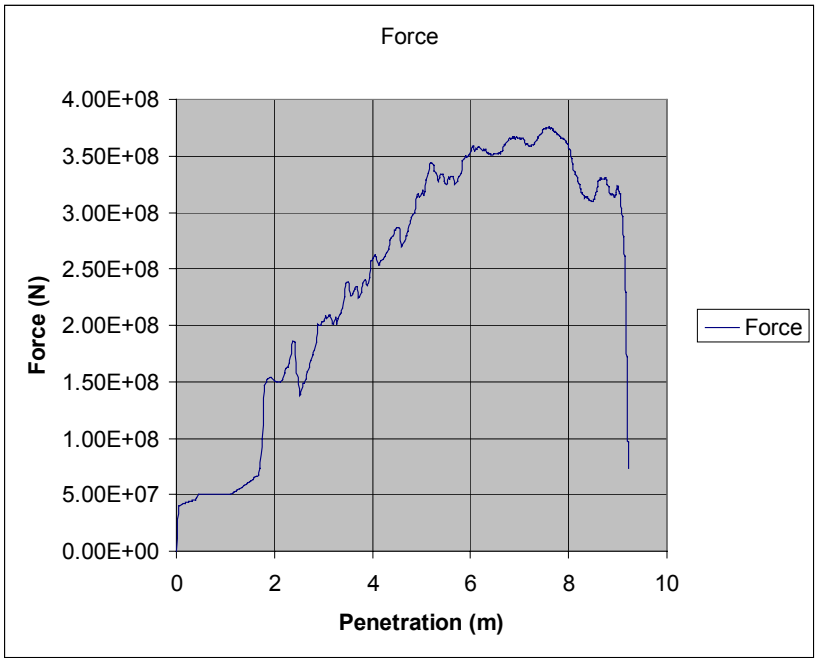

Figure 7.24 – Force vs penetration for Case C-1 (b)

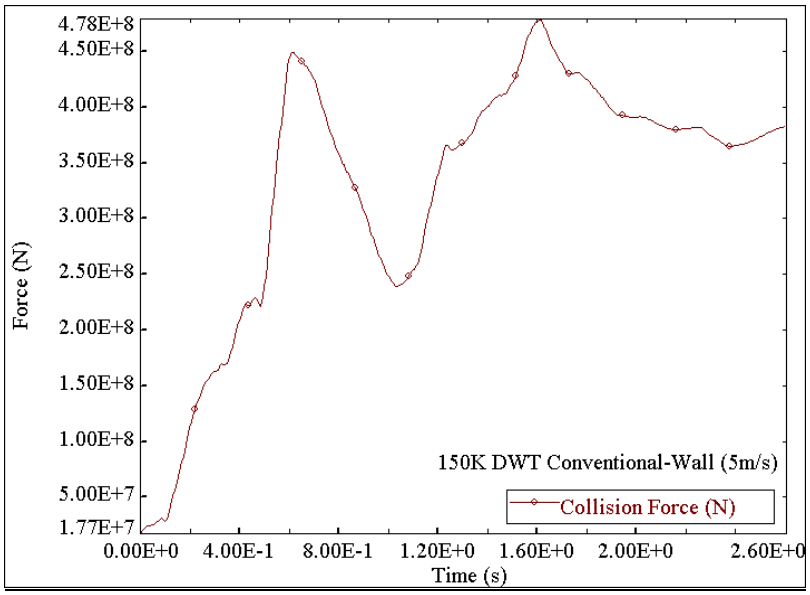

Figure 7.25 - Collision force vs time for Case C-2 (a)

Figure 7.25 shows the collision force plotted against time, for Case C-2 (a). Figure 7.26 shows the force-penetration curve for the same case. Values for maximum collision force, collision duration and maximum penetration have been recorded to be 477MN, 2.53s and 7.2m respectively.

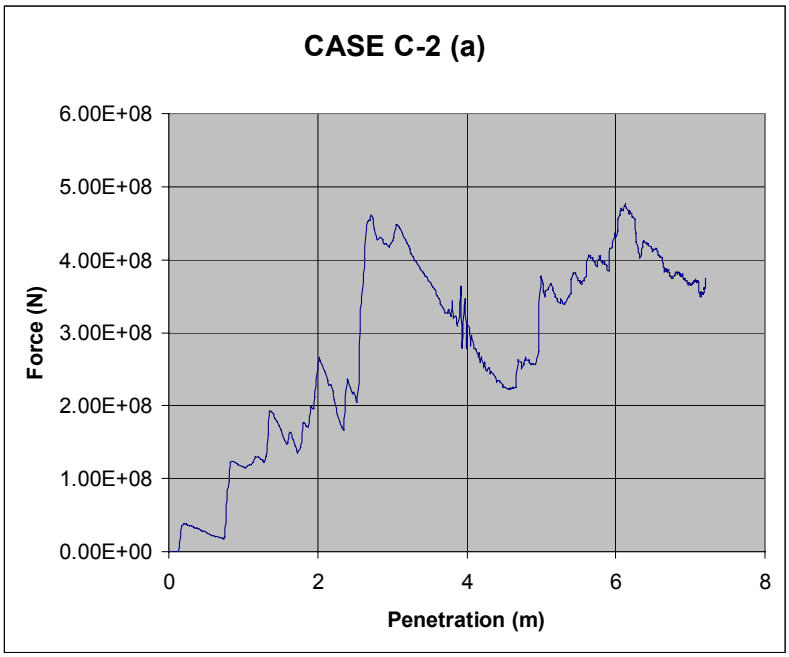

Figure 7.26 – Force vs penetration for Case C-2 (a)

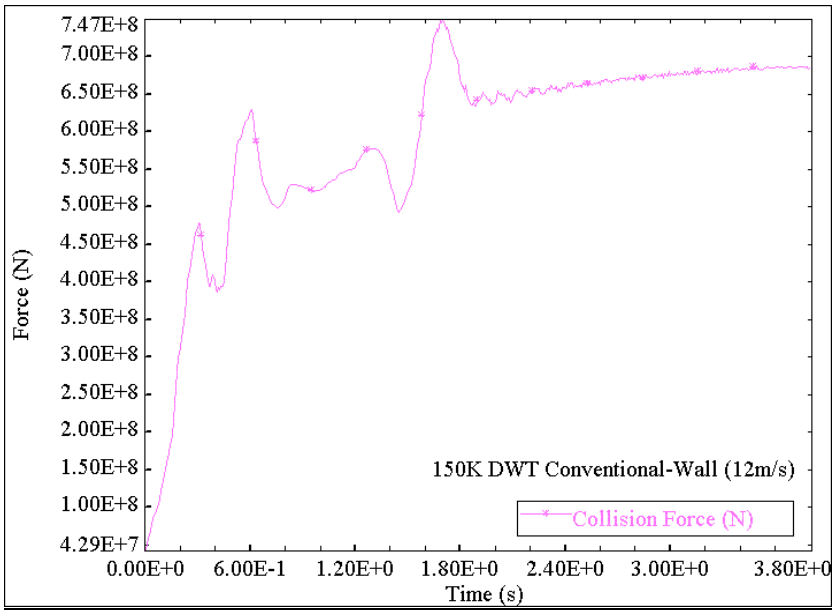

Figure 7.27 - Collision force vs time for Case C-2 (b)

Figure 7.27 shows the collision force plotted against time, for Case C-2 (b). Figure 7.28 shows the force-penetration curve for the same case. Values for maximum collision force, collision duration and maximum penetration have been recorded to be 747MN, 3.8s and 25.0m respectively.

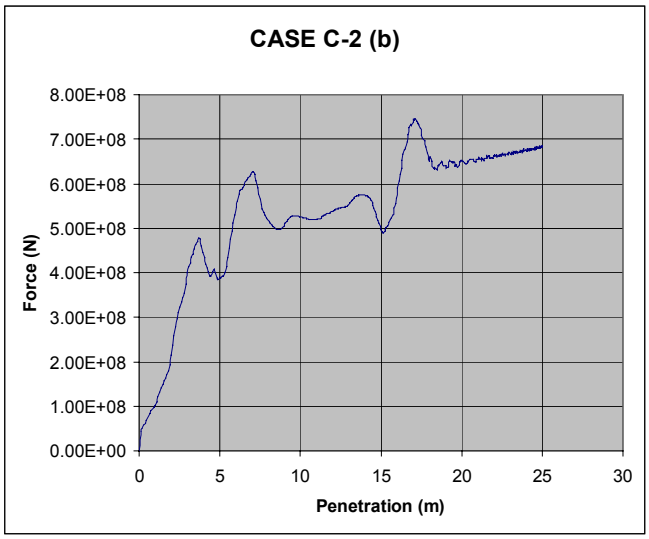

Figure 7.28– Force vs penetration for Case C-2 (b)

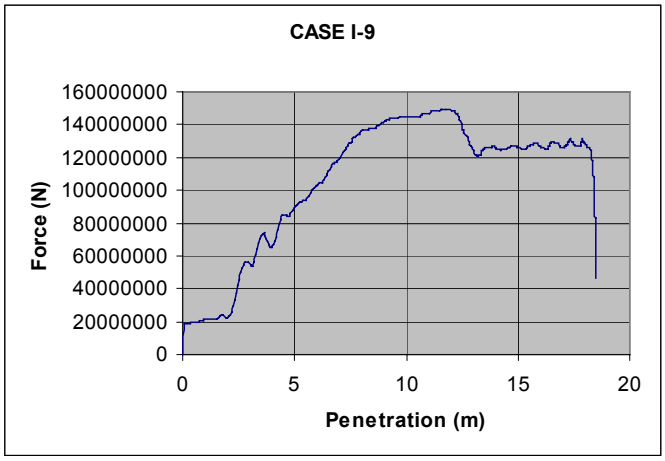

Figure 7.29 – Force vs penetration for Case I-9

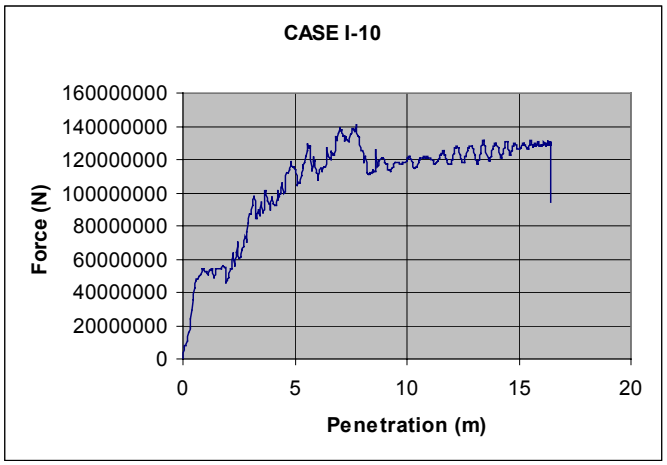

Figure 7.30 – Force vs penetration for Case I-10

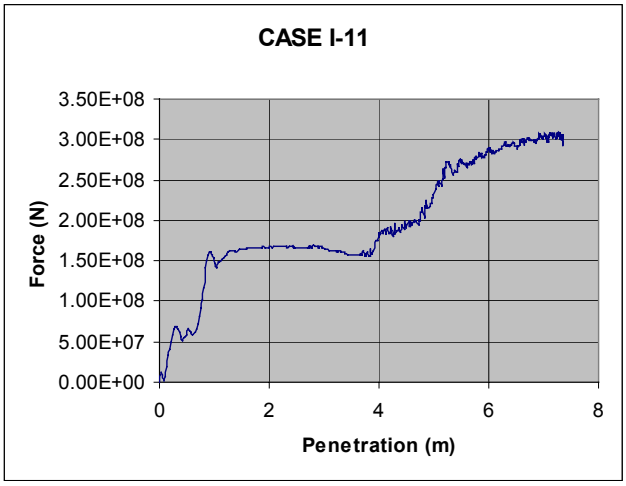

Figure 7.31 – Force vs penetration for Case I-11

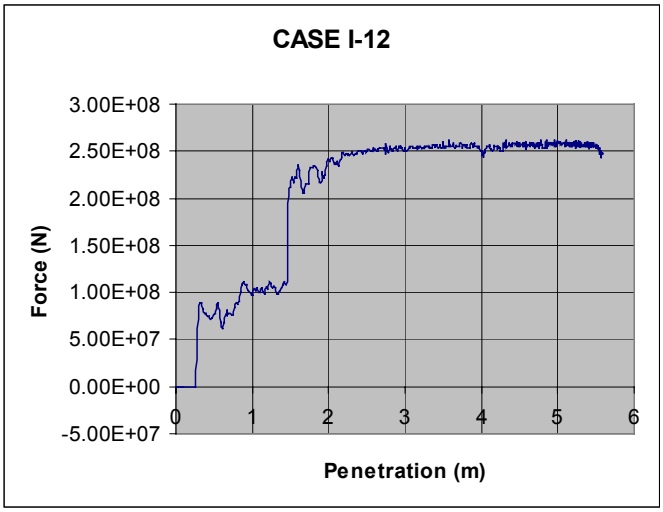

Figure 7.32 - Force vs penetration for Case I-12

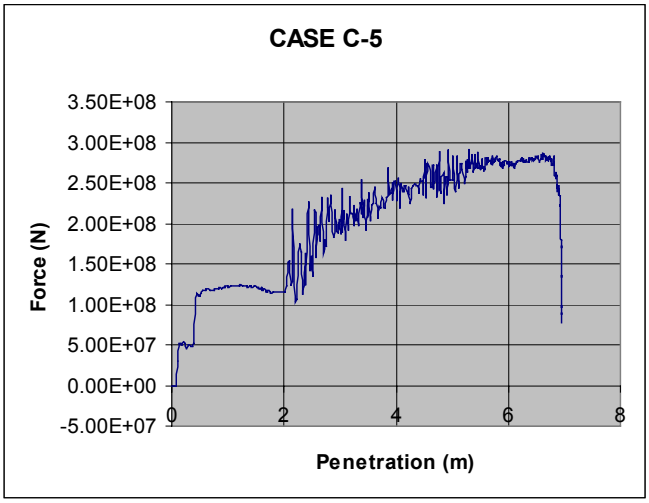

Figure 7.33 - Force vs penetration for Case C-5

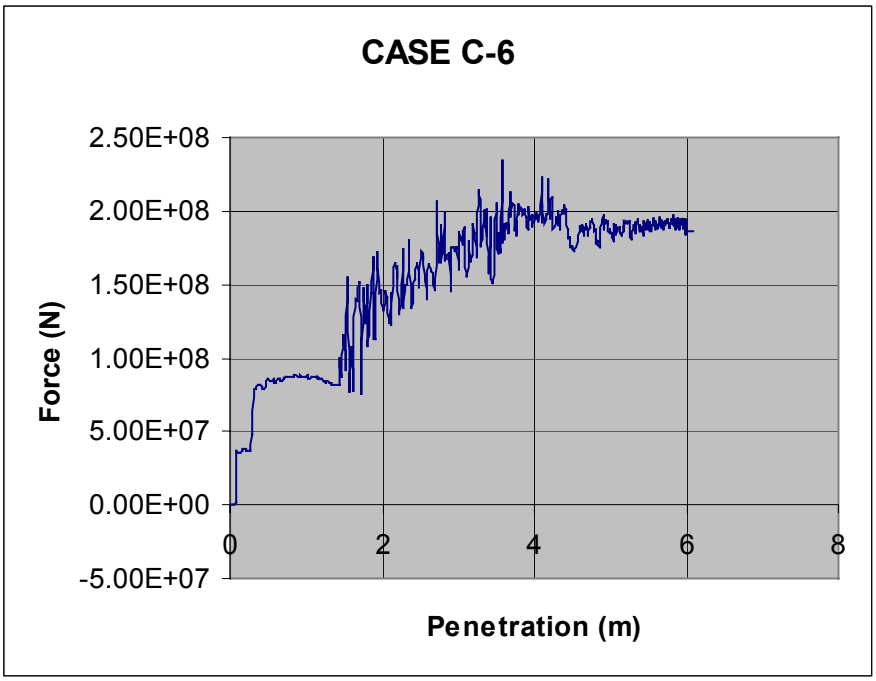

Figure 7.34 - Force vs penetration for Case C-6

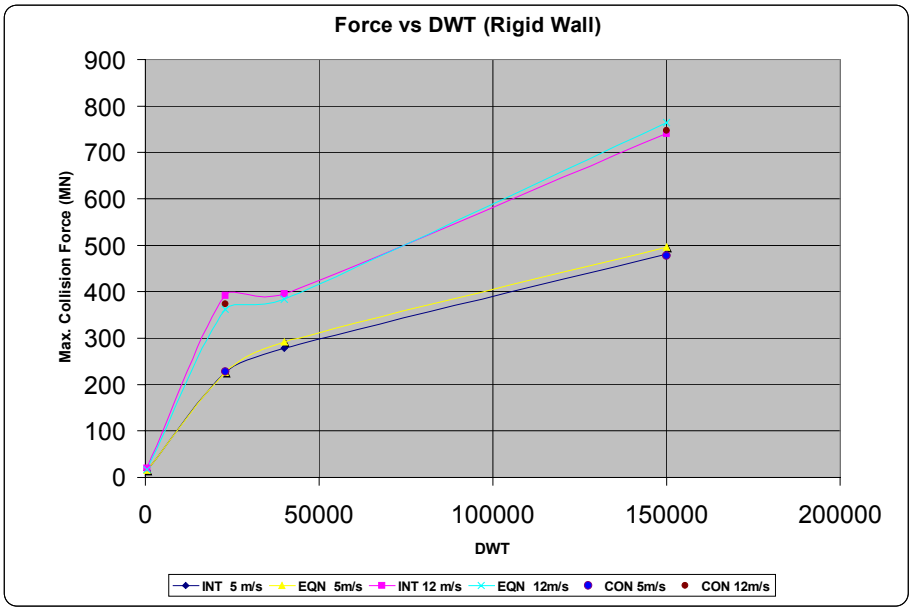

Figure 7.35 – Force vs DWT for various models

Figure 7.35 shows the maximum collision forces plotted as a function of DWT. The two different sets of curves are for the two different speeds. Good correlation is obtained between the intersection, conventional and closed-form calculations. Figure 7.36 shows

the maximum penetration plotted against DWT for the two speeds. It is observed that the intersection and conventional models predict lower penetrations than the closed-form results for higher speeds.

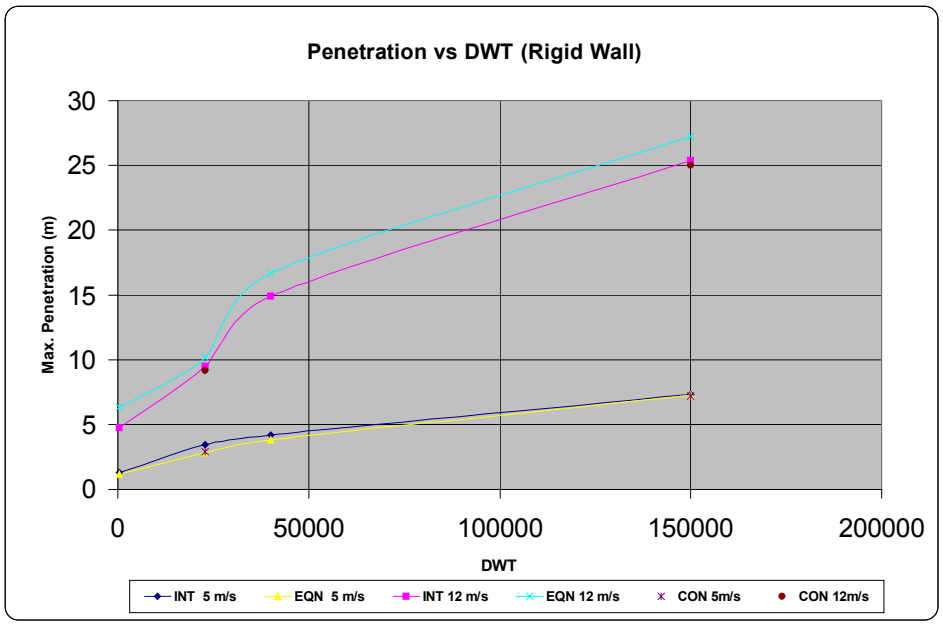

Figure 7.36 – Penetration vs DWT for various models

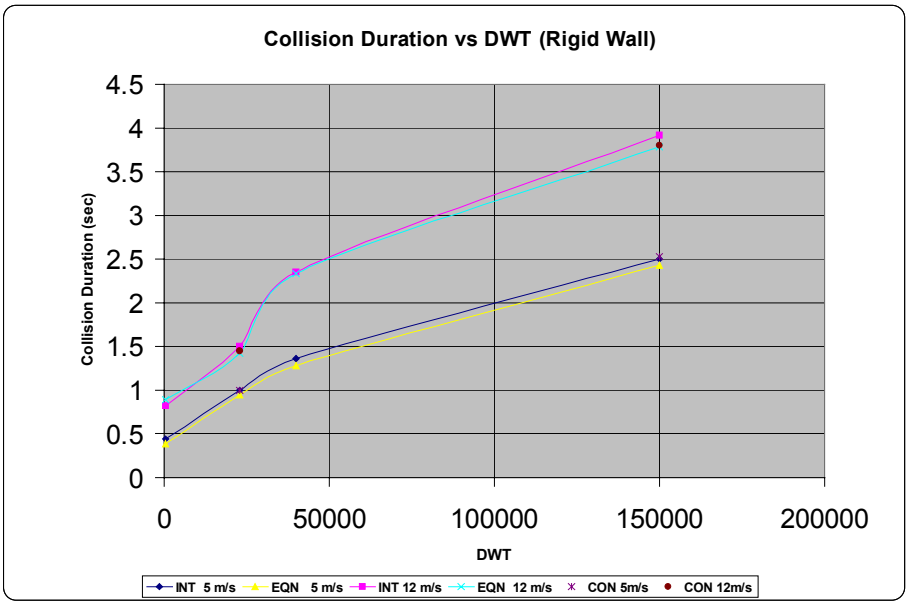

Figure 7.37 – Collision Duration as a function of DWT

Figure 7.37 shows the collision duration plotted as a function of DWT for the two different speeds. Good correlation is obtained between the intersection, conventional and

closed-form calculations. Figure 7.38 shows a comparison of the collision forces for the 23K DWT and 150K DWT ships for the two speeds. It is observed that the intersection and conventional models predict values close to the closed-form values.

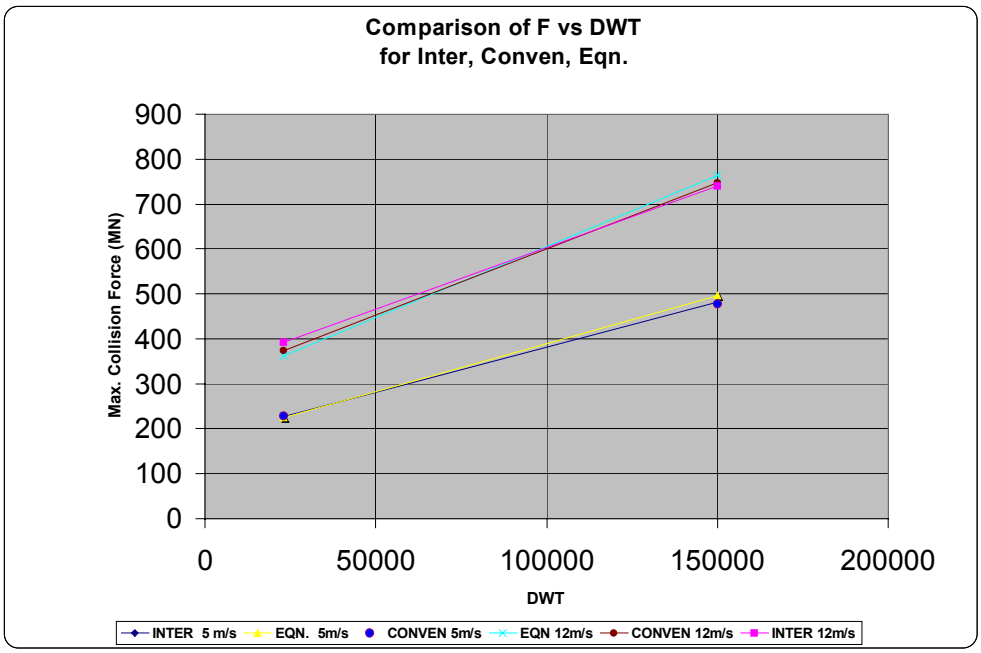

Figure 7.38 – Comparison of F vs DWT for different models

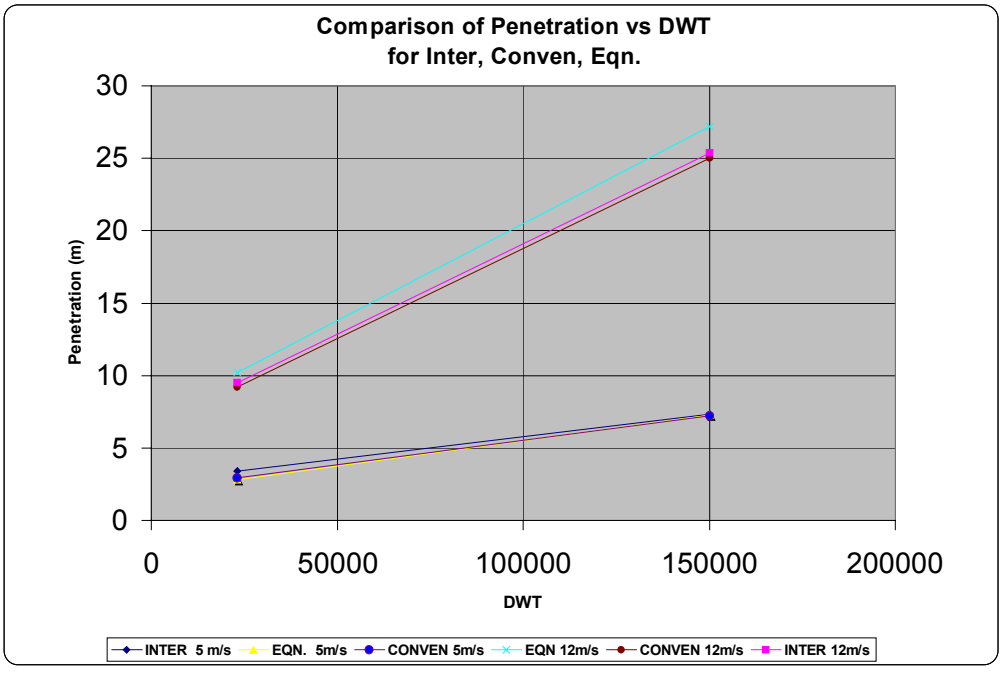

Figure 7.39 – Comparison of maximum penetration vsDWT for various models

Figure 7.39 shows a comparison of the maximum penetration for the 23K DWT and 150K DWT ships for the two speeds. For lower speeds, good correlation is obtained. At higher speeds, the intersection and conventional models predict lower penetration compared to the closed-form results. Collision duration shows a good correlation as seen in Figure 7.40.

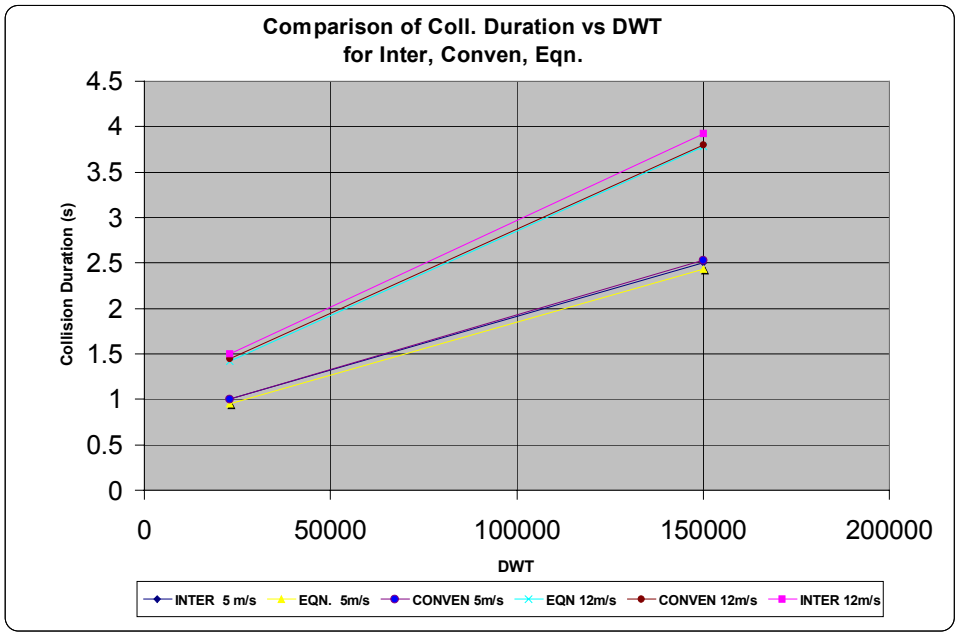

Figure 7.40 – Comparison of Collision Duration vs DWT

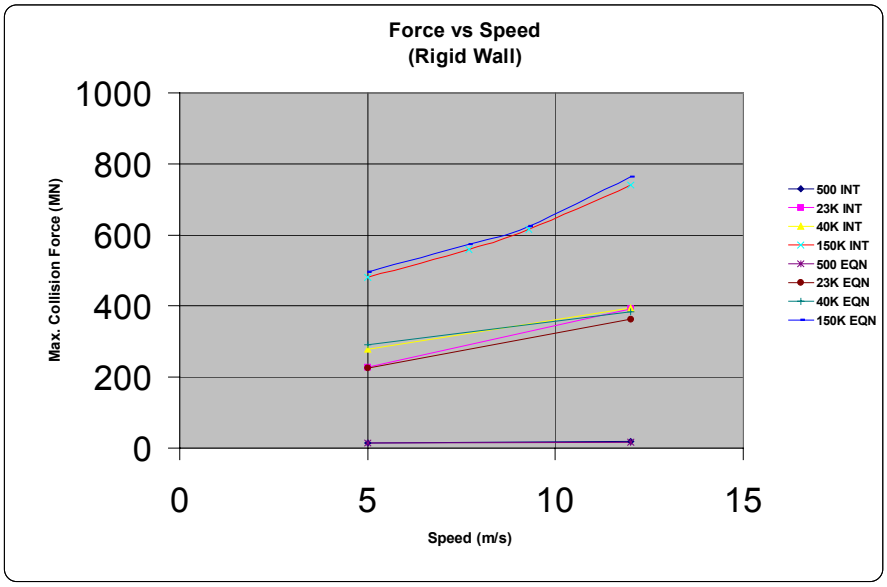

Figure 7.41 – Collision Force vs Striking Speed for different ships

Figure 7.41 compares the variation of collision force with speed for the 23K DWT and 150K DWT. All three results seem to match well. Figure 7.42 compares the variation of maximum penetration with speed for the four basis ships. Again, at lower speeds, there is a good match. At higher speeds, the intersection model, as compared to the closed-form results predicts lower penetration.

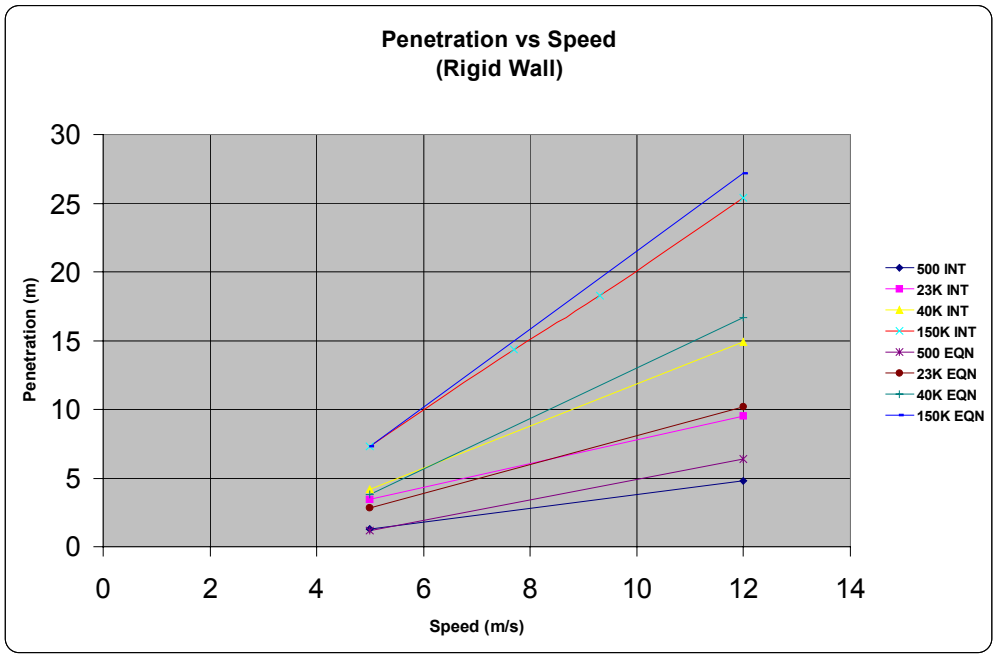

Figure 7.42 – Maximum penetration vs Striking speed for various ships

Figure 7.43 – Collision Duration vs Speed for different ships

Figure 7.43 compares the variation of collision duration with speed for the four basis ships. Figure 7.44 compares the variation of collision force with speed for different models of the 23K and 150K ships.

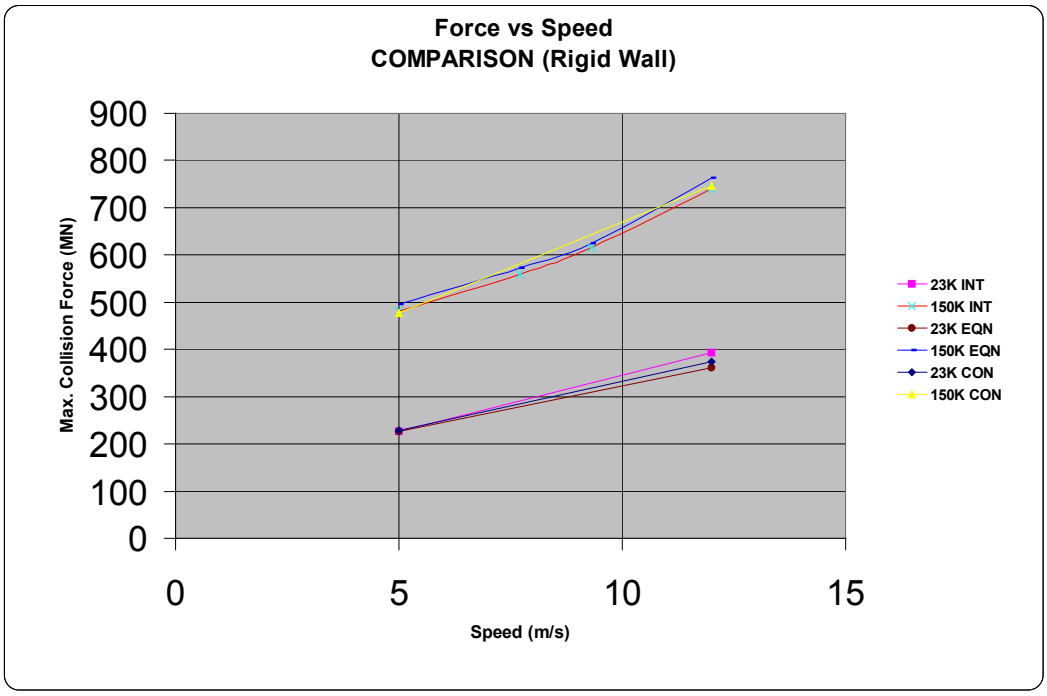

Figure 7.44 – Collision Force vs Speed (23K vs 150K)

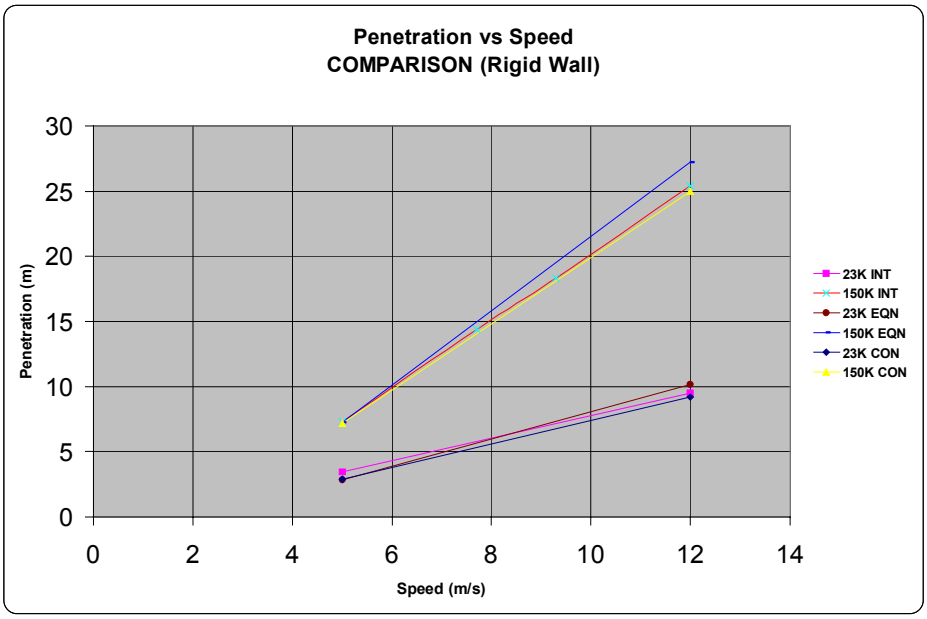

Figure 7.45 – Comparison of Penetration vs speed for 23K and 150K

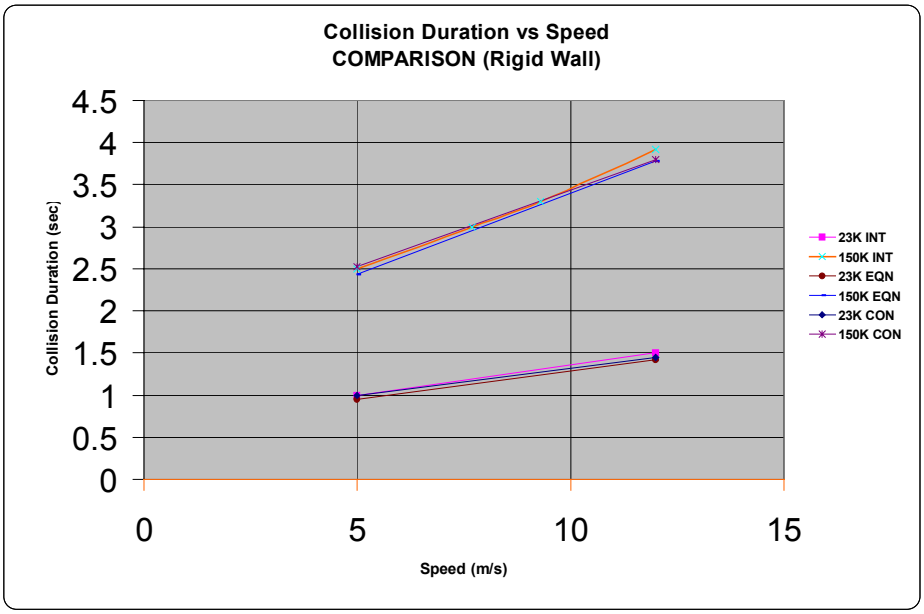

Figure 7.46 – Comparison of collision duration vs speed for 23K and 150K

Figure 7.45 compares the variation of maximum penetration with speed for different models of the 23K DWT and 150K DWT. Again, there is a good match at lower speeds, but at higher speeds, intersection and conventional models predict lower penetration. Figure 7.46 compares the variation of collision duration with speed for different models of 23K and 150K ships. Chapter 8 presents various conclusions derived from the above results and also suggests scope for future research.

Chapter 8 Analysis, Conclusions and Future Research

8.1 ANALYSIS OF RESULTS

This section presents a brief analysis of the important results from Chapter 7. The results presented in Chapter 7 are analyzed to extract useful information and reach important conclusions.

Figures 8.1 (a) and 8.1(b) show results for the 23 kdwt and 150 kdwt ships respectively, using the conventional and intersection element models. Model results are very consistent. Solutions using the conventional model require much more CPU time than the intersection model and since the results are equivalent, the intersection model is the preferred alternative.

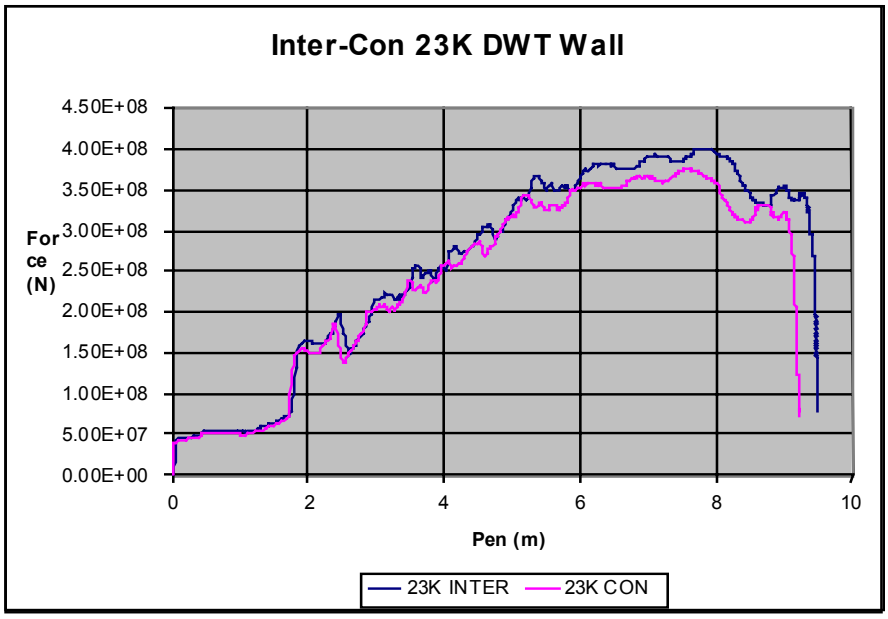

Figure 8.1 (a) – Comparison of F-p curves for Conventional and Intersection Models

Figure 8.2 (a) compares force-penetration results for the 500 DWT intersection-model striking ship for two different speeds. Figures 8.2 (b), (c) and (d) show force-penetration results for the 23K, 40K and 150K striking ship "intersection" models, for two striking speeds (5m/s and 12m/s). Figures 8.2 (e) and 8.2 (f) show a comparison of

force-penetration results for the conventional 23K and 150K striking ships for two different speeds. Each of these figures shows that the relationship between force and penetration is insensitive to striking ship speed and total energy absorbed. This implies that the application of these force-penetration curves to other than rigid wall collisions and for collisions with various absorbed energies is valid.

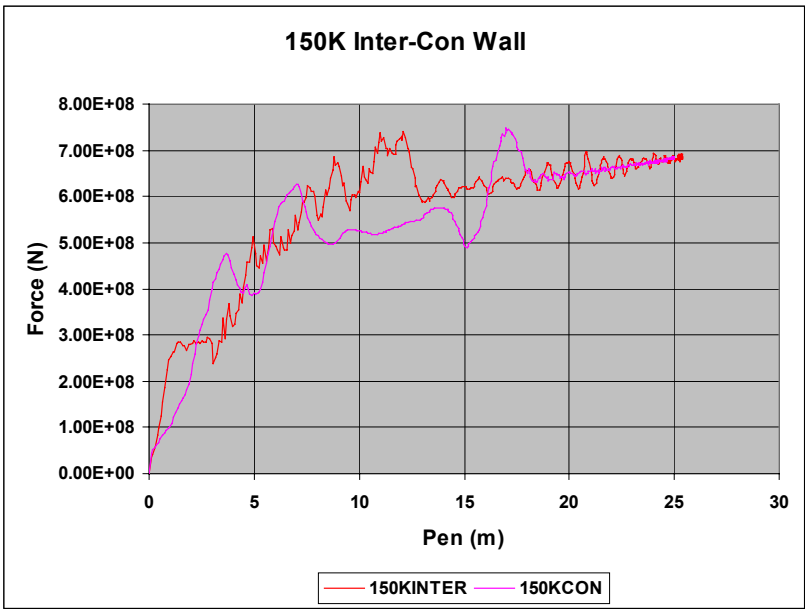

Figure 8.1 (b) – Comparison of F-p curves for Conventional and Intersection Models

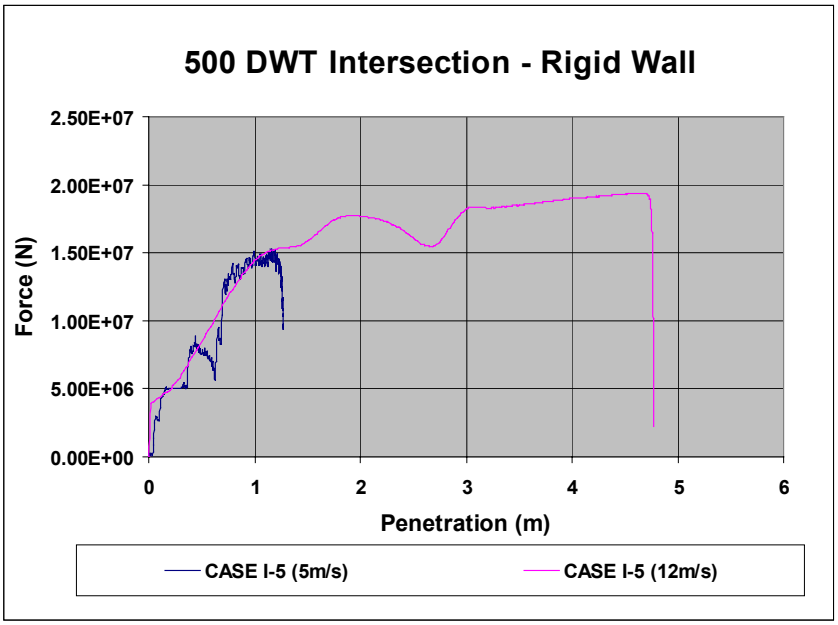

Figure 8.2 (a) – F-d curve for 500 DWT Intersection model

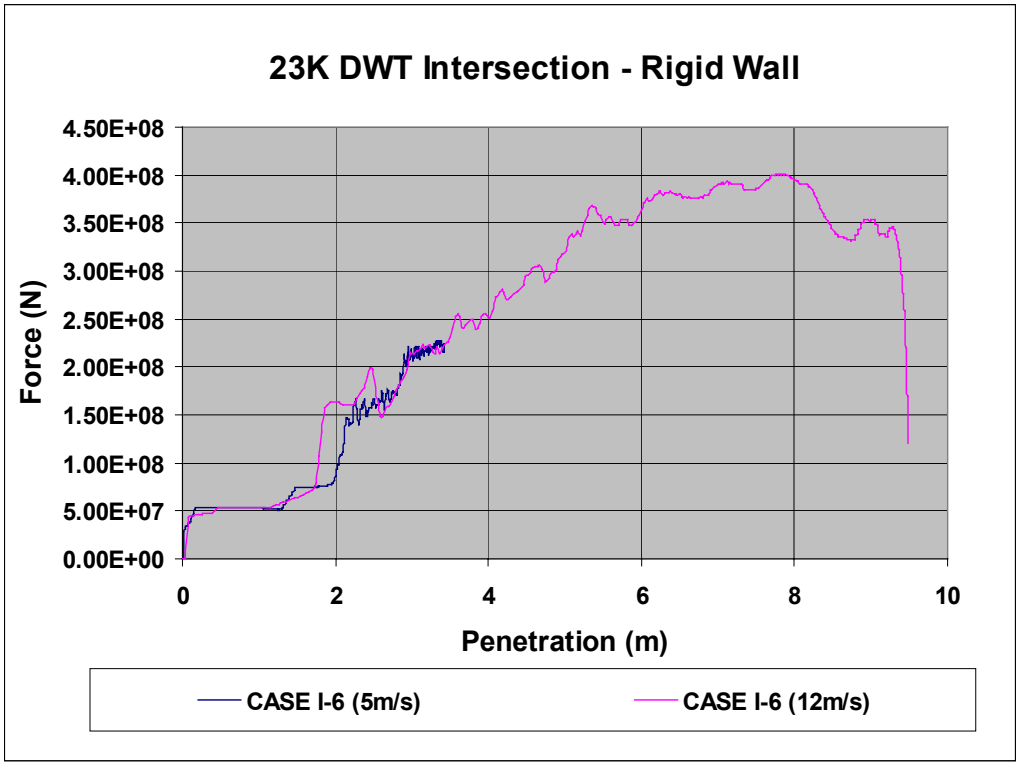

Figure 8.2 (b) – F-d curve for 23K DWT Intersection model

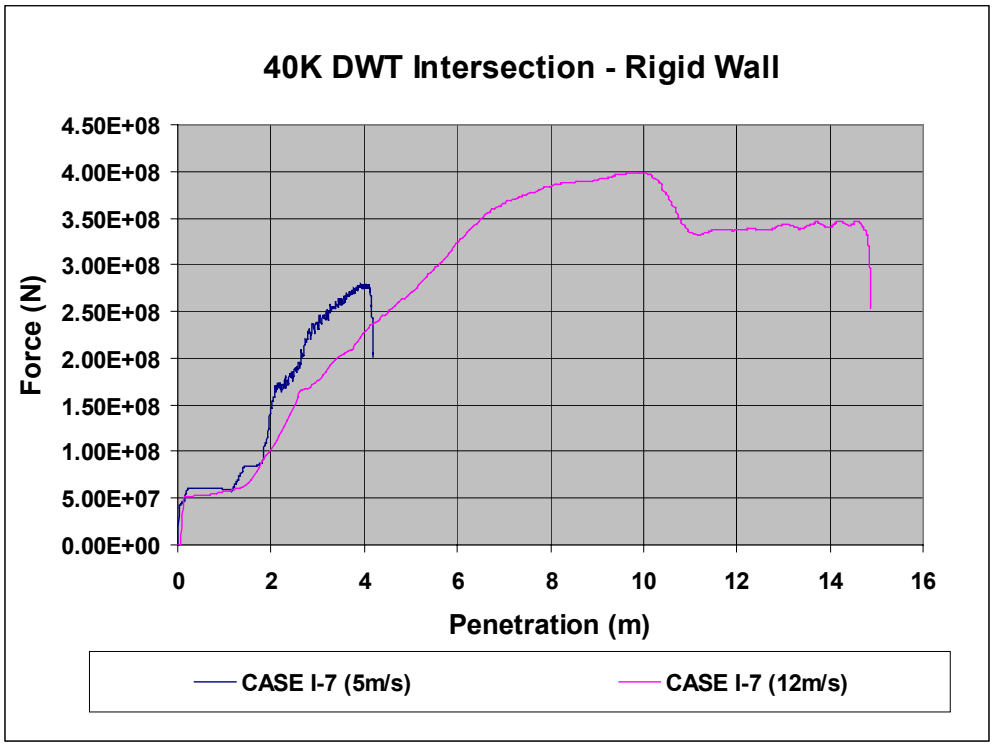

Figure 8.2 (c) – F-d curve for the 40 kdwt intersection model

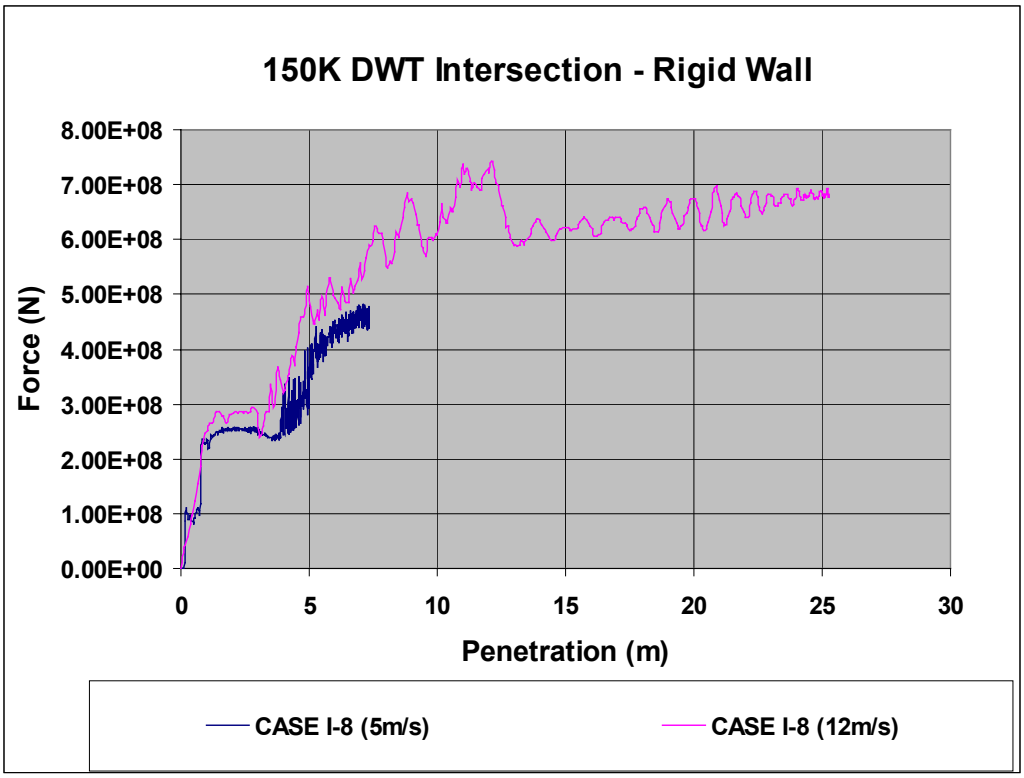

Figure 8.2 (d) – F-d curve for the 150 kdwt intersection model

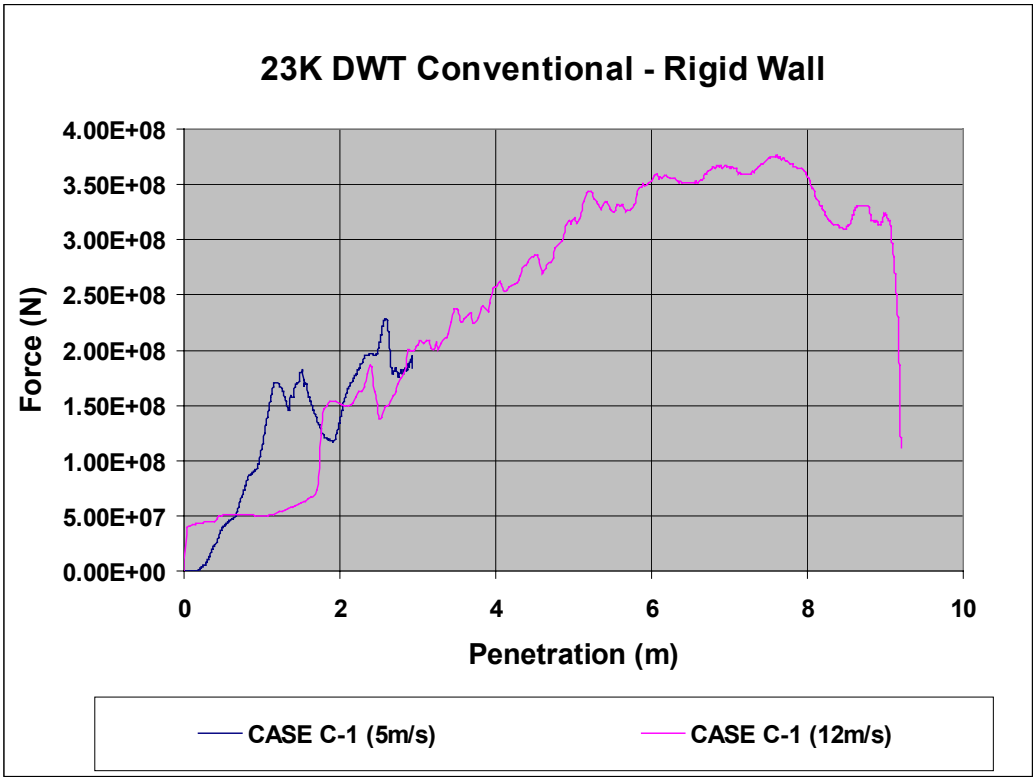

Figure 8.2 (e) – F-d curve for the 23 kdwt conventional model

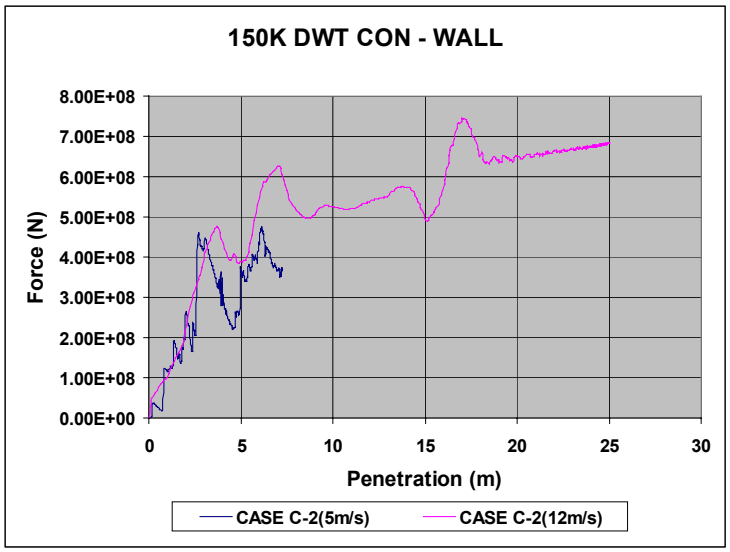

Figure 8.2 (f) – F-d curve for the 150 kdwt conventional model

Pedersen [52] suggests an idealized method to approximate the force-penetration curve for a given ship by fitting a sine-curve to the maximum crushing force and maximum penetration predicted from his closed-form equations. Figure 8.3 (a) through Figure 8.3 (d) show a comparison of the actual force-penetration curves for the four basis ships at two different speeds versus the idealized sine curve suggested by Pedersen. These figures show that this approximation provides reasonable results for lower energy collisions, but not for high-energy collisions.

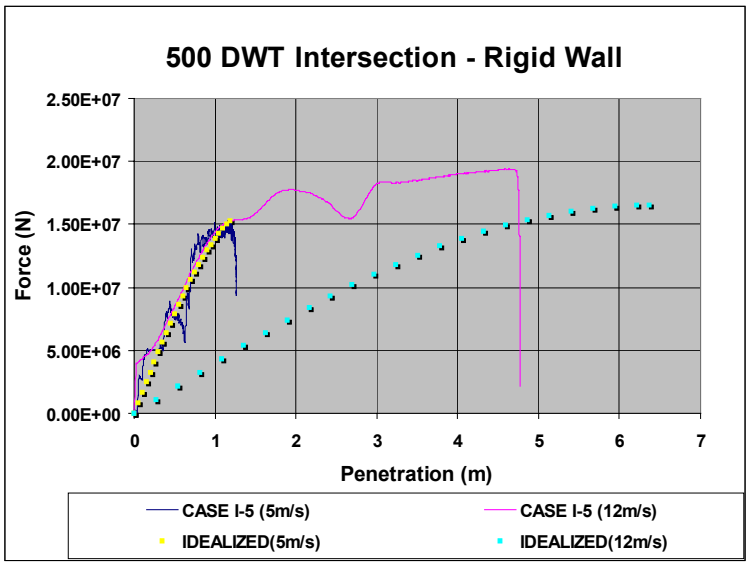

Figure 8.3 (a) – Idealized vs actual Force-penetration curve (500 dwt)

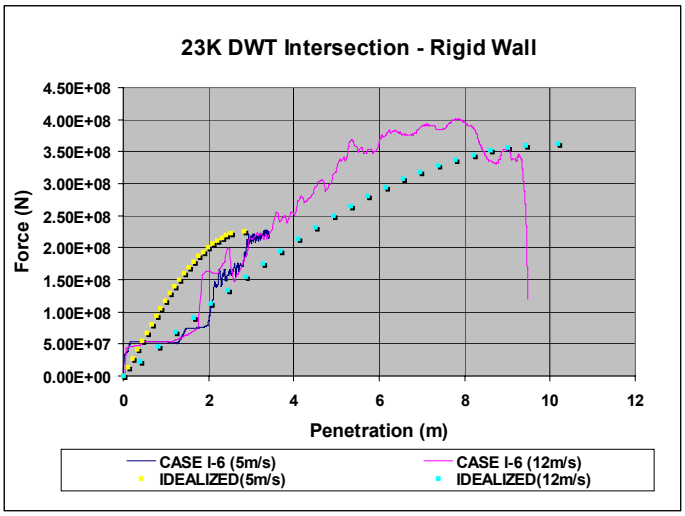

Figure 8.3 (b) – Idealized vs actual Force-penetration curve (23 kdwt)

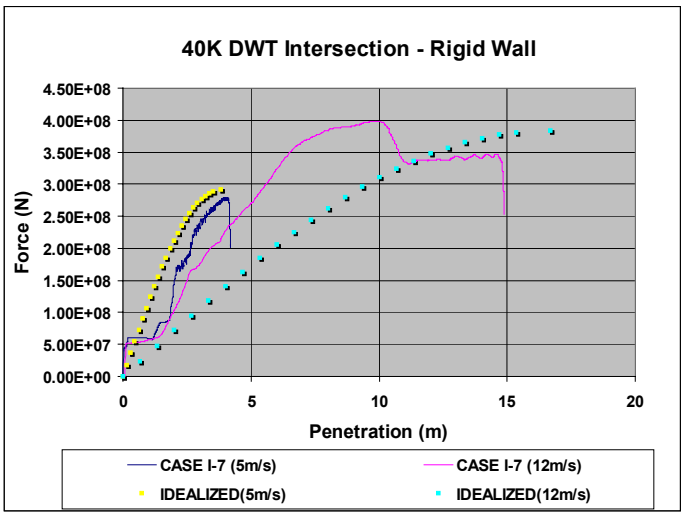

Figure 8.3 (c) – Idealized vs actual Force-penetration curve (40 kdwt)

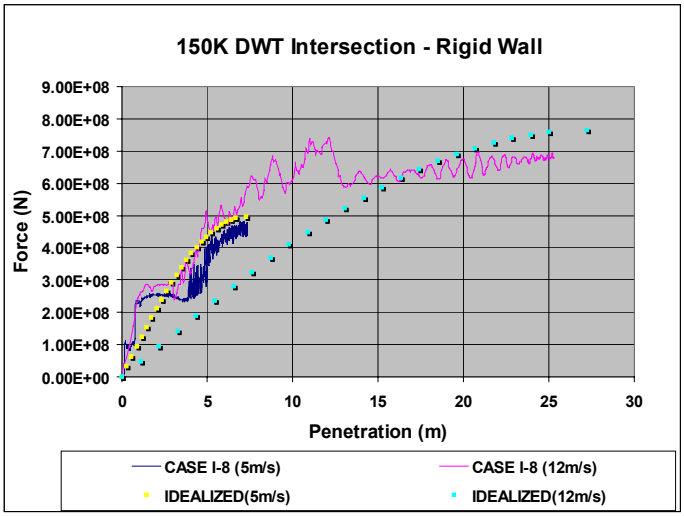

Figure 8.3 (d) – Idealized vs actual force-penetration curve (150 kdwt)

The initial slope of the sine curve suggested by Pedersen [52], does not accurately approximate the initial stiffness of the striking ship at higher speeds. Initial stiffness of the striking ship is very important in the application to struck ship damage. An alternative approach to approximate the initial slope of the force-penetration curve is, to use the stiffness of the first section of the bow. The stiffness of the first section of each of the basis ship striking bows is calculated in Appendix B. Figures 8.4 (a) through 8.4 (d) show the first-section-based approximation to initial stiffness for the basis striking bows.

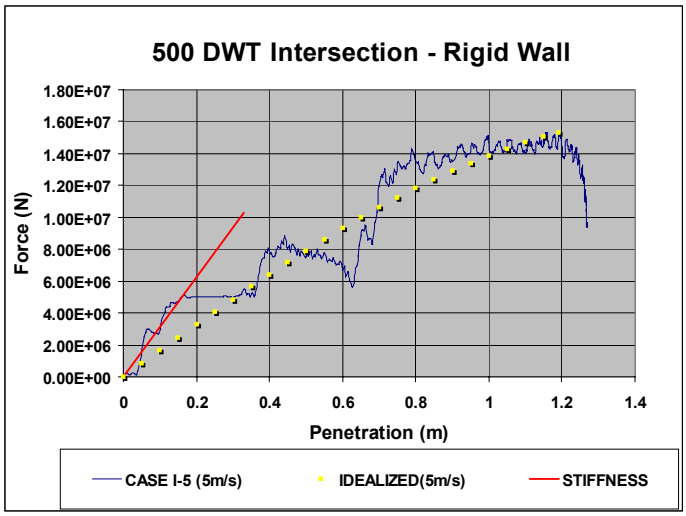

Figure 8.4 (a) – Initial Stiffness of 500 DWT coaster

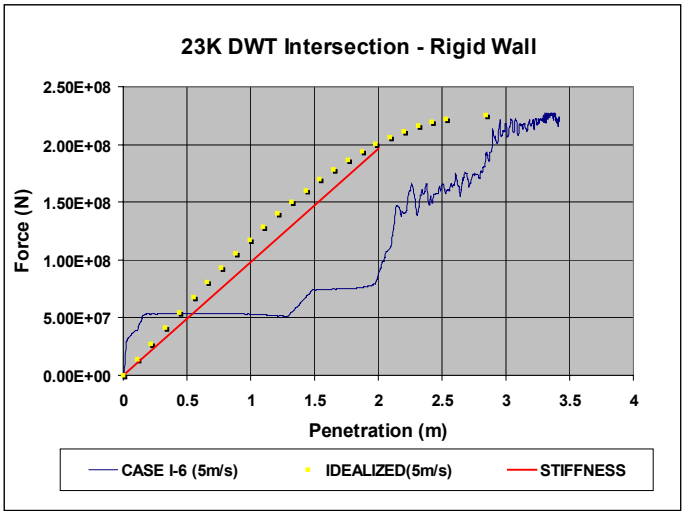

Figure 8.4 (b) – Initial Stiffness of 23K DWT Containership

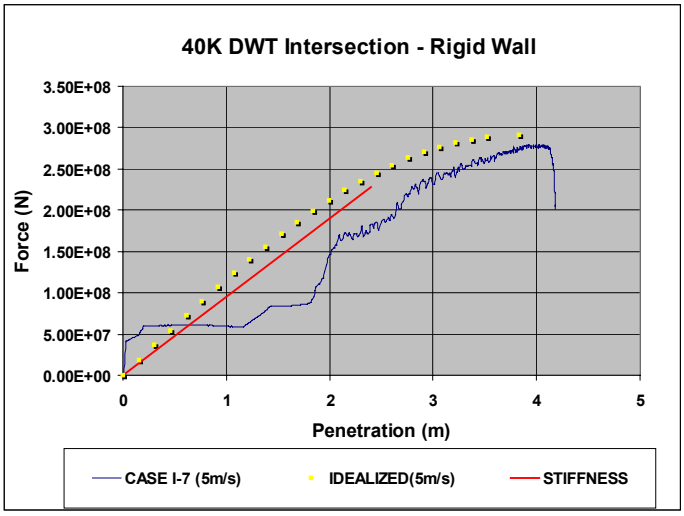

Figure 8.4 (c) – Initial Stiffness of 40K DWT Containership

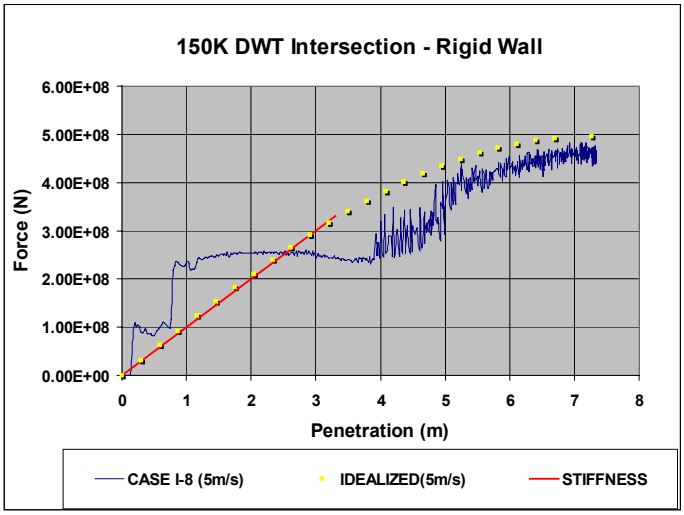

Figure 8.4 (d) – Initial Stiffness of 150K DWT bulk Carrier

Figure 8.5 shows the stiffness (force / sectional area vs penetration) of the bulb uncoupled from that of the bow for each of the basis ships. The bulb is stiffer than the bow in all the cases tested and the total stiffness in each case is the sum of the stiffness of the bulb and the bow. Two possible alternatives for the SIMCOL bow model are to use the total stiffness relationship for the striking wedge or an upper and lower wedge with different bow and bulb stiffness as shown.

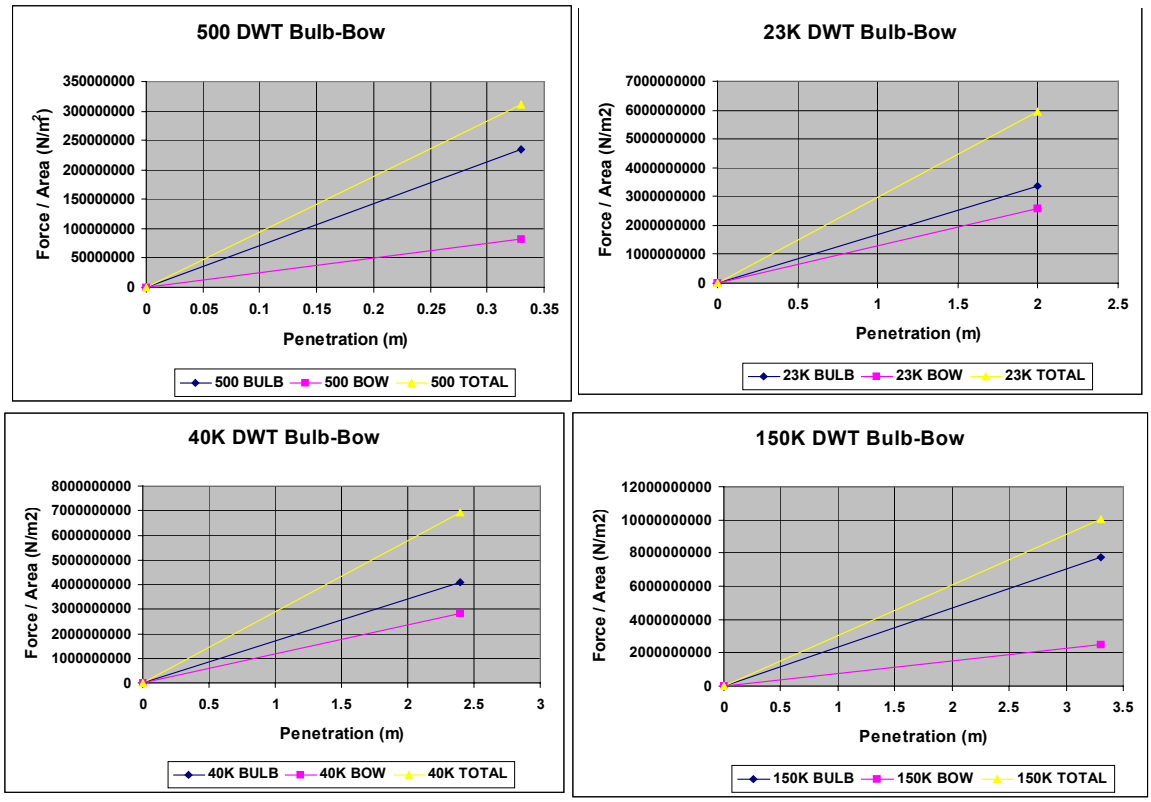

Figure 8.5 – Uncoupled Bow and Bulb Stiffness

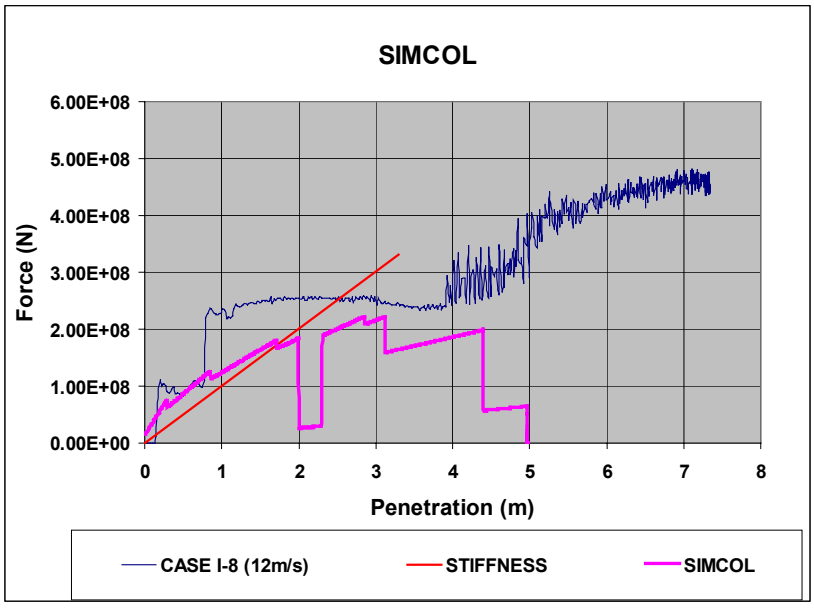

Figure 8.6 – Comparison of SIMCOL initial stiffness to intersection stiffness

Figure 8.6 shows a comparison of the force-penetration curve from SIMCOL (DH150 struck by the 150 kdwt bow) and the first-section based bow stiffness. The initial stiffness of the DH150 side is steeper than the first-section bow stiffness. This

indicates that bow deformation will occur before side deformation and that the assumption of a rigid bow is not valid.

8.2 Energy Balance and Energy Absorption in the Striking Ship

Figure 8.7 (a) shows the results of the 23 kdwt deformable container ship bow striking the deformable SH100 side, Case I-9 (3.6 meters/second). Table 8.1 summarizes these results. All of the kinetic energy is available for deformation in this case because the struck ship is fixed. Side penetration is 1.01 meters and bow crushing is 2.66 meters. When the same bow crushing is applied to the 23kdwt deformable bow / rigid wall force/deformation curve, Figure 8.7 (b), 184 MJ of energy are absorbed. When the same side penetration is applied to the 23kdwt rigid bow / SH100 deformable side force/deformation curve, Figure 8.7 (c), 50.5 MJ of energy are absorbed. The sum of these deformation energies is approximately equal to the total absorbed energy in the fully coupled deformable case. This indicates that for this problem, bow deformation and side deformation may be decoupled into two problems and solved separately. The percentage of the total energy absorbed by the striking ship bow in this case is 79 percent.

Energy absorbed	Area under F-d curve	Penetration (m)	Energy (MJ)
KE available	23 kdwt ship (Δ= 37076 tonne), 3.6 m/s	NA	240.3 MJ
Both ships deformable	23kdwt deformable bow / deformable side w/o sway, I-9, at 3.6 m/s, Figure 8.7a	Bow – 2.66 m Side – 1.01 m	240.3 MJ
Striking ship deformable	23kdwt Deformable bow / Rigid wall, I-6, Figure 8.7b	0 to 2.66	184 MJ
Struck ship deformable	SH100 Deformable side / Rigid bow, R-1, Figure 8.7c	0 to 1.01	50.5 MJ
Total			234.5 MJ
% Striking Ship			**79%**

Table 8.1 – 23kdwt Bow Striking SH100 – Energy Balance

Energy absorbed	Area under F-d curve	Penetration (m)	Energy (MJ)
KE available	150 kdwt ship (Δ= 174850 tonne), 5 m/s	NA	2186 MJ
Both ships deformable	150 kdwt deformable bow / deformable side w/o sway, I-11, at 5 m/s, Figure 8.8a	Bow – 8.4 m Side – 4 m	2186 MJ
Striking ship deformable	150 kdwt Deformable bow / Rigid wall, I-8, Figure 8.8b	0 to 8.4 m (80% area)	1600 MJ
Struck ship deformable	DH150 Deformable side / Rigid bow, R-3, Figure 8.8c	0 to 4 m	640 MJ
Total			2240 MJ
% Striking Ship			**71%**

Table 8.2 – 150kdwt Bow Striking DH150 – Energy Balance

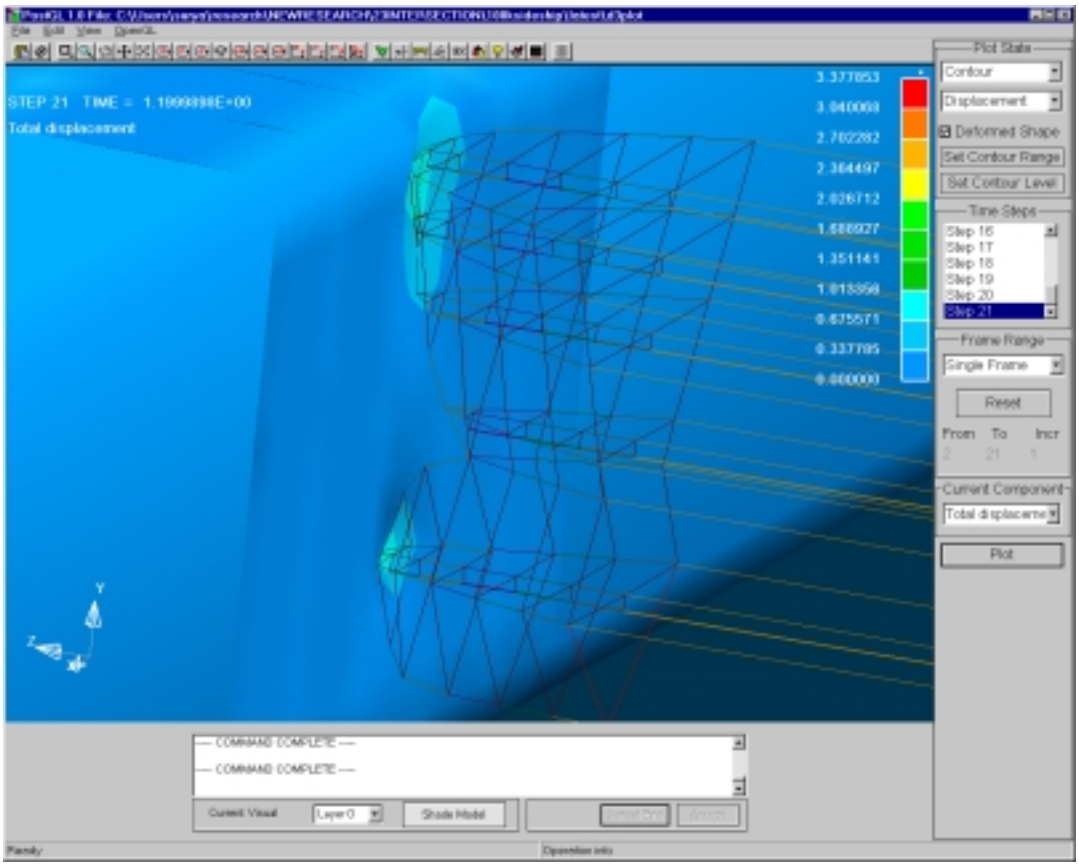

Figure 8.7 (a) – Deformable 23K DWT bow / 100K SH tanker (3.6 m/s), I-9

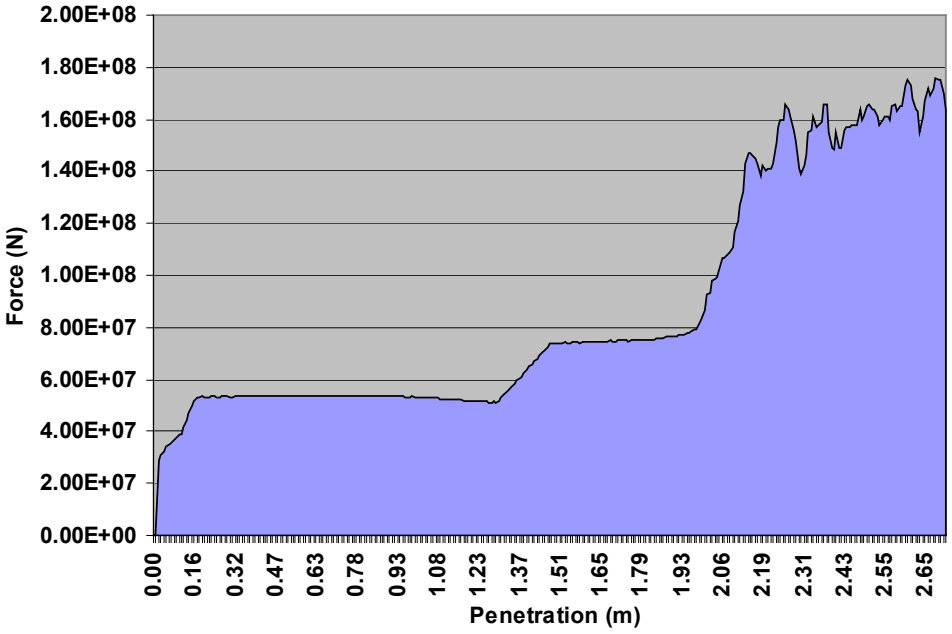

Figure 8.7 (b) – Energy absorption for 23kdwt deformable bow striking rigid wall, I-6

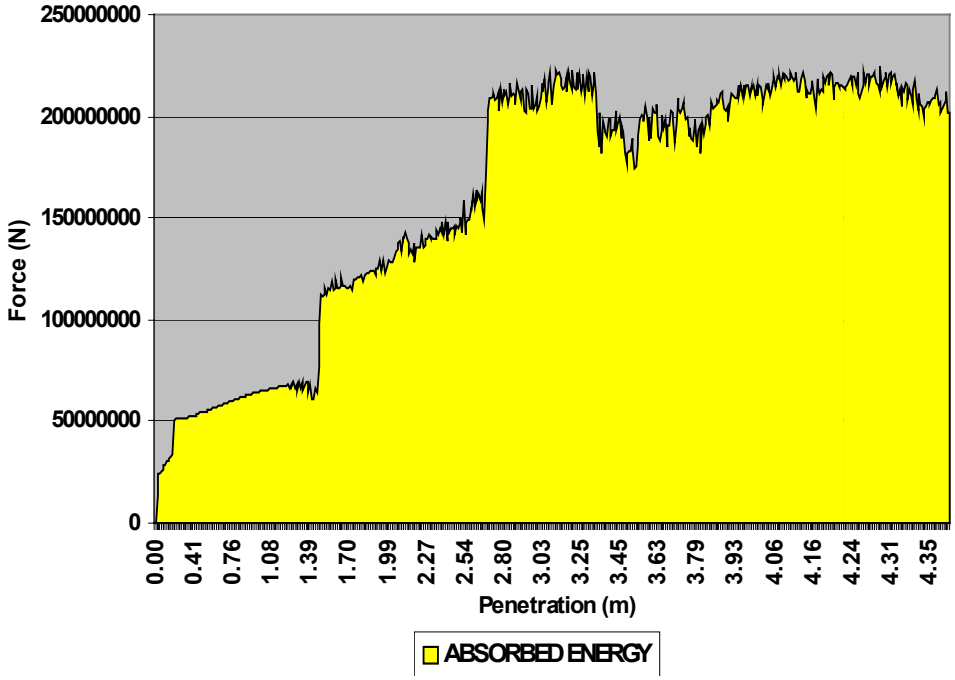

Figure 8.7c – Energy absorption for deformable SH100 struck by rigid 23kdwt bow, R-1

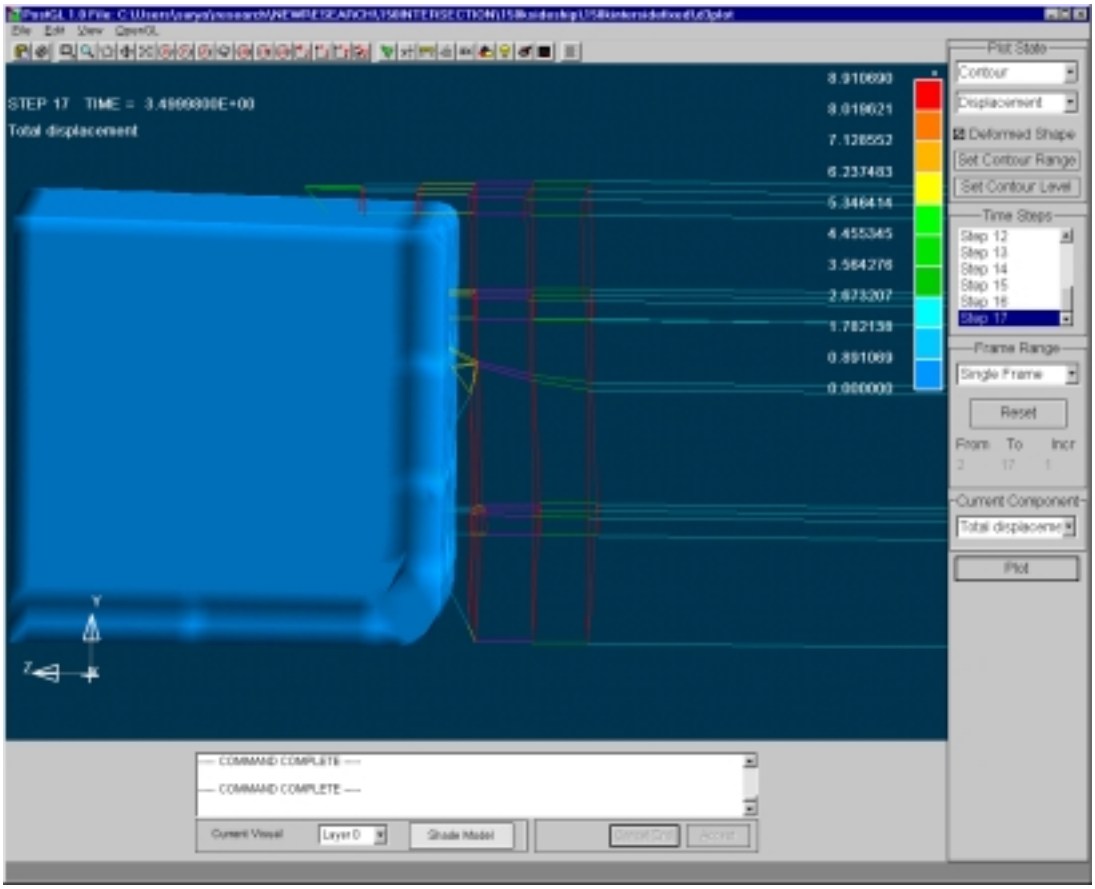

Figure 8.8 (a) – Deformable 150K DWT bow striking 150K DWT DH tanker (5m/s), I-11

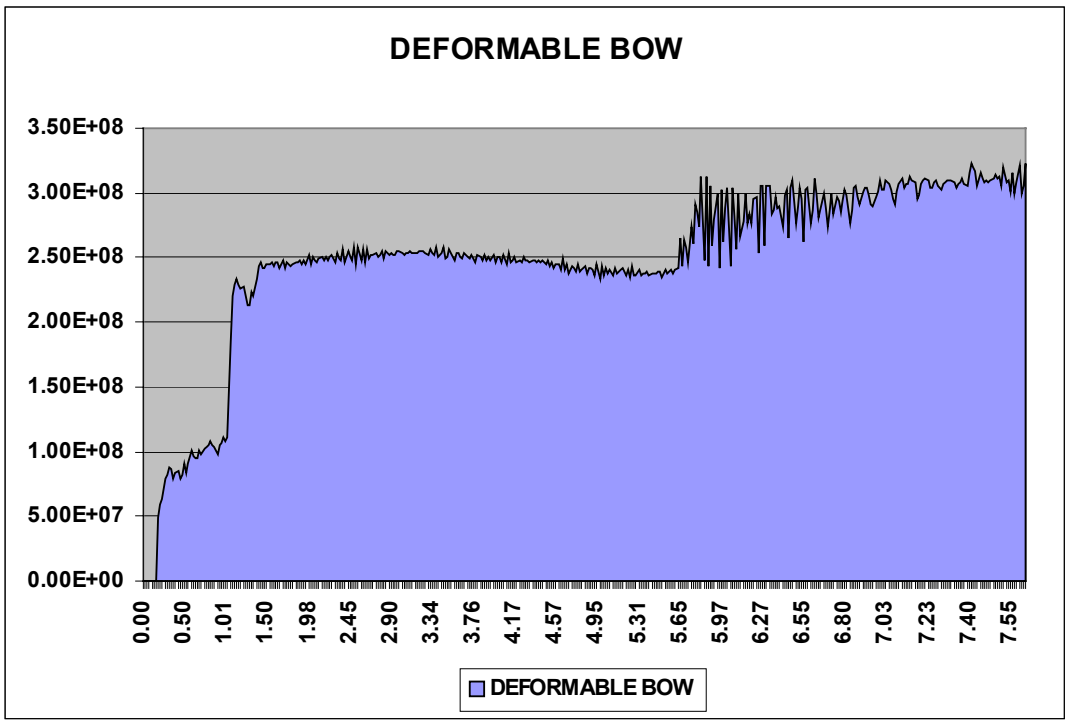

Figure 8.8b – Energy absorption in 150K DWT striking ship (deformable bow striking rigid wall), I-8

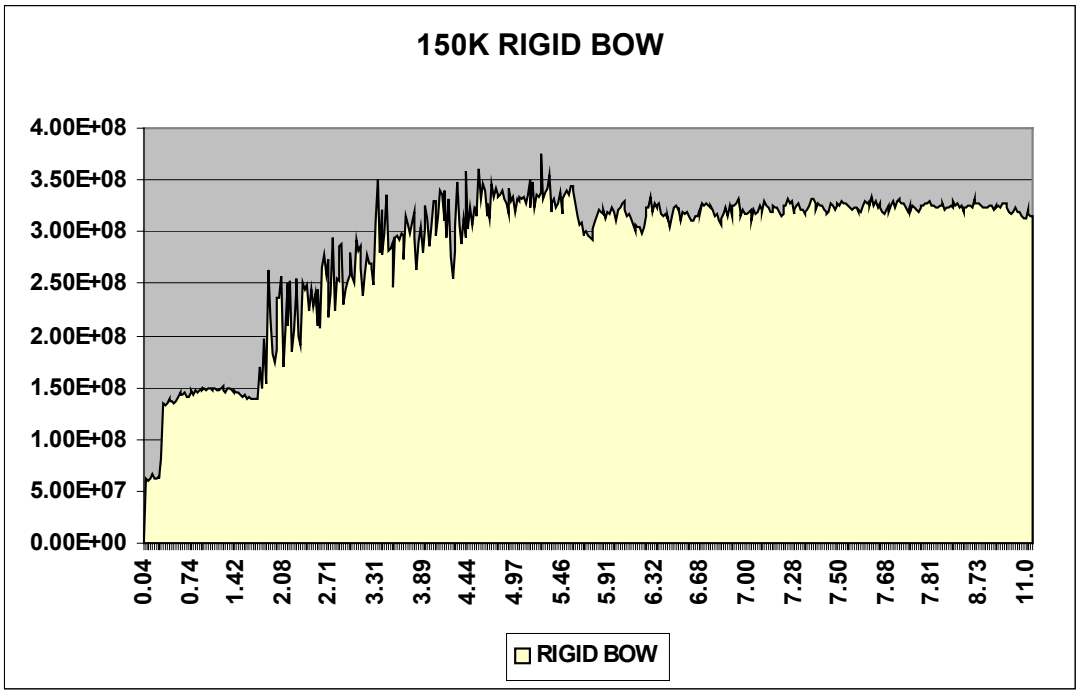

Figure 8.8 (c) – Energy absorption in DH struck ship (rigid bow striking DH tanker), R-3

Figure 8.8(a) shows the results of the 150kdwt deformable bulk carrier bow striking the deformable DH150 side, Case I-11 (5 meters/second, fixed in sway). Table 8.2 summarizes these results. All of the kinetic energy is available for deformation in this case because the struck ship is fixed. Side penetration is 4 meters and bow crushing is 8.4 meters. When the same bow crushing is applied to the 150kdwt deformable bow / rigid wall force/deformation curve, Figure 8.8 (b), and multiplied by the contact fraction of the total area (80%), 1600 MJ of energy are absorbed. When the same side penetration is applied to the 150kdwt rigid bow / DH150 deformable side force/deformation curve, Figure 8.8 (c), 640 MJ of energy are absorbed. The sum of these deformation energies is approximately equal to the total absorbed energy in the fully coupled deformable case. This again indicates that for this problem, bow deformation and side deformation may be decoupled into two problems and solved separately. In this case, 71 percent of the total energy is absorbed by the striking bow.

Figure 8.8 (d) shows DH150 side deformation when struck by the 150 kdwt rigid bow at 3.6 meters per second. Side penetration in this case is 5.63 meters. When applied to the DH150 force/deformation curve, this indicates 1194 MJ are absorbed which compares well with the 1133 MJ of available kinetic energy.

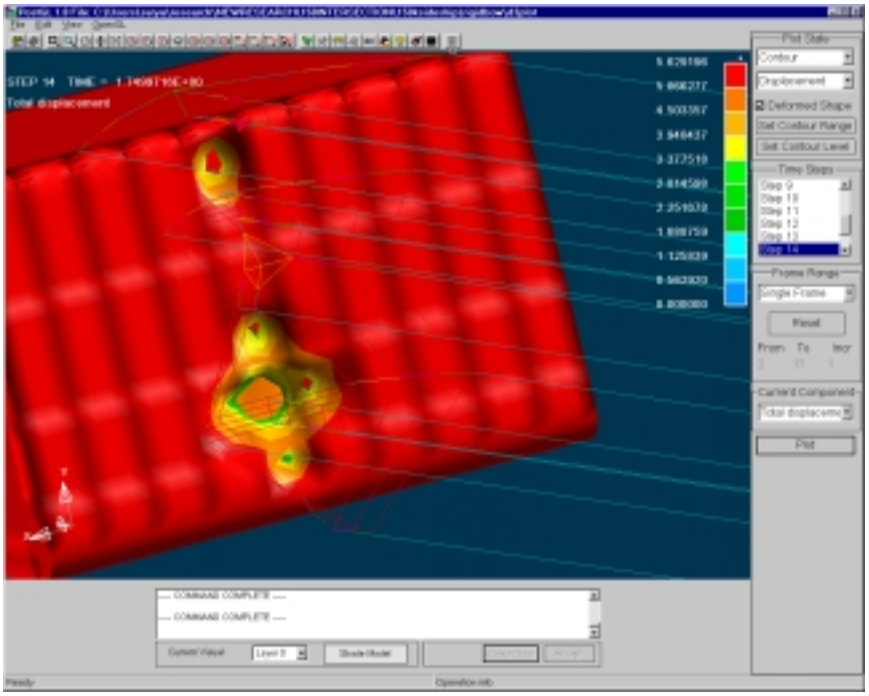

Figure 8.8 (d) – Rigid 150 kdwt bow striking DH150 tanker (3.6 m/s), R-3

8.3 CONCLUSIONS

Based on the results in Chapter 7 and analysis in Sections 8.1 and 8.2, the following conclusions are made:

1. *Bow Geometry - Wedge with limited upper and lower extents is sufficient:* Bow geometry is important to collision simulations. SIMCOL [17] assumes a wedge, with limited upper and lower extents. The assumption of such a wedge shape for the bow is simple and sufficient, as demonstrated by Chen [17]. An infinite wedge is not.
2. *Intersection and conventional models correlate well with closed-form force predictions:* Maximum collision forces predicted by the conventional and intersection element models match well with each other and with the closed-form results calculated using Pedersen [52]'s regression-based formula. (See Figure 7. 38).
3. *Intersection and conventional models predict collision duration that correlates well with closed-form values*. (See Figure 7. 40).
4. *Pedersen's formula conservative:* Pedersen's formula for estimating the maximum penetration may yield conservative results for high-speed collisions. Maximum-penetration values predicted by the intersection and conventional models match well with closed-form results for lower striking speeds (See Figure 7.42). For high striking speeds, intersection and conventional element models predict penetrations lower than the closed-form values (See Figure 7.42).
5. *Intersection element model is sufficient:* The intersection element model is sufficient for finite element analyses because it yields results that are comparable to both the conventional and closed-form calculations. (See Figure 8.1).
6. *Force-penetration curve is independent of striking velocity:* The relationship between collision force and penetration for a specific ship does not depend on the striking speed, but only depends on the structural definition of the ship. The lower the velocity, the lower the maximum value of collision force reached on the curve, but the trend of the curve is the same, regardless of the velocity. Figures 8.1 and 8.2 demonstrate this behavior.

7. *Pedersen's "idealized" approximation is not sufficient for predicting initial bow stiffness:* The "Idealized" sine-curve approximation to the force-penetration curve suggested by Pedersen [52] gives reasonable results for lower striking speeds (See Figure 8.3). At higher speeds and at lower penetrations, this is not a good approximation.

8. *Bow stiffness – better approximation:* The initial stiffness is very important in the application to struck ship damage. Initial stiffness of the striking ship can be better approximated by the stiffness of the first section. Using the values of the stiffness of the first section for each of the basis ships as the initial slope of the force-penetration curve yields a better fit to the curve than the sine-curve fit suggested by Pedersen [52]. (See Figure 8.4).

9. *Bulb should be uncoupled from the bow:* Bulb stiffness is consistently 2-3 times the bow stiffness in the cases tested. This indicates that upper and lower wedges should be considered in SIMCOL.

10. *Striking ship should not be assumed rigid:* Deformation in the striking ship is significant and hence the classic assumption of a rigid bow is not valid. From the results presented in Chapter 4 and the finite element results in Section 8.2, it can be seen that the percentage of energy absorbed by the striking ship bow is significant and is not constant.

11. *SIMCOL, DTU and ALPS/SCOL models are conservative:* SIMCOL, DTU and ALPS/SCOL models predict larger values for penetration due to the assumption of a rigid bow. Hence a deformable bow should be incorporated into these models.

12. *Models for collision deformation may be uncoupled:* Preliminary results indicate that side and bow force/penetration calculations may be made separately, and then compared at each time step to determine their respective deformations.

13. *Bow stiffness is independent of DWT:* Single stiffness values can be used for all ships, regardless of their size. (See Figure 8.9). Except for the 500DWT striking ship, the stiffness for the larger ships is similar. The larger stiffness value should be used for

the single stiffness, since it is conservative, but better than the assumption of infinite stiffness (rigid bow).

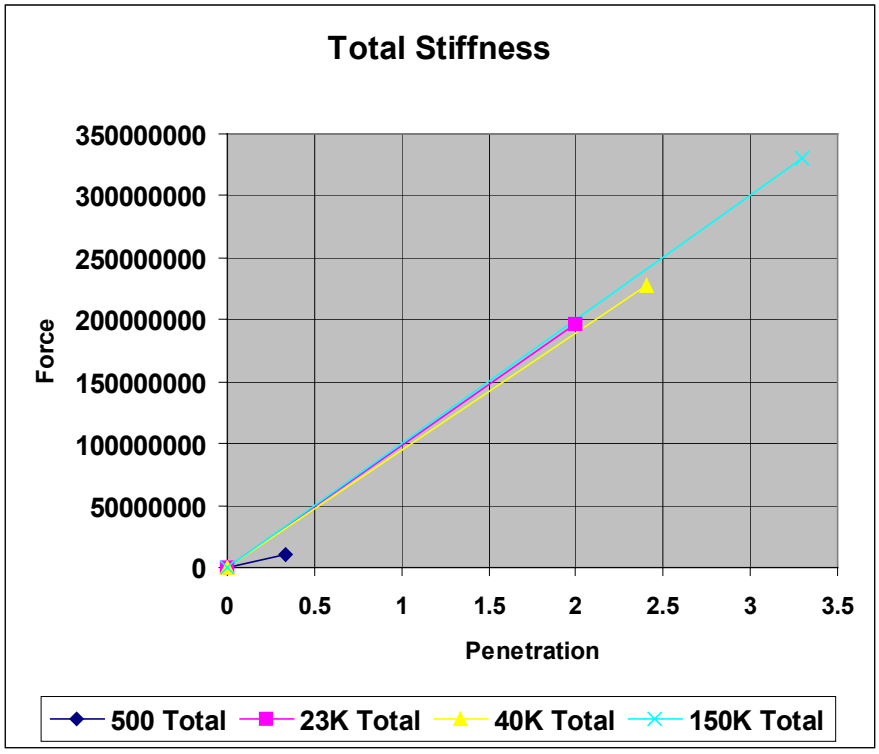

Figure 8.9 – Stiffness of striking ships

8.4 SUGGESTED IMPROVEMENTS TO SIMCOL

Based on the above conclusions, the following suggestions should be implemented into future versions of SIMCOL:

- Deformable wedge-shaped bow with limited upper and lower extents.
- ½ angle, bow height and bow draft to be determined by data analysis.
- Single stiffness for all bows = 100 MN/m.
- Separate upper and lower wedges may be considered as a future additional enhancement if required.

8.5 FUTURE RESEARCH

1. The half-angle measurement is critical to collision calculations. A more rigorous method should be proposed to define the half-angle for striking bows based on penetrating volume.
2. Develop a simplified struck-ship side model for simulation with LS-DYNA. The simplified models developed for the struck-ship side did not give consistent results. Future research should consider using a super-element approach consistent with the elements available in LS-DYNA.
3. Define a regression-based formula to predict the ship scenario parameters, given the type of ship and DWT as described in Chapter 2.
4. Consider oblique angle collisions in LS-DYNA models.
5. Investigate transversely-stiffened bows.

REFERENCES

[1] J. Sirkar et al., "A Framework for Assessing the Environmental Performance of Tankers in Accidental Groundings and Collisions", presented at the SNAME Annual Meeting, October 1997

[2] C. Rawson, K. Crake and A.J. Brown, "Assessing the Environmental Performance of Tankers in Accidental Grounding and Collision" presented at the SNAME Annual Meeting, November 1998

[3] A.J. Brown and M. Amrozowicz, "Tanker Environmental Risk - Putting the Pieces Together", SNAME/SNAJ International Conference on Designs and Methodologies for Collision and Grounding Protection of Ships, August 1996

[4] IMO, "Interim Guidelines for Approval of Alternative Methods of Design and Construction of Oil Tankers under Regulation 13F(5) of Annex I of MARPOL 73/78", Resolution MEPC.66 (37), Adopted September 14, 1995

[5] Amdahl, J. (1983), "Energy Absorption in Ship Platform Impacts", Dr. Ing. Thesis, Report No. UR-83-84, Norwegian Institute of Technology

[6] Amdahl, J. and Kavlie, D. (1992), "Experimental and Numerical Simulation of Double Hull Stranding", Proceedings of the DNV-MIT Workshop on "Mechanics of Ship Collision and Grounding", Oslo

[7] Amdahl, J. and Kavlie, D. (1995), "Design of Tankers for Grounding and Collision", MARIENV '95, 1995.

[8] Ammerman, D.J. and Daidola, J.C (1996), "A Comparison of Methods for Evaluating Structure During Ship Collisions", Proceedings of the Intl. Conference on Design and Methodologies for Collision and Grounding Protection of Ships, San Francisco, August 1996

[9] Ammerman, D.J., Koski, J.A., Sprung, J.L.,, (1997), "SeaRAM: A US DOE Study of Maritime Risk Assessment Data and Methods of Analysis", Sandia National Laboratories

[10] Arita, K (1994), "A Probabilistic Assessment on Protective Structures in Ship Collisions", 63 General Meeting of Ship Research Institute

[11] Arita, K. and Shoji Kuniaki (1995), "Expected Effectiveness of Double Side Structures in Ship Collisions", MARIENV'95, 1995

[12] Bach-Gansmo, O. and Valsgard S., "Simplified stiffness evaluation of a bulbous ship bow", Progress report No. 1, DnV, Report No. 81-0437 (1981). (Rev. no. 1 of 17.02.82)

[13] Bockenhauer, M. and Egge, E.D. (1995), "Assessment of the Collision Resistance of Ships for Classification Purposes", MARIENV'95, 1995

[14] Brown, A.J (1999), "100K DWT Single Hull Tanker from Kuroiwa (1996) – Information Book for Grounding and Collision Analysis", 1999

[15] Brown, A.J (1999), "IMO 150K DWT Double Hull Reference Tanker – Information Book for Grounding and Collision Analysis", 1999

[16] Chang, P.Y., Seibold, F. and Thasantorn, C., "A Rational Methodology for the Prediction of Structural Response due to Collision of Ships.", Paper No. 6, SNAME Annual Meeting, New York, NY, Nov. 13-15, 1980.

[17] Chen Donghui (Jan. 2000), "Simplified Collision Model (SIMCOL)", Dept. of Ocean Engineering, Virginia Tech Thesis, Jan. 2000

[18] Daidola, J.C (1995), "Tanker Structure Behavior During Collision and Grounding", Marine Technology, Vol. 32, No. 1, pp. 20-32, Jan 1995

[19] Egge, E.D. and Bockenhauer, M. (1991), "Calculation of the Collision Resistance of Ships and its Assessment for Classification Purposes", Marine Structures, Vol. 4, pp. 35-56

[20] Gooding, Peter W. (1999), “Collision with a Crushable Bow”, MIT Thesis, 1999

[21] Hagiwara, K., Takanabe, H. and Kawano, H. (1983), “A Proposed Method of Predicting Ship Collision Damage”, International Journal of Impact Engineering, No. 1.A Proposed Method of Predicting Ship Collision Damage”, International Journal of Impact Engineering, No. 1

[22] Hallquist, J.O (1998), “LS-DYNA Examples Manual”, Livermore Software Technology Corporation (LSTC), March 1998

[23] Hallquist, J.O (1998), “LS-DYNA Theoretical Manual”, Livermore Software Technology Corporation (LSTC), May 1998.

[24] Hallquist, J.O (1999), “LS-DYNA Keyword Users Manual – Nonlinear Dynamic Structural Analysis of Structures”, Livermore Software Technology Corporation (LSTC), May 1999.

[25] Hutchison, B. (1986), “Determination of Cargo Damage Risk in Barge Collisions using a Generalized Minorsky Model and Monte Carlo Methods”, SNAME Spring Meeting and Star Symposium, Portland Oregon, 1986

[26] IMO (1995), “Statistical Bow Heights Study for Determination of the Probabilistic Vertical Extent of Damage”, SLF 39/5/, 1995

[27] Ito et. al. (1984, 1985, 1986), "A Simplified Method to Analyze the Strength of Double Hulled Structures in Collision", Journal of Society of Naval Architects of Japan, Vol. 156, pp. 283-295, Vol. 158, pp. 420-434, Vol. 160, pp. 401-409.

[28] Jones, N. (1979), “A Literature Survey on the Collision and Grounding Protection of Ships”, Ship Structure Committee, SSC Report No. 283

[29] Kierkegaard, H. (1993), Ship Bow Response in High Energy Collision", Marine Structures, Vol. 6, pp. 359-376

[30] Kim, J.Y. (1999), "Crushing of a Bow: Theory vs. Scale Model Tests", Joint MIT-Industry Program on Tanker Safety, Report No. 69, June 1999

[31] Kitamura, K. and Akita, M. (1972), "A Study on Collision by an Elastic Stem to the Side Structure of Ships", Trans. SNAJ, 131, 307-317

[32] Kitamura, O. (1996), " Comparative Study on Collision Resistance of Side Structure", Proceedings of the Intl. Conference on Design and Methodologies for Collision and Grounding Protection of Ships, San Francisco, August 1996

[33] Kuroiwa, T. (1995), "Research on Structural Failure of Tankers Due to Collisions and Groundings, Proceedings of the Conference on Prediction Methodology of Tanker Structural Failure (ASIS), Tokyo, Japan, 1995

[34] Kuroiwa, T. and Kawamoto, Y. et. al. (1995), "Numerical Simulation of Collision and Grounding of Ships", Marienv 95

[35] Kuroiwa, T. (1996), Numerical Simulation of Actual Collision and Grounding Experiments, Proceedings of the Intl. Conference on Design and Methodologies for Collision and Grounding Protection of Ships, San Francisco, August 1996

[36] Lehmann, E. and Xing Yu (1996), "Energy Dissipation of Plastic Hinges under Dynamic Loads", Proceedings of the Intl. Conference on Design and Methodologies for Collision and Grounding Protection of Ships, San Francisco, August 1996

[37] Lenselink, H., and Thung, K.G. (1992), "Numerical Simulations of the Dutch-Japanese Full Scale Ship Collision Tests", Proceedings of Conference on Prediction Methodology of Tanker Structural Failure, ASIS, Tokyo, July 1992

[38] Mario Maestro, Alberto Marino (1996), "Search for a Predictive model of structural damage in ship collisions: from a case study to some proposals for a

new approach", Proceedings of the International Conference on "Design Methodologies for Collision and Grounding protection of ships", SNAME/SNAJ, San Francisco, CA, August 22-23, 1996.

[39] McDermott, J. F., Kline, R.G., Jones, E. L., Maniar, N. M., Chiang, W. P. (1974), "Tanker Structural Analysis for Minor Collisions", SNAME Transactions, 1974

[40] Minorsky, V.U. (1959), "An Analysis of Ship Collisions with Reference to Protection of Nuclear Power Plants", Journal of Ship Research, Vol. 3, No. 1, 1959

[41] Murotsu et. Al. (1995), "A System for Collapse and Reliability Analysis of Ship Structures using a Spatial Element Model", Marine Structures, 8, pp. 133-149

[42] Nagasawa, H., et al. (1977), "A Study on the Collapse of Ship Structure in Collision with Bridge Piers", Trans. SNAJ, 142, 345-354

[43] Ohtsubo, H., Wang, G. (1996), "Strength of Ships during Collision and Grounding", Proceedings of the Intl. Conference on Design and Methodologies for Collision and Grounding Protection of Ships, San Francisco, August 1996

[44] Paik, J.K. (1987), "Ultimate Strength Analysis of Ship Structures by Idealized Structural Unit Method", Ph.D. Dissertation, Osaka University

[45] Paik, J.K. (1995), "The Idealized Structural Unit Method: Theory and Application", Dept. of Naval Architecture and Ocean Engineering, Pusan National University, Pusan, Korea, August 1995.

[46] Paik, J.K., and P.T. Pedersen (1995), "Ultimate and Crushing Strength of Plated Structures", Journal of Ship Research, Vol. 39, No. 3, September, 1995

[47] Paik, J. and Pedersen, P.T. (1996), "Modeling of the Internal Mechanics in Ship Collisions", Ocean Engineering, Vol. 23, No. 2, pp. 107-142

[48] Paik, J.K., Chung, J.Y., Chun, M.S. (1996), “On Quasi-Static Crushing of a Stiffened Square Tube”, Journal of Ship Research, Vol. 40, No. 3

[49] Paik, J.K., Yang, S.H. and Thayamballi, A.K. (1996), “Residual Strength Assessment of ships after Collision and Grounding”, Proceedings of the Intl. Conference on Design and Methodologies for Collision and Grounding Protection of Ships, San Francisco, August 1996

[50] Paik, J.K. and Wierzbicki, T. (1997), “A Benchmark Study on Crushing and Cutting of Plated Structures”, Journal of Ship Research, Vol. 41, No. 2

[51] Paik, J.K., Anil K. Thayamballi and W.H. Lee (1998), "A Numerical Investigation of Tripping", Marine Structures, Vol. 11

[52] Pedersen, P.T. et. al. (1993), "Ship Impacts: Bow Collisions", Int. Journal of Impact Engineering, Vol. 13, No. 2, pp. 163-187

[53] Pedersen, P.T. (1994), "Collision and Grounding Mechanics", unpublished

[54] Petersen, M.J. and Pedersen, P.T. (1981), "Collision Between Ships and Offshore Platforms", Offshore Technology Conference, Houston, TX, OTC 4134

[55] Petersen, M.J. (1982), "Dynamics of Ship Collisions", Ocean Engineering, Vol. 9, No. 4, pp. 295-329

[56] Pettersen, E. (1979), "Analysis and Design of Cellular Structures", Dept. of Marine Technology, Norwegian Institute of Technology, Report No. UR-79-02

[57] Reardon, P. and Sprung, J.L. (1996), “Validation of Minorsky’s Ship Collision Model and Use of the Model to Estimate the Probability of Damaging a Radioactive Material Transportation Cask During a Ship Collision”, Proceedings of the Intl. Conference on Design and Methodologies for Collision and Grounding Protection of Ships, San Francisco, August 1996

[58] Reckling, K.A. (1983), "Mechanics of Minor Ship Collisions", International Journal of Impact Engineering, Vol. 1, No. 3, pp. 281-299.

[59] Rosenblatt & Son, Inc (1975), “Tanker Structural Analysis for Minor Collision”, USCG Report, CG-D-72-76.

[60] Sano et. al. (1995), "A Study on the Strength of Double Hull Side Structure of VLCC in Collision", Marienv 95

[61] Sano et. al. (1996), “Strength Analysis of A new Double Hull Structure for VLCC in Collision”, Proceedings of the Intl. Conference on Design and Methodologies for Collision and Grounding Protection of Ships, San Francisco, August 1996

[62] Simonsen, B.C. (1999), “Theory and Validation for the Collision Model”, Joint MIT-Industry Program on Tanker Safety, Report No. 66, June 1999

[63] Sprung, J.L et. al (1998), “Data and methods for the assessment of the risks associated with the maritime transport of radioactive materials and results of the SeaRAM program studies”, Vol. 1 Main Report, Vol. 2 Appendices, Sandia Report, May 1998

[64] Suzuki, K., Ohtsubo, H. (1995), "Crushing Strength of Ship Bow Structure - Calculation of Absorbed Energy and Optimal Design", Marienv95

[65] Ueda, Y., S.M.H. Rashed and J.K. Paik (1995), "Buckling and Ultimate Strength Interactions in Plates and Stiffened Panels under Combined In-Plane Biaxial and Shearing Forces", Marine Structures, Vol. 8

[66] Valsgard, S. and Pettersen, E. (1982), "Simplified Non-Linear Analysis of Ship/Ship Collisions", Norwegian Maritime Research, No. 3, pp. 2-17

[67] Wang, G., Katsuyuki, S., Ohtsubo, H. (1995), "Predicting Collision Strength of Bow Structure", Marienv 95

[68] Wierzbicki, T. (1983), "Crushing Behavior of Plate Intersections", Structural Crashworthiness, edited by A. Jones and T. Wierzbicki, Chapter 3, Butterworth and Co., London

[69] Woisin, G. (1979), "Design Against Collision", International Symposium on Advances in Marine Technology, Trondheim, Norway, 13-15 June, 1979

[70] Yang, P.D.C. and Caldwell, J.B. (1988), "Collision Energy Absorption in Ships Bow Structures", International Journal of Impact Engineering, Vol. 7, No. 2

APPENDIX A
Closed-Form Results

Closed-form calculations for 4 ships using Mathematica

500 DWT Coaster :

Ship Particulars

$LBP = 41.00$;
$B = 9.00$;
$d_{MLD} = 3.50$;
$d = 6.40$;
$T = 3.34$;
$\Delta = 886$;
$V_{service} = 5.00$;
$v_x = V_{service}$;

METHOD 1

Regression-based Crushing load and location of maximum indentation
Calculations based on ship particulars

$\overline{L} = LBP / 275$;

$$m_x = \frac{1.05\ \Delta}{1000};$$

$V_0 = V_{service}$;

$$E_{imp} = \frac{1}{2} m_x V_0^2;$$

$\overline{E}_{imp} = E_{imp} / 1425$;

$$KE = \frac{1}{2} \Delta V_0^2\ 1000\ ;$$

$P_0 = 210$;

$\text{If}\left[\overline{E}_{imp} >= \overline{L}^{2.6}, P_{bow} = P_0\ \overline{L}\left(\overline{E}_{imp} + \left(5.0 - \overline{L}\right)\overline{L}^{1.6}\right)^{0.5}\right]$;

$\text{If}\left[\overline{E}_{imp} < \overline{L}^{2.6}, P_{bow} = 2.24\ P_0\ \left(\overline{E}_{imp}\ \overline{L}\right)^{0.5}\right]$;

Print["Kinetic Energy = ", KE / 10^6 MJ];
Print["Crush Load = ", P_{bow} MN];

$$s_{max} = \frac{\pi}{2} \frac{E_{imp}}{P_{bow}} \text{ metres};$$

Print["Maximum indentation = ", s_{max}];

```
Kinetic  Energy  = 11.075 MJ
Crush  Load  = 15.3069 MN
Maximum  indentation  = 1.19335 metres
```

METHOD 2

Crush Loads for variuos sections based on Summation formula by Yang and Caldwell
Material Properties

$\overline{E} = 209\ 10^9;$
$\sigma_y = 235\ 10^6;$
$\sigma_{0_s} = 1.9\ \sigma_y;$
$s = 0.45;$
$\dot{\epsilon} = \frac{v_x}{s};$
$\sigma_0 = 1.29\ \sigma_{0_s}\ \dot{\epsilon}^{0.037};$

Section 1 (0.33m)

$n_T = 4;$
$n_L = 0;$
$n_c = 1;$
$n_f = 8;$
$n_{AT} = 4;$
$t = 0.007;$
$H = 0.6;$
$\sigma_0 = \frac{\sigma_y + \sigma_{0_s}}{2};$
$b = 6.0;$
$numelem[1] = 6;$

$$P_{mean}[1] = \frac{1}{10^6}\left(N\left[\sigma_0\left(\frac{1.178\ b}{H}\ t^2 + 0.215\ H\sum_{i=1}^{n_{AT}} t + 6.935\sum_{i=1}^{n_{AT}} t^2 + 0.265\ H\sum_{i=1}^{n_T} t + 0.589\sum_{i=1}^{n_T} t^2 + 0.75\ H\sum_{i=1}^{n_c}\sum_{i=1}^{4} t + 0.375\sum_{i=1}^{n_c}\sum_{i=1}^{4} t^2\right)\right]\right)$$

$$Area[1] = \frac{\frac{P_{mean}[1]}{\sigma_0}\ 10^6}{numelem[1]}$$

```
7.7655
0.00379824
```

Section 2 (0.63m)

$n_T = 7;$

$n_L = 4;$

$n_c = 2;$

$n_f = 19;$

$n_{AT} = 11;$

$t = 0.008;$

$H = 0.3;$

$$\sigma_0 = \frac{\sigma_y + \sigma_{0_s}}{2};$$

$b = 24.3;$

$numelem[2] = 11;$

$$P_{mean}[2] = \frac{1}{10^6}\left(N\left[\sigma_0\left(\frac{1.178\ b}{H}t^2 + 0.215\ H\sum_{i=1}^{n_{AT}} t + 6.935\sum_{i=1}^{n_{AT}} t^2 + 0.265\ H\sum_{i=1}^{n_T} t + 0.589\sum_{i=1}^{n_T} t^2 + 0.75\ H\sum_{i=1}^{n_c}\sum_{i=1}^{4} t + 0.375\sum_{i=1}^{n_c}\sum_{i=1}^{4} t^2\right)\right]\right)$$

$$Area[2] = \frac{\frac{P_{mean}[2]}{\sigma_0}\,10^6}{numelem[2]}$$

12.2578

0.00327026

Section 3 (1.33m)

$n_T = 10;$

$n_L = 4;$

$n_c = 2;$

$n_f = 22;$

$n_{AT} = 14;$

$t = 0.009;$

$H = 0.3;$

$$\sigma_0 = \frac{\sigma_y + \sigma_{0_s}}{2};$$

$b = 50;$

$numelem[3] = 18;$

$$P_{mean}[3] = \frac{1}{10^6}\left(N\left[\sigma_0\left(\frac{1.178\ b}{H}t^2 + 0.215\ H\sum_{i=1}^{n_{AT}} t + 6.935\sum_{i=1}^{n_{AT}} t^2 + 0.265\ H\sum_{i=1}^{n_T} t + 0.589\sum_{i=1}^{n_T} t^2 + 0.75\ H\sum_{i=1}^{n_c}\sum_{i=1}^{4} t + 0.375\sum_{i=1}^{n_c}\sum_{i=1}^{4} t^2\right)\right]\right)$$

$$Area[3] = \frac{\frac{P_{mean}[3]}{\sigma_0}\,10^6}{numelem[3]}$$

19.0716
0.00310941

Section 4 (2.43m)

$n_T = 12;$
$n_L = 4;$
$n_c = 0;$
$n_f = 23;$
$n_{AT} = 16;$
$t = 0.009;$
$H = 0.3;$
$\sigma_0 = \frac{\sigma_y + \sigma_{0_s}}{2};$
$b = 50;$
$numelem[4] = 21;$

$$P_{mean}[4] = \frac{1}{10^6}\left(N\left|\sigma_0\left(\frac{1.178\ b}{H}t^2 + 0.215\ H\sum_{i=1}^{n_{AT}} t + 6.935\sum_{i=1}^{n_{AT}} t^2 + 0.265\ H\sum_{i=1}^{n_T} t + 0.589\sum_{i=1}^{n_T} t^2 + 0.75\ H\sum_{i=1}^{n_c}\sum_{i=1}^{4} t + 0.375\sum_{i=1}^{n_c}\sum_{i=1}^{4} t^2\right)\right|\right)$$

$$Area[4] = \frac{\frac{P_{mean}[4]}{\sigma_0}10^6}{numelem[4]}$$

14.7672
0.00206368

DISCUSSION OF THE RESULTS :

METHOD 1

The crushing force for the entire bow structure has been calculated to be **15.3 MN**
The maximum indentation is shown to be **1.19 m**

METHOD 2

The Bow Crushing Forces for various sections obtained using the section – by – section crushing theory and intersection element formulation are summarised below :

```
For[i = 1, i ≤ 4, i++,
 Print["Section ", i, " Pmean =  ", Pmean[i], " MN"]]
Section  1 Pmean =   7.7655  MN
Section  2 Pmean =   12.2578  MN
Section  3 Pmean =   19.0716  MN
Section  4 Pmean =   14.7672  MN
```

```
table = {{0, 0}, {0.33, Pmean[1]}, {0.63, Pmean[2]},
   {1.33, Pmean[3]}, {2.43, Pmean[4]}};
Interpolation[table, InterpolationOrder → 3];
Plot[%[x], {x, 0.0, 2.43}, AxesLabel →
  {"Penetration (m)", "Force (MN)"}]
```

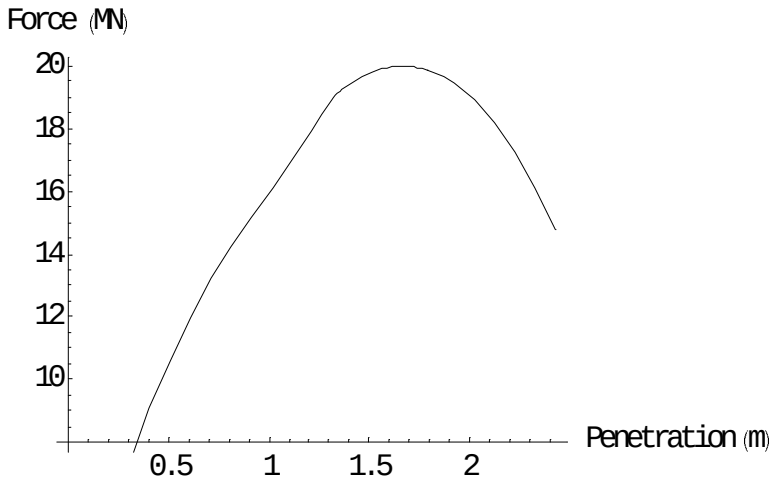

- Graphics -

23, 000 DWT Containership :

Ship Particulars

$LBP = 220.91$;

$B = 26.01$;

$d_{MLD} = 16.11$;

$d = 9.684$;

$T = 9.70$;

$\Delta = 31050$;

$V_{service} = 11.32$;

$v_x = V_{service}$;

METHOD 1

Regression-based Crushing load and location of maximum indentation
Calculations based on ship particulars

$\overline{L} = LBP / 275$;

$m_x = \frac{1.05\ \Delta}{1000}$;

$V_0 = V_{service}$;

$KE = \frac{1}{2} \Delta\ V_0^2\ 1000$;

$E_{imp} = \frac{1}{2} m_x V_0^2$;

$\overline{E}_{imp} = E_{imp} / 1425$;

$P_0 = 210$;

$If\left[\overline{E}_{imp} >= \overline{L}^{2.6}, P_{bow} = P_0\ \overline{L}\left(\overline{E}_{imp} + \left(5.0 - \overline{L}\right)\overline{L}^{1.6}\right)^{0.5}\right]$;

$If\left[\overline{E}_{imp} < \overline{L}^{2.6}, P_{bow} = 2.24\ P_0\ \left(\overline{E}_{imp}\ \overline{L}\right)^{0.5}\right]$;

Print["Kinetic Energy = ", KE / 10^6 MJ];

Print["Crush Load = ", P_{bow} MN];

$s_{max} = \frac{\pi}{2} \frac{E_{imp}}{P_{bow}}$ metres ;

Print["Maximum indentation = ", s_{max}];

```
Kinetic Energy = 1989.41 MJ
Crush Load = 354.74 MN
Maximum indentation = 9.2496 metres
```

METHOD 2

Crush Loads for various sections based on Summation formula by Yang and Caldwell
Material Properties

$\overline{E} = 206\ 10^9;$

$\sigma_y = 245\ 10^6;$

$\sigma_{0_s} = 490\ 10^6;$

$s = 2.0;$

$\dot{\epsilon} = \frac{v_x}{s};$

$\sigma_0 = 1.29\ \sigma_{0_s}\ \dot{\epsilon}^{0.037};$

Section 1 (2.0m)

$n_T = 6;$

$n_L = 7;$

$n_c = 0;$

$n_f = 17;$

$n_{AT} = 13;$

$t = 0.025;$

$H = 2.0;$

$\sigma_0 = \frac{\sigma_y + \sigma_{0_s}}{2};$

$b = 40.43;$

$numelem[1] = 13;$

$$P_{mean}[1] = \frac{1}{10^6}\left(N\left[\sigma_0\left(\frac{1.178}{H}\, b\, t^2 + 0.215\ H \sum_{i=1}^{n_{AT}} t + 6.935 \sum_{i=1}^{n_{AT}} t^2 + 0.265\ H \sum_{i=1}^{n_T} t + 0.589 \sum_{i=1}^{n_T} t^2 + 0.75\ H \sum_{i=1}^{n_c}\sum_{i=1}^{4} t + 0.375 \sum_{i=1}^{n_c}\sum_{i=1}^{4} t^2\right)\right]\right)$$

$$Area[1] = \frac{\frac{P_{mean}[1]}{\sigma_0}\ 10^6}{numelem[1]}$$

107.563

0.0225145

Section 2 (4.0m)

$n_T = 9;$

$n_L = 8;$

$n_c = 0;$

$n_f = 23;$

$n_{AT} = 17;$

$t = 0.030;$

$H = 2.0;$

$$\sigma_0 = \frac{\sigma_y + \sigma_{0_s}}{2};$$

$b = 157;$

$$P_{mean}[2] = \frac{1}{10^6}\left(N\left[\sigma_0\left(\frac{1.178}{H}\, b\, t^2 + 0.215\, H \sum_{i=1}^{n_{AT}} t + 6.935 \sum_{i=1}^{n_{AT}} t^2 + 0.265\, H \sum_{i=1}^{n_T} t + 0.589 \sum_{i=1}^{n_T} t^2 + 0.75\, H \sum_{i=1}^{n_c}\sum_{i=1}^{4} t + 0.375 \sum_{i=1}^{n_c}\sum_{i=1}^{4} t^2\right)\right]\right)$$

$$Area[2] = \frac{\frac{P_{mean}[2]}{\sigma_0}\, 10^6}{numelem[2]}$$

204.515

0.0252956

Section 3 (6.0m)

$n_T = 12;$

$n_L = 9;$

$n_c = 0;$

$n_f = 29;$

$n_{AT} = 21;$

$t = 0.030;$

$H = 2.0;$

$$\sigma_0 = \frac{\sigma_y + \sigma_{0_s}}{2};$$

$b = 312;$

$numelem[3] = 26;$

$$P_{mean}[3] = \frac{1}{10^6}\left(N\left[\sigma_0\left(\frac{1.178}{H}\, b\, t^2 + 0.215\, H \sum_{i=1}^{n_{AT}} t + 6.935 \sum_{i=1}^{n_{AT}} t^2 + 0.265\, H \sum_{i=1}^{n_T} t + 0.589 \sum_{i=1}^{n_T} t^2 + 0.75\, H \sum_{i=1}^{n_c}\sum_{i=1}^{4} t + 0.375 \sum_{i=1}^{n_c}\sum_{i=1}^{4} t^2\right)\right]\right)$$

$$Area[3] = \frac{\frac{P_{mean}[3]}{\sigma_0}\, 10^6}{numelem[3]}$$

280.963

0.0294048

Section 4 (8.0m)

$n_T = 12;$

$n_L = 9;$

$n_c = 0;$

$n_f = 29;$

$n_{AT} = 21;$

$t = 0.030;$

$H = 2.0;$

$$\sigma_0 = \frac{\sigma_y + \sigma_{0_s}}{2};$$

$b = 475;$

$numelem[4] = 28;$

$$P_{mean}[4] = \frac{1}{10^6}\left(N\left[\sigma_0\left(\frac{1.178}{H}\, b\, t^2 + 0.215\, H\sum_{i=1}^{n_{AT}} t + 6.935\sum_{i=1}^{n_{AT}} t^2 + 0.265\, H\sum_{i=1}^{n_T} t + 0.589\sum_{i=1}^{n_T} t^2 + 0.75\, H\sum_{i=1}^{n_c}\sum_{i=1}^{4} t + 0.375\sum_{i=1}^{n_c}\sum_{i=1}^{4} t^2\right)\right]\right)$$

$$Area[4] = \frac{\frac{P_{mean}[4]}{\sigma_0}\, 10^6}{numelem[4]}$$

312.717

0.0303904

Section 5 (10.0m)

$n_T = 12;$

$n_L = 9;$

$n_c = 0;$

$n_f = 29;$

$n_{AT} = 21;$

$t = 0.030;$

$H = 2.0;$

$$\sigma_0 = \frac{\sigma_y + \sigma_{0_s}}{2};$$

$b = 550;$

$numelem[5] = 28;$

$$P_{mean}[5] = \frac{1}{10^6}\left(N\left[\sigma_0\left(\frac{1.178}{H}\, b\, t^2 + 0.215\, H\sum_{i=1}^{n_{AT}} t + 6.935\sum_{i=1}^{n_{AT}} t^2 + 0.265\, H\sum_{i=1}^{n_T} t + 0.589\sum_{i=1}^{n_T} t^2 + 0.75\, H\sum_{i=1}^{n_c}\sum_{i=1}^{4} t + 0.375\sum_{i=1}^{n_c}\sum_{i=1}^{4} t^2\right)\right]\right)$$

$$Area[5] = \frac{\frac{P_{mean}[5]}{\sigma_0}\, 10^6}{numelem[5]}$$

327.328
0.0318103

Section 6 (12.0m)

$n_T = 12;$
$n_L = 9;$
$n_c = 0;$
$n_f = 29;$
$n_{AT} = 21;$
$t = 0.030;$
$H = 2.0;$
$\sigma_0 = \frac{\sigma_y + \sigma_{0_s}}{2};$
$b = 610;$
$numelem[6] = 28;$

$$P_{mean}[6] = \frac{1}{10^6}\left(N\left[\sigma_0\left(\frac{1.178}{H} b t^2 + 0.215 H \sum_{i=1}^{n_{AT}} t + 6.935 \sum_{i=1}^{n_{AT}} t^2 + 0.265 H \sum_{i=1}^{n_T} t + 0.589 \sum_{i=1}^{n_T} t^2 + 0.75 H \sum_{i=1}^{n_c}\sum_{i=1}^{4} t + 0.375 \sum_{i=1}^{n_c}\sum_{i=1}^{4} t^2\right)\right]\right)$$

$$Area[6] = \frac{\frac{P_{mean}[6]}{\sigma_0} 10^6}{numelem[6]}$$

339.016
0.0329462

DISCUSSION OF THE RESULTS :

METHOD 1

The crushing force for the entire bow structure has been calculated to be **354.74 MN**
The maximum indentation is shown to be **9.25 m**

METHOD 2

The Bow Crushing Forces for various sections obtained using the section – by – section crushing theory and intersection element formulation are summarised below :

```
For[i = 1, i ≤ 6, i++,
 Print["Section ", i, " Pmean =   ", Pmean[i], " MN"]]
Section  1 Pmean =   107.563  MN
Section  2 Pmean =   204.515  MN
Section  3 Pmean =   280.963  MN
Section  4 Pmean =   312.717  MN
Section  5 Pmean =   327.328  MN
Section  6 Pmean =   339.016  MN
```

```
table = {{0, 0}, {2.4, Pmean[1]}, {4.8, Pmean[2]}, {7.2, Pmean[3]},
   {9.6, Pmean[4]}, {12, Pmean[5]}, {14.4, Pmean[6]}};
Interpolation[table, InterpolationOrder → 3];
Plot[%[x], {x, 0, 14.4}, AxesLabel →
  {"Penetration (m)", "Force (MN)"}]
```

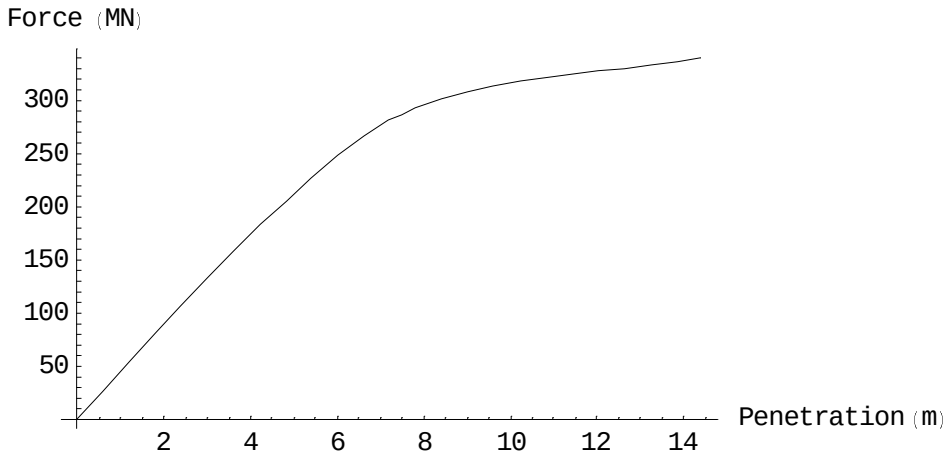

- Graphics -

40, 000 DWT Containership :

Ship Particulars

$LBP = 211.50$;
$B = 32.20$;
$d_{MLD} = 21.00$;
$d = 24.00$;
$T = 11.90$;
$\Delta = 54000$;
$V_{service} = 12.90$;
$v_x = V_{service}$;

METHOD 1

Regression-based Crushing load and location of maximum indentation
Calculations based on ship particulars

$\overline{L} = LBP / 275$;

$$m_x = \frac{1.05\ \Delta}{1000};$$

$V_0 = V_{service}$;

$$KE = \frac{1}{2}\ \Delta\ V_0^{\,2}\ 1000\ ;$$

$$E_{imp} = \frac{1}{2}\ m_x\ V_0^{\,2};$$

$\overline{E}_{imp} = E_{imp} / 1425$;
$P_0 = 210$;
If$\left[\overline{E}_{imp} >= \overline{L}^{2.6},\ P_{bow} = P_0\ \overline{L}\left(\overline{E}_{imp} + \left(5.0 - \overline{L}\right)\overline{L}^{1.6}\right)^{0.5}\right]$;
If$\left[\overline{E}_{imp} < \overline{L}^{2.6},\ P_{bow} = 2.24\ P_0\ \left(\overline{E}_{imp}\ \overline{L}\right)^{0.5}\right]$;
Print["Kinetic Energy = ", KE / 10^6 MJ];
Print["Crush Load = ", P_{bow} MN];

$$s_{max} = \frac{\pi}{2}\ \frac{E_{imp}}{P_{bow}}\ \text{metres};$$

Print["Maximum indentation = ", s_{max}];

```
Kinetic Energy = 4493.07 MJ
Crush Load = 398.583 MN
Maximum indentation = 18.5923 metres
```

METHOD 2

Crush Loads for variuos sections based on Summation formula by Yang and Caldwell
Material Properties

$\overline{E} = 209\ 10^9;$

$\sigma_y = 235\ 10^6;$

$\sigma_{0_s} = 1.9\ \sigma_y;$

$s = 2.40;$

$\dot{\epsilon} = \frac{v_x}{s};$

$\sigma_0 = 1.29\ \sigma_{0_s}\ \dot{\epsilon}^{0.037};$

Section 1 (2.4m)

$n_T = 6;$

$n_L = 7;$

$n_c = 0;$

$n_f = 17;$

$n_{AT} = 13;$

$t = 0.025;$

$H = 2.40;$

$\sigma_0 = \frac{\sigma_y + \sigma_{0_s}}{2};$

$b = 40.43;$

$numelem[1] = 13;$

$$P_{mean}[1] = \frac{1}{10^6}\left(N\left[\sigma_0\left(\frac{1.178}{H}\, b\, t^2 + 0.215\ H \sum_{i=1}^{n_{AT}} t + 6.935 \sum_{i=1}^{n_{AT}} t^2 + 0.265\ H \sum_{i=1}^{n_T} t + 0.589 \sum_{i=1}^{n_T} t^2 + 0.75\ H \sum_{i=1}^{n_c}\sum_{i=1}^{4} t + 0.375 \sum_{i=1}^{n_c}\sum_{i=1}^{4} t^2\right)\right]\right)$$

$$Area[1] = \frac{\frac{P_{mean}[1]}{\sigma_0}\ 10^6}{numelem[1]}$$

113.83

0.0256968

Section 2 (4.8m)

$n_T = 9;$

$n_L = 8;$

$n_c = 0;$

$n_f = 23;$

$n_{AT} = 17;$

$t = 0.030;$

$H = 2.4;$

$$\sigma_0 = \frac{\sigma_y + \sigma_{0_s}}{2};$$

$b = 157;$

$numelem[2] = 22;$

$$P_{mean}[2] = \frac{1}{10^6}\left(N\left[\sigma_0\left(\frac{1.178}{H}\, b\, t^2 + 0.215\, H\sum_{i=1}^{n_{AT}} t + 6.935\sum_{i=1}^{n_{AT}} t^2 + 0.265\, H\sum_{i=1}^{n_T} t + 0.589\sum_{i=1}^{n_T} t^2 + 0.75\, H\sum_{i=1}^{n_c}\sum_{i=1}^{4} t + 0.375\sum_{i=1}^{n_c}\sum_{i=1}^{4} t^2\right)\right]\right)$$

$$Area[2] = \frac{\frac{P_{mean}[2]}{\sigma_0}\, 10^6}{numelem[2]}$$

209.599

0.0279596

Section 3 (7.2m)

$n_T = 12;$

$n_L = 9;$

$n_c = 0;$

$n_f = 29;$

$n_{AT} = 21;$

$t = 0.030;$

$H = 2.4;$

$$\sigma_0 = \frac{\sigma_y + \sigma_{0_s}}{2};$$

$b = 312;$

$numelem[3] = 26;$

$$P_{mean}[3] = \frac{1}{10^6}\left(N\left[\sigma_0\left(\frac{1.178}{H}\, b\, t^2 + 0.215\, H\sum_{i=1}^{n_{AT}} t + 6.935\sum_{i=1}^{n_{AT}} t^2 + 0.265\, H\sum_{i=1}^{n_T} t + 0.589\sum_{i=1}^{n_T} t^2 + 0.75\, H\sum_{i=1}^{n_c}\sum_{i=1}^{4} t + 0.375\sum_{i=1}^{n_c}\sum_{i=1}^{4} t^2\right)\right]\right)$$

$$Area[3] = \frac{\frac{P_{mean}[3]}{\sigma_0}\, 10^6}{numelem[3]}$$

282.584

0.0318961

Section 4 (9.6m)

$n_T = 12;$

$n_L = 9;$

$n_c = 0;$

$n_f = 29;$

$n_{AT} = 21;$

$t = 0.030;$

$H = 2.4;$

$$\sigma_0 = \frac{\sigma_y + \sigma_{0_s}}{2};$$

$b = 475;$

$numelem[4] = 28;$

$$P_{mean}[4] = \frac{1}{10^6}\left(N\left[\sigma_0\left(\frac{1.178}{H}\, b\, t^2 + 0.215\, H \sum_{i=1}^{n_{AT}} t + 6.935 \sum_{i=1}^{n_{AT}} t^2 + 0.265\, H \sum_{i=1}^{n_T} t + 0.589 \sum_{i=1}^{n_T} t^2 + 0.75\, H \sum_{i=1}^{n_c}\sum_{i=1}^{4} t + 0.375 \sum_{i=1}^{n_c}\sum_{i=1}^{4} t^2\right)\right]\right)$$

$$Area[4] = \frac{\frac{P_{mean}[4]}{\sigma_0}\, 10^6}{numelem[4]}$$

307.119

0.0321894

Section 5 (12.0m)

$n_T = 12;$

$n_L = 9;$

$n_c = 0;$

$n_f = 29;$

$n_{AT} = 21;$

$t = 0.030;$

$H = 2.4;$

$$\sigma_0 = \frac{\sigma_y + \sigma_{0_s}}{2};$$

$b = 550;$

$$P_{mean}[5] = \frac{1}{10^6}\left(N\left[\sigma_0\left(\frac{1.178}{H}\, b\, t^2 + 0.215\, H \sum_{i=1}^{n_{AT}} t + 6.935 \sum_{i=1}^{n_{AT}} t^2 + 0.265\, H \sum_{i=1}^{n_T} t + 0.589 \sum_{i=1}^{n_T} t^2 + 0.75\, H \sum_{i=1}^{n_c}\sum_{i=1}^{4} t + 0.375 \sum_{i=1}^{n_c}\sum_{i=1}^{4} t^2\right)\right]\right)$$

$$Area[5] = \frac{\frac{P_{mean}[5]}{\sigma_0}\, 10^6}{numelem[5]}$$

318.409

0.0333727

Section 6 (14.4m)

$n_T = 12;$

$n_L = 9;$

$n_c = 0;$

$n_f = 29;$

$n_{AT} = 21;$

$t = 0.030;$

$H = 2.4;$

$$\sigma_0 = \frac{\sigma_y + \sigma_{0_s}}{2};$$

$b = 610;$

$numelem[6] = 28;$

$$P_{mean}[6] = \frac{1}{10^6}\left(N\left[\sigma_0\left(\frac{1.178}{H} b t^2 + 0.215\ H \sum_{i=1}^{n_{AT}} t + 6.935 \sum_{i=1}^{n_{AT}} t^2 + 0.265\ H \sum_{i=1}^{n_T} t + 0.589 \sum_{i=1}^{n_T} t^2 + 0.75\ H \sum_{i=1}^{n_c}\sum_{i=1}^{4} t + 0.375 \sum_{i=1}^{n_c}\sum_{i=1}^{4} t^2\right)\right]\right)$$

$$Area[6] = \frac{\frac{P_{mean}[6]}{\sigma_0} 10^6}{numelem[6]}$$

327.44

0.0343193

DISCUSSION OF THE RESULTS :

METHOD 1

The crushing force for the entire bow structure has been calculated to be **398.58 MN**
The maximum indentation is shown to be **18.59 m**

METHOD 2

The Bow Crushing Forces for various sections obtained using the section – by – section crushing theory and intersection element formulation are summarised below :

```
For[i = 1, i ≤ 6, i++,
 Print["Section ", i, " Pmean =   ", Pmean[i], " MN"]]
Section  1 Pmean =   113.83  MN
Section  2 Pmean =   209.599  MN
Section  3 Pmean =   282.584  MN
Section  4 Pmean =   307.119  MN
Section  5 Pmean =   318.409  MN
Section  6 Pmean =   327.44  MN
```

```
table = {{0, 0}, {2.4, Pmean[1]}, {4.8, Pmean[2]}, {7.2, Pmean[3]}
   , {9.6, Pmean[4]}, {12, Pmean[5]}, {14.4, Pmean[6]}};
Interpolation[table, InterpolationOrder → 3];
Plot[%[x], {x, 0, 14.4}, AxesLabel →
  {"Penetration (m)", "Force (MN)"}]
```

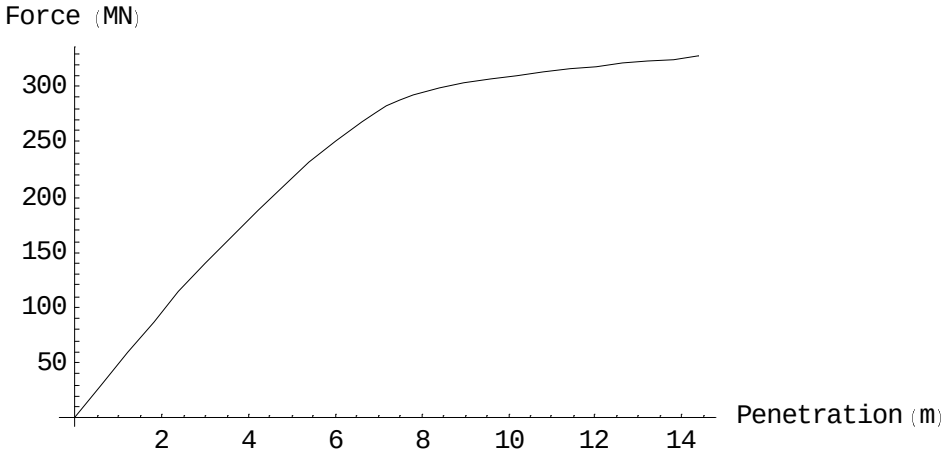

- Graphics -

150, 000 DWT Bulk Carrier :

Ship Particulars

$LBP = 274.50$;
$B = 47.00$;
$d_{MLD} = 21.60$;
$d = 26.00$;
$T = 15.96$;
$\Delta = 174850$;
$V_{service} = 9.3$;
$v_x = V_{service}$;

METHOD 1

Regression-based Crushing load and location of maximum indentation Calculations based on ship particulars

$\overline{L} = LBP / 275$;

$$m_x = \frac{1.05\ \Delta}{1000};$$

$V_0 = V_{service}$;

$$E_{imp} = \frac{1}{2} m_x V_0^2;$$

$$KE = \frac{1}{2} \Delta V_0^2\ 1000;$$

$\overline{E}_{imp} = E_{imp} / 1425$;
$P_0 = 210$;
$If\left[\overline{E}_{imp} >= \overline{L}^{2.6}, P_{bow} = P_0\ \overline{L}\left(\overline{E}_{imp} + \left(5.0 - \overline{L}\right)\overline{L}^{1.6}\right)^{0.5}\right]$;
$If\left[\overline{E}_{imp} < \overline{L}^{2.6}, P_{bow} = 2.24\ P_0\ \left(\overline{E}_{imp}\ \overline{L}\right)^{0.5}\right]$;
Print["Kinetic Energy = ", KE / 10^6 MJ];
Print["Crush Load = ", P_{bow} MN];

$$s_{max} = \frac{\pi}{2} \frac{E_{imp}}{P_{bow}} \text{ metres};$$

Print["Maximum indentation = ", s_{max}];

```
Kinetic Energy = 7561.39 MJ
Crush Load = 648.182 MN
Maximum indentation = 19.2404 metres
```

METHOD 2

Crush Loads for variuos sections based on Summation formula by Yang and Caldwell
Material Properties

$\overline{E} = 209\ 10^9;$

$\sigma_y = 315\ 10^6;$

$\sigma_{0_s} = 1.9\ \sigma_y;$

$s = 3.30;$

$\dot{\epsilon} = \frac{v_x}{s};$

$\sigma_0 = 1.29\ \sigma_{0_s}\ \dot{\epsilon}^{0.037};$

Section 1 (3.3m)

$n_T = 5;$

$n_L = 4;$

$n_c = 1;$

$n_f = 13;$

$n_{AT} = 9;$

$t = 0.030;$

$H = 3.3;$

$\sigma_0 = \frac{\sigma_y + \sigma_{0_s}}{2};$

$b = 50;$

$numelem[1] = 9;$

$$P_{mean}[1] = \frac{1}{10^6}\left(N\left[\sigma_0\left(\frac{1.178}{H}\,b\,t^2 + 0.215\,H\sum_{i=1}^{n_{AT}} t + 6.935\sum_{i=1}^{n_{AT}} t^2 + 0.265\,H\sum_{i=1}^{n_T} t + 0.589\sum_{i=1}^{n_T} t^2 + 0.75\,H\sum_{i=1}^{n_c}\sum_{i=1}^{4} t + 0.375\sum_{i=1}^{n_c}\sum_{i=1}^{4} t^2\right)\right]\right)$$

$$Area[1] = \frac{\frac{P_{mean}[1]}{\sigma_0}\,10^6}{numelem[1]}$$

317.888

0.0773308

Section 2 (4.8m)

$n_T = 8;$
$n_L = 5;$
$n_c = 1;$
$n_f = 20;$
$n_{AT} = 13;$
$t = 0.030;$
$H = 3.3;$
$\sigma_0 = \frac{\sigma_y + \sigma_{0_s}}{2};$
$b = 200;$

$$P_{mean}[2] = \frac{1}{10^6}\left(N\left[\sigma_0\left(\frac{1.178}{H}\, b\, t^2 + 0.215\, H \sum_{i=1}^{n_{AT}} t + 6.935 \sum_{i=1}^{n_{AT}} t^2 + 0.265\, H \sum_{i=1}^{n_T} t + 0.589 \sum_{i=1}^{n_T} t^2 + 0.75\, H \sum_{i=1}^{n_c}\sum_{i=1}^{4} t + 0.375 \sum_{i=0}^{n_c}\sum_{i=1}^{4} t^2\right)\right]\right)$$

$numelem[2] = 16;$

$$Area[2] = \frac{\frac{P_{mean}[2]}{\sigma_0}\, 10^6}{numelem[2]}$$

427.481
0.058495

Section 3 (7.2m)

$n_T = 7;$
$n_L = 8;$
$n_c = 0;$
$n_f = 20;$
$n_{AT} = 15;$
$t = 0.030;$
$H = 3.3;$
$\sigma_0 = \frac{\sigma_y + \sigma_{0_s}}{2};$
$b = 375;$

$$P_{mean}[3] = \frac{1}{10^6}\left(N\left[\sigma_0\left(\frac{1.178}{H}\, b\, t^2 + 0.215\, H \sum_{i=1}^{n_{AT}} t + 6.935 \sum_{i=1}^{n_{AT}} t^2 + 0.265\, H \sum_{i=1}^{n_T} t + 0.589 \sum_{i=1}^{n_T} t^2 + 0.75\, H \sum_{i=1}^{4} t + 0.375 \sum_{i=1}^{4} t^2\right)\right]\right)$$

$numelem[3] = 24;$

$$Area[3] = \frac{\frac{P_{mean}[3]}{\sigma_0}\, 10^6}{numelem[3]}$$

465.465
0.0424617

Section 4 (9.6m)

$n_T = 7;$

$n_L = 8;$

$n_c = 0;$

$n_f = 20;$

$n_{AT} = 15;$

$t = 0.030;$

$H = 3.3;$

$$\sigma_0 = \frac{\sigma_y + \sigma_{0_s}}{2};$$

$b = 575;$

$$P_{mean}[4] = \frac{1}{10^6}\left(N\left[\sigma_0\left(\frac{1.178}{H}\, b\, t^2 + 0.215\, H \sum_{i=1}^{n_{AT}} t + 6.935 \sum_{i=1}^{n_{AT}} t^2 + 0.265\, H \sum_{i=1}^{n_T} t + 0.589 \sum_{i=1}^{n_T} t^2 + 0.75\, H \sum_{i=1}^{4} t + 0.375 \sum_{i=1}^{4} t^2\right)\right]\right)$$

$numelem[4] = 18;$

$$Area[4] = \frac{\frac{P_{mean}[4]}{\sigma_0}\, 10^6}{numelem[4]}$$

494.813

0.0601853

Section 5 (12.0m)

$n_T = 7;$

$n_L = 8;$

$n_c = 0;$

$n_f = 20;$

$n_{AT} = 15;$

$t = 0.030;$

$H = 3.3;$

$$\sigma_0 = \frac{\sigma_y + \sigma_{0_s}}{2};$$

$b = 700;$

$$P_{mean}[5] = \frac{1}{10^6}\left(N\left[\sigma_0\left(\frac{1.178}{H}\, b\, t^2 + 0.215\, H \sum_{i=1}^{n_{AT}} t + 6.935 \sum_{i=1}^{n_{AT}} t^2 + 0.265\, H \sum_{i=1}^{n_T} t + 0.589 \sum_{i=1}^{n_T} t^2 + 0.75\, H \sum_{i=1}^{4} t + 0.375 \sum_{i=1}^{4} t^2\right)\right]\right)$$

$numelem[5] = 18;$

$$Area[5] = \frac{\frac{P_{mean}[5]}{\sigma_0}\, 10^6}{numelem[5]}$$

513.156
0.0624163

Section 6 (14.4m)

$n_T = 7;$

$n_L = 8;$

$n_c = 0;$

$n_f = 20;$

$n_{AT} = 15;$

$t = 0.030;$

$H = 3.3;$

$\sigma_0 = \frac{\sigma_y + \sigma_{0_s}}{2};$

$b = 850;$

$$P_{mean}[6] = \frac{1}{10^6}\left(N\left|\sigma_0\left(\frac{1.178}{H}\, b\, t^2 + 0.215\, H \sum_{i=1}^{n_{AT}} t + 6.935 \sum_{i=1}^{n_{AT}} t^2 + 0.265\, H \sum_{i=1}^{n_T} t + 0.589 \sum_{i=1}^{n_T} t^2 + 0.75\, H \sum_{i=1}^{4} t + 0.375 \sum_{i=1}^{4} t^2\right)\right|\right)$$

$numelem[6] = 18;$

$$Area[6] = \frac{\frac{P_{mean}[6]}{\sigma_0}\, 10^6}{numelem[6]}$$

535.167
0.0650936

DISCUSSION OF THE RESULTS :

METHOD 1

The crushing force for the entire bow structure has been calculated to be **648.182 MN**
The maximum indentation is shown to be **19.24 m**

METHOD 2

The Bow Crushing Forces for various sections obtained using the section – by – section crushing theory and intersection element formulation are summarised below :

```
For[i = 1, i ≤ 6, i++,
 Print["Section ", i, " Pmean =   ", Pmean[i], " MN"]]
```

```
Section  1 Pmean =   317.888  MN
Section  2 Pmean =   427.481  MN
Section  3 Pmean =   465.465  MN
Section  4 Pmean =   494.813  MN
Section  5 Pmean =   513.156  MN
```

Section 6 P_{mean} = 535.167 MN

```
table = {{0, 0}, {3.2, Pmean[1]}, {6.4, Pmean[2]}, {9.6, Pmean[3]}
   , {12.8, Pmean[4]}, {16, Pmean[5]}, {19.2, Pmean[6]}};
Interpolation[table, InterpolationOrder → 3];
Plot[%[x], {x, 0, 19.2}, AxesLabel →
  {"Penetration (m)", "Force (MN)"}]
```

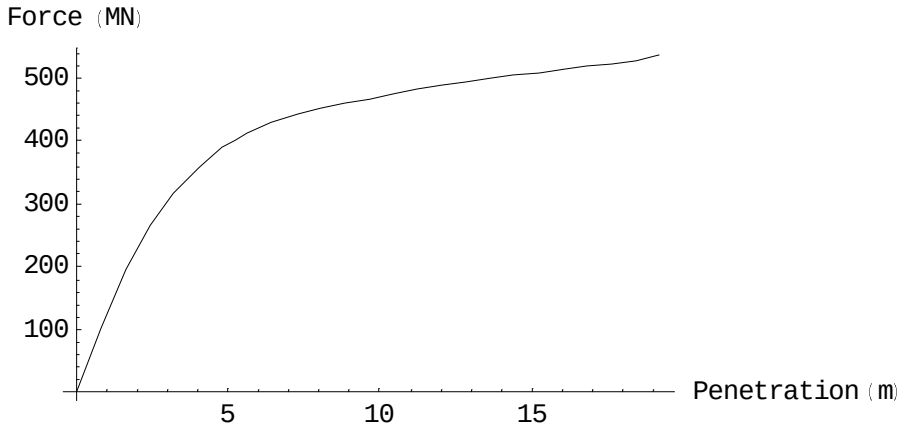

- Graphics -

APPENDIX B

Ship particulars and bow scantlings

500 DWT Coaster

Principal Particulars:

LBP	: 41.0 m
Breadth moulded	: 9.00 m
Depth mld to main deck	: 3.50 m
Depth to shelter deck	: 6.40 m
Max. Draft	: 3.34 m
Displacement	: 886 tons
Speed	: 5.0 m/s (9.70 knots)

The bow is stiffened by transverse stiffeners/frames with spacing 0.3 m below 3.9 m abl and 0.6 m in shelter deck and in side shell above longitudinal stringer 3.9 m abl. The most important structural data for the bow are:

Plate thickness, bottom up to 1.0 m abl	: 9.0 mm
Plate thickness, side shell up to 4.0 m abl	: 14.0 mm
Plate thickness, side shell above 4.0 m abl	: 7.0 mm
Plate thickness, shelter deck	: 7.0 mm
(Main Deck is not present in forepeak)	
CL-girder, shelter deck	: 300 x 8/100 x 10 (L)
CL-girder along stem line above bulb	: 300 x 8/100 x 10 (L)
Horizontal stringer 3.9 m abl	: 300 x 8/100 x 10 (L)
Longitudinal CL-girder, bottom	: 500 x 8/100 x 10 (L)
Breast hooks between 1.7 & 3.4m abl (4 off)	: 200 x 8 (Fl)
CL-bulkhead in bulb	: 6.0 mm

23,000 DWT Containership

Principal dimensions:

LBP	: 211.50 m
Breadth moulded	: 32.20 m
Depth mld to main deck	: 21.00 m
Depth to shelter deck	: 24.00 m
Max. Draft	: 11.90 m
Displacement (Loaded)	: 54,000 tons
Max. Service Speed	: 11.3 m/s (21.97 knots)

The bulbous bow is stiffened longitudinally. The transverse frames supporting the longitudinals have a spacing of 2.4 m. The most important structural data for the bow are:

Bottom:

Plate thickness	: 19.0 mm
Longitudinals, spacing 0.8 m	: L 250 X 90 X 12 / 16
CL-Girder	: L 1900 X 250 X 15 / 25

Side shell:

Plate thickness, side shell up to 6.1 m abl	: 17.0 mm
Plate thickness, side shell between 6.1 and 12.3 m abl	: 35.0 mm
Plate thickness, side shell between 12.3 and 21.0 m abl	: 16.0 mm
Plate thickness, side shell above 21.0 m abl	: 14.0 mm
Longitudinals below 5.2 m abl and above 13.6 m abl (spacing 0.8 m)	: L250 x 90 x 10/15
Longitudinals between 6.6 and 12.0 m abl, spacing 0.6 m	: L250 x 90 x 12/16

Forecastle deck, 24.0 m abl

Plate thickness	: 15.0 mm
Longitudinals, spacing 0.8 m	: L150 x 100 x 9
CL-girder	: L700 x 150 x 12/12

Main deck,21.0 m abl

Plate thickness	: 11.0 mm
Longitudinals, spacing 0.8 m	: L150 x 100 x 9
CL-girder	: L700 x 150 x 12/12

Deck 17.6 m abl

Plate thickness	: 11.0 mm
Longitudinals, spacing 0.8 m	: L150 x 100 x 9
CL-girder	: L700 x 150 x 12/12

Deck 12.8 m abl

Plate thickness	: 15.0 mm
Longitudinals, spacing 0.8 m	: L200 x 90 x 9/14
CL-girder	: L700 x 150 x 12/12

Deck (not water-tight), 6 m abl

Plate thickness	: 11.0 mm
Longitudinals, spacing 0.8 m	: Fl. 150 x 12

40,000 DWT Containership

Principal dimensions:

LBP	: 211.50 m
Breadth moulded	: 32.20 m
Depth mld to main deck	: 21.00 m
Depth to shelter deck	: 24.00 m
Max. Draft	: 11.90 m
Displacement (Loaded)	: 54,000 tons
Max. Service Speed	: 11.3 m/s (21.97 knots)

The bulbous bow is stiffened longitudinally. The transverse frames supporting the longitudinals have a spacing of 2.4 m. The most important structural data for the bow are:

Bottom:

Plate thickness	: 19.0 mm
Longitudinals, spacing 0.8 m	: L 250 X 90 X 12 / 16
CL-Girder	: L 1900 X 250 X 15 / 25

Side shell

Plate thickness, side shell up to 6.1 m abl	: 17.0 mm
Plate thickness, side shell between 6.1 and 12.3 m abl	: 35.0 mm
Plate thickness, side shell between 12.3 and 21.0 m abl	: 16.0 mm
Plate thickness, side shell above 21.0 m abl	: 14.0 mm
Longitudinals below 5.2 m abl and above 13.6 m abl (spacing 0.8 m)	: L250 x 90 x 10/15
Longitudinals between 6.6 and 12.0 m abl, spacing 0.6 m	: L250 x 90 x 12/16

Forecastle deck, 24.0 m abl

Plate thickness	: 15.0 mm
Longitudinals, spacing 0.8 m	: L150 x 100 x 9
CL-girder	: L700 x 150 x 12/12

Main deck,21.0 m abl

Plate thickness	: 11.0 mm
Longitudinals, spacing 0.8 m	: L150 x 100 x 9
CL-girder	: L700 x 150 x 12/12

Deck 17.6 m abl

Plate thickness	: 11.0 mm
Longitudinals, spacing 0.8 m	: L150 x 100 x 9
CL-girder	: L700 x 150 x 12/12

Deck 12.8 m abl

Plate thickness	: 15.0 mm
Longitudinals, spacing 0.8 m	: L200 x 90 x 9/14
CL-girder	: L700 x 150 x 12/12

Deck (not water-tight), 6 m abl

Plate thickness	: 11.0 mm
Longitudinals, spacing 0.8 m	: Fl. 150 x 12

150,000 DWT Bulk Carrier

Ship Particulars

LBP	: 274 m
Breadth moulded	: 47.0 m
Depth molded	: 21.6 m
Depth to forecastle deck	: 26.0 m
Max. Draft	: 15.96 m
Displacement	: 174850 tons
Max. service speed	: 7.7 m/s (15.00 knots)

The bow is stiffened longitudinally. The transverse frames supporting the longitudinals have a spacing of 3.2 m. The most important structural data for the bow are:

Material

Yield Stress for plates and stiffeners (σ_Y)	: 315 Mpa
Ratio between ultimate and Yield stress (σ_u/σ_Y)	: 1.6

Bottom

plate thickness	: 18.0 mm
longitudinals, spacing	: L450 x 150 x 12/16
CL-Girder	: L2500 x 400 x 15/25

Side shell

Plate thickness, side shell up to 8.1 m abl	: 18.0 mm
Plate thickness, side shell between 8.1 and 17.0 m abl	: 33.0 mm
Plate thickness, side shell between 17.0 and 26.0 m abl	: 16.0 mm
Longitudinals between 1.2 and 6.8 m abl, spacing 0.8 m	: L450 x 150 x 12/16
Longitudinals between 8.4 and 16.2 m abl, spacing 0.6 m	: L400 x 100 x 19/19

Longitudinals between 17.4 and 24.8 m abl, spacing 0.8 m : L350 x 100 x 12/17

Forecastle deck, 26.0 m abl

Plate thickness	: 13.0 mm
Longitudinals, spacing	: L250 x 90 x 12/16
CL-girder	: L1400 x 250 x 12/25

Tank top, 20.0 m abl

Plate thickness	: 13.0 mm
Longitudinals, spacing	: L250 x 90 x 12/16
CL-girder	: L1400 x 250 x 12/25

Deck (not water-tight), 7.7 m abl

Plate thickness	: 13.0 mm
Longitudinals, spacing	: L250 x 90 x 12/16
CL-girder	: L1400 x 250 x 12/25

Breast hooks

Number of breast hooks	: 32
Cross-section	: 1200 x 15
Length	: 3000 mm
CL-girder along stem line cross-section	: T1400 x 250 x 12/25
CL-bulkhead in bulb fwd F.P (plate thickness)	: 12mm
Vertical stiffening spacing	: 0.8 m

APPENDIX C

Example of an LS-DYNA input deck

```
*KEYWORD
$---+----1----+----2----+----3----+----4----+----5----+----6----+----7----+----8
$
$ DYNA3D(936) DECK WAS WRITTEN BY: ETA/FEMB VERSION 26
$ DATE  : Nov 11, 1999 at 10:22:33
$ PREPARED BY: SURYANARAYANA VAKKALANKA (M.S)
$ AEROSPACE AND OCEAN ENGINEERING, VIRGINIA TECH.
$
$---+----1----+----2----+----3----+----4----+----5----+----6----+----7----+----8
$                (1) TITLE CARD.
$---+----1----+----2----+----3----+----4----+----5----+----6----+----7----+----8
*TITLE
150K SPEED12
$---+----1----+----2----+----3----+----4----+----5----+----6----+----7----+----8
$                (2) CONTROL CARDS.
$---+----1----+----2----+----3----+----4----+----5----+----6----+----7----+----8
*CONTROL_TERMINATION
$   ENDTIM    ENDCYC     DTMIN    ENDNEG    ENDMAS
  .400E+01         0      .000      .000      .000
*CONTROL_TIMESTEP
$   DTINIT      SCFT      ISDO    TSLIMT      DTMS      LCTM     ERODE     MS1ST
      .000      .900         0
*CONTROL_HOURGLASS
$      IHQ        QH
         1      .100
```

```
*CONTROL_BULK_VISCOSITY
$      Q2       Q1
   1.500     .060
*CONTROL_SHELL
$  WRPANG   ITRIST    IRNXX   ISTUPD   THEORY      BWC    MITER
  20.000        2       -1        0        2        2        1
*CONTROL_CONTACT
$  SLSFAC   RWPNAL   ISLCHK   SHLTHK   PENOPT   THKCHG    ORIEN
    .100
$  USRSTR   USRFAC    NSBCS   INTERM    XPENE
       0        0       10        0    4.000
*CONTROL_ENERGY
$    HGEN     RWEN    SLNTEN     RYLEN
       1        2        1        1
*CONTROL_DAMPING
$  NRCYCK    DRTOL   DRFCTR   DRTERM   TSSFDR   IRELAL    EDTTL
IDRFLG
     250     .001     .995
*CONTROL_OUTPUT
$   NPOPT    NEECHO   NREFUP   IACCOP    OPIFS   IPNINT   IKEDIT
       0        0        0        0     .000        0      100
$---+----1----+----2----+----3----+----4----+----5----+----6----+----7----+----8
$                (3) DATABASE CONTROL CARDS - ASCII HISTORY FILE
$---+----1----+----2----+----3----+----4----+----5----+----6----+----7----+----8
$*DATABASE_HISTORY_OPTION
$     ID1      ID2      ID3      ID4      ID5      ID6      ID7      ID8
$
$OPTION : BEAM    BEAM_SET   NODE   NODE_SET
$        SHELL   SHELL_SET  SOLID  SOLID_SET
$        TSHELL  TSHELL_SET
$---+----1----+----2----+----3----+----4----+----5----+----6----+----7----+----8
```

```
$                (4) DATABASE CONTROL CARDS FOR ASCII FILE
$---+----1----+----2----+----3----+----4----+----5----+----6----+----7----+----8
$---+----1----+----2----+----3----+----4----+----5----+----6----+----7----+----8
$*DATABASE_OPTION
$      DT
$
$OPTION : SECFORC RWFORC NODOUT ELOUT  GLSTAT
$        DEFORC  MATSUM NCFORC RCFORC DEFGEO
$        SPCFORC SWFORC ABSTAT NODFOR BNDOUT
$        RBDOUT  GCEOUT SLEOUT MPGS   SBTOUT
$        JNTFORC AVSFLT MOVIE
*DATABASE_GLSTAT
  .800E-02
*DATABASE_RCFORC
  .800E-02
$---+----1----+----2----+----3----+----4----+----5----+----6----+----7----+----8
$                (5) DATABASE CONTROL CARDS FOR BINARY FILE
$---+----1----+----2----+----3----+----4----+----5----+----6----+----7----+----8
*DATABASE_BINARY_D3PLOT
$  DT/CYCL     LCDT    NOBEAM
  .200E+00
*DATABASE_BINARY_D3THDT
$  DT/CYCL     LCDT    NOBEAM
  .200E+00
$*DATABASE_BINARY_OPTION
$  DT/CYCL     LCDT    NOBEAM
$
$OPTION : D3DRFL D3DUMP RUNRSF INTFOR
$---+----1----+----2----+----3----+----4----+----5----+----6----+----7----+----8
*DATABASE_EXTENT_BINARY
         0        0        3        0        1        1        1        1
```

```
        0       0       0       0       0       0
$---+----1----+----2----+----3----+----4----+----5----+----6----+----7----+----8
$                  (6) DEFINE PARTS CARDS
$---+----1----+----2----+----3----+----4----+----5----+----6----+----7----+----8
*PART
$HEADING
 PART PID =       8 PART NAME :TRANS
$     PID     SID     MID    EOSID    HGID    GRAV   ADPOPT    TMID
        8       8       4
*PART
$HEADING
 PART PID =       1 PART NAME :WALL
$     PID     SID     MID    EOSID    HGID    GRAV   ADPOPT    TMID
        1       1       1
*PART
$HEADING
 PART PID =       9 PART NAME :MASS
$     PID     SID     MID    EOSID    HGID    GRAV   ADPOPT    TMID
        9      18       3
*PART
$HEADING
 PART PID =       2 PART NAME :LONG1
$     PID     SID     MID    EOSID    HGID    GRAV   ADPOPT    TMID
        2       2       2
*PART
$HEADING
 PART PID =       3 PART NAME :LONG2
$     PID     SID     MID    EOSID    HGID    GRAV   ADPOPT    TMID
        3       3       2
*PART
$HEADING
```

```
 PART PID =        4 PART NAME :LONG3
$     PID      SID      MID     EOSID     HGID     GRAV    ADPOPT     TMID
        4        4        2
*PART
$HEADING
 PART PID =        5 PART NAME :LONG4
$     PID      SID      MID     EOSID     HGID     GRAV    ADPOPT     TMID
        5        5        2
*PART
$HEADING
 PART PID =        6 PART NAME :LONG5
$     PID      SID      MID     EOSID     HGID     GRAV    ADPOPT     TMID
        6        6        2
*PART
$HEADING
 PART PID =        7 PART NAME :LONG6
$     PID      SID      MID     EOSID     HGID     GRAV    ADPOPT     TMID
        7        7        2
$---+----1----+----2----+----3----+----4----+----5----+----6----+----7----+----8
$                 (7) MATERIAL CARDS
*MAT_PLASTIC_KINEMATIC
$MATERIAL NAME:TRANS
$     MID       RO        E       PR     SIGY     ETAN     BETA
        4 7.850E+03 2.090E+11 2.800E-01 4.567E+08 4.567E+08 0.000E+00
$     SRC       SRP       FS
 4.000E+01 5.000E+00 0.000E+00
*MAT_RIGID
$MATERIAL NAME:WALL
$     MID       RO        E       PR        N    COUPLE        M     ALIAS
        1 7.850E+03 2.090E+11 2.800E-01 0.000E+00 0.000E+00 0.000E+00
$     CMO      CON1      CON2
```

```
      1.0       7.0       7.0
$LCO or A1        A2        A3        V1        V2        V3
*MAT_PLASTIC_KINEMATIC
$MATERIAL NAME:MASS
$     MID        RO         E        PR      SIGY      ETAN      BETA
         3 1.525E+06 2.090E+11 2.800E-01 4.567E+08 4.567E+08 0.000E+00
$     SRC       SRP        FS
 0.000E+00 0.000E+00 0.000E+00
*MAT_PLASTIC_KINEMATIC
$MATERIAL NAME:FLOWSTRE
$     MID        RO         E        PR      SIGY      ETAN      BETA
         2 7.850E+03 2.090E+11 2.800E-01 4.567E+08 4.567E+08 0.000E+00
$     SRC       SRP        FS
 4.000E+01 5.000E+00 0.000E+00
$---+----1----+----2----+----3----+----4----+----5----+----6----+----7----+----8
$                 (7.1) SECTION CARDS
$---+----1----+----2----+----3----+----4----+----5----+----6----+----7----+----8
*SECTION_BEAM
$PROPERTY NAME:TRUSS
$     SID    ELFORM      SHRF   QR/IRID       CST
         8         3
  .900E+00
*SECTION_SHELL
$PROPERTY NAME:WALL
$     SID    ELFORM      SHRF       NIP     PROPT   QR/IRID     ICOMP
         1         2  .100E+01       3.0       1.0        .0
$      T1        T2        T3        T4      NLOC
 1.000E-06 1.000E-06 1.000E-06 1.000E-06
*SECTION_BEAM
$PROPERTY NAME:MASS
$     SID    ELFORM      SHRF   QR/IRID       CST
```

18 3

.900E+00

***SECTION_BEAM**

$PROPERTY NAME:LONG1

$ SID ELFORM SHRF QR/IRID CST

2 3

.773E-01

***SECTION_BEAM**

$PROPERTY NAME:LONG2

$ SID ELFORM SHRF QR/IRID CST

3 3

.585E-01

***SECTION_BEAM**

$PROPERTY NAME:LONG3

$ SID ELFORM SHRF QR/IRID CST

4 3

.425E-01

***SECTION_BEAM**

$PROPERTY NAME:LONG4

$ SID ELFORM SHRF QR/IRID CST

5 3

.602E-01

***SECTION_BEAM**

$PROPERTY NAME:LONG5

$ SID ELFORM SHRF QR/IRID CST

6 3

.624E-01

***SECTION_BEAM**

$PROPERTY NAME:LONG6

$ SID ELFORM SHRF QR/IRID CST

7 3

```
 .651E-01
$---+----1----+----2----+----3----+----4----+----5----+----6----+----7----+----8
$                (8) NODAL POINT CARDS
$---+----1----+----2----+----3----+----4----+----5----+----6----+----7----+----8
*NODE
$  NODE             X             Y             Z     TC     RC
     1  .251391800E+05  .129386200E+05  .138082400E+05
     2  .251503900E+05  .129386200E+05  .138082400E+05
     3  .251616000E+05  .129386200E+05  .138082400E+05
     4  .251461400E+05  .129273900E+05  .138082400E+05
     5  .251422400E+05  .129202200E+05  .138082400E+05
        .
        .
        .
        .
   240  .251585400E+05  .129202200E+05  .136932400E+05
   241  .251503900E+05  .129202200E+05  .136932400E+05
   242  .251503900E+05  .129188200E+05  .136932400E+05
   243  .251503900E+05  .129126200E+05  .136932400E+05
   244  .251506400E+05  .129372200E+05  .136932400E+05
   245  .251506400E+05  .129312200E+05  .136932400E+05
   246  .251506400E+05  .129188200E+05  .136932400E+05
$---+----1----+----2----+----3----+----4----+----5----+----6----+----7----+----8
$                (9) SOLID ELEMENT CARDS
$---+----1----+----2----+----3----+----4----+----5----+----6----+----7----+----8
*ELEMENT_SOLID
$   EID     PID      N1      N2      N3      N4      N5      N6      N7      N8
$---+----1----+----2----+----3----+----4----+----5----+----6----+----7----+----8
$                (10) BEAM ELEMENT CARDS
$---+----1----+----2----+----3----+----4----+----5----+----6----+----7----+----8
*ELEMENT_BEAM
```

```
$   EID     PID      N1      N2      N3
        1       8       1       2
        2       8       2       3
        3       8       4       5
        4       8       5       6
        5       8       6       7
              .
              .
              .
      349       7       1     231
      350       7      58     232
      351       7       2     229
      352       7      79     244
      353       7     238      80
      354       7      81     245
      355       7     242      65
      356       7      74     246
$---+----1----+----2----+----3----+----4----+----5----+----6----+----7----+----8
$                   (11) SHELL ELEMENT CARDS
$---+----1----+----2----+----3----+----4----+----5----+----6----+----7----+----8
```

***ELEMENT_SHELL**

```
$   EID     PID      N1      N2      N3      N4
        95       1      86      89      88      87
        96       1      89      91      90      88
        97       1      91      93      92      90
        98       1      93      95      94      92
        99       1      95      97      96      94
       100       1      97      99      98      96
              .
              .
              .
```

```
    190       1     190     191     202     201
    191       1     191     192     203     202
    192       1     192     193     204     203
    193       1     193     194     205     204
    194       1     194     195     206     205
$---+----1----+----2----+----3----+----4----+----5----+----6----+----7----+----8
$                (12) SPRING OR DAMPER ELEMENT CARDS
$---+----1----+----2----+----3----+----4----+----5----+----6----+----7----+----8
*ELEMENT_DISCRETE
$   EID     PID      N1      N2     VID              S      PF
*ELEMENT_MASS
$   EID     NID            MASS
$---+----1----+----2----+----3----+----4----+----5----+----6----+----7----+----8
$                (14) HOURGLASS AND BULK PROPERTIES CARDS
$---+----1----+----2----+----3----+----4----+----5----+----6----+----7----+----8
$*HOURGLASS
$     IHQ       QH      IBQ       Q1       Q2
$
$---+----1----+----2----+----3----+----4----+----5----+----6----+----7----+----8
$                (15) DEFINE SET CARDS
$---+----1----+----2----+----3----+----4----+----5----+----6----+----7----+----8
$---+----1----+----2----+----3----+----4----+----5----+----6----+----7----+----8
$                (16) BOUNDARY CONDITION CARDS
$---+----1----+----2----+----3----+----4----+----5----+----6----+----7----+----8
*BOUNDARY_SPC_NODE
$ NID/NSID      CID     DOFX     DOFY     DOFZ    DOFRX    DOFRY    DOFRZ
       1        0        1        1        0        1        1        1
       2        0        1        1        0        1        1        1
       3        0        1        1        0        1        1        1
       4        0        1        1        0        1        1        1
       5        0        1        1        0        1        1        1
```

```
        .
        .
        .
    241     0     1     1     0     1     1     1
    242     0     1     1     0     1     1     1
    243     0     1     1     0     1     1     1
    244     0     1     1     0     1     1     1
    245     0     1     1     0     1     1     1
    246     0     1     1     0     1     1     1
$---+----1----+----2----+----3----+----4----+----5----+----6----+----7----+----8
$               (17) LOCAL COORDINATE SYSTEM
$---+----1----+----2----+----3----+----4----+----5----+----6----+----7----+----8
$---+----1----+----2----+----3----+----4----+----5----+----6----+----7----+----8
$               (18) NODAL CONSTRAINT CARDS
$---+----1----+----2----+----3----+----4----+----5----+----6----+----7----+----8
$---+----1----+----2----+----3----+----4----+----5----+----6----+----7----+----8
$               (19) INITIAL CARDS
$---+----1----+----2----+----3----+----4----+----5----+----6----+----7----+----8
*INITIAL_VELOCITY_NODE
$    NID       VX       VY       VZ      VXR      VYR      VZR
       1 0.000E+00 0.000E+00 1.200E+01 0.000E+00 0.000E+00 0.000E+00
       2 0.000E+00 0.000E+00 1.200E+01 0.000E+00 0.000E+00 0.000E+00
       3 0.000E+00 0.000E+00 1.200E+01 0.000E+00 0.000E+00 0.000E+00
       4 0.000E+00 0.000E+00 1.200E+01 0.000E+00 0.000E+00 0.000E+00
       5 0.000E+00 0.000E+00 1.200E+01 0.000E+00 0.000E+00 0.000E+00
        .
        .
        .
     240 0.000E+00 0.000E+00 1.200E+01 0.000E+00 0.000E+00 0.000E+00
     241 0.000E+00 0.000E+00 1.200E+01 0.000E+00 0.000E+00 0.000E+00
     242 0.000E+00 0.000E+00 1.200E+01 0.000E+00 0.000E+00 0.000E+00
```

243 0.000E+00 0.000E+00 1.200E+01 0.000E+00 0.000E+00 0.000E+00

244 0.000E+00 0.000E+00 1.200E+01 0.000E+00 0.000E+00 0.000E+00

245 0.000E+00 0.000E+00 1.200E+01 0.000E+00 0.000E+00 0.000E+00

246 0.000E+00 0.000E+00 1.200E+01 0.000E+00 0.000E+00 0.000E+00

$---+----1----+----2----+----3----+----4----+----5----+----6----+----7----+----8

$ (22) DEFINE CONTACT SURFACE

$---+----1----+----2----+----3----+----4----+----5----+----6----+----7----+----8

***CONTACT_NODES_TO_SURFACE_TITLE**

$ CID IF. NAME

9 NODES

$ SSID MSID SSTYP MSTYP SBOXID MBOXID SPR MPR

2 3 4 0 0 0 0 0

$ FS FD DC V VDC PENCHK BT DT

0.000E+00 0.000E+00 0.000E+00 0.000E+00 0.000E+00 0 0.000E+00 1.000E+20

$ SFS SFM SST MST SFST SFMT FSF VSF

.100E+01 .100E+01 .100E+01 .100E+01 .100E+01 .100E+01

***SET_NODE_LIST**

$ SID DA1 DA2 DA3 DA4

2

$ NID1 NID2 NID3 NID4 NID5 NID6 NID7 NID8

1 2 3 4 5 6 7 8

9 10 11 12 13 14 15 16

17 18 19 20 21 22 23 24

25 26 27 28 29 30 31 32

33 34 35 36 37 38 39 40

41 42 43 44 45 46 47 48

49 50 51 52 53 54 55 56

57 58 59 60 61 62 63 64

65 66 67 68 69 70 71 72

73 74 75 76 77 78 79 80

81 82 83 84 85 225 226 227

```
      228     229     230     231     232     233     234     235
      236     237     238     239     240     241     242     243
      244     245     246
*SET_SEGMENT
$     SID      DA1      DA2      DA3      DA4
        3
$      N1       N2       N3       N4       A1       A2       A3       A4
       86       89       88       87
       89       91       90       88
       91       93       92       90
       93       95       94       92
       95       97       96       94
          .
          .
          .
      190      191      202      201
      191      192      203      202
      192      193      204      203
      193      194      205      204
      194      195      206      205
$---+----1----+----2----+----3----+----4----+----5----+----6----+----7----+----8
$                 (23) DEFINE RIGID WALL
$---+----1----+----2----+----3----+----4----+----5----+----6----+----7----+----8
$                 (24) NODAL RIGID BODY CARDS
$---+----1----+----2----+----3----+----4----+----5----+----6----+----7----+----8
$                 (25) JOINT CARDS
$---+----1----+----2----+----3----+----4----+----5----+----6----+----7----+----8
$---+----1----+----2----+----3----+----4----+----5----+----6----+----7----+----8
$---+----1----+----2----+----3----+----4----+----5----+----6----+----7----+----8
*END
```

*LS-DYNA KEYWORDS are shown in bold-faced text.

The * preceding the keywords is a must and should not be ignored

The $ preceding a line means that that line is a dummy line and will not be executed during the run.

APPENDIX D

Closed Form Drawings

150K DWT

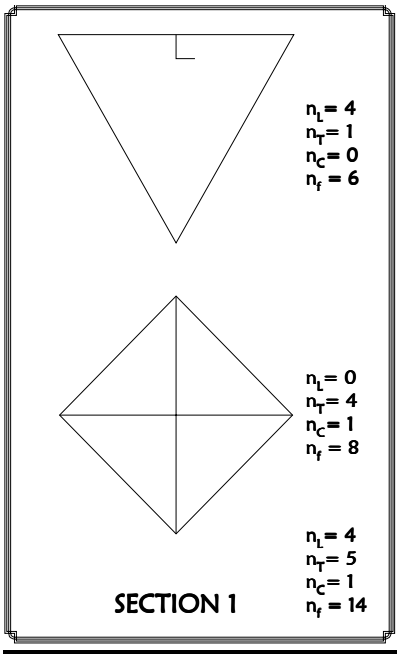

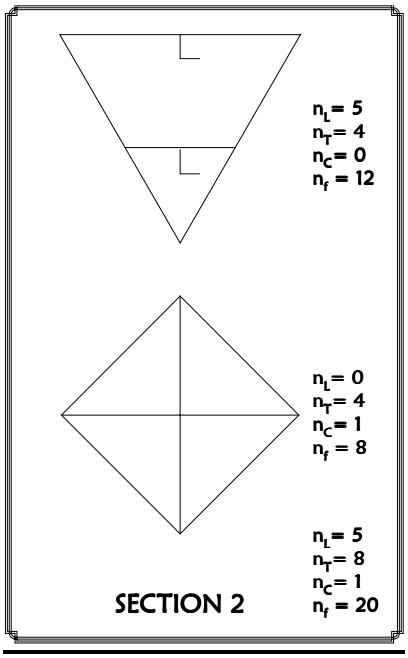

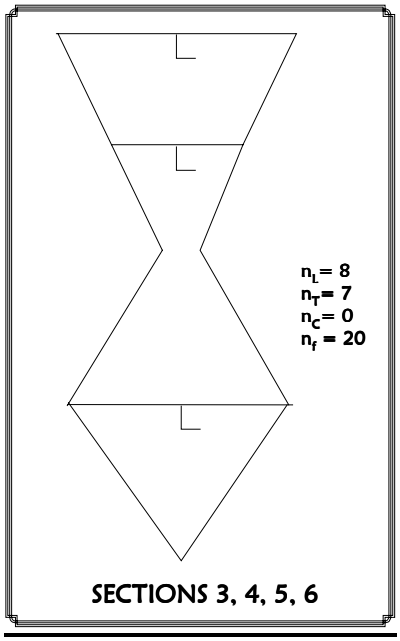

40K DWT

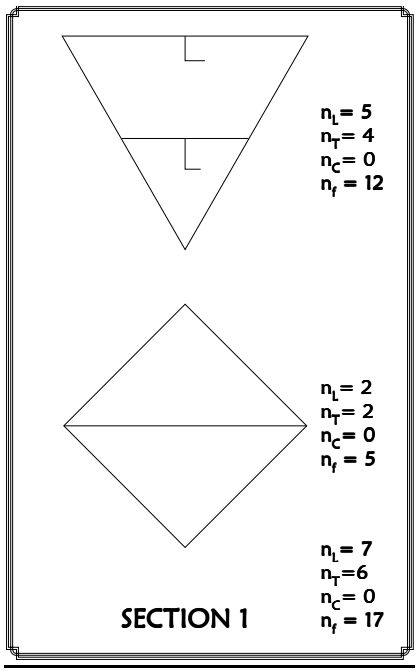
n_L= 5
n_T= 4
n_C= 0
n_f = 12
n_L= 2
n_T= 2
n_C= 0
n_f = 5
n_L= 7
n_T=6
n_C= 0
n_f = 17
SECTION 1

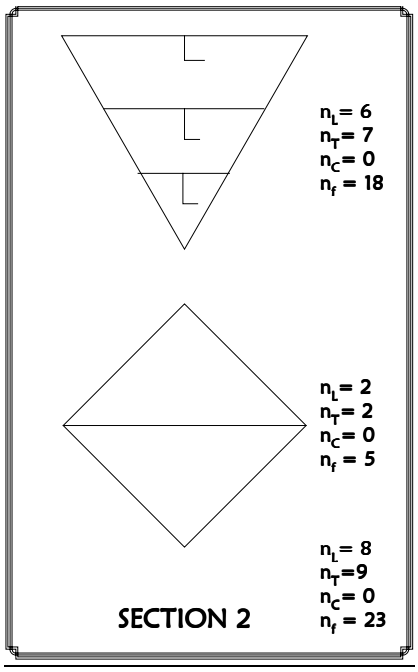
n_L= 6
n_T= 7
n_C= 0
n_f = 18
n_L= 2
n_T= 2
n_C= 0
n_f = 5
n_L= 8
n_T=9
n_C= 0
n_f = 23
SECTION 2

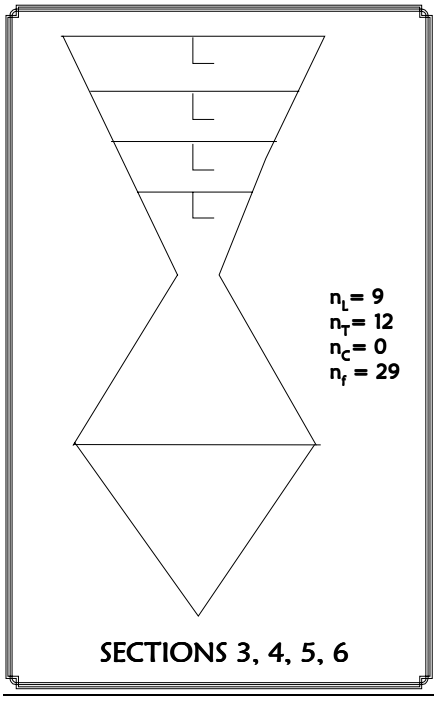
n_L= 9
n_T= 12
n_C= 0
n_f = 29
SECTIONS 3, 4, 5, 6

23K DWT

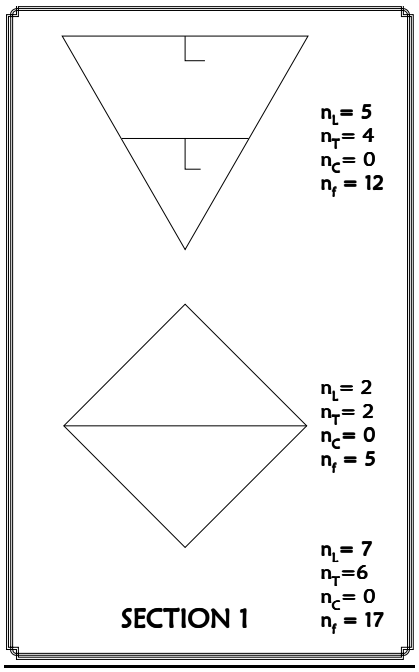
n_L= 5
n_T= 4
n_C= 0
n_f = 12
n_L= 2
n_T= 2
n_C= 0
n_f = 5
n_L= 7
n_T=6
n_C= 0
n_f = 17
SECTION 1

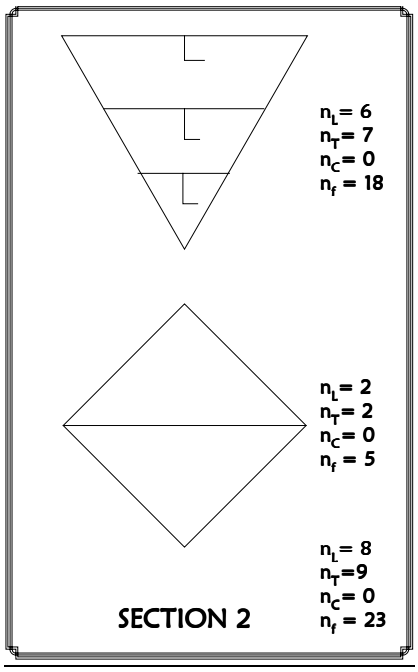
n_L= 6
n_T= 7
n_C= 0
n_f = 18
n_L= 2
n_T= 2
n_C= 0
n_f = 5
n_L= 8
n_T=9
n_C= 0
n_f = 23
SECTION 2

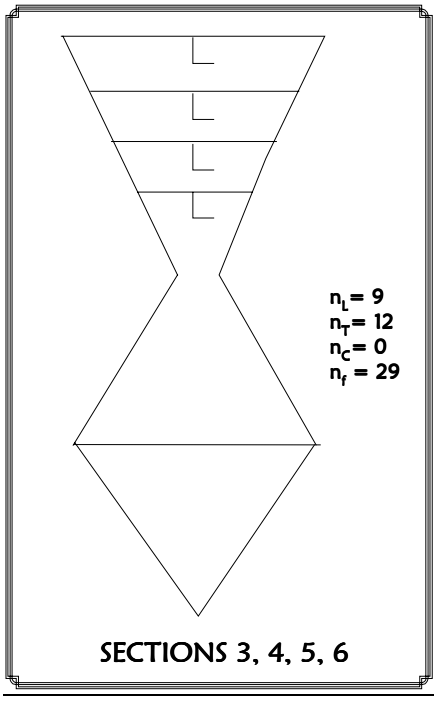
n_L= 9
n_T= 12
n_C= 0
n_f = 29
SECTIONS 3, 4, 5, 6

500 DWT

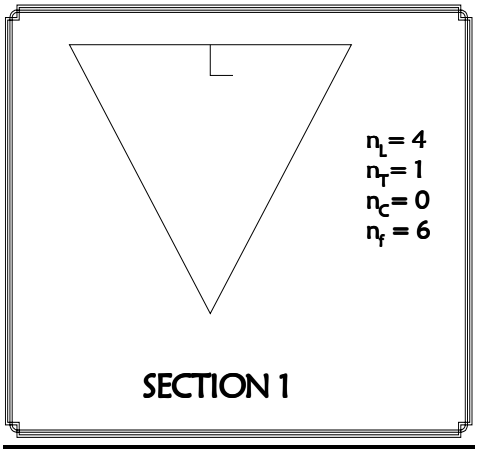
$n_L = 4$
$n_T = 1$
$n_C = 0$
$n_f = 6$
SECTION 1

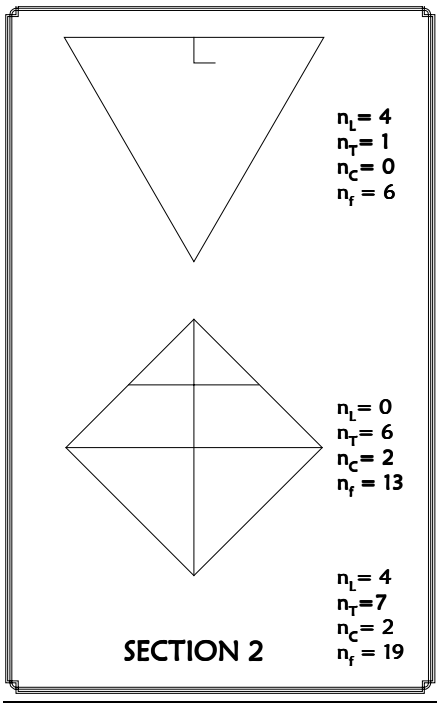
$n_L = 4$
$n_T = 1$
$n_C = 0$
$n_f = 6$
$n_L = 0$
$n_T = 6$
$n_C = 2$
$n_f = 13$
$n_L = 4$
$n_T = 7$
$n_C = 2$
$n_f = 19$
SECTION 2

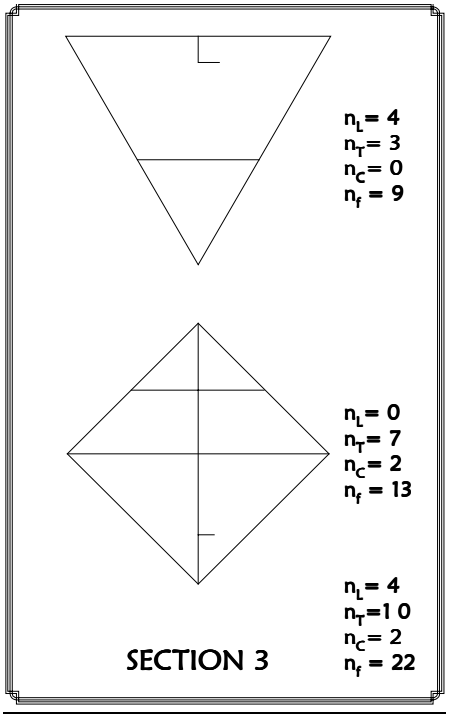
$n_L = 4$
$n_T = 3$
$n_C = 0$
$n_f = 9$
$n_L = 0$
$n_T = 7$
$n_C = 2$
$n_f = 13$
$n_L = 4$
$n_T = 10$
$n_C = 2$
$n_f = 22$
SECTION 3

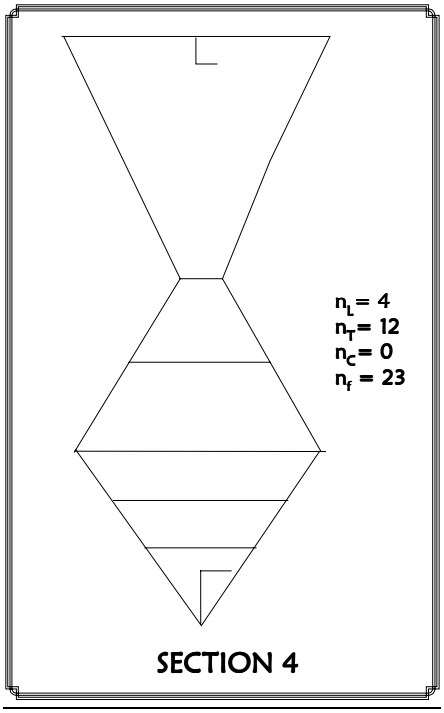
$n_L = 4$
$n_T = 12$
$n_C = 0$
$n_f = 23$
SECTION 4

VITA

Suryanarayana Vakkalanka was born in Hyderabad, India on 24 June, 1977. He did his schooling at Siva Sivani Public School, Hyderabad, India and his pre-university schooling at Little Flower Junior College, Hyderabad, India.

He joined the Indian Institute of Technology, Madras, India in 1994 and graduated with a Bachelor of Technology (B.Tech) in Naval Architecture in June 1998.

He then attended Virginia Polytechnic Institute and State University (Virginia Tech), Blacksburg, USA for his graduate studies. He received his Master of Science (M.S) in Ocean Engineering in March 2000. His areas of interest are ship collisions and finite element analysis. Currently, he is working with Microstrategy Inc., Falls Church, VA, USA.